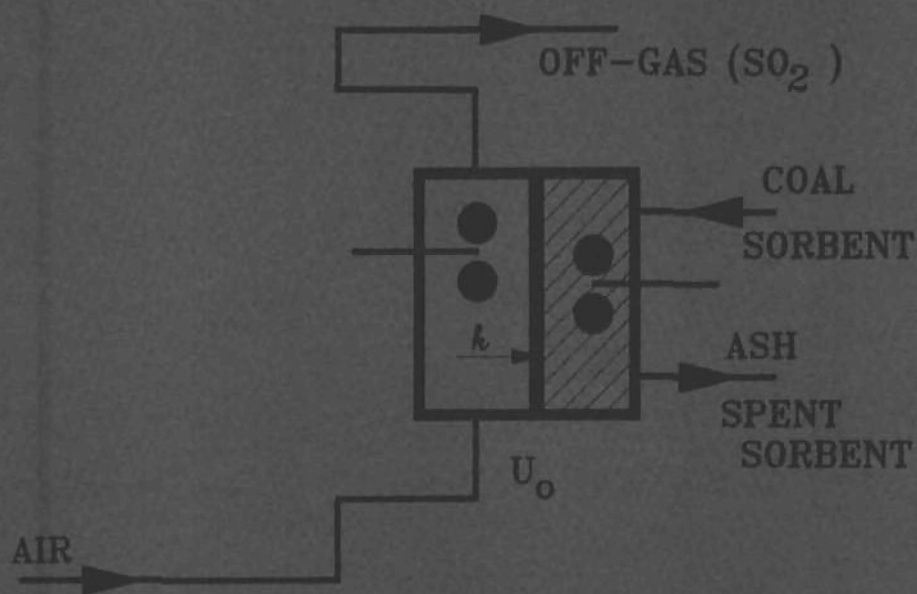


# Sulfur Retention and Particle Motion during Fluidized Bed Combustion of Coal



J.C. Schouten

TR diss  
1619

Sulfur Retention  
and  
Particle Motion  
during  
Fluidized Bed Combustion of Coal

6400 dg

217 0689

700 class 1619

Copyright © 1988 by J.C. Schouten, Delft, The Netherlands.

No part of this publication may be reproduced, stored in a retrieval system or transmitted, in any form, or by any means, electronic, mechanical photocopying, recording or otherwise, without the written prior permission of the author.

# Sulfur Retention and Particle Motion during Fluidized Bed Combustion of Coal

## PROEFSCHRIFT

ter verkrijging van de graad van  
doctor aan de Technische Universiteit Delft,  
op gezag van de Rector Magnificus,  
prof.dr. J.M. Dirken,  
in het openbaar te verdedigen  
ten overstaan van een commissie  
door het College van Dekanen daartoe aangewezen,

op donderdag 24 maart 1988  
te 14.00 uur

door

JACOB CORNELIS SCHOUTEN

scheikundig ingenieur

geboren op 29 juni 1959 te Apeldoorn



Delft University Press / 1988

TR diss  
1619

Dit proefschrift is goedgekeurd door de promotor prof.dr.s. P.J. van den Berg en door de toegevoegd promotor ir. C.M. van den Bleek.

De promotiecommissie wordt gevormd door:

**voorzitter:**

De Rector Magnificus der Technische Universiteit Delft of diens vervanger.

**promotor:**

prof.dr.s. P.J. van den Berg (Technische Universiteit Delft, Faculteit der Scheikundige Technologie en der Materiaalkunde)

**toegevoegd promotor:**

ir. C.M. van den Bleek (Technische Universiteit Delft, Faculteit der Scheikundige Technologie en der Materiaalkunde)

**leden:**

prof. B. Scarlett, M.Sc. (Technische Universiteit Delft, Faculteit der Scheikundige Technologie en der Materiaalkunde)

prof. dipl.-ing. K.R.G. Hein (Technische Universiteit Delft, Faculteit der Werktuigbouwkunde)

prof.dr.ir. J.J.H. Brouwers (Universiteit Twente, Faculteit der Werktuigbouwkunde)

dr.ir. H.A. Masson (Université Libre Bruxelles, Mécanique Appliquée, Brussel, België)

Ir. C.M. van den Bleek heeft als begeleider in hoge mate bijgedragen aan het totstandkomen van het proefschrift. Het College van Dekanen heeft hem als zodanig aangewezen.

## STELLINGEN

behorende bij het proefschrift  
ter verkrijging van de graad van  
doctor in de technische wetenschappen

SULFUR RETENTION and PARTICLE MOTION  
during FLUIDIZED BED COMBUSTION of COAL

van

Jaap Schouten

Delft, 24 maart 1988

1. Er bestaat een paradox tussen enerzijds de veelzijdige en complexe onderlinge samenhang van de fysische verschijnselen en chemische processen in een wervelbedreaktor en anderzijds de betrekkelijke eenvoud van de modellen waarmee deze verschijnselen en processen (veelal) onafhankelijk van elkaar worden beschreven.
  2. Een sluggend fluide bed bestaat uit twee duidelijk onderscheidbare delen met verschillende aanwezigheidswaarschijnlijkheden van de vaste stof. Het beddeel boven de bedhoogte bij minimale fluidisatie kan beschouwd worden als een grote 'splash zone' waar de aanwezigheidswaarschijnlijkheden in axiale richting sterk afneemt t.g.v. een verdunningseffect [1]. Bij de keuze van de plaats van continue aftap van sorbentmateriaal in een FBC-installatie moet rekening worden gehouden met dit fluid dynamisch gedrag van het bed. Wanneer de vaste stof onderhevig is aan segregatie, dient de sorbentaftap gekozen te worden beneden of boven de bedhoogte bij minimale fluidisatie afhankelijk van de aard van de segregatie van het sorbentmateriaal ('jetsam' of 'flotsam').
- [1] Dit proefschrift.
3. De enige juiste manier voor het vaststellen van de wijze van gasdoorstroming en gasoverdracht tussen fasen in een fluide bed is het experimenteel bepalen van de axiale en radiale concentratieprofielen in zowel de bellen als de dichte fase in het bed [1]. Het toepassen van theoretische reactormodellen, met behulp waarvan de discriminatie tussen verschillende gasdoorstromingsmogelijkheden (zoals 'ISTR' of '(dispersed) plug flow'; 'fast bubble' of 'slow bubble') geschiedt op grond van alleen de concentratie aan de uitgang van de reactor [2], moet worden afgewezen.

[1] Almstedt, A.-E. and Ljungstrom, E.B., Proc. 9th Int. Conf. on FBC, volume 1, 575-585, Boston, USA, May 3-7, 1987.

[2] Van der Looij, J.M.P., Proc. Int. Symp. on Multiphase Flows. ISMF 1987, volume 1, 19-27, Zhejiang University, Hangzhou, People's Republic of China, August 3-5, 1987.

4. Voor de uitvoering van representatieve zwavelretentie-experimenten tijdens stationaire bedrijfstoestand in een FBC-installatie vormt het een essentiële voorwaarde dat een meting niet eerder wordt uitgevoerd dan na een periode van ten minste 5 maal de gemiddelde sorbentverblijftijd. Als criterium voor het bereiken van de stationaire toestand moet daarbij niet gehanteerd worden het constant zijn van bijv. de gemiddelde bedtemperatuur en/of gassamenstelling (zoals veelvuldig in de praktijk wordt toegepast), maar veeleer het constant zijn van de gemiddelde samenstelling van het sorbentmateriaal in het bed.

Van den Bleek, C.M. and Schouten, J.C., Written comment on Proc. 9th Int. Conf. on FBC, Boston, USA, May 3-7, 1987 (to be published by the Amer. Soc. Mech. Eng. (ASME)); Delft, June 3rd, 1987.

5. In de zwavelretentiemodellering is het gebruik van eenvoudige (empirische) kinetiekrelaties voor de sulfatatiereactie essentieel voor het verkrijgen van een eenvoudig en inzichtelijk model ([1] en [2]). Wanneer deze relaties echter niet correct worden toegepast in zowel de vaste-fase balans als de gas-fase balans, worden weliswaar eenvoudige doch incorrecte vergelijkingen verkregen voor de zwaveldoorbraakconcentratie en de molaire calcium/zwavel-verhouding in de reactorvoeding ([3] en [4]).

[1] Schouten, J.C. and Van den Bleek, C.M., Shorter Communication submitted for publication to Chem. Eng. Sci., 1986.

[2] Schouten, J.C. and Van den Bleek, C.M., Proc. 9th Int. Conf. on FBC, volume 2, 749-761, Boston, USA, May 3-7, 1987.

[3] Zheng, J., Yates, J.G. and Rowe, P.N., Chem. Eng. Sci., 37 (2), 167, 1982.

[4] Noordergraaf, I.W., PhD Thesis, Department of Chemical Engineering and Chemistry, Delft University of Technology, The Netherlands, 1985.

6. Bij het ontwerpen van een fluïde-bed-reaktor verdient het aanbeveling om de toepassing van een 'konisch' gevormde reaktor te onderzoeken. In een dergelijke reaktor worden de verschillende verschijnselen en processen in het bed simultaan beïnvloed door de gelijktijdige verandering in axiale richting van de beddiameter, de H/D-verhouding en de superfiële gassnelheid.

In de wervelbedverbranding van steenkool biedt een konische reaktor de volgende voordelen: verbetering van de zwavelretentie door vergroting van de gasverblijftijd [1]; afname van segregatie t.g.v. de toenemende beddiameter [2]; vergroting van het koolverbrandingsrendement door vermindering van fines-elutriatie; afname van NOx-vorming d.m.v. getrapte verbranding in een 'sandwiched B-A' fluïde bed [3].

Een 'serieschakeling' van reaktordelen met verschillende diameters biedt in dit kader eveneens aantrekkelijke mogelijkheden.

[1] Ulerich, N.H., Newby, R.A. and Keairns, D.L., Report EPRI CS-3330, Project 1336-1, 5-6/5-7, Westinghouse Electric Corporation, Research and Development Center, Pittsburgh (PA), USA, December 1983.

[2] Dit proefschrift.

[3] Masson, H.A. and Stievenart, Ph., Lezing gepresenteerd op WUB werkgroep bijeenkomst, Universiteit Twente, Enschede, 18 september 1987.

7. De mate van zwavelretentie in een fluïde-bed-verbrandingsinstallatie kan niet voortdurend toenemen door vergroting van de hoeveelheid actief sorbent materiaal in het bed. Dit houdt in dat bij een bepaalde maximale CaO-omzetting niet altijd een beduidende toename van de zwavelretentie bij een constante (Ca/S)-verhouding kan worden verkregen door het gebruik van een ander sorbent materiaal met een grotere maximale CaO conversie.

Dit proefschrift.

8. De beweging van de vaste fase in een fluïde bed wordt meestal beschreven met het verschijnsel 'dispersie', dat gebaseerd is op de willekeurige beweging van de deeltjes (bijv. het één-dimensionale dispersie model van Taylor [1]). Deze aanpak is vergelijkbaar met de diffusie van molekulen in een gas, welke gerelateerd is aan een concentratiegradiënt. Op dezelfde wijze wordt de dispersie van deeltjes gerelateerd aan een verschil in deeltjesconcentratie in het bed. Een aannemelijke fysische verklaring voor deze beschrijving van het deeltjestransport is niet voorhanden. Het is beter de beweging van vaste stof in een fluïde bed te beschrijven met een twee-fasen model waarbij er deeltjesuitwisseling plaats vindt tussen omhoog- en omlaaggerichte convectieve stromen van vaste stof [2].

[1] Avidan, A. and Yerushalmi, J., *AIChE J.*, 31 (5), 835, 1985.

[2] Schouten, J.C., Masson, H.A. and Van den Bleek, C.M., Proc. Int. Symp. on Multiphase Flows, ISMF 1987, volume 1, 237-243, Zhejiang University, Hangzhou, People's Republic of China, August 3-5, 1987.

9. Bij de bestudering van de chemische en/of intrinsieke kinetiek van een batch gas-vast-reactie op laboratoriumschaal is de keuze van de reactor van wezenlijk belang. In het algemeen geldt de regel dat deze reactie ook moet worden bestudeerd in het type reactor waarin op praktijkschaal het proces wordt uitgevoerd. De aard van de gas-vast-menging in deze reactor bepaalt niet de grootte van de chemische/intrinsieke reactiesnelheid (want kinetiek en hydrodynamica vormen uiteraard onafhankelijke systeemeigenschappen), maar kan wel van invloed zijn op de grootte van de conversie van verschillende vaste-stof-deeltjes op hetzelfde tijdstip in de reactor en daarmee op de vereiste complexiteit van de te hanteren kinetische relaties.

Dit proefschrift.

10. De algemene toepasbaarheid van een mathematisch fysisch/chemisch model ten behoeve van wetenschappelijke en/of industriële (proces)technologische toepassing wordt bepaald door drie factoren welke, in volgorde van belangrijkheid, gegeven zijn als:
1. de eenvoud van het gebruik van het model; zowel ten aanzien van de berekening van de fysisch/chemische modelparameters, als ten aanzien van de vereiste (numerieke) berekeningsmethode;
  2. de mogelijkheid tot experimentele toetsing en nauwkeurige kwantitatieve validatie van het model;
  3. de mogelijkheid tot en de betrouwbaarheid van de modelmatige opschaling van laboratoriumgegevens naar pilot-plant of grootschalige toepassingen.



11. De overtuigingskracht welke spreekt uit een politieke redevoering is voornamelijk gelegen in een afgewogen toepassing van de uitspraak van Einstein dat "everything should be made as simple as possible, but not simpler".

12. Corrosiebestrijding in de agrarische sector vraagt om actie; rust roest ook in de landbouw!

Schouten, J.C., Landbouwmecanisatie, 34 (5), 551-553, 1983.

Schouten, J.C. en Gellings, P.J., TH&MA, Extern kwartaalblad THTwente, 9, 18-21, Juli 1983.

13. Bedrijven en instellingen die thans niet deelnemen aan de trend om meer vrouwen aan te trekken voor leidinggevende functies, zullen daarvan in de toekomst hinder ondervinden in hun relaties met partners, concurrenten en klanten.

14. De instelling van een Corrosie Informatie Transfer Punt ten behoeve van de agrarische sector is zeer gewenst.

Schouten, J.C., Report Steel/Sem.10/R.4 (34 pages), Steel Committee of the Economic Commission for Europe (ECE) of the United Nations Organization (UNO), Geneva, Switzerland, January 1984.

Schouten, J.C., Metaal&Techniek, 29 (6), 40-42, 1984.

Schouten, J.C., Metaal&Techniek, 29 (7), 28-31, 1984.

15. Grappige stellingen bestaan niet: als grappig bedoelde stellingen zijn meestal flauw, ver gezocht, vervelend of irritant en bovendien vaak stilistisch onnodig ingewikkeld.

16. De 'corrosiebeschermingsfactor' en de 'corrosie conditie' vormen bruikbare grootheden bij de technisch-economische analyse van corrosiekosten en mogelijke besparingen [1], zowel voor afzonderlijke bedrijven als voor totale bedrijfstakken [2].

[1] Schouten, J.C. and Gellings, P.J., Br. Corros. J., 19 (4), 159-164, 1984.

[2] Schouten, J.C. and Gellings, P.J., J. Agr. Engng. Res., 36, 217-231, 1987.

17. Het niveau, de kwaliteit en de werkwijze van de Nederlandse volksvertegenwoordiging moeten worden verbeterd door:

a. uitbreiding van het aantal leden der Tweede Kamer van 150 naar 250;

b. afschaffing van de Eerste Kamer;

c. het wijzigen van het parlamentslidmaatschap van een 'volledige' in een 'deeltijd' functie: volksvertegenwoordigers moeten naast de functie van parlamentslid andere politieke en/of maatschappelijke betrekkingen vervullen; bijvoorbeeld in het bedrijfsleven, de vakbond, het openbaar bestuur, de financiële wereld, het onderwijs, het wetenschappelijk onderzoek, de gezondheidszorg, de land- en tuinbouw enz.

d. een aanzienlijke vergroting van de bereidheid van oud-bewindspersonen om na het minister- of staatssecretarisschap voor een periode van ten minste vier jaren deel uit te maken van het parlement.

Extended Epstein - Heisenberg Principle.

In a R&D orbit, only two of the existing three parameters can be defined simultaneously. These parameters are: task, time and resources.

1. If one knows what the task is, and there is a time limit allowed for the completion of the task, then one cannot guess how much it will cost.
2. If the time and resources are clearly defined, then it is impossible to know what part of the R&D task will be performed.
3. If one is given a clearly defined R&D goal and a definite amount of money which has been calculated to be necessary for the completion of the task, one cannot predict if and when the goal will be reached.

If one is lucky enough and can accurately define all three parameters, then what one deals with is not in the realm of R&D.

(in: Arthur Bloch, Murphy's Law Complete - all the reasons why everything goes wrong, Methuen London Ltd., Great Britain, 1985.)

## ACKNOWLEDGEMENTS

This thesis is a part of the research program on the regenerative desulfurization during the fluidized bed combustion of coal as it is carried out at the Department of Chemical Engineering and Chemistry of the Delft University of Technology.

I would like to acknowledge gratefully:

- \* the financial support given by the Commission of the European Communities (Contract no. EN3F-0014-NL (CDF)), the Netherlands Research Association 'Stichting voor de Technische Wetenschappen STW' (research project no. 700-349-173), the Netherlands Management Office for Energy Research PEO (Contract no. 20.35-016.30) and Shell Internationale Petroleum Maatschappij B.V.;
- \* the succesful cooperation with the 'Institut National des Industries Extractives INIEX' in Liège (Belgium) in using different fluidized bed facilities.

Furthermore I am grateful to all persons who have contributed to the realization of this thesis by their scientific, technical or administrative support.

Because the mentioning of many names provides the possibility of forgetting some, I will only mention three: I want to thank Cor van den Bleek for his stimulating support and encouragement; further I want to thank Gerrit Hakvoort for his helpful suggestions; finally I am grateful to Henri Masson for his enthusiastic cooperation.

## CONTENTS

### SUMMARY / SAMENVATTING

CHAPTER 1: INTRODUCTION and SCOPE of THESIS	1
1.1 The D.U.T. research on FBC	1
1.2 Overview of the research work: list of publications	1
1.3 Overview of the thesis	7
CHAPTER 2: SULFUR RETENTION during FLUIDIZED BED COMBUSTION of COAL	9
2.1 Introduction	9
2.2 J.C. Schouten and C.M. van den Bleek Prediction and Optimization of Sulfur Retention in the Fluidized Bed Combustion of Coal: the D.U.T. SURE model (submitted for publication in Chem. Eng. Sci., 1987)	10
2.3 J.C. Schouten and C.M. van den Bleek The Influence of Oxygen-Stoichiometry on Desulfurization during FBC: a Simple SURE Modeling Approach (submitted for presentation at the 10th Int. Symp. on Chemical Reaction Engineering, ISCRE 10, 1988)	63
2.4 Comments	78
CHAPTER 3: PARTICLE MOTION in SLUGGING GAS FLUIDIZED BEDS	91
3.1 Introduction	91
3.2 J.C. Schouten, P.J.M. Valkenburg and C.M. van den Bleek Segregation in a Slugging FBC Large Particle System (accepted for publication in Powder Technol., 1987)	92
3.3 J.C. Schouten, H.A. Masson and C.M. van den Bleek The Motion of Particles in a Slugging Gas Fluidized Bed (submitted for publication in Powder Technol., 1987)	120
3.4 Comments	155
NOTATION	168
REFERENCES	172
CURRICULUM VITAE	177

## SUMMARY

A key feature of fluidized bed coal combustion (FBC) is the possibility of the in-situ removal of the sulfur, by natural or synthetic sorbents, which is released from the burning coal. However, the consumption of the sorbent should be maintained at a reasonably low level in order to reduce the solid waste disposal as well as to achieve an acceptable cost of energy relative to conventional technologies. These considerations, together with others (like the interaction between  $\text{SO}_x$ - and  $\text{NO}_x$ -removal), make clear that much research on its environmental performance is still needed before FBC 'comes of age'.

The research described in this thesis is predominantly focussed on two subjects, which are both related to the removal of sulfur during FBC:

1. the modeling of sulfur retention, and
2. the motion of particles in slugging gas fluidized beds.

### 1. the modeling of sulfur retention (chapter 2).

Starting from an evaluation of retention models given in literature a simple analytical Sulfur RETention (SURE) model is described which can be used for the prediction and optimization of sulfur retention during FBC.

The SURE model is based on a simple approach to the sulfation kinetics: the sorbent sulfation rate is first order in the  $\text{SO}_2$  (or  $\text{SO}_3$ ) concentration and first order in the reactive sorbent surface area. Two-phase plug flow as well as one-phase ideally mixed gas flow are considered.

The decrease of the desulfurization efficiency during staged combustion as well as the temperature-dependency of the sulfure capture process can theoretically be explained by the formation of  $\text{SO}_3$  as a gaseous intermediate reactant in the sorbent sulfation reaction.

The model provides analytical equations for the dimensionless sulfur outlet concentration in case of unsteady state sulfation and for the molar calcium to sulfur ratio in the reactor feed during steady state operation; the latter being a function of fluid bed reactor conditions, coal and sorbent properties, and the stoichiometric in-bed air ratio.

The SURE model shows good agreement with experimental data obtained from the literature. It is argued that the sorbent residence time is an important system parameter, which importance is generally neglected during sulfur capture experimentations in pilot-plants.

Finally, the retention index is introduced which is a useful parameter for optimization of the retention performance of a combustor. The index facilitates the choice of an appropriate action in the minimization of the calcium to sulfur feed ratio (e.g. change of particle size or superficial gas velocity).

## 2. the motion of particles in slugging gas fluidized beds (chapter 3).

The particles applied in FBC systems are generally B- or D-type of powders and differ significantly in size and density (coal, ash, sorbent). Their fluidization behaviour is strongly influenced by the presence of closely packed internals as heat exchanger tubes. Consequently, the fluidization is mostly of the slugging type and shows remarkable agreement with the mode of fluidization in relatively small diameter fluid beds.

Therefore slugging, particle mixing and segregation are investigated in small diameter beds (3.5 to 15 cm ID) with two different experimental techniques: abrupt defluidization and a radio-active tracer technique.

The slugging beds are characterized by dimensionless slug parameters which are obtained from visual bed height measurements. It is observed that square-nosed slugging is likely to occur at  $H_{mf}/D$ -ratios of more than 4. The distance between two successive gas slugs is found to be independent of gas velocity, while the average length of solids slugs equals about 80% to more than 90% of the bed height at minimum fluidization.

The extent of segregation increases with a larger  $H_{mf}/D$ -ratio, a smaller bed diameter and a decreasing gas velocity. However, at a gas velocity of three times the minimum fluidization velocity still a significant degree of segregation is measured. Based on experimentations it is further suggested that segregation becomes nil beyond a critical value of the bed diameter (about 23 cm at a  $H_{mf}/D$ -ratio of 2 and an excess gas velocity of 0.3 m/s).

Finally, dynamic radio-active tracer experiments are presented, which clearly show that a slugging bed consists of two regions: above and below the position of the bed height at minimum fluidization. The influence is shown of the axial bed position, the gas velocity and the  $H_{mf}/D$ -ratio on the particle velocity, on the probability of changes in the direction of the particle's displacement and on its presence probability.

The observed decrease of the presence probability along the bed height in a single-component bed is defined as 'solids dilution' and is explained by a balance of the drag force and gravity force acting on the particle.

Based on these observations a general model for the motion of solids in slugging gas fluidized beds is introduced. The mechanism of solids motion is based on convective and dispersive solids flows which differ in magnitude in the upper and lower part of the bed.

A comparison between the experimentally observed normalized presence probability of the tracer and the fitted solids concentration according to the model shows a good agreement which is further applied for a diagnostic evaluation of solids motion in slugging gas fluidized beds.

## SAMENVATTING

Een wezenlijke eigenschap van wervelbedverbranding van steenkool (WBV) vormt de mogelijkheid om de zwavel die vrijkomt bij de koolverbranding in situ te vangen m.b.v. een natuurlijk of synthetisch sorbent materiaal. Het verbruik van dit sorbent moet echter in een aanvaardbare omvang worden gerealiseerd om enerzijds de vast-afval problematiek te beperken en om anderzijds een acceptabel niveau van energiekosten te verkrijgen in vergelijking met conventionele energietechnologieën. Deze overwegingen tezamen met anderen, zoals de interactie tussen  $SO_x$ - and  $NO_x$ -verwijdering, maken duidelijk dat nog veel onderzoek ten aanzien van de milieuaspecten nodig is alvorens WBV als een 'volwassen' technologie kan worden aangemerkt.

Het onderzoek beschreven in dit proefschrift is voornamelijk gericht op twee onderwerpen, welke beide betrekking hebben op de verwijdering van zwavel tijdens wervelbedverbranding van steenkool:

1. de modellering van zwavelretentie, en
2. de beweging van deeltjes in sluggende, gas-gefludiseerde bedden.

### 1. de modellering van zwavelretentie (hoofdstuk 2).

Uitgaande van een evaluatie van retentiemodellen in de literatuur, wordt een eenvoudig, analytisch model beschreven dat kan worden gebruikt voor de voorspelling en optimalisatie van zwavelretentie tijdens WBV. Dit model is gebaseerd op een eenvoudige benadering van de sulfatatiekinetiek: de sorbent sulfatatiesnelheid is eerste orde in de  $SO_2$  (of  $SO_3$ ) concentratie en eerste orde in het reactieve sorbent oppervlak. Zowel twee-fasen propstroming als de één-fase ideaal geroerde tank worden beschouwd.

De afname van de ontzwavelingsefficiëncy tijdens getrapte verbranding en de temperatuurafhankelijkheid van het zwavelvangstproces kunnen theoretisch worden verklaard met behulp van de vorming van  $SO_3$  als gasvormig tussenproduct in de sorbent-sulfatatiereactie.

Het model biedt analytische vergelijkingen voor de dimensieloze zwavelconcentratie tijdens niet-stationaire sulfatatie en voor de molaire calcium-zwavel verhouding in de reactorvoeding tijdens stationaire operatie; de laatste is een functie van reactor condities, van kool- en sorbent-eigenschappen en van de stoichiometrische luchtverhouding in het bed.

Het model toont goede overeenstemming met experimentele gegevens uit de literatuur. Aangetoond wordt dat de sorbentverblijftijd een belangrijke systeemgrootte is, welke in het algemeen wordt veronachtzaamd tijdens zwavelvangstexperimenten in (kleinschalige) proefopstellingen.

Ten slotte wordt de retentie-index geïntroduceerd, welke een bruikbare grootte vormt voor de optimalisatie van de mate van retentie in een verbrandingsinstallatie. De index vergemakkelijkt de keuze van een geschikte aktie m.b.t. de minimalisatie van de molaire calcium-zwavel verhouding (bijv. verandering van de deeltjesgrootte of de superficiële gassnelheid).

## 2. deeltjesbeweging in sluggende gas-gefluidiseerde bedden (hoofdstuk 3).

De deeltjes die toegepast worden in WBV-systemen zijn doorgaans B- of D-type poeders en verschillen aanzienlijk in grootte en dichtheid (kool, as en sorbent). Hun fluïdisatiegedrag wordt sterk beïnvloed door de aanwezigheid van de dichtgepakte warmtewisselaarpipen in het bed (schijnbare beddiameter van ongeveer 10 cm). Dientengevolge wordt de fluïdisatie meestal gekarakteriseerd door 'slugging' en toont opvallende gelijkenis met de wijze van fluïdisatie in wervelbedden van relatief kleine inwendige diameter.

Daarom zijn slugging, deeltjesmenging en segregatie in kleine bedden (3.5 tot 15 cm ID) onderzocht met behulp van twee verschillende experimentele technieken: abrupte defluïdisatie en een radio-actieve tracer techniek.

De sluggende bedden worden gekarakteriseerd door dimensieloze slugparameters, welke worden verkregen m.b.v. visuele bedhoogtemetingen. Getoond wordt dat 'square-nosed slugging' optreedt bij  $H_{mf}/D$ -verhoudingen groter dan 4. De afstand tussen twee opeenvolgende gaslugs is onafhankelijk van de gassnelheid, terwijl de gemiddelde lengte van de deeltjesslugs ongeveer 80% tot zelfs meer dan 90% van de bedhoogte bij minimale fluïdisatie bedraagt.

De mate van segregatie neemt toe met een grotere  $H_{mf}/D$ -verhouding, een kleinere beddiameter en een afnemende superfiële gassnelheid. Bij een gassnelheid van driemaal de minimale fluïdisatiesnelheid wordt echter nog steeds een significant niveau van segregatie gemeten. Op grond van experimenten wordt verondersteld dat segregatie nihil wordt boven een kritieke grootte van de beddiameter (ongeveer 23 cm bij een  $H_{mf}/D$ -verhouding van 2 en bij een gassnelheid van 0.3 m/s boven de minimale fluïdisatiesnelheid).

Vervolgens worden dynamische radio-actieve tracer experimenten gepresenteerd, welke duidelijk aantonen dat een sluggend bed bestaat uit een tweetal delen: onder en boven de positie van de bedhoogte bij minimale fluïdisatie. De invloed wordt getoond van de axiale positie in het bed, de superfiële gassnelheid en de  $H_{mf}/D$ -verhouding, op de deeltjessnelheid, op de waarschijnlijkheid van een verandering in de richting van de deeltjesverplaatsing en op de aanwezigheidswaarschijnlijkheid van het tracerdeeltje.

De waargenomen afname van de aanwezigheidswaarschijnlijkheid langs de bedhoogte in een bed van een enkelvoudige component, wordt gedefinieerd als 'deeltjesverdunding' en wordt verklaard met behulp van een evenwicht tussen de 'meesleurkracht' en de zwaartekracht welke op een deeltje werken.

Gebaseerd op deze waarnemingen wordt een algemeen model voor de beweging van deeltjes in een sluggend, gas-gefluidiseerd bed geïntroduceerd. Het mechanisme van deeltjesbeweging is gebaseerd op convectieve en dispersieve vaste-stof stromen, welke verschillen in grootte in het bovenste en onderste deel van het bed.

Een vergelijking tussen de experimenteel waargenomen genormaliseerde aanwezigheidswaarschijnlijkheid van de tracer en de 'gefitte' deeltjesconcentratie volgens het model tonen een goede overeenstemming, welke verder wordt gebruikt voor een evaluatie van deeltjesbewegingen in sluggende bedden.



### 1.1 The D.U.T. research on FBC

The research on sulfur retention during the fluidized bed combustion of coal at the Department of Chemical Engineering and Chemistry at the Delft University of Technology (D.U.T.) started in March 1980. The program is presently managed by prof. drs. P.J. van den Berg and ir. C.M. van den Bleek.

The research was carried out from January 1980 to March 1984 by PhD student ir. I.W. Noordergraaf (graduated May 1985). Noordergraaf started the work on sulfur capture during fluidized bed combustion of coal with use of a synthetic sorbent material. Further he paid attention to the external mass transfer phenomena and the fluid dynamical behaviour of large particles.

This work was continued in January 1984 and in August 1984 respectively by the PhD students ir. J.C. Schouten (financially supported by the Netherlands Research Organization STW) and ir. P.J.M. Valkenburg. A new aspect in the research program was the study with use of thermal analytical techniques of the release of sulfur during the combustion of coal.

In April 1986 a research project on the regenerative sulfur retention during FBC was started being financially supported by the Commission of the European Communities and the Netherlands Management Office for Energy Research PEO. Two PhD students have been appointed for the synthesis and testing of sorbent materials and for the design of a sorbent-regenerator (ir. A.E. Duisterwinkel and ir. E.H.P. Wolff).

### 1.2 Overview of the research work: list of publications

The work of the present author has predominantly been focussed on three topics in the D.U.T. research program:

1. the release of sulfur during coal combustion,
2. the retention of sulfur during the fluidized bed combustion of coal,
3. the motion of particles in slugging gas fluidized beds.

A collection of 14 papers has been written on these respective topics of the D.U.T. research program. The author of this thesis is first author of 11 papers and co-author of 3 papers. Some of these papers have already been published in conference proceedings or journals, while others have been submitted or accepted for presentation at conferences or publication in journals:

<u>journals</u>	-published:	2 papers
	-accepted for publication:	1 paper
	-submitted for publication:	4 papers
<u>conferences</u>	-published in proceedings:	6 papers
	-submitted for presentation:	1 papers

First, a list of these publications is given together with a short abstract of the papers so as to provide a comprehensive overview of the author's work. Further, in the next section of this chapter, it is indicated what the general scope of the present thesis will be and which papers therefore have been included in this thesis.

List of publications:

1. the release of sulfur during coal combustion

- 1.1 Schouten, J.C., Hakvoort, G., Valkenburg, P.J.M. and Van den Bleek, C.M., "An Approach with Use of EGA to the Mechanism of Sulfur Release during Coal Combustion", Proc. 10th Nordic Symp. and Joint Nordic-English Symp. on Thermal Analysis and Calorimetry, Bergen, Norway, August 20-22, 1986; in: Thermochimica Acta, 114, 171-178, 1987.

In this paper a reaction scheme for the release of sulfur from pyrite ( $\text{FeS}_2$ ) in coal is presented. The decomposition of pyrite is a complicated process composed of several overlapping reactions. The reaction scheme is verified by thermogravimetric experiments with combustion of pyrite, FeS, coal and coal with additions of pyrite. The results are in good qualitative agreement with the proposed reaction scheme.

- 1.2 Schouten, J.C., Blommaert, F.Y., Hakvoort, G. and Van den Bleek, C.M., "A Thermal Analytical Study on the Release of Sulfur during Coal Combustion", Proc. 1987 Int. Conf. on Coal Science, Maastricht, The Netherlands, October 26-30, 1987; in: Coal Science and Technology 11, J.A. Moulijn, K.A. Nater and H.A.G. Chermin (Eds.), 837-840, Elsevier, Amsterdam, 1987.

In this second paper thermal analytical experiments with relatively high heating rates (up to 70 °C/min) are presented. X-ray diffraction is used to determine the composition of specific samples at the end of relevant sulfur release peaks. The reaction products of pyrite combustion are  $\text{FeS}_{(1+x)}$ , FeS and  $\text{Fe}_2\text{O}_3$ .  $\text{FeSO}_4$  is not detected as such, however it can occur as an intermediate reaction product. Separate coal devolatilization and subsequent char combustion experiments are carried out with three coal types with

different sulfur compositions in order to determine the distribution of sulfur over volatiles and char. The main conclusion is that in case of three different coal types all organic sulfur is released during coal devolatilization, while pyritic sulfur is predominantly released during the combustion of the char.

- 1.3 Schouten, J.C., Ingwersen, M.J. and Van den Bleek, C.M., "The Release of Sulfur from a Batch Addition of Coal to a Fluid Bed", Proc. 1987 Int. Conf. on Coal Science, Maastricht, The Netherlands, October 26-30, 1987; in: Coal Science and Technology 11, J.A. Moulijn, K.A. Nater and H.A.G. Chermin (Eds.), 841-844, Elsevier, Amsterdam, 1987.

In the last paper in this series batch-wise sulfur release experiments are presented which are carried out in a 5 cm ID diameter laboratory-scale fluidized bed. In case of one coal type it is confirmed that the organic sulfur is released during coal devolatilization, while pyritic sulfur is oxidized during char combustion. In case of another coal type a different type of behaviour was found.

## 2. the retention of sulfur during the fluidized bed combustion of coal

- 2.1 Schouten, J.C., Singh, P.C., Valkenburg, P.J.M. and Van den Bleek, C.M., "Sulfur Release and Capture in Fluidized Bed Coal Combustion: A Review", submitted for publication in Chem. Eng. Res. Des., 1986.

In this review paper some important variables that determine sulfur release are discussed as coal devolatilization, the position of sulfur generation and the effect of bed variables as temperature and excess air. The advantages of synthetic, regenerative sorbents are discussed vis.a.vis the more commonly available natural sorbents as limestone or dolomite. The effects of additives, hydration,  $\text{NO}_x$ -interaction and freeboard are summarized, together with variables affecting sulfur capture as the (Ca/S) ratio, particle size, temperature, gas velocity, pressure, etc. Further the review provides a summary of 22 typical experimental studies on sulfur capture during FBC as well as an overview of typical sulfur retention models in literature.

- 2.2 Hakvoort, G., Van den Bleek, C.M., Schouten, J.C. and Valkenburg, P.J.M., "TG Study of Sorbent Materials for Desulfurization of Combustion Gases at High Temperature", Proc. 10th Nordic Symp. and Joint Nordic-English Symp. on Thermal Analysis and Calorimetry, Bergen, Norway, August 20-22, 1986; in: Thermochimica Acta, 114, 103-108, 1987.

A thermogravimetric study is summarized on the sulfation and regeneration of CaO-impregnated  $\alpha$ -Al<sub>2</sub>O<sub>3</sub> (pellets) which is a synthetic sorbent that is used in the D.U.T. research program.

- 2.3 Schouten, J.C. and Van den Bleek, C.M., "A Critical Remark on the Use of Semi-empirical Models for Desulfurization in Fluid Bed Coal Combustion", Shorter Communication submitted for publication in Chem. Eng. Sci., 1986.

In this paper some serious concerns are brought forward with respect to the correct application of simple (semi-empirical) sulfation kinetic equations in sulfur retention models as given in the literature. It is illustrated that two sulfation models in literature are fundamentally incorrect, because the mass conservation laws are not correctly applied.

- 2.4 Schouten, J.C. and Van den Bleek, C.M., "The D.U.T. SURE model: A Simple Approach in FBC Sulfur Retention Modeling", Proc. 9th Int. Conf. on Fluidized Bed Combustion, volume 2, 749-761, Boston, USA, May 3-7, 1987.

A simple mathematical sulfur retention (SURE) model is described that can be used for the prediction and optimization of the retention of sulfur during FBC. Starting from an evaluation of retention models in literature this model is based on a simple approach to the sulfation kinetics: the sorbent sulfation rate is first order in the gaseous sulfur concentration as well as in the reactive sorbent surface. The model provides a simple analytical expression for the molar (Ca/S) ratio in the reactor feed as a function of the required level of sulfur retention in the bed, the maximum CaO utilization of the sorbent and a dimensionless model parameter: the retention parameter.

- 2.5 Schouten, J.C. and Van den Bleek, C.M., "Prediction and Optimization of Sulfur Retention in the Fluidized Bed Combustion of Coal: the D.U.T. SURE model", submitted for publication in Chem. Eng. Sci., 1987.

In this paper a non-steady state modeling approach is added to the steady state approach as is outlined in the previous paper. Hereto relations are derived for the gaseous sulfur outlet concentration (sulfur breakthrough) as a function of the dimensionless breakthrough time in the case of unsteady state combustor operation due to a batch addition of sorbent or a sulfur step input on a bed containing a fixed amount of sorbent. The CaO conversion and the sulfur outlet concentration are compared with literature data from which the sulfation kinetic reaction rate parameter is calculated.

- 2.6 Valkenburg, P.J.M., Singh, P.C., Schouten, J.C. and Van den Bleek, C.M., "Sulfation Studies in a Fixed Bed Reactor on Synthetic Sorbents for Possible Use in the Regenerative Sulfur Capture Process in Fluidized Bed Combustion of Coal", Proc. 9th Int. Congr. on Chemical Engineering, CHISA 1987, Prague, Czechoslovakia, August 30 - September 4, 1987.

A fixed bed sorption study is presented in which the SURE model approach as outlined in the previous papers is used to describe the non-steady state sulfation of the synthetic sorbent (paper 2.2) in a fixed bed reactor. The influence of oxygen on the rate of sulfation is explained by the formation of the intermediate reactant  $SO_3$ . In order to fit the data the model is extended to describe the sulfation at two different reactive surfaces, which have kinetic reactivities towards  $SO_3$  uptake which differ an order in magnitude.

- 2.7 Schouten, J.C. and Van den Bleek, C.M., "The Influence of Oxygen-Stoichiometry on Desulfurization during FBC: A Simple SURE Modeling Approach", submitted for presentation at the 10th Int. Symp. on Chemical Reaction Engineering, ISCRE 10, Basle, Switzerland, August 29 - September 1, 1988.

In the last paper of this series the influence of oxygen-stoichiometry on the desulfurization efficiency in a FBC combustor is discussed. The effect of a decreasing sulfur removal at low oxygen concentrations (at low in-bed air ratios) is explained by the formation of  $SO_3$ . The steady state SURE model is extended and now provides an analytical equation for the (Ca/S) ratio which is also a function of the coal properties and of the in-bed stoichiometric air ratio.

### 3. the motion of particles in slugging gas fluidized beds

- 3.1 Schouten, J.C., Valkenburg, P.J.M. and Van den Bleek, C.M., "Segregation in a Slugging FBC Large Particle System", accepted for publication in Powder Technology, 1987.

Segregation and slugging experiments are presented which have been carried out at ambient conditions with a binary large particle system representing the ash-coal/sorbent mixture in a fluid bed combustor. The slugging beds are characterized by dimensionless slug parameters which are obtained from visual bed height measurements. The influence of the superficial gas velocity, the bed diameter and the bed aspect ratio on the extent of segregation is investigated. A simple segregation model is introduced which is based on a mechanism of segregation in slugging gas fluidized beds that is proposed being based on experimental observations.

- 3.2 Schouten, J.C., Masson, H.A. and Van den Bleek, C.M., "A Model for the Segregation of Large Particles in Slugging Gas Fluidized Beds", Proc. Int. Symp. on Multiphase Flows, ISMF 1987, volume 1, 237-243, Zhejiang University, Hangzhou, People's Republic of China, August 3-5, 1987.

In this paper a simple approach is given to the modeling of segregation in (round- and square-nosed) slugging beds. The segregation mechanism is based on a segregative upwards flow of particles in the particle slug, a convective downwards flow of particles in the gas slug, together with particle dispersion of particle exchange between the particle and gas slug. The dispersion coefficients calculated with the model as a function of the superficial gas velocity and of the bed diameter are well in agreement with the equation derived by Thiel and Potter.

- 3.3 Schouten, J.C., Masson, H.A. and Van den Bleek, C.M., "The Motion of Particles in a Slugging Gas Fluidized Bed", submitted for publication in Powder Technology, 1987.

An experimental study is presented with the objective to investigate with a dynamic radioactive tracer technique the movement of sorbent particles in a one- and two-component 10 cm ID fluid bed. Information is obtained on the presence probability of the tracer particle as a function of the bed height, the frequency of passage of the tracer at a given level, the probability for a direction change, the magnitude of the up- and downward velocities of the tracer as a function of the bed height and on the random diffusion- (or dispersion-) like character of the particles trajectories. This information is applied to obtain a qualitative description of the mechanism of particle motion in these systems. Furthermore, a general model for the motion of particles in slugging fluidized beds is formulated based on this mechanistic description.

- 3.4 Valkenburg, P.J.M., Schouten, J.C. and Van den Bleek, C.M., "The Non-Steady State Segregation of Particles in Gas Fluidized Beds", Proc. 5th Eng. Found. Conf. on Fluidization, Elsinore, Denmark, May 18-23, 1986; in: Fluidization, (Eds. K. Østergaard and A. Sørensen), Engineering Foundation, New York, 193-200, 1986.

In the last paper of this series a modeling approach is given on the non-steady state segregation of particles. It is shown that a pulse-like input of slightly denser tracer particles results in a significant maximum in the particle distribution curve. This maximum can be described with a non-steady state model equation which is based on the segregation model as introduced in paper 3.1.

### 1.3 Overview of the thesis

A selection of four papers has been included in the present thesis (see section 1.2: papers 2.5, 2.7, 3.1 and 3.3); this selection consists predominantly of papers which have not been published so far and which provide a comprehensive and characteristic overview of the authors work on the modeling of sulfur retention during FBC and the motion of particles in gas fluidized beds.

The selected four papers are presented in two chapters. In chapter 2 predominantly the modeling of sulfur retention during the fluidized bed combustion of coal will be considered. In chapter 3 the results obtained on different aspects concerning the motion and hydrodynamics of particles in gas fluidized beds will be discussed. The main subjects considered are slugging, segregation and mixing.

Each respective chapter begins with an introduction in which a short overview is given of the subject and the papers which are presented in that specific chapter.

Furthermore, in the last section of each chapter some comments on all the papers (including those not printed in this thesis) are added, in order to increase their coherence or to supply some extra information so as to enlarge the general understanding. Sometimes a formula or expression in a comment may be a little difficult to understand without having read the original paper; however, the comments have been written in such a way that the general 'message' which it contains can easily be understood.

The notation applied in the respective papers and comments is explained in one overall notation list which is given at the end of the thesis. This is also the case with the references mentioned in the papers and comments which are gathered in one overall list.

Finally, it should be noticed that the present text of the papers, as they are inserted in the respective chapters in this thesis, might differ sometimes a little from the text of the original papers which have been submitted for publication. Principally, this has been done in order to increase the mutual style and form; consequently, no fundamental alterations have been included.

## 2.1 Introduction

This chapter gives an impression of the theoretical work which has been carried out by the author on the derivation of a mathematical model for the description of sulfur retention during the fluidized bed combustion of coal. No experimental results will be presented or discussed other than those available in the literature: these experimental data are predominantly applied to validate the proposed retention model.

In the first paper (chapter 2.2) a simple mathematical sulfur retention (SURE) model is described which can be used for the prediction and optimization of the retention of sulfur during FBC. Starting from an evaluation of retention models in literature this model is based on a simple approach to the sulfation kinetics: the sorbent sulfation rate is first order in the gaseous sulfur concentration, and first order in the reactive sorbent surface. The model provides a simple analytical expression for the molar (Ca/S) ratio in the reactor feed as a function of **a**, the required level of sulfur retention in the bed, **b**, the maximum CaO utilization of the sorbent, and **c**, a dimensionless model parameter: the retention parameter. Furthermore relations are derived for the gaseous sulfur reactor outlet concentration (sulfur breakthrough) as a function of the dimensionless breakthrough time in the case of unsteady state combustor operation due to a batch addition of sorbent or a sulfur step input on a bed containing a fixed amount of sorbent. The CaO conversion and the sulfur outlet concentration are compared with literature data from which the sulfation kinetic reaction rate parameter is calculated.

In the second paper (chapter 2.3) the influence of oxygen-stoichiometry on the desulfurization efficiency is discussed. The effect of a decreasing sulfur removal at low oxygen concentrations (at low in-bed air ratios) is explained by the formation of SO<sub>2</sub> as a gaseous intermediate reactant in the sulfation reaction. The steady state SURE model is extended and now provides an analytical equation for the (Ca/S) ratio which is also a function of the coal properties and of the in-bed stoichiometric air ratio. A good qualitative agreement with literature data is reported. Furthermore the importance of the sorbent residence time with respect to model validation is discussed.



2.2 PREDICTION and OPTIMIZATION of SULFUR RETENTION  
in the FLUIDIZED BED COMBUSTION of COAL:  
the D.U.T. SURE model

submitted for publication in Chem. Eng. Sci., 1987

SUMMARY	12
1. INTRODUCTION	12
1.1 Sulfur release and capture during FBC	12
1.2 Sulfur retention modeling	14
2. THE SURE MODEL	19
2.1 Sulfation kinetic term	19
2.2 Choice of fluid dynamical reactor model	19
2.3 Summary of SURE model assumptions	20
2.3.1 One-phase model	20
2.3.2 Two-phase model	21
2.3.3 Both models	21
3. SULFUR BREAKTHROUGH AT UNSTEADY STATE OPERATION	22
3.1 One-phase model	22
3.2 Two-phase model	24
4. (Ca/S) RATIO AT UNSTEADY STATE OPERATION	25
4.1 One-phase model	25
4.2 Two-phase model	27
5. COMPARISON OF MODEL CALCULATIONS WITH EXPERIMENTAL DATA	28
5.1 Sulfation kinetic term	28
5.2 Sulfur breakthrough at unsteady state operation	32
5.2.1 CaO conversion	32
5.2.2 Sulfur outlet concentration	33
5.3 Sulfur retention at steady state operation	34
6. MODEL PARAMETER SENSITIVITY ANALYSIS	39
6.1 Calculation of model parameters	39
6.2 Comparison of one- and two-phase model	39
6.2.1 Sulfur breakthrough at unsteady state operation	39
6.2.2 (Ca/S) ratio at steady state operation	40
6.3 Level of sulfur retention	44
6.3.1 Influence of maximum sorbent conversion	44
6.3.2 Influence of retention parameter	45
6.4 Influence of reactor circumstances and sorbent properties on sulfur retention	46
6.4.1 Sorbent residence time	47
6.4.2 Sorbent particle size	48
6.4.3 Superficial gas velocity	49

7. OPTIMIZATION OF THE (Ca/S) RATIO	50
7.1 Retention index RI	50
7.2 Choice of parameter change cpc	52
8. CONCLUSIONS	54
APPENDIX 1: THE MODEL PARAMETERS	55
1. Maximum gas exchange ratio $P_0$	55
2. Two-phase gas flow parameter $m$	58
3. Retention parameter $M$	59
4. Maximum conversion $\alpha$	60
5. Magnitude of model $\alpha^{\max}$ parameters	60
APPENDIX 2: MODEL LIMITATION DUE TO OXYGEN CONSUMPTION	61

# PREDICTION and OPTIMIZATION of SULFUR RETENTION

in the FLUIDIZED BED COMBUSTION of COAL:

the D.U.T. SURE model

J.C. Schouten and C.M. van den Bleek

## SUMMARY

In this paper the D.U.T. SU(lfur)RE(tention) model is described which is a simple mathematical model that can be used for the prediction and optimization of the retention of sulfur during the fluidized bed combustion of coal. Starting from an evaluation of retention models given in literature the SURE model is based on a simple approach to the sulfation kinetics: the sorbent sulfation rate is a. first order in the gaseous sulfur component concentration, and b. first order in the reactive sorbent surface. The fluid dynamical part of the SURE model is based on the two-phase theory of fluidization with plug flow of gas in the bubble phase and an ideally mixed dense phase. Also the case of a high gas exchange between both phases is considered resulting in a one-phase ideally stirred tank model. In the case of steady state combustor operation the one-phase SURE model provides a simple analytical expression for the molar (Ca/S) ratio in the reactor feed as a function of a. the required level of sulfur retention in the bed, b. the maximum CaO utilization of the sorbent, and c. a dimensionless model parameter: the retention parameter. The one-phase SURE model is compared with sulfation experiments derived from the literature in order to check its general validity. A parameter sensitivity analysis is given from which the relative importance of the respective (dimensionless) model parameters is deduced. Finally, the retention index is introduced which is a parameter that is very useful for the judgement of the sulfur retention performance of the combustor. It can be used to optimize both the fluid bed operating conditions and the sorbent properties in order to obtain the minimum possible (Ca/S) ratio at a specific required level of sulfur retention.

## 1. INTRODUCTION

### 1.1 Sulfur release and capture during FBC

Fluidized beds are used for many different chemical engineering applications. One of these is the production of energy from coal, although this technique is still under development and many problems concerning the fundamentals of fluidization, combustion, gas transfer, heat exchange etc. have to be solved yet (LaNauze, 1985).

One of the advantages of the fluidized bed coal combustion technique is the possibility of the in-situ removal of the sulfur released from the coal by the addition of a natural sorbent material (limestone or dolomite) or a synthetic sorbent. Much research has been carried out in this field, experimentally as well as theoretically: a comprehensive literature review on sulfur release and capture in the fluidized bed combustion of coal is provided by Schouten et al. (1986).

They concluded that in general 25% to 60% of the sulfur in coal is released with the volatiles; the absolute percentage increases with increasing temperature and is probably not dependent on total volatile yield. In general more than 90% of the sulfur in volatiles is present as H<sub>2</sub>S. The major portion of the volatile sulfur is released near the coal feed point, while the remaining sulfur is released during subsequent char combustion in the bed.

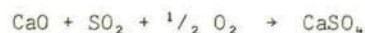
It is clear that under oxidizing circumstances in the bed the sulfur is predominantly released in the form of sulfur dioxide which originates from the combustion of the organic and pyritic sulfur (FeS<sub>2</sub>) in the coal. In general it can be assumed that the rate of release of sulfur from coal, at high combustion rates as practised in fluid bed combustion, is linearly dependent on the rate of coal combustion (Schouten et al., 1986; Schouten et al., 1987c). A reaction scheme for the release of sulfur from pyrite in coal is given by Schouten et al. (1987c).

In a reducing atmosphere it is possible that also hydrogen sulfide and COS are emitted, where H<sub>2</sub>S for example originates from the reaction of hydrogen with the pyrite in coal:



The formation of these reduced sulfur species is of importance in the multi-stage sub-stoichiometric fluid bed coal firing which may be necessary in order to reduce the NO<sub>x</sub>-emission significantly (as for example in the limestone injection multistage burner LIMB of the U.S. Environmental Protection Agency; Borgwardt et al., 1984).

In general lime offers the possibility of the capture of sulfur in the case of SO<sub>2</sub> as well as of the reduced sulfur species H<sub>2</sub>S and COS (Simons and Rawlins, 1980; Borgwardt et al., 1984) according to the following reactions:



It is important to notice that in the case of hydrogen sulfide capture the calcium utilization can reach 100% when initial particle porosities are greater than 42% (Simons and Garman, 1986), while the maximum conversion in the once-through use of lime-sorbent in the case of SO<sub>2</sub> capture is generally smaller than 45% due to the difference in the molar volumes of the respective reaction products, which influences the occurrence of pore plugging. Further Simons and Rawlins (1980) concluded that any procedure

which utilizes limestone removal of  $\text{SO}_2$  is potentially capable of removing  $\text{H}_2\text{S}$  at approximately the same rate.

So lime-based sorbents can be used in oxidizing as well as reducing atmospheres. However, the capture of  $\text{H}_2\text{S}$  and  $\text{COS}$  instead of  $\text{SO}_2$  may have important implications for the research on the regenerative removal of sulfur by natural and synthetic sorbent materials as presently carried out in The Netherlands at the Delft University of Technology and Twente University (Kamphuis et al., 1987).

So it is concluded that the type of sulfation process greatly influences the optimum use of the sorbent material. However, also other phenomena and parameters are of great importance for the prediction and optimization of sulfur retention in fluid bed coal combustion. Here we can think of for example reactor operating conditions like the  $(\text{Ca}/\text{S})$  ratio or the superficial gas velocity, but also sorbent properties as pore volume and particle size (Schouten et al., 1986). In this paper it is tried to establish which parameters and phenomena are important and in what way they can eventually be influenced to obtain an optimum high level of sulfur retention in a fluid bed combustor.

## 1.2 Sulfur retention modeling

One useful way to determine the most important parameters that influence the sulfation performance of a fluid bed coal combustor is to obtain a mathematical reactor model which describes the main chemical and physical phenomena. A detailed analysis of model calculation results, together with a model parameter sensitivity analysis, will in many cases give useful insight in the sulfation process.

At least 40 overall fluidized bed coal combustion system models have been published in literature. The majority of these models has been reviewed by Olofsson (1980), Park et al. (1980), LaNauze and Jung (1982) and LaNauze (1985). These reviews are based on a summary of the basic model assumptions. However, these summaries are essentially point by point comparisons of the various models, rather than critical assessments of the models's predictive capabilities or accessibility (Preto, 1985).

LaNauze (1985) concludes that in general the models meet only with limited success in their ability to predict combustion performance, carbon loading or gas concentration and temperature profiles. The accuracy with which some critical parameters are known or can be estimated is not great, which allows reasonable variation in predictions by adjusting parameters such as the cross-flow factor, bubble size or chemical rate. Preto (1985) adds to this that the available models are in some cases overcomplicated,

with the inclusion of irrelevant minutiae, and in other cases too rudimentary, with the exclusion of important factors.

In most cases the validity of these overall system models can be questioned as for example is demonstrated for the sulfur retention prediction of the MIT system model (Molayem et al., 1982). However, also comprehensive models have been developed (e.g. Wells et al., 1982), which are reasonably accurate, but these are also quite complicated and require significant computing facilities.

It is remarkable that only a few models as reviewed by LaNauze (1985) incorporate sulfur release as well as sulfur capture. Therefore eight typical fluid bed retention models have been listed in Table 1 which showed a reasonable to very good agreement between the calculated prediction of the sulfur capture efficiency and experimental combustor data (Ho et al. (1986) presented only model calculations based on experimental data). It is remarkable that the modeling of the sulfation process in only two of the models summarized in Table 1 is based on a fundamental structural gas-solid reaction model (see Ramachandran and Doraiswamy (1982) for a comprehensive review of these models). Many workers have used these type of models for the modeling of the sulfur retention reaction of calcium oxide and sulfur dioxide in other types of reactors (as differential reactors or thermobalances).

The common gas-solid reaction models which have been in use so far are the kinetic model (for example Borgwardt (1970) and Borgwardt and Harvey (1972)), the grain model (Ishida and Wen, 1971; Wen and Ishida, 1973; Ranade and Harrison, 1979), the pore model (Ramachandran and Smith, 1977; Georgakis et al., 1977; Chrostowski and Georgakis, 1978; Georgakis et al., 1979; Dogu, 1981; Bhatia and Perlmutter, 1981; Christman and Edgar, 1983; Bhatia, 1985; Simons and Garman, 1986) and the volume reaction model (Fan et al., 1977; 1978; 1984).

One major disadvantage of the application of structural gas solid reaction models to overall fluid bed combustion system models is mentioned by Fieldes (1979), Lee and Georgakis (1981), Fee et al. (1983) and Dennis and Fieldes (1986). They argued that detailed reaction models that take into account changes of structural solid properties are highly non-linear. Therefore it is very difficult to incorporate them easily into fluid dynamical models of a fluidized bed combustor without resort to excessively long computer calculations for each size of stone in the feed. This will especially hold for the mathematical modeling of the unsteady state sulfur release and absorption of sulfur from a batch addition of coal and/or sorbent material. Such a rigorous analysis of the  $SO_2$  or  $H_2S/COS$  sulfation

Table 1: Overview of typical fluid bed sulfur retention models, which show good agreement with experimental combustor data; (see for description Table 2).

<u>Author(s)</u>	<u>A</u>	<u>B</u>	<u>C</u>	<u>D</u>	<u>E</u>	<u>F</u>	<u>G</u>	<u>H</u>
Bethell et al. (1973)	1	1	1/yes	1+2	3a	yes/2	no	2
Chen and Saxena (1977)	3	1	1/yes	1+2	3b	yes/2	no	2
Rajan et al. (1978)	2a	2	2/yes	1	1a	yes	no	2
Rajan and Wen (1980)	2a	2	2/yes	1+3	1a	yes	yes	2
Lee et al. (1980) Lee and Georgakis (1981)	2b	3	1/no	1	2+3b	no	no	1
Zheng et al. (1982)	2b	3	1/no	1	2+3c	no	no	1
Fee et al. (1983)	2c	3	1/no	1	2+3b	no	no	1
Fee et al. (1984)	2c	3	1/no	1	2+3b	no	yes	1
Ho et al. (1986)	2c	1	1/no	1	1b	no	no	2
-----								
Schouten and Van den Bleek (this work)	2c	3	1/no	1	3c+4	no	no	1

Table 2: Description of typical fluid bed sulfur retention models as summarized in Table 1.

A. Fluid bed model.

- 1) One phase model.
- 2a) Two phase bubbling bed model, clouded bubbles; bubble phase and emulsion phase; bubble size dependent on bed height; minimum fluidization conditions in the emulsion phase; gas exchange between bubble and emulsion phase is axially distributed (compartments in series model).
- 2b) Two phase bubbling bed model; bubble phase and emulsion phase; average bubble size; minimum fluidization conditions in the emulsion phase; average gas exchange coefficient.

Table 2 continued ...

- 2c) Two phase bubbling bed model; bubble phase and emulsion phase; average bubble size; minimum fluidization conditions in the emulsion phase; gas exchange between phases is uniform or non-uniform according to fast and slow bubble regimes.
- 3) Three phase bubbling bed model: bubble, cloud-wake and emulsion phase; bubble size is dependent on bed height; minimum fluidization conditions in the emulsion phase; gas exchange between phases is based on average bubble volume.

B. Gas flow pattern.

- 1) Plug flow of gas in all phases.
- 2) Mixed flow in all phases.
- 3) Plug flow in bubble phase; emulsion phase well mixed.

C. Solids flow.

- 1) Solids ideally mixed (in emulsion phase).
- 2) Solids well mixed in a number of compartments.
- 3) Solids diameter distribution is considered: yes / no.

D. Sulfur release.

- 1) Sulfur release rate is proportional to coal (char) combustion rate (or coal feed rate).
- 2) Sulfur release is not uniform over the bed height.
- 3) Sulfur release during devolatilization is considered and is taken temperature dependent.

E. Sulfur capture.

- 1a) Grain model of Wen and Ishida (1973) is used to calculate limestone reactivity.
- 1b) Grain model of Hartman and Coughlin (1976) is used.
- 2) Semi-empirical sulfur capture kinetic equation is used.
- 3) Kinetic rate data obtained from:
  - a) fixed bed laboratory experiments;
  - b) thermogravimetric analysis;
  - c) fluid bed batch experiments.
- 4) Sulfation rate is linear proportional to reactive sorbent surface.

F. Elutriation.

- 1) Elutriation is considered: yes / no.
- 2) Recirculation of elutriated particles.

G. Freeboard.

- 1) Freeboard sulfur retention is considered: yes / no.

H. Model complexity.

- 1) Simple analytical expressions are applied.
- 2) More complex (numerical) calculations are needed.



reaction results in mathematical expressions that are too complicated for practical engineering applications.

Further Fieldes (1979) concluded that using a computer to solve equations describing particle sulfation also divorces the user sometimes from physical reality, as he illustrated clearly with two mistakes in the application of solid reaction models in literature. In one case he showed that still reasonable fits of solid conversion against time were derived in the work of Hartman and Couglin (1976) with an incorrect value of the effective surface rate constant forcing the adjusted effective product diffusion coefficient to a rather low value (this was also noticed by Simons and Rawlins (1980) who suggested that the diffusion coefficient was a factor 20 to low).

Consequently, another important disadvantage of the structural gas-solid reaction models is that they require thorough knowledge of particle properties as pore size distribution and grain diameter that are strongly stone dependent, as well as physical constants as the solid diffusion coefficient which are extremely difficult to determine experimentally. So far the solid-state diffusion coefficient of  $\text{SO}_2$  through a nonporous layer of  $\text{CaSO}_4$  was obtained by adjusting it in a pore or grain model. A comprehensive summary of the diffusivity estimates as obtained by different authors is given by Marsh and Ulrichson (1985).

However, it must be noticed that the disadvantages as mentioned above of course do not detract from the conceptual contribution of the fundamental gas-solid reaction models to the basic understanding of the influence of the solids structure (grains and pores) on the overall reaction rate.

To avoid the possible extensive computation as well as the problem of experimental determination of physical constants or solid properties, a more recent trend in the fluid bed modeling of sulfur retention is based on the experimental observation that the decay in the overall solids conversion can easily be fitted by an exponential, reciprocal or other type of empirical relation (see Table 1). These models provide simple analytical expressions for the sulfur retention as a function of the molar (Ca/S) ratio that can easily be applied to real combustors (for example Lee et al., 1980; Lee and Georgakis, 1981; Zheng et al., 1982; Fee et al., 1983; Fee et al., 1984; Noordergraaf et al., 1985; Dennis and Fieldes, 1986). The sorbent parameters in these models, which describe the sulfation kinetics, are obtained either from thermogravimetric analysis data (e.g. Fee et al., 1983; 1984) or from batchwise sulfation experiments in fluid beds (Zheng et al., 1982; Noordergraaf et al., 1985; Dennis and Fieldes, 1986). However, some critical

remarks can be made to the experimental approaches and fundamental correctness of some of these models (Schouten and Van den Bleek, 1986).

In general it can be concluded that the use of a simple (semi-empirical) description of the complicated sulfation reaction is very promising, especially in the modeling of sulfur retention in fluid bed combustors, where certainly the urgent need for practical engineering models is present.

## 2. THE SURE MODEL

### 2.1 Sulfation kinetic term

Therefore in this paper a fluid bed Sulfur RETention (SURE) model is presented in which the sulfation kinetic term is based on two simple assumptions: the sorbent sulfation rate (i.e. the rate of decrease of reactive sorbent surface) is first order in the gaseous sulfur ( $\text{SO}_2$  or  $\text{H}_2\text{S}/\text{COS}$ ) concentration and first order in the reactive sorbent surface.

After the work of Borgwardt (1970) the first assumption has been generally applied in several sulfation studies on the capture of  $\text{SO}_2$  with lime. Recently also Marsh and Ulrichson (1985) showed in a detailed sulfation study that between 740 and 930 °C the reaction is clearly first order in  $\text{SO}_2$ ; further they reported, just as Borgwardt (1970) and other workers, that above 740 °C the  $\text{SO}_2$  capture is zero order in oxygen. Simons and Rawlins (1980) and Simons and Garman (1986) showed that the same assumptions hold also for the capture of  $\text{H}_2\text{S}$ ; further they determined the intrinsic  $\text{H}_2\text{S}$  reaction rate at one-half of the  $\text{SO}_2$  rate.

The second kinetic model assumption is based on the fact that the sulfation rate ceases due to the decrease of the reactive surface area and eventually due to an alternative deactivation mechanism like the plugging of pores and the associated loss in internal surface area (see e.g. Simons and Garman, 1986).

### 2.2 Choice of fluid dynamical reactor model

The kinetic term has to be fit into a fluid dynamical reactor model. The choice of the type of fluid dynamical reactor model is strongly dependent on *the mode of fluidization and gas transport that is present in fluid bed coal combustors*. A correct model choice can only be made when model discrimination can be carried out based on combustor data on the axial concentration profiles in the bubble phase as well as in the emulsion phase. *Experimental data on this matter are very limited which makes it rather difficult to choose the correct fluid dynamical model for the gas transport in coal combustors*. Therefore model discrimination can in most cases only be

performed based on the reactor outlet concentration. Especially in the case of sulfur retention this is difficult, because generally combustor data demonstrate a significant scatter which is sometimes in the order of the difference between calculated outcomes of different models.

In general one has to decide between plug flow of gas in the reactor or ideally mixed flow; secondly, one can eventually distinguish two gas phases (bubble phase and emulsion phase) with either uniform mass transfer between these phases (corresponding to a slow bubble regime) or non-uniform mass transfer (corresponding to a fast bubble regime). Further, in the situation of the two-phase model one has to decide between plug flow or ideally mixed flow in the separate phases; actually there is a range of choices between the two extremes. One can superimpose axial diffusion and mixing on the plug flow model, however the additional complexity is of questionable value in absence of discriminating information.

The linear gas velocity in the emulsion phase in fluid bed combustors is generally higher than the bubble (or slug) rise velocity, due to the relatively large particles present (500  $\mu\text{m}$  to sometimes more than 10 mm). This means that the bubbles are 'swept' through with gas, resulting in the same concentration in both phases. This would imply the choice of a one-phase reactor model.

However, it has to be noticed that in the case of fluid bed coal combustion also the reactive solids concentration (i.e. the interfacial area of coal and/or sorbent material) plays an important role in the final reactor model choice. Noordergraaf et al. (1986) and De Kok et al. (1986) have shown that at low values of the solids concentration (i.e. a  $< 2 \text{ m}^2/\text{m}^3$ ) the bubble to emulsion phase mass transfer resistance is negligible, while at higher values of the interfacial area the gas to solids mass transfer in the emulsion phase can be neglected. This implies that at low values of the reactive solids concentration the gas transport can be described with a one-phase model, while at higher values a two-phase model should be used.

Proceeding with these considerations it is understandable that in the present paper both type of models will be compared.

### 2.3 Summary of SURE model assumptions

First, the respective model assumptions as discussed in sections 2.1 and 2.2 will be summarized:

#### 2.3.1 One-phase model

The fluid bed is considered as an ideally stirred tank reactor:

\* ideally mixed gas flow;

\* solids ideally mixed.

### 2.3.2 Two-phase model

The fluid bed is considered to consist of two phases:

- \* the bubble phase is in plug flow;
- \* the emulsion phase is ideally mixed;
- \* the solids are present in the emulsion phase and are ideally mixed:  
all sulfur is released in the emulsion phase (as  $\text{SO}_2$ );
- \* non-uniform mass transfer between both phases.

### 2.3.3 Both models

For both models the following assumptions apply:

- \* the sulfur release rate is linear dependent on the feed rate and sulfur content of the coal;
- \* the sulfur capture rate is linear dependent on the reactive sorbent surface area and first order in the gaseous sulfur concentration;
- \* the sorbent particles are of uniform size;
- \* elutriation and freeboard phenomena are not taken into account.

The one- and two-phase SURE models are compared in the case of unsteady and steady state fluid bed combustor operation. Hereto relations are derived in respectively sections 3 and 4 for:

- a. the gaseous sulfur outlet concentration as a function of time (sulfur breakthrough) in the case of unsteady state operation due to a batch addition of sorbent or a sulfur step input on a bed containing a fixed amount of sorbent;
- b. the (Ca/S) ratio needed to obtain a specific level of sulfur retention under steady state operating conditions.

In section 5 the SURE models are compared with experimental kinetic and combustor data in order to check the general validity. Further, in section 6 a model parameter sensitivity analysis is given from which the relative importance of the respective dimensionless model parameters will be deduced. Hereafter the influence of the main fluid bed reactor conditions (as gas velocity and solids residence time) and sorbent properties (as particle diameter) on the level of sulfur retention will be determined. The model parameters are calculated with correlations and relations obtained from literature (Appendix 1).

Finally, the retention index is introduced in section 7 which is shown to be a useful tool in the analyzing of fluid bed reactor operating conditions and different sorbent properties to enable a proper choice of the

combustor operating circumstances and the type of sorbent required for an optimum (Ca/S) ratio at a specific required level of sulfur retention.

### 3. SULFUR BREAKTHROUGH AT UNSTEADY STATE OPERATION

In this section relations for the sulfur breakthrough time according to the respective SURE models will be derived proceeding with the model assumptions given in section 2.3.

#### 3.1 One-phase model

In the case of unsteady state combustor operation the sulfur mass balance is given as (out = in - conversion - accumulation):

$$U_0 F c(t) = \phi_S - k S(t) c(t) - \epsilon H F \left( \frac{dc(t)}{dt} \right) \quad [1]$$

$k$  is the overall sulfation rate constant, which is a combination of external mass transfer limitations and sulfation kinetics (intrinsic kinetics+intra-particle mass transfer phenomena). This differential equation is written in dimensionless form as:

$$\left[ \tau_g / \tau_{br} \right] \left( \frac{dX(\theta)}{d\theta} \right) = 1 - X(\theta) [P_0 \sigma(\theta) + 1] \quad [2]$$

$$\tau_g \text{ is the gas residence time, which is defined as: } \tau_g = \epsilon H / U_0 \quad [3]$$

where  $\epsilon$  is the average bed porosity,  $H$  is the average expanded bed height and  $U_0$  is the superficial gas velocity.

$\tau_{br}$  is the sulfur breakthrough time which equals:

$$\tau_{br} = q S_0 / \phi_S = \alpha_{max} N_{CaO,0} / \phi_S \quad [4]$$

where  $q$  is the CaO surface concentration (mol/m<sup>2</sup>),  $\alpha_{max}$  is the maximum CaO conversion (which can be smaller than unity due to pore plugging) and  $N_{CaO,0}$  is the initial amount of CaO in the bed. Further  $\theta$  is the dimensionless time, which is defined as  $t/\tau_{br}$ .

$\sigma(\theta)$  is the dimensionless reactive sorbent surface  $S/S_0$  at time  $\theta$ ; and  $c_0$  is defined as the initial gaseous sulfur concentration:

$$c_0 = \phi_S / (U_0 F) \quad [5]$$

$P_o$  is the maximum gas exchange ratio related to the finally reacted sorbent surface  $S_o$  in the bed as defined by Schouten and Van den Bleek (1986):

$$P_o = k S_o / (U_o F) \quad \text{or} \quad P_o = k \alpha_{\max} S_A / (U_o F) \quad (P_o > 0) \quad [6]$$

where  $S_A$  is the initial total available reactive sorbent surface.

In general the sulfur breakthrough time is much larger than the gas residence time. When realistic average data are taken for the respective parameters (e.g.  $\epsilon = 0.7$  [-];  $H = 1$  m;  $U_o = 1-2$  m/s and  $\alpha_{\max} = 0.4$  [-];  $\phi_S = 0.01-0.1$  mol/s;  $N_{CaO,o} = 100-1000$  mol), then it is easy to calculate that  $\tau_g < 1$  sec and  $\tau_{br} \gg 400$  sec. This means that in general  $\tau_g / \tau_{br} \ll 0.0025$ , which implies that the sulfur capture reaction is a rather slow reaction compared to the residence time of the gaseous sulfur in the bed. So the accumulation term in the mass balance, Eq.[1], is very small and can be neglected (or in Eq.[2]:  $(\tau_g / \tau_{br}) (dX(\theta)/d\theta) = 0$ ). Consequently the pseudo-steady state approximation can be applied in this reaction system.

So from Eq.[2] the dimensionless sulfur concentration  $X(\theta)$  in the outlet of the reactor as a function of time is then obtained as:

$$X(\theta) = c(\theta)/c_o = 1 / [1 + P_o \sigma(\theta)] \quad \text{where} \quad X(\theta=0) = 1 / [1 + P_o] \quad [7]$$

Further the conversion of the sorbent in the reactor as a function of time is obtained from the following sorbent mass balance (CaO accumulation =  $SO_2$  or  $H_2S/COS$  conversion):

$$\zeta q \left( \frac{dS(t)}{dt} \right) = -k S(t) c(t) \quad \text{or} \quad \left( \frac{d\sigma(t)}{dt} \right) = -k / (\zeta q) \sigma(t) c(t) \quad [8]$$

In dimensionless form:  $\left( \frac{d\sigma(\theta)}{d\theta} \right) = -P_o \sigma(\theta) X(\theta)$  with b.c.:  $\sigma(\theta=0) = 1$ .

The stoichiometric coefficient  $\zeta$  (mol  $SO_2$  or  $H_2S$  or  $COS$  / mol CaO) equals 1. Substitution of Eq.[7] in Eq.[8] and solution of the differential equation leads to:

$$\theta = 1 + [1/P_o] \left[ \ln P_o - \left\{ \frac{1-X}{X} \right\} - \ln \left\{ \frac{1-X}{X} \right\} \right] \quad [9]$$

In principle this equation describes implicitly the breakthrough of sulfur in a fluid bed reactor as a function of two dimensionless model parameters: the maximum gas exchange ratio ( $P_o$ ) and the maximum conversion of CaO ( $\alpha_{\max}$ ).

### 3.2 Two-phase model

In the same way the breakthrough equation in case of the two-phase model is derived as:

$$\Theta = [1/m] \left[ 1 - \frac{m \cdot (1-X)}{P_0 \cdot (X+m-1)} \right] - [1/P_0] \ln \left[ \frac{m \cdot (1-X)}{P_0 \cdot (X+m-1)} \right] \quad [10]$$

Here the dimensionless sulfur breakthrough concentration at  $\Theta=0$  equals:

$$X(\Theta=0) = \frac{m + P_0 - (1-m)}{m + P_0} \quad [11]$$

$$\text{with: } m = 1 - u \exp[-N_0/u] \quad (0 < m \leq 1) \quad [12]$$

$$\text{where: } u = 1 - [U_e/U_0] \quad (0 \leq u \leq 1) \quad [13]$$

$$\text{and: } N_0 = HK/U_0 \quad (N_0 > 0) \quad [13a]$$

So the two-phase model equation contains next to the maximum gas exchange ratio  $P_0$  and the maximum CaO conversion  $\alpha_{\max}$  one extra dimensionless parameter,  $m$ , which will be defined as the two-phase gas flow parameter. This parameter expresses the influence of mass transfer between the bubble and emulsion phase ( $N_0$ ) together with the distribution of the convective gas flow over both phases ( $u$ ):  $N_0$  is the number of mass transfer units and  $u$  is the dimensionless excess gas velocity in the bubble phase.  $K$  is the mass transfer coefficient based on the total reactor volume;  $U_e$  is the superficial gas velocity in the emulsion phase.

When  $N_0 \rightarrow \infty$  or when  $u = 0$  then  $m = 1$ , in which case Eq.[9] equals Eq.[10] and the one-phase model and two-phase model become theoretically the same. Of course this is clear for the situation where no bubble phase is present ( $U_0 = U_e$  and consequently  $u = 0$ ). However, it means also that the gas flow in the bed can be considered as ideally mixed in the case that the gas transfer between both phases is very high ( $N_0 \rightarrow \infty$ ), while the bubble phase is still in plug flow. So this result confirms the general applied assumption that the gas flow in slow bubble beds, with a high throughflow of gas in the bubble phase as well as in the emulsion phase, can theoretically be considered as ideally mixed.

#### 4. (Ca/S) RATIO AT STEADY STATE OPERATION

Proceeding with the model assumptions as summarized in section 2.3 now a derivation will be given of expressions for the (Ca/S) ratio at a specific level of retention in case of the one- and two-phase SURE models.

##### 4.1 One-phase model

The sulfur retention is defined as  $R = 1 - (c/c_0)$ , so proceeding with the mass balance given in Eq.[1], without the accumulation term in steady state situation, it is derived that:

$$R = 1 - 1 / [1 + P_0 \sigma_{avg} / \alpha_{max}] \quad [14]$$

Here in the case of steady state operation  $\sigma_{avg}$  ( $= S/S_A$ ) is the average fractional reactive sorbent surface in the bed and is based on the initial total available surface  $S_A$ . It is calculated from the solids residence time distribution function  $E(t)$  and the fractional reactive surface  $\sigma(t)$  as a function of time according to:

$$\sigma_{avg} = \int_0^{\tau} E(t) \sigma(t) dt \quad [15]$$

$\tau$  is the maximum possible reaction time, for example the pore plugging time when the reaction product blocks the pores before total conversion of the sorbent has been reached. It should be noticed that no reactive surface area is present at  $t > \tau$  and therefore  $\sigma(t > \tau) = 0$ .

The solids residence time function of solids in a fluid bed has been determined by Yagi and Kunii (1961) to be equal to that of an ideally stirred tank:

$$E(t) = [1/\tau_s] \exp[-t/\tau_s] \quad [16]$$

The conversion of freshly added sorbent in the reactor as a function of time is obtained from the sorbent mass balance as given in Eq.[8]. At steady state operation the sulfur dioxide (or hydrogen sulfide, COS concentration) in the reactor may be assumed to be constant, consequently the fractional reactive surface in the reactor as a function of time is given as:

$$\sigma(t) = \exp[-\frac{k}{q} c t] \quad [17]$$

The minimum fractional sorbent reactive surface is derived with Eq.[17] as:



$$\sigma_{\min} = \exp\left[-\frac{k}{q} c \tau\right] = 1 - \alpha_{\max} \quad [18]$$

The average fractional reactive surface  $\sigma_{\text{avg}}$  is subsequently obtained from Eqs.[15]...[17] as:

$$\sigma_{\text{avg}} = \left[ \frac{1}{1 + \frac{kc\tau_s}{q}} \right] \left[ 1 - \exp\left(-\left\{\frac{1}{\tau_s} + \frac{kc}{q}\right\} \tau\right) \right] \quad [19]$$

In the same way the average sorbent conversion in the bed is derived from:

$$\alpha_{\text{avg}} = \int_0^{\tau} E(t) (1-\sigma(t)) dt + \int_{\tau}^{\infty} E(t) (1-\sigma(\tau)) dt \quad [20]$$

$$\text{This leads to: } \alpha_{\text{avg}} = (1-\sigma_{\text{avg}}) - (1-\alpha_{\max}) \exp[-\tau/\tau_s] \quad [21]$$

The solids residence time  $\tau_s$  is calculated from the maximum total amount of Ca in the bed ( $qS_A$ ) and the molar calcium feed rate ( $\phi_{Ca}$ ) as:

$$\tau_s = \frac{N_{CaO} \Delta}{\phi_{Ca}} = \frac{q S_A}{\phi_{Ca}} = [q S_0] / [\alpha_{\max} \phi_{Ca}] \quad [22]$$

Next to Eq.[14] the retention R is also defined by Eq.[23] from which the gaseous sulfur reactor outlet concentration c can be calculated:

$$R = 1 - [U_0 F c] / \phi_S \quad [23]$$

The calcium to sulfur ratio (Ca/S) in the reactor feed is derived from:

$$(Ca/S) = \phi_{Ca} / \phi_S \quad [\text{mol Ca/mol S}] \quad [24]$$

Combination of the Eqs.[14], [18] and [21]...[24] results in the following expressions for the average fractional reactive surface  $\sigma_{\text{avg}}$ , the average sorbent conversion  $\alpha_{\text{avg}}$  and the molar calcium to sulfur ratio (Ca/S) as a function of the level of retention R in the reactor:

$$\sigma_{\text{avg}} = \frac{1 - (1-\alpha_{\max}) \exp\left[-\frac{\ln(1-\alpha_{\max})}{M[1-R]}\right]}{1 + M[1-R]} \quad [25]$$

$$\alpha_{\text{avg}} = \sigma_{\text{avg}} M [1-R] \quad [26]$$

$$(Ca/S) = R / \alpha_{\text{avg}} \quad [27]$$

where the dimensionless parameter  $M$  is defined as the retention parameter which is given by:

$$M = \frac{k \tau_s \phi_s}{U_o F q} \quad [28]$$

When the maximum conversion of the sorbent is  $\alpha_{\max} = 1$  [-] then the retention  $R$  can be written explicitly as a function of the calcium to sulfur molar ratio  $(Ca/S)$  according to:

$$R = \frac{1}{2} \left[ \left( \frac{M+1}{M} + (Ca/S) \right) - \left\{ \left( \frac{M+1}{M} + (Ca/S) \right)^2 - 4(Ca/S) \right\}^{1/2} \right] \quad [29]$$

When the required sulfur reactor outlet concentration  $c$  is known the corresponding level of retention  $R$  can be calculated from Eq.[23]. With the correct values of the retention parameter  $M$  and the maximum conversion  $\alpha_{\max}$  the value of the calcium to sulfur ratio  $(Ca/S)$  is then obtained from the Eqs.[25]...[27].

#### 4.2 Two-phase model

In the same way as is demonstrated for the one-phase model the  $(Ca/S)$  ratio in case of the two-phase model is derived as:

$$\sigma_{\text{avg}} = \frac{1 - (1 - \alpha_{\max}) \exp\left[-\frac{\ln(1 - \alpha_{\max})}{(M/m) [1-R]}\right]}{1 + (M/m) [1-R]} \quad [30]$$

$$\alpha_{\text{avg}} = \sigma_{\text{avg}} (M/m) [1-R] \quad [31]$$

$$(Ca/S) = R / \alpha_{\text{avg}} \quad [32]$$

with  $m$  as given by Eq.[12]:  $m = 1 - u \exp[-N_o/u]$ .

When the maximum conversion of the sorbent is  $\alpha_{\max} = 1$  [-] then the retention  $R$  can be written in this case explicitly as a function of the calcium to sulfur molar ratio  $(Ca/S)$  as:

$$R = \frac{1}{2} \left[ \left( \frac{M+m}{M} + (Ca/S) \right) - \left\{ \left( \frac{M+m}{M} + (Ca/S) \right)^2 - 4(Ca/S) \right\}^{1/2} \right] \quad [33]$$

It is obvious that in the case of  $SO_2$  capture the SURE model does not take into account the effect that also oxygen is needed for this reaction. In fact it is implicitly assumed that the reaction is zero order in oxygen. However, oxygen is also used for the volatiles and char combustion, so at high oxygen consumption rates this theoretically may cause the situation

that the model still predicts a certain level of retention, while in practice no oxygen is available. Hereto in Appendix 2 a condition is derived which relates the level of retention to the coal feed rate and according to which the SURE model can be correctly applied in the case of SO<sub>2</sub> capture.

An advantage of the one- and two-phase SURE models as presented in sections 3 and 4 is that they provide simple analytical expressions for the calculation of the key variables (as the (Ca/S) ratio) as a function of dimensionless system parameters. This greatly enlarges the ease of application of the model, for example in overall fluid bed system models, while also direct insight can be obtained concerning the relevance of reactor and sorbent properties for the sulfur retention.

However, in general the usefulness of a mathematical model is only decided by its realistic outcomes and predictive capacity. Therefore in the next section 5 model calculations will be compared with experimental data obtained from the literature.

## 5. COMPARISON OF MODEL CALCULATIONS WITH EXPERIMENTAL DATA

### 5.1 Sulfation kinetic term

The retention model presented in this paper is fundamentally based on a rather simple approach to the sulfation kinetics. Therefore it is necessary to check the general validity of the kinetic model assumptions. This will be done in this section by fitting the model expressions to sulfation data derived from literature.

Many sulfation studies (e.g. Borgwardt, 1970; Borgwardt and Harvey, 1972; Hartman and Coughlin, 1976; Simons and Rawlins, 1980; Borgwardt et al., 1984) have been conducted in differential reactors to explore the reaction mechanism and the intrinsic sulfation reaction rate. In this case it can be written according to the simple assumptions on which the kinetic term in the present model is based that:

$$\alpha = \alpha_{\max} \left[ 1 - \exp\left[ -\frac{k_s c_o}{q} t \right] \right] \quad \text{or in dimensionless form:}$$

$$\Lambda = 1 - \exp[-\Pi] \quad \text{with } \Lambda = \alpha/\alpha_{\max} \quad \text{and } \Pi = t/t_o \quad [34]$$

where  $t_o = q/(k_s c_o)$ .

The molar surface CaO concentration  $q$  can be calculated from the respective equations as given in Appendix 1. The SO<sub>2</sub> concentration  $c_o$  equals 3000 ppm in case of Borgwardt's experiments.

In Figure 1 the dimensionless conversion  $\Lambda$  is plotted as a function of the dimensionless time  $\Pi$ . The shaded area covers 15 data-sets (with 131 points  $\Lambda$  vs  $\Pi$ ) obtained by fitting Eq.[34] to 15 experimental curves of Borgwardt (1970) and Borgwardt and Harvey (1972) in case of the  $\text{SO}_2$  sulfation with limestone or dolomite. Their data of the smaller particle sizes (96  $\mu\text{m}$  and 250  $\mu\text{m}$ ) have been taken to be more sure that the effect of mass transfer limitation is very limited.

The model fit is rather good, which indicates that the sulfation kinetic term used is suitable for the modeling of this type of gas-solid reaction. In Table 3 the fitted values of the maximum conversion  $\alpha_{\text{max}}$  and the time constant  $t_0$  have been summarized, together with the sulfation kinetic rate constant  $k_s$  as calculated from  $t_0$ . It is observed that  $k_s$  ranges between 119 mm/s and 677 mm/s, where the latter value is rather high compared to the others. The average rate constant for the sulfation of the different stones (calcined at 980 °C) equals 253 mm/s at 760 °C ( $\sigma_{n-1} = 29$  mm/s), while at 980 °C the average value of  $k_s$  equals 260 mm/s ( $\sigma_{n-1} = 210$  mm/s).

Borgwardt and Harvey (1972) reported an average kinetic rate constant of 2.2 mm/s at 980 °C based on the initial total (BET) specific CaO surface area, while Marsh and Ulrichson (1985) in a detailed rate and diffusional study on the reaction of calcium oxide with sulfur dioxide reported a value of 2.1 mm/s at the same temperature. Consequently, the kinetic rate constant is more than 100 times higher when  $k_s$  is based on the initial total particle outer surface, as is the case in the SURE model presented here.

The kinetic sulfation rate constant  $k_s$  for the sulfation reaction  $\text{CaO} + \text{SO}_2 + \frac{1}{2} \text{O}_2 \rightarrow \text{CaSO}_4$  is reported by Dennis and Fieldes (1986) to be independent of particle diameter and dependent on temperature, as would be expected. They experimentally obtained a rate constant  $k_s$  based on particles outer surface that varied between 179 mm/s and 216 mm/s for Penrith limestone when the temperature varied between 825 and 975 °C. According to Zheng et al. (1982) a comparison of published data reported by Fieldes and Davidson gives surface rate constants in the range of 65 to 260 mm/s for a variety of limestone types under various conditions.

Consequently the order of magnitude of the fitted and reported values is the same, variations are either due to different reaction temperatures, different calcination temperatures or are related to the properties of the original rocks (Borgwardt and Harvey, 1972).

The effect of reaction temperature on the reaction rate can be incorporated using the appropriate value of the activation energy of the respective sulfation reactions. The  $\text{SO}_2$  sulfation activation energy is reported by Borgwardt (1970) to range between 34 and 76 kJ/mole for calcines

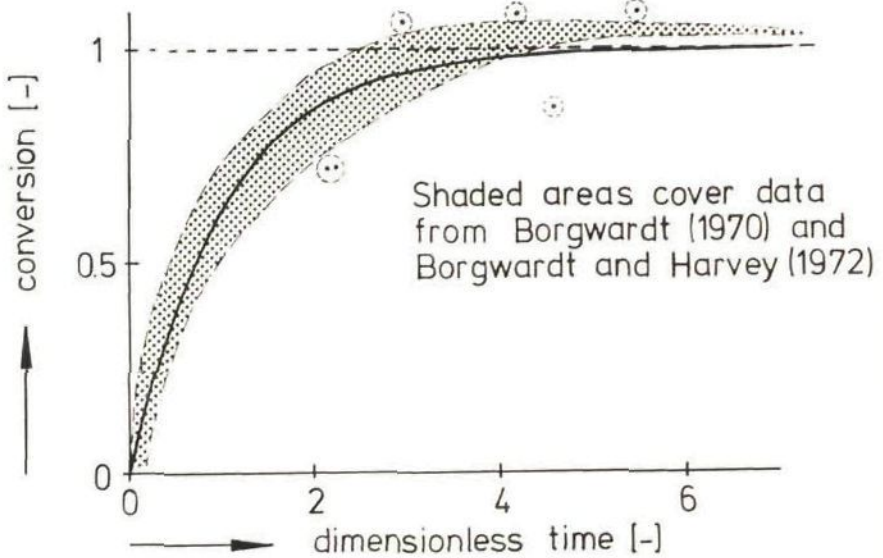


Figure 1: The dimensionless conversion  $\lambda$  as a function of the dimensionless time  $\Pi$ , Eq.[34], for experimental data of Borgwardt (1970) and Borgwardt and Harvey (1972); see also Table 3.

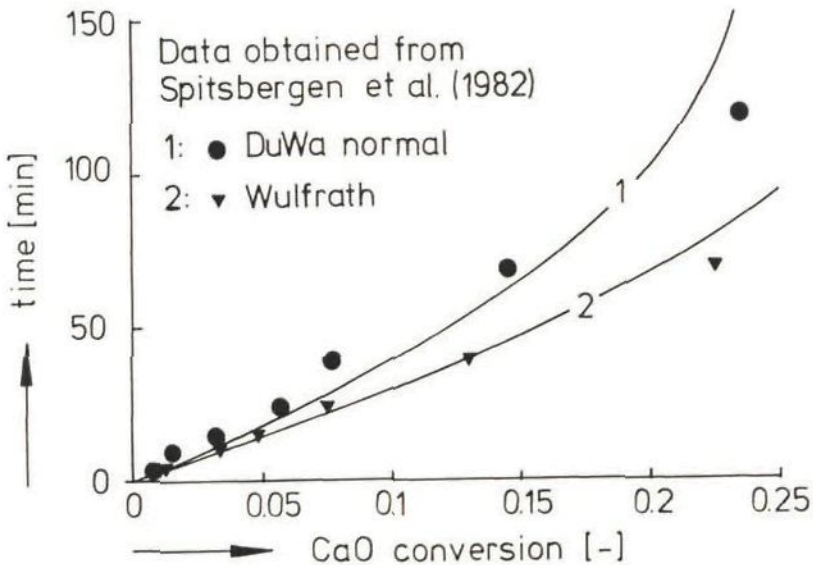


Figure 2: Comparison between the non-steady state one-phase SURE model, Eq.[35], and CaO conversion data of Spitsbergen et al. (1982) for two limestone types: DuWa C. normal and Wulfrath; see also Table 4.

Table 3: Time constant  $t_0$ , maximum conversion  $\alpha_{\max}$  and kinetic rate constant  $k_s$  obtained from experimental data of  
a. Borgwardt (1970) and b. Borgwardt and Harvey (1972).

Reference	sorbent type	particle size [ $\mu\text{m}$ ]	T <sub>calc</sub> [ $^{\circ}\text{C}$ ]	T <sub>react</sub> [ $^{\circ}\text{C}$ ]	$t_0$ [sec]	$\alpha_{\max}$ [-]	$k_s$ [mm/s]
a.	dolomite 1351	96	980	650	40.8	0.069	147
a.	"	96	980	760	28.9	0.126	232
a.	"	96	980	870	49.4	0.226	150
a.	"	96	980	980	51.4	0.388	158
a.	"	250	980	870	107.5	0.252	180
b.	limestone type 1	96	980	980	22.3	0.167	677
b.	limestone type 2	96	980	980	127.1	0.485	119
b.	limestone type 3	250	980	980	186.7	0.459	191
b.	"	96	980	980	104.1	0.524	132
b.	limestone type 4	250	980	980	92.6	0.322	415
b.	"	96	980	980	115.2	0.583	128
b.	"	96	1100	760	22.0	0.072	553
b.	"	96	980	760	44.5	0.150	273
b.	"	96	890	760	76.2	0.315	160
b.	"	96	790	760	71.2	0.442	171

T<sub>calc</sub> = temperature at which sorbent is calcined  
T<sub>react</sub> = temperature at which reaction is carried out

of different limestones (between 650 and 980 °C). Wen and Ishida (1973) reported an average value of 73.3 kJ/mole, found by applying the grain model to other researchers' data. According to Marsh and Ulrichson a range of 65.3 to 74.5 kJ/mole was determined by Hatfield et al. (1970), while from own experiments they found a value of 80.0 kJ/mole (740 - 930 °C).

More scatter exists in the activation energies reported for the H<sub>2</sub>S sulfation reaction: Simons and Rawlins found a value of 42 kJ/mole (in case of Glasshouse stone), while Borgwardt et al. (1984) measured an activation energy of CaO reaction with H<sub>2</sub>S or COS of 130 kJ/mole (in case of Fredonia White (BCR 2061) limestone).

## 5.2 Sulfur breakthrough at unsteady state operation

### 5.2.1 CaO conversion

In this section the validity of the fluid-dynamical part of the model will be checked by fitting the model expressions to CaO conversion data of the SO<sub>2</sub> sulfation reaction obtained by Spitsbergen et al. (1982) and Akse et al. (1983) in a 4 cm ID quartz fluid bed at 1 m/s. Hereto 6 different types of limestone are compared, each with an average particle diameter of 925 μm (-1000μm +850μm). The one-phase model equation (m=1; Eq.[9]) will be used, where the sulfur breakthrough time is explicitly written as a function of the solids conversion (with  $\sigma(t) = \alpha(t)/\alpha_{\max}$ ) as:

$$\Theta = 1 - \sigma(t) - (1/P_0) \ln [\sigma(t)] \quad [35]$$

The magnitude of the maximum CaO conversion  $\alpha_{\max}$  is taken as reported by Akse et al. (1983) for these limestones; further  $\tau_{br}$  is calculated from the data supplied, so the maximum gas exchange ratio  $P_0$  is the only parameter that has to be obtained by fitting. Finally, the kinetic sulfation rate constant  $k_s$  is then calculated from  $P_0$ . The results are summarized in Figure 2 and Table 4.

In general the one-phase model, Eq.[35], fits the experimental conversion data moderately well; the corresponding values of the kinetic constant  $k_s$  at 850 °C range between 52 and 108 mm/s. Compared to the values as reported in section 5.1 these rate constants of the SO<sub>2</sub> sulfation reaction are low, but they are still of the same order of magnitude and in the same range.

So the one-phase SURE model fits the solids conversion data reasonably well and gives fitted values of the intrinsic rate constant which are realistic and that agree with other data reported in literature.

Table 4: Sulfur breakthrough time  $\tau_{br}$ , maximum exchange parameter  $P_0$  and kinetic rate constant  $k_s$  calculated from CaO conversion data reported by Spitsbergen et al. (1982); the maximum CaO conversion  $\alpha_{max}$  is obtained from reported data of Akse et al. (1983).

The data were obtained in a 4 cm ID quartz fluid bed at 850 °C;  
 $U_0 = 1$  m/s,  $d_0 = 925$   $\mu$ m (-1000+850  $\mu$ m);  $c_0 = 2000$  ppm SO<sub>2</sub>;  
 limestone batch 25 g.

limestone type	$\alpha_{max}$ [-]	$\tau_{br}$ [min]	$P_0$ [-]	$k_s$ [mm/s]
Carmeuse Engis	0.308	45	0.757	60
Nekami	0.400	58	0.867	52
Dornap	0.342	51	0.804	57
Wulfrath	0.331	49	1.120	96
Hawthorn	0.312	40	0.999	82
DuWa C. Normal	0.256	38	1.017	108

### 5.2.2 Sulfur outlet concentration

The validity of the fluid-dynamical part of the model will also be checked by fitting the dimensionless outlet sulfur concentration to experimental data of Zheng et al. (1982), Noordergraaf (1985) and Dennis and Fieldes (1986). This is done for  $m=1$ , so in case of the one-phase model. The results are summarized in a dimensionless form in Figure 3 according to:

$$F(X) = \{ (1-\theta) P_0 + \ln P_0 \} = \left[ \frac{(1-X)}{X} \right] + \ln \left[ \frac{(1-X)}{X} \right] \quad [36]$$

The shaded area in the graph covers 8 data sets of Zheng et al., 3 of Noordergraaf and 1 of Dennis and Fieldes. It is shown that the model gives a reasonable fit of the data. Unfortunately the information supplied by Zheng et al. and Dennis and Fieldes is too limited to calculate accurately the sulfation rate constant  $k_s$  from the fitted value of  $P_0$ . However, in case of



Noordergraaf's data, calculation of the kinetic rate constant is possible; the results are summarized in Table 5.

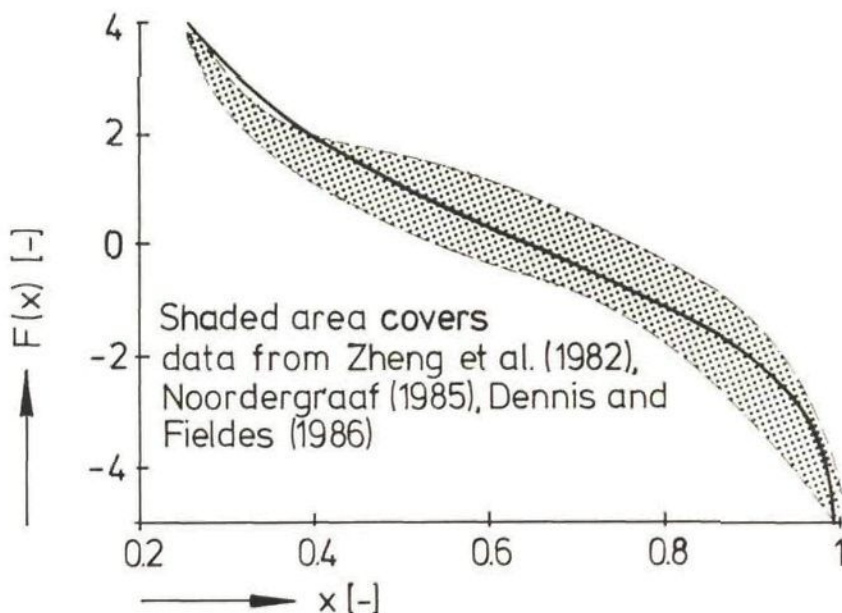


Figure 3: Dimensionless plot of sulfur breakthrough in a fluid bed according to the one-phase SURE model, Eq.[36]; comparison with experimental data of Zheng et al. (1982), Noordergraaf (1985) and Dennis and Fieldes (1986); see also Table 5.

It is observed that the maximum CaO conversion in case of Noordergraaf's data is very high. This is due to the fact that here a synthetic sorbent material (CaO on  $\alpha$ -Al<sub>2</sub>O<sub>3</sub> carrier) is used with large pores that inhibit deactivation phenomena like pore plugging. The corresponding values of the kinetic rate constant  $k_s$  vary between 38 and 80 mm/s at 850 °C, which are low compared to the rate constants as reported in section 5.1, but still of the same order of magnitude.

### 5.3 Sulfur retention at steady state operation

In this section a comparison is given of model calculations and predictions and steady state experimental retention data as derived from different literature sources (Lee and Georgakis (1981), Zheng et al. (1982), Ekinici et al. (1982) and Fee et al. (1983)).

Table 5: Sulfur breakthrough time  $\tau_{br}$ , maximum exchange parameter  $P_0$ , maximum CaO conversion  $\alpha_{max}$  and kinetic reaction rate constant  $k_s$  obtained from data of a. Zheng et al. (1982) (10 cm ID bed), b. Noordergraaf (1985) (10 cm ID bed) and c. Dennis and Fieldes (1986) (8 cm ID bed).

Reference	sorbent type	$U_0$ [m/s]	$d_0$ [mm]	T [°C]	$\tau_{br}$ [min]	$\alpha_{max}$ [-]	$P_0$ [-]	$k_s$ [mm/s]
a.	limestone 1359	0.2	0.15	850	8.1	-	2.29	-
a.	"	0.2	0.15	800	7.4	-	2.62	-
a.	"	0.2	0.62	800	2.5	-	0.75	-
a.	"	0.2	0.62	850	1.9	-	0.66	-
a.	"	0.35	0.15	800	5.7	-	3.28	-
a.	"	0.35	0.15	850	5.0	-	2.59	-
a.	"	0.35	0.62	800	2.5	-	0.81	-
a.	"	0.35	0.62	850	2.2	-	0.94	-
b.	synthetic sorbent	1.0	2.5 mm pellets	850	18.2	0.815	0.984	80
b.	"	1.25	"	850	22.7	1	1.396	51
b.	"	1.5	"	850	19.2	1	1.371	38
c.	Penrith limestone	$>5 U_{mf}$	0.78	875	224.0	-	0.608	-

The calculation of the retention parameter M is based on the plant operating circumstances as given by the respective authors and further based on the correlations given in Appendix 1. However, unfortunately in general it is not possible to obtain the average sorbent residence time  $\tau_s$  accurately as needed to calculate M from Eq.[A1.24]. Therefore the average sorbent residence time has been calculated together with the maximum CaO sorbent conversion from a least-squares fit of the experimental data to the respective model equations. The maximum conversion will be compared with the values as reported by the respective authors.

In Figure 4 the model fit is compared with combustor retention data as given by Fee et al. (1983) in case of the Babcock and Wilcox 0.98 m<sup>2</sup> plant with a once-through sorbent usage. The fitted value of the retention parameter M equals 1.20 [-], which is in agreement with an average sorbent residence time of 25 minutes in case of  $k_s = 200$  mm/s. Although this value of  $\tau_s$  is rather low, it is not unrealistic in this specific situation. However, when a lower value of  $k_s$ , e.g. 50 mm/s as reported in sections 5.1 and 5.2, is used then the sorbent residence time should equal 73 minutes.

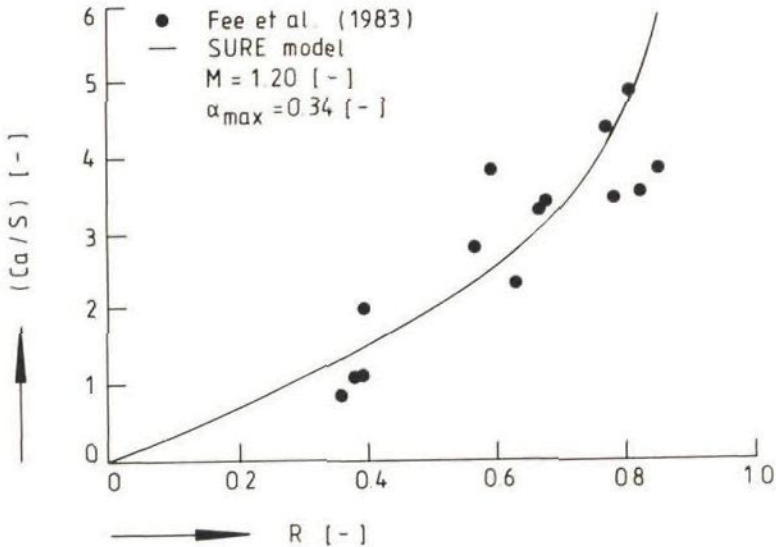


Figure 4: The (Ca/S) ratio as a function of retention R: comparison between the one-phase SURE model, Eq.[27], and experimental data of Fee et al. (1983) ( $U_o = 2.54$  m/s;  $H = 0.42$  m;  $F = 0.98$  m<sup>2</sup>;  $d_o = 0.9$  mm).

Consequently these calculations illustrate clearly that also the sulfation kinetic rate constant should be known quite accurately to obtain a correct value of the retention parameter M (this will be especially important in the case of the capture of reduced sulfur species in multi-stage combustion: since the residence time of the limestone particles in the reducing zone is short the feasibility of improving the overall sulfur capture by CaS formation will depend predominantly on reaction kinetics; Borgwardt et al., 1984).

The fitted value of the maximum CaO sorbent conversion equals 34%, where the average value reported by Fee et al. (1983) in this specific case (Lowellville limestone;  $d_o = 0.9$  mm) is 32% as determined in a TGA-test,

while a value of 36% was reported in a 3.34 m<sup>2</sup> combustor facility. The agreement between these values is very good, indicating that the prediction of the SURE model is realistic.

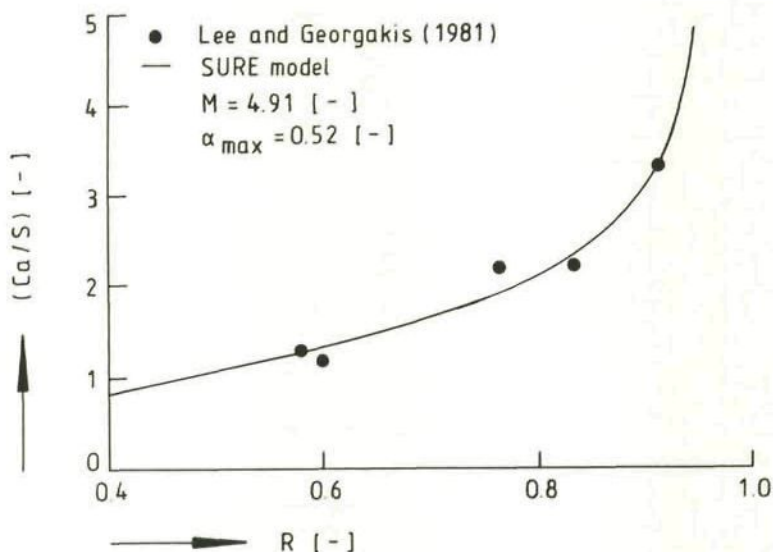


Figure 5: The  $(Ca/S)$  ratio as a function of retention  $R$ : comparison between the one-phase SURE model, Eq.[27], and experimental data of Lee and Georgakis (1981) ( $U_0 = 1.22$  m/s;  $H = 0.67$  m;  $F = 0.4$  m<sup>2</sup>;  $d_0 = 0.58$  mm).

In Figure 5 the model fit is shown of retention plant data as given by Lee and Georgakis (1981) in case of a 0.4 m<sup>2</sup> fluid bed facility. The fitted value of the retention parameter equals 4.91 [-], from which the sorbent residence time is approximated as 25 minutes in case of a kinetic sulfation rate constant  $k_s$  of 200 mm/s. When here also the value of 50 mm/s is used a sorbent residence time of 78 minutes results.

The fitted value of the maximum conversion equals 52%, where Lee and Georgakis (1981) report a value in this specific case (Limestone 18;  $d_0 = 580$   $\mu$ m) of 51%; again the agreement is very good as is also observed from a comparison of the SURE model fits with other conversion data reported by Lee and Georgakis (1981) as shown in Figure 6.

In Figure 7 the fitted values of the maximum sorbent conversion have been summarized as a function of the respective sorbent particle diameters obtained from several literature sources. In general it can be concluded that the maximum conversion varies between 0.3 and 0.7 for particle diameters in between 500  $\mu$ m and 1500  $\mu$ m.

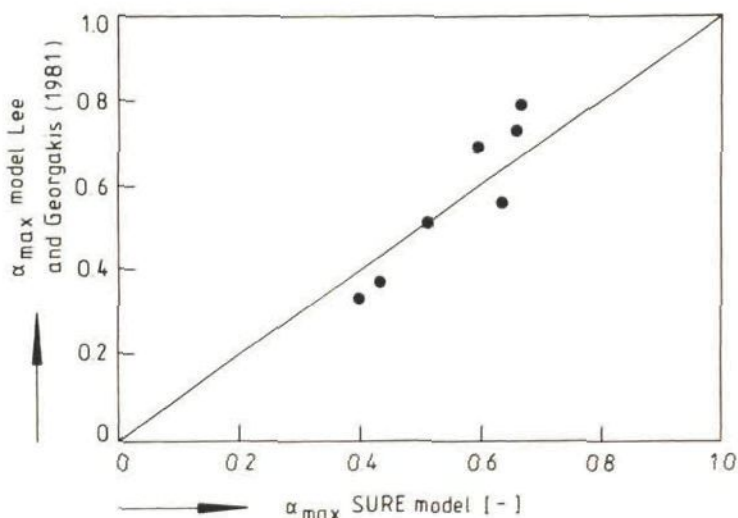


Figure 6: Comparison between the maximum CaO conversion as obtained by Lee and Georgakis (1981) and the fitted values according to the one-phase SURE model.

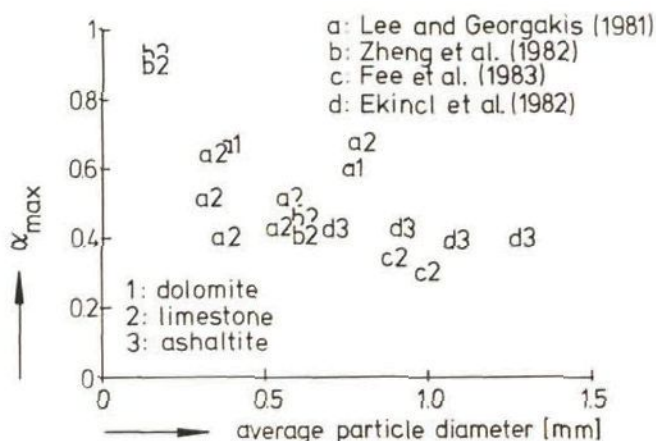


Figure 7: Overview of fitted values of the maximum CaO conversion as a function of the respective sorbent particle diameter as obtained from 4 different literature sources.

The general conclusion which can be drawn so far from the results presented in sections 5.1 to 5.3 is that the one-phase SURE model fits experimental data rather good and gives realistic predictions of the kinetic rate constant  $k_s$ , the maximum CaO conversion and the sorbent residence time. So a further application and analysis of the model will be put forward in the following section.

## 6. MODEL PARAMETER SENSITIVITY ANALYSIS

### 6.1 Calculation of model parameters

In Appendix 1 a summary is given of equations derived from literature from which characteristic average values of the dimensionless model parameters  $P_0$ ,  $m$ ,  $M$  and  $\alpha_{\max}$  are obtained. These characteristic values will be used for the model parameter sensitivity analysis as outlined in the next sections.

### 6.2 Comparison of one- and two-phase model

#### 6.2.1 Sulfur breakthrough at unsteady state operation

In Figures 8 and 9 a comparison is given of the one- and two-phase models with parameter values of  $P_0$  respectively 1 [-] and 3 [-]. It is observed that with a lower value of the maximum exchange parameter the difference between the one- and two-phase model increases. The lines drawn at different values of  $m$  go all more or less through the same point. Behind this point the two models do not differ much anymore. This means that especially the beginning of the breakthrough of sulfur is important for the comparison of the two models; when  $X > 0.8$  [-] then the difference between the models becomes less.

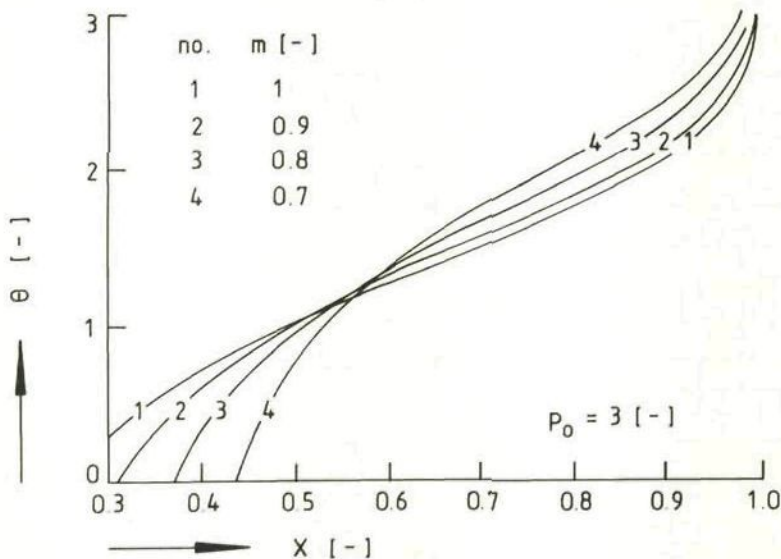


Figure 8: SURE model sensitivity analysis; comparison of one- and two-phase SURE models in case of sulfur breakthrough at unsteady state combustor operation, Eq.[10], at a fixed value of the maximum exchange parameter  $P_0 = 3$  [-] and different values of the two-phase gas flow parameter  $m$ .

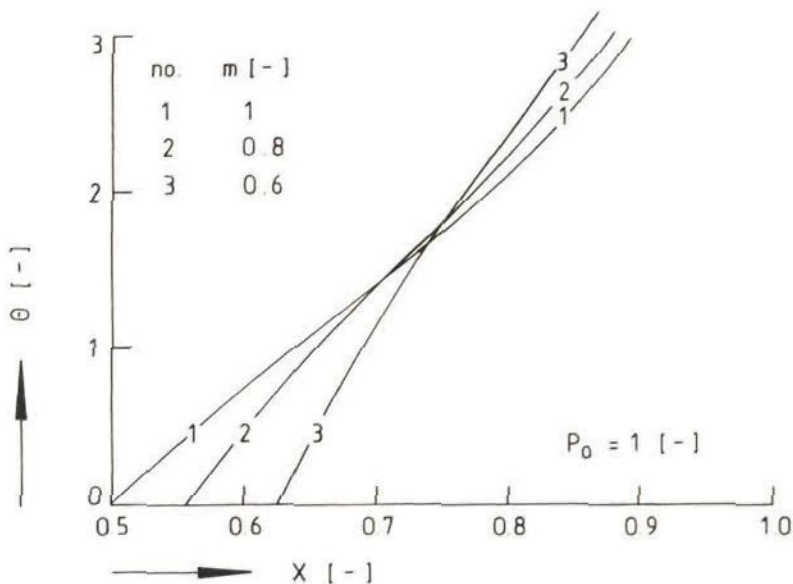


Figure 9: SURE model sensitivity analysis; comparison of one- and two-phase SURE models in case of sulfur breakthrough at unsteady state combustor operation, Eq.[10], at a fixed value of the maximum exchange parameter  $P_0 = 1$  [-] and different values of the two-phase gas flow parameter  $m$ .

### 6.2.2 (Ca/S) ratio at steady state operation

In Figure 10 the two-phase gas flow parameter  $m$  is plotted as a function of the number of transfer units  $N_0$  at different values of the dimensionless excess gas velocity  $u$ . It is observed that  $m$  varies between 0.5 [-] and almost 1 [-] for characteristic values of  $N_0$  (0.5 - 3 [-]) and  $u$  ( $> 0.6$  [-]). In Figure 11 the product  $M(1-R)$  is given as a function of the level of retention  $R$  at different values of the retention parameter  $M$ . It is observed that at characteristic values of  $R$  ( $> 0.8$ ) the value of  $M(1-R)$  decreases significantly. Further in Figure 12 the ratio between the (Ca/S) ratio of the one-phase model and the two-phase model is demonstrated as a function of the product  $M(1-R)$  at different values of the two-phase gas flow parameter  $m$  for an average value of the maximum conversion  $\alpha_{\max}$  of 0.5 [-]. It is observed that this ratio is always smaller than 2 at the characteristic values of  $m$  ( $m > 0.5$  [-]); the (Ca/S) ratio of the one-phase model is always higher than that of the two-phase model. Further this graph makes clear that the difference between both models becomes very small when  $M(1-R) > 1$  and  $m > 0.7$  [-]. However, it is concluded from Figure 11 that at a retention

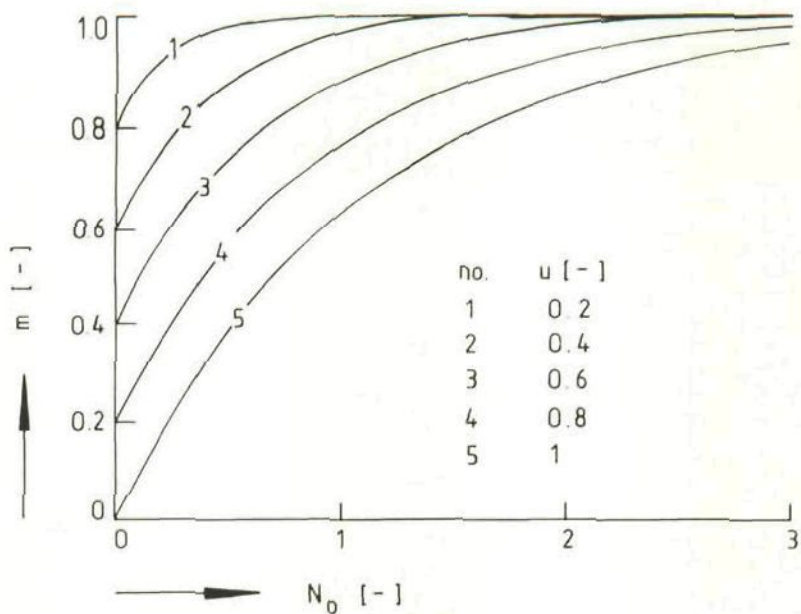


Figure 10: SURE model sensitivity analysis; the two-phase gas flow parameter  $m$  as a function of the number of mass transfer units  $N_D$  at different values of the dimensionless excess gas velocity in the bubble phase  $u$ , Eq.[12].

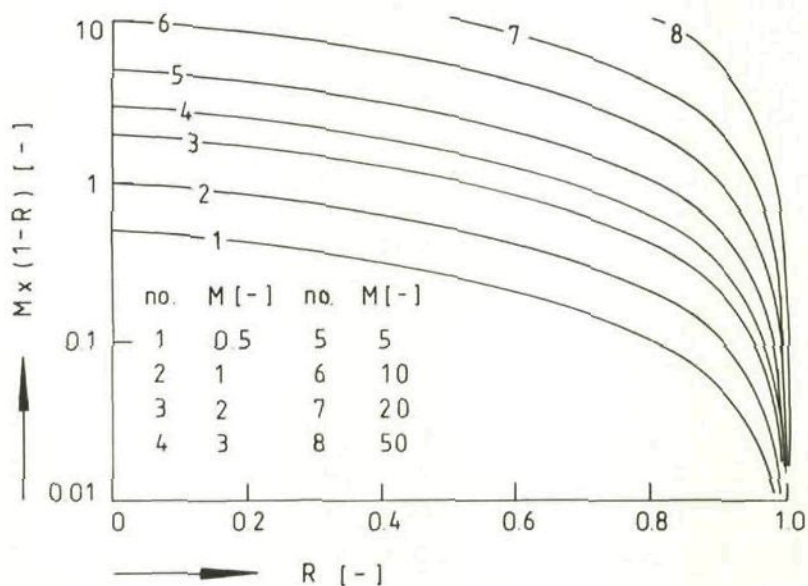


Figure 11: SURE model sensitivity analysis; the product  $M(1-R)$  as a function of the level of retention  $R$  at different values of the retention parameter  $M$ .



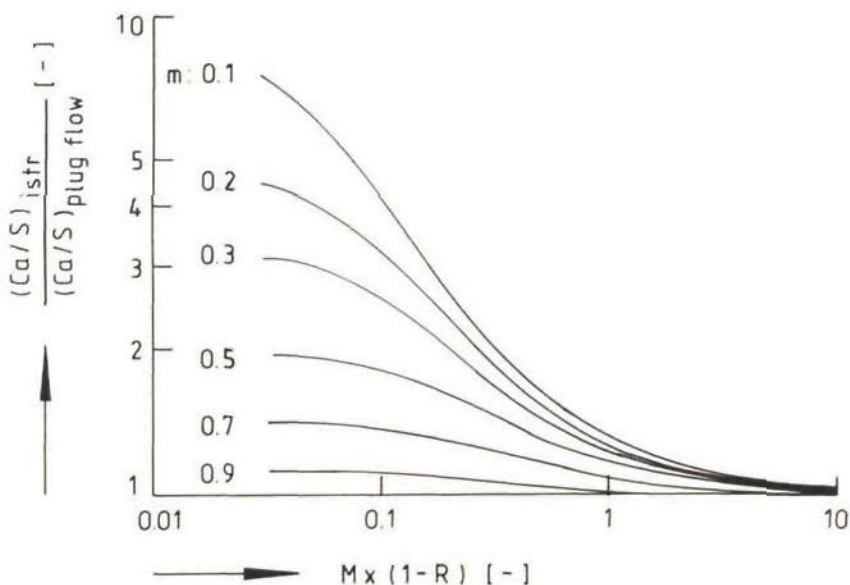


Figure 12: SURE model sensitivity analysis; the ratio between the (Ca/S) ratio as obtained from the one-phase SURE model (istr=ideally stirred tank reactor), Eq.[27], and the two-phase SURE model (with plug flow in the bubble phase), Eq.[32], as a function of the product  $M(1-R)$  at different values of the two-phase gas flow parameter  $m$  and at a value of the maximum CaO conversion of 0.5 [-].

level  $R > 0.8$  this is only the case at high values of  $M (> 10)$  together with a relative high level of gas exchange ( $N_o > 1 - 2$  [-]); Figure 10).

This effect is also illustrated in Figures 13 and 14 where the retention  $R$  is plotted as a function of the (Ca/S) ratio with respectively  $M = 1$  [-] and  $M = 10$  [-] ( $\alpha_{max} = 1$  [-] in both cases). It is concluded that at a low level of gas exchange in the emulsion phase ( $M = 1$  [-]) the models differ clearly, however when  $M = 10$  [-] the difference becomes significantly less even at low values of  $m$ .

So it can be concluded from this parameter sensitivity analysis that it will strongly depend on the actual combustor conditions which model will provide the best prediction of the (Ca/S) ratio at a required level of retention. In general it can be concluded that at relatively high levels of gas exchange between the phases ( $N_o \gg 2$  [-]) both models will give almost the same outcomes (because then  $m \rightarrow 1$  [-]).

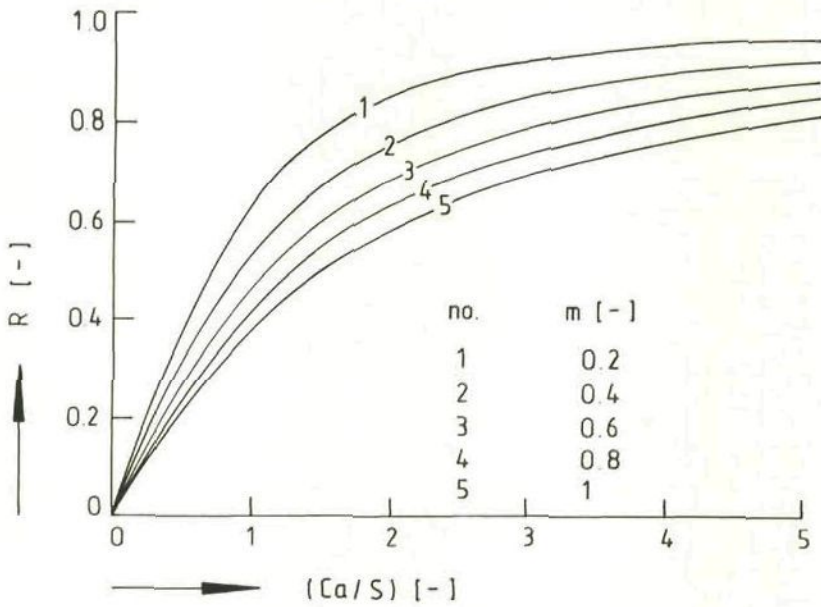


Figure 13: SURE model sensitivity analysis; the level of retention  $R$  as a function of the  $(Ca/S)$  ratio, Eq.[33], at different values of the two-phase gas flow parameter  $m$ ;  $\alpha_{max} = 1$  [-];  $M = 1$  [-].

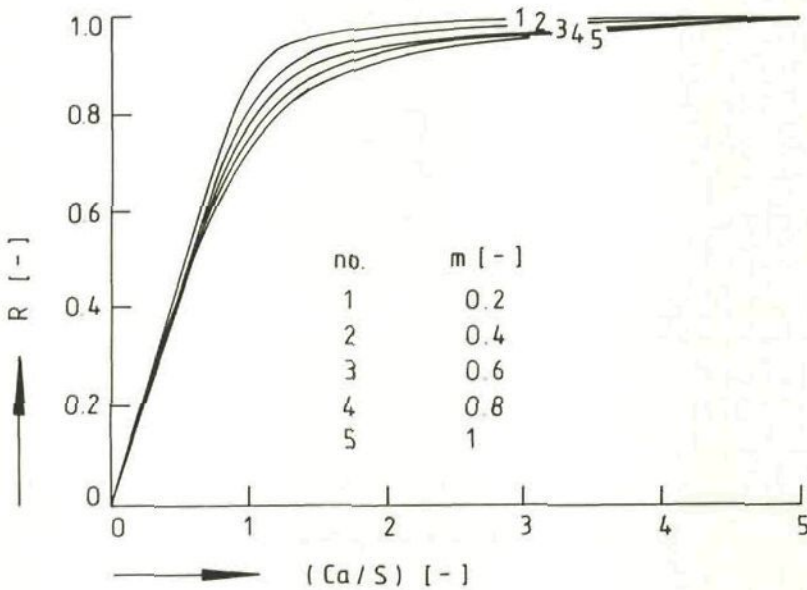


Figure 14: SURE model sensitivity analysis; the level of retention  $R$  as a function of the  $(Ca/S)$  ratio, Eq.[33], at different values of the two-phase gas flow parameter  $m$ ;  $\alpha_{max} = 1$  [-];  $M = 10$  [-].

### 6.3 Level of sulfur retention

In this section it is analyzed in what way the level of sulfur retention is influenced by the the maximum conversion  $\alpha_{\max}$  and the retention parameter  $M$  in relation to the  $(\text{Ca}/\text{S})$  ratio.

#### 6.3.1 Influence of maximum sorbent conversion

In Figure 15 the  $(\text{Ca}/\text{S})$  ratio is shown as a function of the level of sulfur retention  $R$  at a fixed value of the retention parameter  $M = 2 [-]$  in the case of the slow bubble model ( $m = 1 [-]$ ). It is concluded that the maximum conversion of  $\text{CaO}$  in the sorbent,  $\alpha_{\max}$ , strongly influences the  $(\text{Ca}/\text{S})$  ratio necessary to obtain a specific required retention  $R$  when  $\alpha_{\max}$  ranges between about 0.1 and 0.5. However, in this specific situation where  $M = 2 [-]$  the influence of the maximum conversion is very limited above the value of about 0.5  $[-]$ : especially the difference between  $\alpha_{\max}$  of 0.7 and 0.9 is very small.

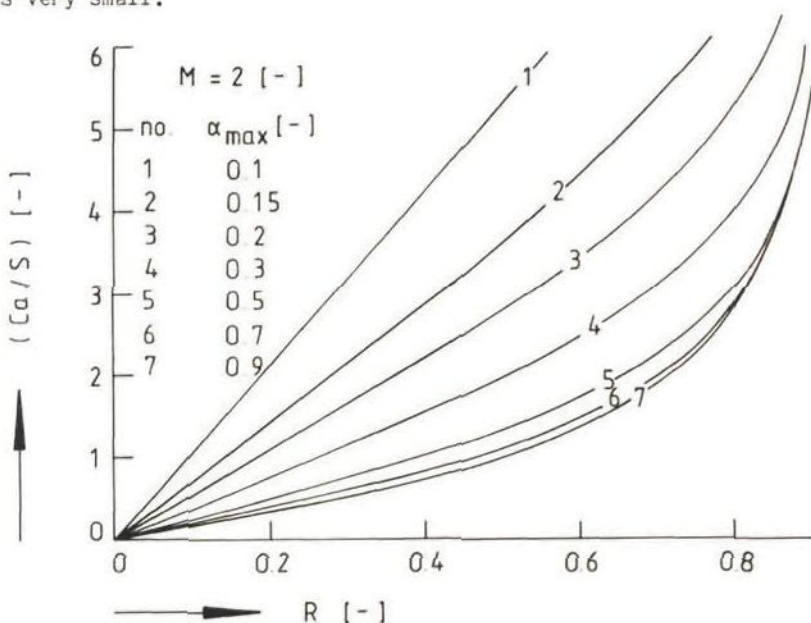


Figure 15: SURE model sensitivity analysis; the  $(\text{Ca}/\text{S})$  ratio of the one-phase model, Eq.[27], as a function of the level of retention  $R$  at a fixed value of the retention parameter  $M = 2 [-]$  and at different values of the maximum  $\text{CaO}$  conversion  $\alpha_{\max}$ .

This implies in general that at a certain level of the maximum  $\text{CaO}$  conversion no significant increase in the sulfur retention can be obtained at a fixed  $(\text{Ca}/\text{S})$  ratio by increasing the maximum sorbent utilization in the reactor (for example by using another sorbent type).

### 6.3.2 Influence of retention parameter

The same effect can be observed in Figure 16 where the  $(Ca/S)$  ratio at  $m = 1$  [-] has been plotted as a function of the retention  $R$  at a fixed value of  $\alpha_{max} = 0.5$  [-]. In this case it is concluded that the retention parameter strongly influences the  $(Ca/S)$  ratio needed to obtain a specific required level of retention when it is smaller than about  $M = 10$  [-]. Above this level the influence of  $M$  is limited, especially when the required retention  $R$  is smaller than about 0.9.

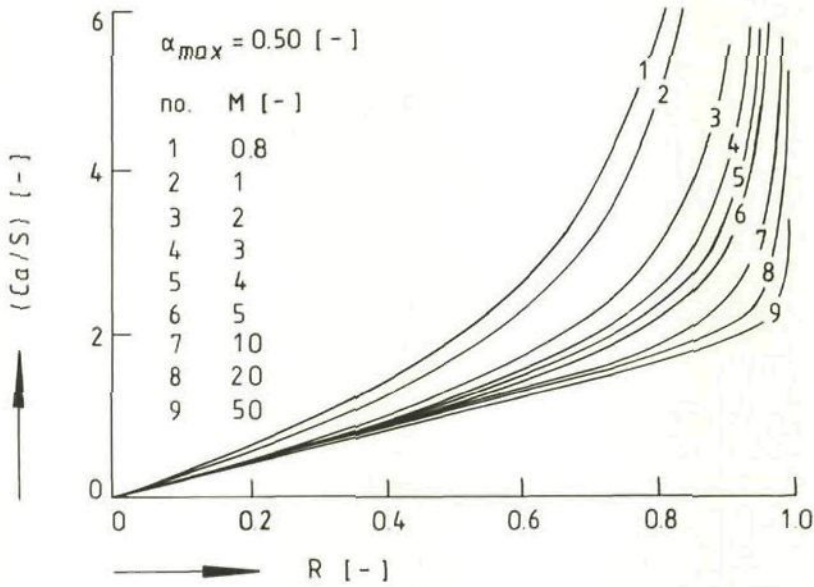


Figure 16: SURE model sensitivity analysis; the  $(Ca/S)$  ratio of the one-phase model, Eq.[27], as a function of the level of retention  $R$  at a fixed value of the maximum  $CaO$  conversion  $\alpha_{max} = 0.5$  [-] and at different values of the retention parameter  $M$ .

In general these effects, obtained from analyzing Figures 15 and 16, mean that the retention in a fluid bed coal combustor cannot always continuously be increased by adding the same extra amount of sorbent to the bed. Especially at high levels of the retention parameter  $M$  and/or the maximum sorbent conversion  $\alpha_{max}$  the required retention level can already be obtained by just a relatively small increase of the  $(Ca/S)$  ratio. For example, it can be derived from Figure 15 ( $M = 2$  [-]) that at a maximum conversion of 0.3 the  $(Ca/S)$  ratio must be increased with 1.5 units from 2.3 to 3.8 to let the retention increase to 80%. However, at a maximum conversion of the sorbent of 0.7 and a  $(Ca/S)$  ratio of 2.3 an absolute increase with about 0.1 units to 2.4 is already sufficient to obtain the required retention level of 80%.

#### 6.4 Influence of reactor circumstances and sorbent properties on sulfur retention

As can be concluded from the definition of the retention parameter M (see hereto also Appendix 1) and from Eq.[25] the level of sulfur retention R is predominantly influenced by two groups of parameters:

##### 1) fluid bed reactor circumstances:

- \* the sorbent residence time  $\tau_s$ ;
- \* the superficial gas velocity  $U_0$ ;
- \* the mass transfer coefficient in the dense phase  $k_g$   
(or the corresponding Sherwood number Sh);
- \* the bed temperature T;

##### 2) sorbent properties:

- \* the average sorbent particle diameter  $d_0$ ;
- \* the maximum sorbent CaO conversion  $\alpha_{max}$ ;
- \* the sulfation kinetic rate constant  $k_s$ ;

next to the most important parameter, i.e.:

- \* the (Ca/S) ratio in the reactor feed.

In the following sections it is illustrated how the level of retention is effected by the sorbent residence time, the average sorbent particle diameter and the superficial gas velocity at different levels of the (Ca/S) ratio.

The mass transfer coefficient is predominantly effected by the sorbent particle diameter at a fixed value of the average bed particle diameter  $d_p$  (see Eq.[A1.6] and [A1.7], page 57) and also by the bed temperature.

The kinetic sulfation rate constant is temperature dependent and determined by the type of sorbent used. So a higher temperature would imply a higher retention parameter M caused by an increase of the sulfation rate. However, an other sorbent type might also give a higher value of M even at lower temperatures. Because this implies that temperature and sorbent type are closely linked therefore just an average common case is considered here with  $k_s = 200$  mm/s.

Because the effect of the maximum sorbent CaO conversion has already been outlined in detail in Figure 15, the value  $\alpha_{max} = 1$  [-] has been chosen in this case. The slow bubble regime is considered, so  $m = 1$  [-]. Further

the following average reactor circumstances and sorbent properties have been chosen:

$$U_o = 2 \text{ m/s}; \phi_S/F = 0.03 \text{ mol/s/m}^2; \tau_s = 2 \text{ hr}; d_o = d_p = 1 \text{ mm};$$

$$\rho_o = 2700 \text{ kg/m}^3; x_{\text{CaCO}_3} = 0.95 [-].$$

The equations given in Appendix 1 are used to calculate the other relevant parameters, like e.g. the Sherwood number.

#### 6.4.1 Sorbent residence time

In Figure 17 it is shown that the sorbent residence time is a very important parameter: at a (Ca/S) ratio of 2 the sulfur retention increases from about 70% to 85% when the sorbent residence is increased from 1 to 3 hours. However, it is also obvious that the same effect results when the (Ca/S) ratio is increased from 2 to 4 at a residence time of 1 hour.

The sorbent residence time can be increased by increasing the cyclone recycle ratio which will also result in a decrease of the average sorbent particle diameter in the bed. As a result of both effects the retention parameter M will increase, which will give a higher level of retention at the same (Ca/S) ratio.

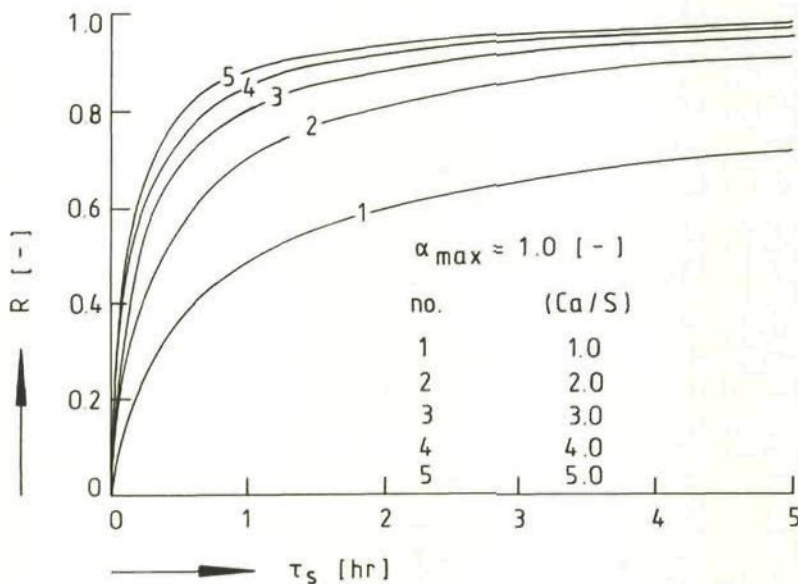


Figure 17: The level of sulfur retention R as a function of the sorbent residence time  $\tau_s$  in case of the one-phase SURE model, Eq.[29], at different values of the (Ca/S) ratio;  $\alpha_{\max} = 1 [-]$ .

The effect of recycle ratio on retention has already been experimentally confirmed in a 20 MW facility by Bass and High (1984): they showed that  $\text{SO}_2$  retention could be increased by 10% with the addition of multiclone catch recycle (recycle ratio increased from 0 to 3).

The effect of solid in-bed residence time on sulfur retention has also been reported by Duqum et al. (1985) in a 2 MW and a 20 MW unit. They showed that an increase of solid residence time from 30 to 120 hours increased the spent bed lime utilization from about 33% to about 42%; further the sulfur capture increased with about 10% when the recycle ratio was increased from 1 to 6.

#### 6.4.2 Sorbent particle size

The effect of sorbent particle size is illustrated in Figure 18. At a (Ca/S) ratio of 2 the level of retention decreases from about 85% to 72% when the average sorbent particle diameter is increased from 1 to 2 mm. But the level of retention will stay at about 85% when the (Ca/S) ratio is increased from 2 to more than 3.

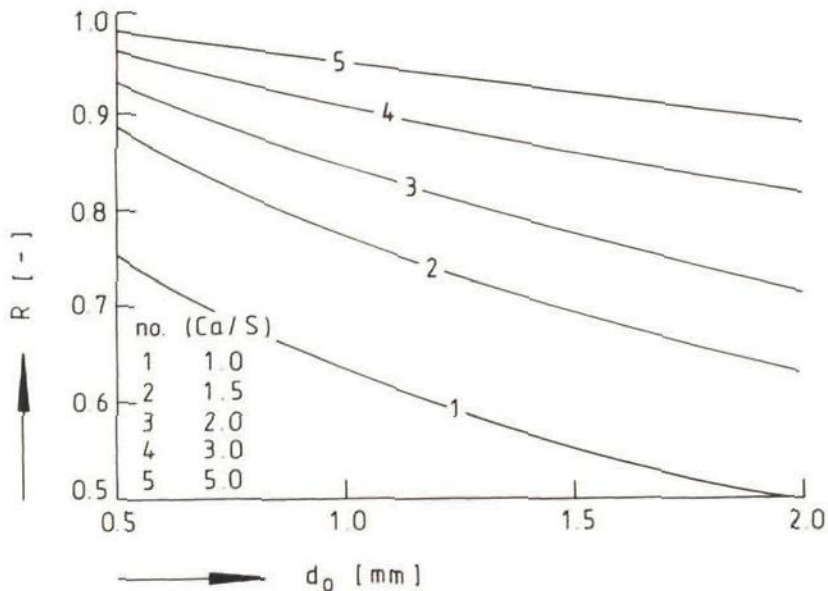


Figure 18: The level of sulfur retention  $R$  as a function of the average sorbent particle diameter  $d_0$  in case of the one-phase SURE model, Eq.[29], at different values of the (Ca/S) ratio;  $\alpha_{\max} = 1$  [-].

The effect of particle diameter has been experimentally observed for example by Anthony et al. (1985) in a 0.155 m<sup>2</sup> AFBC pilot plant: they reported that sulfur retention is optimum in the particle size range of 0.5 to 1.0 mm. Increasing the limestone particle diameter much above 1 mm drastically reduced the sulfur capture.

Jonke et al. (1972) found that for particles of 1000 μm the retention was about 87% and for smaller particles (630 μm) the retention was about 93% for a common (Ca/S) ratio of 4.0, temperature of 840 °C and gas velocity of 0.91 m/s.

These observations agree qualitatively with the SURE model calculations.

#### 6.4.3 Superficial gas velocity

Finally, the effect of the superficial gas velocity is shown in Figure 19. At a (Ca/S) ratio of 1.5 the level of retention decreases from about 83% to 74% when the gas velocity is increased from 1 to 2 m/s. The level of retention will only remain at about 83% when the (Ca/S) ratio is increased to more than 2.

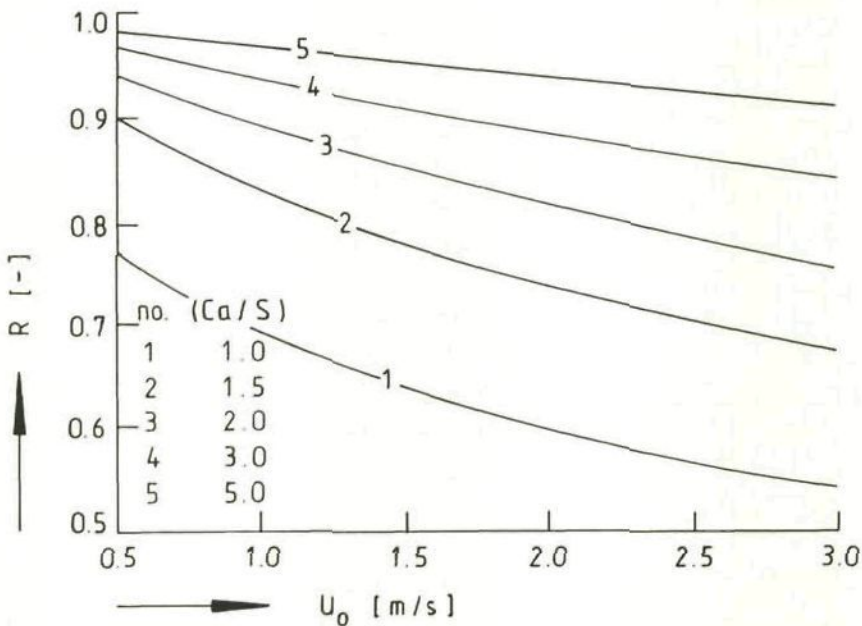


Figure 19: The level of sulfur retention  $R$  as a function of the superficial gas velocity  $U_0$  in case of the one-phase SURE model ( $m = 1$  [-]), Eq.[29], at different values of the (Ca/S) ratio;  $\alpha_{\max} = 1$  [-].

The effect of gas velocity is experimentally confirmed by Duqum et al. (1985) who reported that the sulfur capture decreased as much as 15% as the



superficial gas velocity was increased from 5 to 12 ft/s for a (Ca/S) ratio of 2.5 - 3.0 and a recycle ratio of 1 - 2.

Tang et al. (1982) reported a drop in the sulfur retention of about 40% for a comparatively narrow range of (Ca/S) ratio between 2.5 and 3.0, when the fluidizing velocity was increased from 1.5 to 3.7 m/s.

Rajan and Wen (1980) discussed the effect of fluidizing velocity on sulfur retention efficiency. At low velocities (1 m/s), elutriation is small, and hence the average bed particle size is small. Also the gas and solids residence times are increased. This implies a greater reactivity of the limestone particles (sulfur retention 85%). But at higher fluidizing velocities (2.4 m/s), entrainment is large, and the particles entrained are also larger. Bed particle sizes are consequently larger, resulting in lower reactivities (retention 70%). Also the residence times will be shorter. A combination of these effects results in a lower SO<sub>2</sub> retention efficiency at higher velocities.

However, the general experimental trends observed are also clearly predicted by the SURE model as indicated in Figure 19.

## 7. OPTIMIZATION OF THE (Ca/S) RATIO

### 7.1 Retention index RI

As is outlined in detail in section 6 the level of retention R is dependent on reactor conditions and sorbent properties. In order to minimize limestone purchase and preparation costs as well as the solid waste disposal, it is clear that the combustor must be operated at the lowest possible (Ca/S) ratio where still the required retention R can be established. This requires specific operating circumstances (see also comment 5, page 87) and sorbent properties. However, in general the reactor conditions are determined by coal combustion efficiency requirements, where only small variations in for example the superficial gas velocity are possible. Further the sorbent properties cannot be varied widely, because they are restricted by the types of sorbent available (which restrict the maximum possible conversion) and the available particle diameter fractions.

For a proper optimization it has to be evaluated which parameter should be adapted or changed first to obtain the highest reduction of the (Ca/S) ratio at the required level of retention: for example the retention parameter (via e.g. increase of the recycle ratio which enlarges the sorbent residence time) and/or the choice of another sorbent diameter fraction and/or even the choice of another type of limestone (natural or synthetic) with a higher maximum conversion.

With respect to these considerations the retention index RI is introduced to enable comparison and optimization of the combination of the fluid bed reactor circumstances and the sorbent properties. This index is given on a scale of 0 to 100 and is defined as the ratio between the stoichiometric calcium to sulfur ratio and the actual calcium to sulfur ratio in the feed at the required level of retention R:

$$RI = 100 \frac{(Ca/S)_{\text{stoichiometric}}}{(Ca/S)_{\text{actual}}} = 100 \frac{\alpha_{\text{avg}} * (Ca/S)_{\text{actual}}}{(Ca/S)_{\text{actual}}} = 100 \alpha_{\text{avg}} \quad [37]$$

The retention index becomes in the case of the two-phase model (with  $m = 1$  [-] in case of the one-phase model):

$$RI = 100 \left[ \frac{(M/m) [1-R]}{1 + (M/m) [1-R]} \right] \left[ 1 - (1 - \alpha_{\text{max}}) \exp \left\{ - \frac{\ln (1 - \alpha_{\text{max}})}{(M/m) [1-R]} \right\} \right] \quad [38]$$

Consequently, the retention index defined in this manner is equal to the percentual average conversion of the sorbent in the bed and is dependent on respectively the retention parameter M, the two-phase gas flow parameter m and the maximum sorbent conversion  $\alpha_{\text{max}}$ . The value of the retention R is fixed at 0.8, which corresponds with the required level of desulfurization for a 3.5% sulfur coal in order to meet the EPA standard for new coal-fired plants of 1.2 lb SO<sub>2</sub>/MBtu (0.54 kg/MJ) of fuel burned.

When RI equals 100 [-] then the retention performance is optimum (the combustor operates at stoichiometric conditions:  $R = (Ca/S) = 0.8$  [-] and  $\alpha_{\text{max}} = 1$  [-]) and the calcium to sulfur ratio cannot be decreased. However, when  $RI < 100$  [-] then the general retention performance of the combustor could be increased for example by either increasing the retention parameter M (for example by decreasing the sorbent particle size or increasing the sorbent residence time) or by increasing the maximum sorbent conversion  $\alpha_{\text{max}}$  (for example by means of additives to the sorbent or the use of a sorbent with a higher initial porosity). A change of the two-phase gas flow parameter m is less likely, because it depends strongly on the mode of fluidization and gas transfer in the bed.

In Figure 20 the retention index is plotted as a function of the maximum conversion at different values of the retention parameter M. In this graph also two experimental values of the retention index have been indicated, which were calculated from two retention plant data-sets of Lee and Georgakis (1981). These values were obtained by fitting the SURE model to these data-sets, whereafter the fitted values of M and  $\alpha_{\text{max}}$  were used to calculate RI. In case of data-set 'a2' the sorbent is better utilized,

because RI and, consequently, the average sorbent conversion in the bed is higher than in the case of 'a1'. This means that the retention of 80% can be obtained at a lower  $\langle Ca/S \rangle$  ratio.

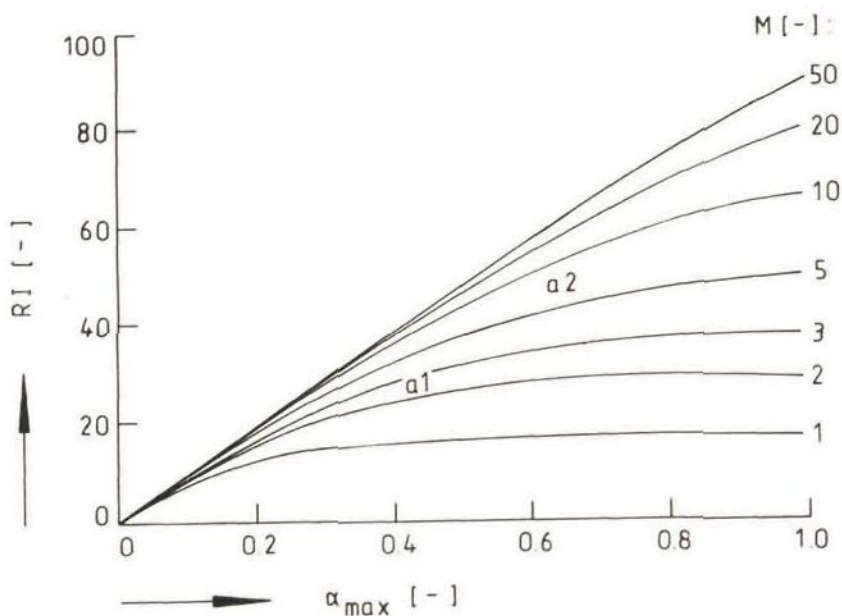


Figure 20: The retention index RI at  $R = 0.8$  [-], Eq.[38], as a function of the maximum conversion at different values of the retention parameter; two data-sets derived from Lee and Georgakis (1981) have been indicated (a1:  $d_0 = 0.55$  mm;  $U_0 = 0.79$  m/s; a2:  $d_0 = 0.79$  mm;  $U_0 = 0.91$  m/s).

In general Figure 20 illustrates clearly that at a low retention parameter  $M$  (e.g.  $M = 1$  [-]) the retention index cannot be increased by increasing the maximum conversion from for example 0.5 to 0.7: this has no effect at all. In that case the retention index can only be increased by increasing  $M$ . However, at a high retention parameter (e.g.  $M = 20$  [-]) an increase of the maximum conversion gives a considerable increase in the retention index, especially at low levels of  $\alpha_{max}$ .

## 7.2 Choice of parameter change cpc

Which parameter should be changed depends on the actual situation: sometimes a change of  $M$  will lead to a better result than an improvement of the sorbent maximum sulfation capacity. For this purpose the choice of parameter change (cpc) is introduced, which is defined as the ratio between the change of the retention index due to a change in  $M$  and the change of the retention index due to a change in  $\alpha_{max}$ :

$$cpc = \frac{\left[\frac{\partial RI}{\partial M}\right]_{m, \alpha_{max}, R}}{\left[\frac{\partial RI}{\partial \alpha_{max}}\right]_{m, M, R}} \quad \text{with:} \quad [39]$$

$$\begin{aligned} \left[\frac{\partial RI}{\partial M}\right]_{m, \alpha_{max}, R} = & \frac{[1-R] \left[1 - (1-\alpha_{max}) \exp\left(-\frac{\ln(1-\alpha_{max})}{(M/m)[1-R]}\right)\right]}{m \left[1 + (M/m)[1-R]\right]^2} + \\ & + \frac{(1-\alpha_{max}) \ln(1-\alpha_{max}) \exp\left(-\frac{\ln(1-\alpha_{max})}{(M/m)[1-R]}\right)}{M \left[1 + (M/m)[1-R]\right]^2} \end{aligned} \quad [40]$$

and:

$$\left[\frac{\partial RI}{\partial \alpha_{max}}\right]_{m, M, R} = \exp\left(-\frac{\ln(1-\alpha_{max})}{(M/m)[1-R]}\right) \quad [41]$$

When  $cpc > 1$  [-] then the retention parameter  $M$  should be changed first to obtain a higher retention index value, while  $\alpha_{max}$  should be changed first when  $cpc < 1$  [-]. Change of the retention parameter  $M$  implies that it must be enlarged, for example by the use of a smaller sorbent particle diameter or by increasing the solids residence time (e.g. by recycling of bed material). Change of  $\alpha_{max}$  means for example that another sorbent type with a higher initial porosity should be applied.

In Figure 21 the  $cpc$  is demonstrated as a function of the maximum conversion at different values of the retention parameter  $M$ . In this graph also the value of  $cpc$  has been indicated which is calculated from retention combustor data of Lee and Georgakis (1981) and Zheng et al. (1982). In case of data-sets 'a1' and 'a2' it is concluded that the retention performance can only be improved by increasing the maximum conversion ( $cpc < 1$  [-]); however, the data-set of Zheng et al. (1982) illustrates that the retention performance of their combustor should be improved by increasing the retention parameter  $M$  ( $cpc > 1$  [-]).

In general Figure 21 makes clear that the situation where  $cpc < 1$  [-] is derived alone in cases where  $M < 5$  [-]. When  $M > 5$  [-] then an increase of the retention index is only obtained when the maximum conversion of the sorbent is improved. So in the case that  $M < 5$  [-] and  $cpc > 1$  [-] the  $(Ca/S)$  ratio can be decreased by changing e.g.  $\tau_s$  or  $d_o$ . It means further that those changes in the parameters should be effected which causes that  $M > 5$  [-]. Hereafter improvement of  $(Ca/S)$  is only realized by using another sorbent type with a higher maximum conversion.

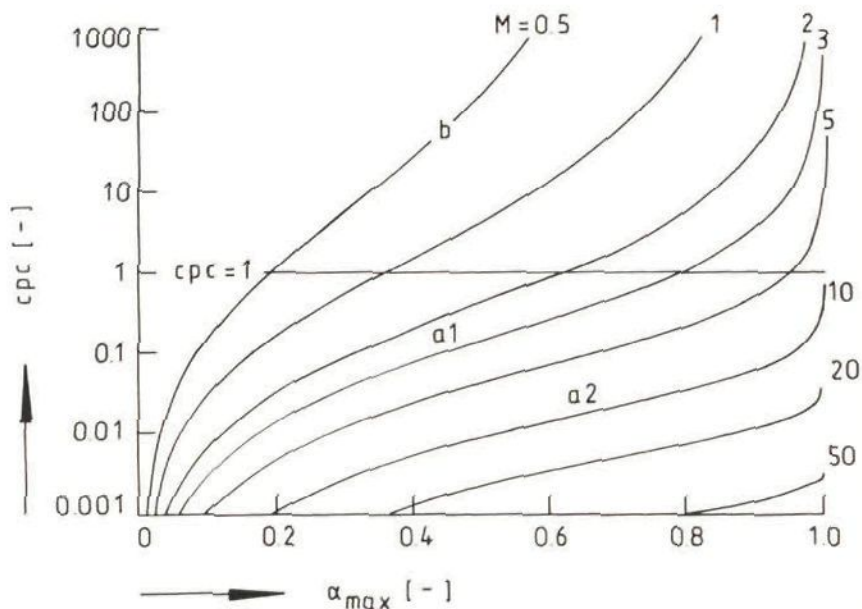


Figure 21: The choice of parameter change  $cpc$ , Eq.[39], as a function of the maximum CaO conversion  $\alpha_{max}$  at different values of the retention parameter  $M$ ; three data-sets derived from experimental data of Lee and Georgakis (1981), a1 and a2, and of Zheng et al. (1982), b, have been indicated.

## 8. CONCLUSIONS

The following conclusions have been obtained:

1. The simple sulfation kinetic term agrees well with CaO conversion data obtained from Borgwardt (1970) and Borgwardt and Harvey (1972).
2. The one-phase SURE model fits experimental data of CaO conversion and sulfur breakthrough in fluid beds obtained from Spitsbergen et al. (1982), Zheng et al. (1982), Noordergraaf (1985) and Dennis and Fieldes (1986) rather good.
3. Also good fits are derived between the one-phase SURE model and (Ca/S) ratios at different levels of retention obtained from Lee and Georgakis (1981), Zheng et al. (1982), Ekinci et al. (1982) and Fee et al. (1983).
4. The one-phase SURE model gives realistic predictions of the  $SO_2$  sulfation kinetic rate constant (varying between 40 and 700 mm/s), the maximum CaO conversion (in general 0.3 to 0.7 [-]) and the sorbent residence time.

5. The model parameter sensitivity analysis shows that it will strongly depend on the actual combustor conditions which fluid dynamical model (one or two-phase) will provide the best prediction of the (Ca/S) ratio at a required level of retention. In general it is concluded that at relatively high levels of gas exchange between the bubble and dense phase ( $N_0 \gg 2 [-]$ ) both models will give almost the same outcomes (because then  $m \rightarrow 1 [-]$ ).
6. The sensitivity analysis makes further clear that the retention in a fluid bed coal combustor cannot always continuously be increased by enlarging the amount of active sorbent in the bed. This implies e.g. that at a certain level of maximum CaO conversion no significant increase in the sulfur retention at a fixed (Ca/S) ratio can be obtained by increasing the maximum sorbent utilization in the reactor (for example by using another sorbent type).
7. The influence of the sorbent residence time, the sorbent particle size and the superficial gas velocity on sulfur retention is very good qualitatively predicted by the one-phase SURE model. It is discussed that the sorbent residence time and particle size are both influenced by the recycle of cyclone catch, which combined effect will increase the sulfur retention.
8. A detailed examination of the retention index, used for the optimization of sulfur retention, shows that at a value of the retention parameter M higher than 5 generally only improvement of the (Ca/S) ratio is obtained by increasing the maximum sorbent conversion.
9. Finally, it may be stated that the SURE model can be used as a diagnostic tool for analysis of operational data as well as a predictive tool for analysis of plants under construction or design. However, it is advisable that the direct predictive capacity of the SURE model will be determined by a detailed validation against experimental retention results of different FBC units.

#### APPENDIX 1: THE MODEL PARAMETERS

##### 1. Maximum gas exchange ratio $P_0$

The maximum gas exchange ratio  $P_0$  is defined by Schouten and Van den Bleek (1986) and equals the ratio between the maximum gas flow transferred between gas phase and sorbent surface and the total gas flow in the bed:

$$P_0 = \frac{k S_A}{U_0 F} = \frac{k \alpha_{\max} S_A}{U_0 F} \quad [A1.1]$$

For practical purposes the maximum gas exchange ratio will also be given as:

$$P_o = \frac{k a_o H}{U_o} = \frac{k \alpha_{\max} a_A}{U_o} \quad [A1.2]$$

where  $a_o$  is the initial sorbent interfacial area ( $m^2$  initial sorbent surface per  $m^3$  total reactor volume). In agreement with the definition of the sulfation rate parameter  $k$ , that is based on the particle outer surface area,  $a_o$  is derived from the outer surface area of spherical particles as:

$$a_o = \frac{6 W_o}{d_o \rho_o HF} = \frac{6 \alpha_{\max} W_A}{d_o \rho_o HF} \quad [A1.3]$$

where  $d_o$  is the initial average sorbent particle diameter,  $\rho_o$  is the initial sorbent density and  $W_o$  is the initial mass of sorbent in the bed.

$k$  is the overall sulfation rate parameter which can be a combination of mass transfer limitations and sulfation kinetics. Dennis and Fieldes (1986) concluded that the effect of external mass transfer resistance from the bulk gas to the surface of the limestone particle is of importance, especially at early times in the sulfation reaction. In general the mass transfer coefficient  $k_g$  is of the order 0.2 - 0.6 m/s considering the range of typical particle diameters used in fluidized bed desulfurization (500  $\mu m$  - 2000  $\mu m$ ).  $k_g$  is calculated from the appropriate Sherwood number as:

$$k_g = Sh D / d_o \quad [A1.4]$$

The rate konstant  $k_s$  for the sulfation reaction  $CaO + SO_2 + 1/2 O_2 + CaSO_4$  varies between about 40 mm/s and 700 mm/s as is discussed in section 5.1 and 5.2. Actually  $k_s$  represents intrinsic kinetics at the reaction site plus intraparticle mass transfer phenomena (as pore and product layer diffusion). An average value of 200 mm/s will be used in the respective model calculations (for example in sections 5.3 and 6.4). This value implies that the overall sulfation rate parameter,  $k$ , generally varies between about 100 mm/s and 150 mm/s, where  $k$  is calculated from:  $k = 1/(1/k_g + 1/k_s)$ . E.g. Dennis and Fieldes (1986) reported values of  $k$  between 113 and 161 mm/s.

With combination of Eq.[A1.2]...[A1.4]  $P_o$  is finally written as:

$$P_o = \left[ \frac{d_o}{Sh D} + \frac{1}{k_s} \right]^{-1} \left[ \frac{6 \alpha_{\max} W_A}{\rho_o d_o U_o F} \right] \quad [A1.5]$$

The Sherwood number is obtained from the 'gas renewal theory' of LaNauze (1985):

$$Sh = 2 \epsilon_{mf} + \left[ \frac{4 \epsilon_{mf} d_o (U_{mf}/\epsilon_{mf} + u_b)}{\pi D} \right]^{1/2} \quad \text{when } d_o/d_p > = 3-5 \quad [A1.6]$$

and:

$$Sh = 2 \epsilon_{mf} + \left[ \frac{4 d_o U_{mf}}{\pi D} \right]^{1/2} \quad \text{when } d_o/d_p < 3 \quad [A1.7]$$

The bubble rise velocity  $u_b$  is obtained from the relation proposed by Weimer and Clough (1983):

$$u_b = C (U_o - U_e) + 0.71 \left[ g d_b \frac{(\rho_p - \rho_g)}{\rho_p} (1 - \epsilon_b) \right]^{1/2} \quad [A1.8]$$

C is a distribution coefficient that is related to the degree of uniformity of the bubble volume fraction over the bed cross section; Weimer and Clough (1983) give averages values of  $C = 1.29 - 1.39$ . Here  $C = 1.35$  is suggested.

$$\text{The bubble fraction } \epsilon_b \text{ is given by: } \epsilon_b = 1 - H_{mf}/H \quad [A1.9]$$

The average expanded bed height H is given by an empirical correlation of Babu et al. (1978):

$$H / H_{mf} = 1 + \left[ \frac{1.9544 (U_o - U_{mf})^{0.738} d_p^{1.006} \rho_p^{0.736}}{U_{mf}^{0.937} \rho_g^{0.126}} \right] \text{ (c.g.s.)} \quad [A1.10]$$

The emulsion phase gas velocity  $U_e$  is not always equal to the minimum fluidization velocity  $U_{mf}$ , but it can be increased owing to the flow of gas between neighbouring bubbles, leading to an average particulate phase superficial gas velocity as given by Clift et al. (1983):

$$U_e = U_{mf} \left[ 1 + 1.5 (\epsilon_b)^{2/3} \right] \quad [A1.11]$$

However, this effect is not always taken into account in the derivation of other parameters as for example the gas exchange coefficient. Therefore it is assumed here that still  $U_e = U_{mf}$ .

The minimum fluidization velocity  $U_{mf}$  is evaluated from the correlation given by Wen and Yu (1966):

$$U_{mf} = \frac{\mu}{\rho_g d_p} \left[ \left\{ (33.7)^2 + 0.0408 Ar \right\}^{1/2} - 33.7 \right] \quad [A1.12]$$

$$\text{with the Archimedes number: } Ar = \left[ \frac{d_p^3 \rho_g (\rho_p - \rho_g) g}{\mu^2} \right] \quad [A1.13]$$



The bubble size  $d_b$  increases with increasing gas flow and increasing height above the distributor. Many relations have been derived for the bubble diameter in small particle systems, e.g. Mori and Wen (1975). However, these small particle correlations largely underpredict the bubble size for large particle systems as is indicated by Glicksman et al. (1981).

Furthermore the presence of heat exchanger tubes in FBC units is also a complicating feature. These internals influence the fluidization behaviour, which sometimes changes to slugging, and they inhibit the growth of bubbles or may even act as a bubble splitter in the case of horizontal tubes, while they promote the occurrence of bubble chains between the pipes in the case of vertical tubes (Kool (1985); Noordergraaf et al. (1987)). Kool (1985) showed that the relation of Yacono and Angelino (1978) can be used for large particle systems. The average bubble diameter according to this relation is given by:

$$d_b = 1.75 \beta (U_o - U_e) H^{3/4} \quad \text{with } 0.28 < \beta < 1.2 ; \quad d_b \leq d_{\max} \quad [\text{A1.14}]$$

$d_{\max}$  is the maximum bubble size which can be approximated by the pitch between the pipes, which is in general about 10 cm.

## 2. Two-phase gas flow parameter m

The two-phase gas flow parameter  $m$  is defined as:

$$m = 1 - u \exp[ - N_o / u ] \quad [\text{A1.15}]$$

The dimensionless excess gas velocity in the bubble phase,  $u$ , is obtained from:

$$u = 1 - U_e / U_o \quad [\text{A1.16}]$$

with  $U_e = U_{mf}$ . The minimum fluidization velocity is calculated from the correlation of Wen and Yu (1966), Eq.[A1.12].

$$\text{The number of transfer units } N_o \text{ is defined by: } N_o = H K / U_o \quad [\text{A1.17}]$$

where the average expanded bed height  $H$  is obtained from the correlation of Babu et al. (1978), Eq.[A1.10]. The mass transfer coefficient  $K$  is related to the mass transfer coefficient  $K_{be}$  based on the bubble volume according to:

$$K = \epsilon_b K_{be} \quad [\text{A1.18}]$$

Yates (1983) has reviewed the available expressions for the interchange coefficient  $K_{be}$  and recommends the use of the expression developed by Sit and Grace (1981):

$$K_{be} = \frac{1.5 U_{mf}}{d_b} + \frac{12}{d_b^{3/2}} \left[ \frac{D \epsilon_{mf} u_b}{\pi} \right]^{1/2} \quad [A1.19]$$

### 3. Retention parameter M

M is a model parameter that contains parameters determined by the fluid bed reactor dimensions (F), the fluidizing conditions ( $\tau_s, U_o$ ), the required coal feed rate ( $\phi_s$ ) as well as by the sorbent applied (q); the parameter k can be a combination of mass transfer limitations ( $k_g$ ) and sulfation kinetics ( $k_s$ ):

$$M = \frac{k \tau_s \phi_s}{U_o F q} \quad [A1.20]$$

In agreement with the definitions of  $k_g$  and  $k_s$ , which are based on the volume of gas exchanged between bulk gas and the particle outer surface, it is clear that the molar surface concentration q should also be based on the particle outer surface area according to:

$$q = \frac{\text{moles of CaO in a particle}}{\text{particle outer surface area}} = \frac{W_{CaCO_3} \cdot 1000 / M_{CaCO_3}}{\pi d_o^2} = (5/3) x_{CaCO_3} \rho_o d_o \quad [A1.21]$$

The sorbent residence time is a parameter which is not easy to obtain. However, it can be approximated by the average residence time of all solids in the bed:

$$\tau_s = W_{bed} / \phi_{solids} \quad [A1.22]$$

The molar sulfur feed rate  $\phi_s$  is simply calculated from the coal feed rate according to:

$$\phi_s = (10/32) x_s \phi_{coal} \quad (x_s \text{ in wt.}\%) \quad [A1.23]$$

The retention parameter M is subsequently derived from :

$$M = \frac{3}{5} \left[ \frac{d_p}{Sh D} + \frac{1}{k_s} \right]^{-1} \left[ \frac{\tau_s \phi_s}{x_{CaCO_3} \rho_o d_o U_o F} \right] \quad [A1.24]$$

#### 4. Maximum CaO conversion $\alpha_{\max}$

The sulfation of sorbent material is a complex coupling of chemical reactions with the mass transport through a time-varying porous structure. The molar volume of the reaction product  $\text{CaSO}_4$  is sufficiently large that the pores of the CaO may completely plug prior to total CaO utilization. Many models describe this process, see e.g. Simons and Garman (1986). In their pore plugging model they derived an equation for the maximum CaO conversion, which is a function of the sorbent initial porosity. This equation can be used to calculate  $\alpha_{\max}$  in the case of pore plugging:

$$\alpha_{\max} = [1/(z-1)] [\epsilon_p^0 / (1-\epsilon_p^0)] \quad [\text{A1.25}]$$

$z$  is the ratio between the molar volumes of the reaction product  $\text{CaSO}_4$  and the reactant CaO ( $z = 3.06$ ).  $\epsilon_p^0$  is the initial porosity of the calcined sorbent.

#### 5. Magnitude of model parameters

Proceeding with the relations given above characteristic values of the respective model parameters will be calculated in order to carry out a model sensitivity analysis. The calculation of the respective model parameters is based on realistic values of fluid bed combustor dimensions, fluidizing conditions and sorbent properties. The data are summarized in Table A1.

Because sulfur breakthrough experiments are in general carried out with an interfacial sorbent surface ( $1-10 \text{ m}^2/\text{m}^3$ ) which is much smaller than the interfacial sorbent surface available during steady combustor operation ( $> 1000 \text{ m}^2/\text{m}^3$ ) this lower value will be used for the sensitivity analysis of the unsteady state models.

Using the data in Table A1 and the equations given above it can be estimated that in general the model parameters range between:

$$P_0: 0.5 - 5 [-]; \quad N_0: 0.5 - 3 [-]; \quad u > 0.6 [-];$$

$$m: 0.5 - 1 [-]; \quad M: 0.5 - 50 [-]; \quad \alpha_{\max}: 0.2 - 0.8 [-].$$

Table A1: Average combustor operating conditions and sorbent properties.

Combustor operating conditions		Sorbent properties
$H_{mf}$ : 0.3 m	$\epsilon_{mf}$ : 0.43 [-]	$d_o$ : 0.5 - 2 mm
$U_o$ : 1 - 3 m/s	$T$ : 850 °C	$\rho_o$ : 2700 kg/m <sup>3</sup>
$\phi_S/F$ : 0.01 - 0.05 mol/s/m <sup>2</sup>		$\epsilon_p^o$ : 0.4 - 0.6 [-]
$d_p$ : 0.5 - 2 mm	$\rho_p$ : 2600 kg/m <sup>3</sup>	$x_{CaCO_3}$ : 0.95 [-]
$a_o$ : 1 - 10 m <sup>2</sup> /m <sup>3</sup> (calculation of $P_o$ )		
$\tau_S$ : > (>>) 1 hr		

## APPENDIX 2: MODEL LIMITATION DUE TO OXYGEN CONSUMPTION

It is obvious that the role of oxygen has not been taken into account in the sulfur capture kinetic equations as applied in the SURE models. The reaction is considered to be of zero order in oxygen. This implies that it is assumed that there are no limitations to the supply of oxygen. However, situations can exist where this is not the case. For example when under steady state operation the feed rate of coal is very high almost all oxygen supplied will be used for the combustion of volatiles and char, while few oxygen remains for the capture reaction. Therefore a condition has to be derived, which relates the level of retention to the coal feed rate and according to which the models can be correctly applied. Hereto the overall oxygen balance is formulated as:

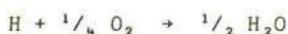
$$\{\text{oxygen out of reactor}\} = \{\text{oxygen input}\} - \{\text{oxygen consumed by reaction}\}$$

$$\{\text{oxygen out of reactor (O}_2)\} = \{ U_o F c_{\text{uit}} \}$$

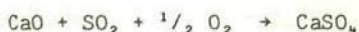
$$\{\text{oxygen input}\} = \{ U_o F c_{\text{in}} + 1/2 \phi_O \}$$

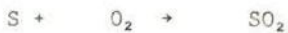
The oxygen consumed by reaction is based on complete combustion of the coal components C, H, N and S and on the sulfur capture reaction:

combustion reactions:



sulfur capture reaction:





$$\text{So: } \{ \text{oxygen consumed by reaction} \} = \{ \phi_C + 1/4 \phi_H + \phi_N + \phi_S + 1/2 \alpha_{\text{avg}} \phi_{\text{Ca}} \}$$

$$\text{Further: } \alpha_{\text{avg}} \phi_{\text{Ca}} = \alpha_{\text{avg}} (\text{Ca/S}) \phi_S = R \phi_S$$

Substitution of the respective parts of the balance in the overall oxygen balance gives:

$$\eta = \frac{c_{\text{in}} - c_{\text{uit}}}{c_{\text{in}}} = \frac{\phi_S (1+R/2) + \phi_C + \phi_N + 1/4 \phi_H - 1/2 \phi_O}{U_o F c_{\text{in}}}, \text{ with } 0 \leq \eta \leq 1$$

If all oxygen is consumed then  $\eta = 1$ . Because it is obvious that always  $\eta \geq 0$ , the condition can be formulated as follows:  $\eta < 1$ . Rearranging of the above equation leads subsequently to the condition:

$$R < \Delta = 2 * \left\{ \left[ \frac{U_o F c_{\text{in}}}{\phi_S} + 1/2 \frac{\phi_O}{\phi_S} - 1 \right] - \left[ \frac{\phi_C}{\phi_S} + \frac{\phi_N}{\phi_S} + 1/4 \frac{\phi_H}{\phi_S} \right] \right\} \quad [\text{A2.1}]$$

In general this condition is easily met under practical oxidizing conditions (excess air  $> 1$ ) as is illustrated for example in Table A2 in the case of an experiment in the 4 MW<sub>th</sub> TNO AFBB facility (Brem, 1986).

However, at small excess air ratios ( $\approx 1$ ) this condition becomes important, where at values smaller than 1 (sub-stoichiometric firing) next to SO<sub>2</sub> also reduced sulfur species like H<sub>2</sub>S and COS may be formed.

Table A2: The model condition  $\Delta$  (Eq.[A2.1]) in the case of an experiment (nr. 97) in the 4 MW<sub>th</sub> TNO AFBB facility (Brem, 1986).

$U_o = 2.0 \text{ m/s}$	$(\text{Ca/S}) = 1.9 \text{ [-]}$	American coal (Virg):
$F = 2.25 \text{ m}^2$	$R = 0.71 \text{ [-]}$	$\phi_S = 0.0608 \text{ mol/s}$
$H = 1.07 \text{ m}$		$\phi_O/\phi_S = 8.2 \text{ [-]}$
$T = 1115 \text{ K}$		$\phi_C/\phi_S = 47.2 \text{ [-]}$
$p = 1.0 \text{ atm}$		$\phi_H/\phi_S = 87.5 \text{ [-]}$
$c_{\text{in}} = 2.29 \text{ mol/m}^3$		$\phi_N/\phi_S = 2.1 \text{ [-]}$
Model condition (given by Eq.[A2.1]): $\Delta = 2 * 101.7$ ; so: $R \ll \Delta$		

## 2.3 The INFLUENCE of OXYGEN-STOICHIOMETRY on DESULFURIZATION during FBC:

### a SIMPLE SURE MODELING APPROACH

submitted for presentation at the 10th Int. Symp. on  
Chemical Reaction Engineering, ISCRE 10,  
Basle, Switzerland, August 29 - September 1, 1988

SUMMARY	64
1. INTRODUCTION	64
1.1 Sulfur retention during FBC	64
1.2 Effect of the air ratio on desulfurization	65
1.3 Role of oxygen in the sulfation mechanism: SO <sub>3</sub> formation	65
2. THE Sulfur RETention MODEL	66
2.1 SURE model assumptions	66
2.2 SURE model mass balances	67
2.3 Oxygen concentration	68
2.4 (Ca/S) ratio	69
3. COMPARISON WITH EXPERIMENTAL DATA	72
3.1 Oxygen concentration	72
3.2 Sensitivity analysis: influence of $\lambda$ on retention	72
3.3 Diagnostic evaluation of model and experiments: the sorbent residence time	73
4. CONCLUSION	76
APPENDIX 1	76
APPENDIX 2	77

# The INFLUENCE of OXYGEN-STOICHIOMETRY on DESULFURIZATION during FBC:

## a SIMPLE SURE MODELING APPROACH

J.C. Schouten and C.M. van den Bleek

### SUMMARY

In this paper an extension is presented of the simple Sulfur Retention SURE model which was published earlier by the authors (Schouten and Van den Bleek, 1987). The present model explains the effect of a decreasing desulfurization efficiency during staged Fluidized Bed Combustion of coal by the relatively fast formation of  $SO_3$  as a gaseous intermediate reactant in the sorbent sulfation reaction. The SURE model provides an analytical expression for the molar (Ca/S) ratio in the reactor feed as a function of the degree of sulfur retention, the maximum sorbent conversion and three dimensionless model parameters. These parameters are functions of fluid bed operating conditions, coal and sorbent properties and the stoichiometric air ratio.

It is shown that the oxygen concentration and the decrease in sulfur retention at lower stoichiometric air ratios can readily be described by the model equations.

Furthermore, the SURE model is applied as a diagnostic tool for the analysis of plant operational data obtained from the recent literature. It is concluded from an evaluation of SURE model calculations and experimental data that the sorbent residence time is a crucial system parameter. It is demonstrated that the observed neglect of the influence of the sorbent residence time on the steady state character of many retention experimentations gives rise to serious doubt on the reliability and usefulness of these measurements for model verification purposes.

### 1. INTRODUCTION

#### 1.1 Sulfur retention during FBC

One of the advantages of the fluidized bed coal combustion technique is the possibility of the in-situ removal of sulfur, released from coal, by addition of a natural (limestone or dolomite) or a synthetic sorbent material. The main fluid bed reactor quantities that influence the degree of desulfurization are respectively: the sorbent residence time (Van den Bleek and Schouten, 1987), the superficial gas velocity, the bed temperature and the mass transfer coefficient in the dense phase. The main sorbent properties are respectively: the average sorbent particle diameter, the maximum sorbent CaO conversion and the sulfation kinetic rate constant. The most important system parameter is, of course, the (Ca/S) molar ratio in the reactor feed (Schouten and Van den Bleek, 1987).

Research activities on emissions from fluid bed coal combustors are more and more concerned with the reduction of  $NO_x$ -emissions by means of staged (sub-stoichiometric) combustion. However,  $SO_x$ - and  $NO_x$ -emissions are found to be strongly interrelated: in general  $SO_x$ -emissions increase with a lower

primary air ratio (e.g. Valk et al., 1987), while  $\text{NO}_x$ -emissions may increase with a higher sorbent hold-up and a lower sorbent fractional sulfation (e.g. Hirama et al., 1987). It is remarkable that none of the main overall FBC sulfur retention models in literature, as summarized by Schouten and Van den Bleek (1987), incorporate these effects of oxygen on the sulfation reaction. This is mainly due to the fact that these models are applied to describe FBC desulfurization in case of relatively high air ratios ( $\lambda > 1.2$ ) where the influence of the high oxygen concentration in the bed on the extent of sulfur capture is small or even negligible.

Therefore in this paper an extension is presented of the earlier published simple FBC Sulfur RETention (SURE) model (Schouten and Van den Bleek, 1987), which now includes the effect of oxygen on the degree of sulfur capture. First, a survey will be given of some literature results so as to conclude what the effect of oxygen and its role in the sulfation mechanism may be.

### 1.2 Effect of the air ratio on desulfurization

For example, the effect of excess air is demonstrated by Terada et al. (1982): they showed in a experimental study on two-stage combustion that this technique is very effective to reduce the  $\text{NO}_x$ -emission. They reported a decrease in the  $\text{NO}_x$ -emission from about 240 ppm to less than 100 ppm when the in-bed air ratio was decreased from about 1.05 to 0.88 (3.3 to 3.6%  $\text{O}_2$  in flue gas). At the same time the  $\text{SO}_x$ -retention decreased from about 95% to less than 90% at a relatively high (Ca/S) ratio of 5.

A same effect was observed by Inoue et al. (1982): reduction of the in-bed air ratio from 1.0 to 0.9 caused a drop of the desulfurization efficiency of about 5%.

Valk et al. (1987) reported a more significant decrease in the extent of sulfur capture: the  $\text{SO}_2$  emission almost doubled when the primary air stoichiometry is reduced from 1.1 to 0.6. Further they concluded from analysis of bed, cyclone and baghouse filter material that the main sulfation reaction product is  $\text{CaSO}_4$ ; even at the lowest air level of 0.6 no reaction product as CaS was formed due to the capture of reduced sulfur species like  $\text{H}_2\text{S}$ .

### 1.3 Role of oxygen in the sulfation mechanism: $\text{SO}_3$ formation

Fieldes et al. (1979) reported that the maximum conversion of limestone particles in a fluidized bed is influenced by the concentration of  $\text{SO}_2$  as well as of  $\text{O}_2$  in the inlet gas. A plausible explanation is provided by Burdett (1980) who demonstrated the maximum sulfation capacity to be



dependent on the concentration of  $\text{SO}_3$  in the reactor.  $\text{SO}_3$  is an important intermediate gaseous reactant in the sulfation reaction according to:



Burdett (1980) showed that the maximum conversion of limestone sulfated with 435 vpm  $\text{SO}_2$  at 810 °C is comparable to that measured with 500 vpm  $\text{SO}_2$  with 2%  $\text{O}_2$  at the same temperature. Burdett et al. (1983) concluded that the maximum concentration of  $\text{SO}_3$  in the combustor is governed by thermodynamic considerations; the equilibrium conversion of  $\text{SO}_2$  to  $\text{SO}_3$  increases with rising pressure and falling temperature. At 850 °C and 10%  $\text{O}_2$  in the flue gas, a potential exists for about 15% of the sulfur dioxide to be present as  $\text{SO}_3$  at atmospheric pressure, but this increases up to 44% at 20 bar. They concluded that also the reaction rates are sufficiently high at the temperatures in question for FBC to consider  $\text{SO}_3$  present. They measured representative steady state  $\text{SO}_3$  concentrations corresponding to a degree of oxidation of  $\text{SO}_2$  of about 2 to 3%.

In recent work it has been shown that the effect of oxygen on the sulfation of a synthetic CaO sorbent material in a fixed bed reactor can very well be explained by the formation of  $\text{SO}_3$  (Valkenburg et al., 1987). Model predictions based on this approach showed to be in good agreement with experiments. Therefore this ' $\text{SO}_3$ -explanation' of the oxygen influence will be adopted here as a basis for the extension of the SURE model. First, a summary of the main model assumptions and mass balances will be given.

## 2. THE SULFUR RETENTION MODEL

### 2.1 SURE model assumptions

1. The choice of the type of fluid-dynamical reactor model is strongly dependent on the mode of fluidization and gas transport that is present in a fluid bed coal combustor.

Recently, Almstedt (1987) and Almstedt and Ljungström (1987) demonstrated with capacitance and oxygen probe measurements that the visible bubble flow rate in a FBC combustor is much smaller than predicted by the two-phase theory of fluidization. This is a result of the bubble growth and rise velocity being limited by the horizontal in-bed cooling tubes giving the bed a slugging fluid-dynamical character. This in turn causes a significant amount of the gas to pass the bed as a through-flow through the bubbles (or gas slugs) and through the dense phase between the vertically aligned bubbles. Further no variation in the oxygen

concentration due to the presence of bubbles can be seen caused by the rapid inter-phase gas exchange which results in a high and even oxygen concentration throughout the bed.

Consequently, in the present paper the one-phase ideally mixed gas flow model (ISTR) will be applied, which corresponds with these experimental results.

2. Furthermore, the solids are assumed to be ideally mixed due to the relatively high sorbent residence time with respect to the gas residence time; particles are spherical and of uniform size.
3. Elutriation and freeboard phenomena are not taken into account.
4. The coal combustion rate is assumed to be first order in the oxygen concentration and first order in the total external reactive coal surface area.
5. The sorbent CaO sulfation rate is first order in the gaseous sulfur  $SO_2$  concentration and first order in the total external reactive sorbent surface area.
6. Finally, it is assumed that the rate of  $SO_3$  formation is high.

## 2.2 SURE model mass balances

The conversion of freshly added coal to the reactor is obtained from the following coal mass balance: (coal accumulation) = ( $O_2$  conversion);

$$\zeta_1 q_1 \frac{d-S_1(t)}{dt} = -k_1 S_1(t) c_1 \quad [1]$$

The conversion of freshly added sorbent to the reactor under steady state conditions (constant concentrations) is obtained from the following CaO mass balance: (CaO accumulation) = ( $SO_3$  conversion);

$$\zeta_3 q_3 \frac{d-S_3(t)}{dt} = -k_3 S_3(t) c_3 \quad [2]$$

The oxygen mass balance is given as: (oxygen out) = + (oxygen in) - (oxygen consumed by coal combustion) - (oxygen consumed by  $SO_3$  formation). This leads to the following expression:

$$\phi_V c_1 = \phi_V c_{in} - k_1 S_1 c_1 - 1/2 (k_1 c_2 c_1^{1/2} - k_1/K_0 c_3) \epsilon V \quad [3]$$

It is clear that the magnitude of the oxygen consumption in the reactor is predominantly determined by the extent of coal combustion; therefore in the subsequent model derivation the following assumption is applied:

$$k_1 S_1 c_1 \gg \frac{1}{2} (\kappa_1 c_2 c_1^{1/2} - \kappa_1/K_0 c_3) \epsilon V \quad [4]$$

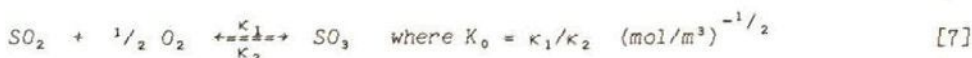
The SO<sub>2</sub> mass balance reads: (SO<sub>2</sub> out) = + (SO<sub>2</sub> in) - (SO<sub>2</sub> consumed by SO<sub>3</sub> formation reaction), resulting in:

$$\phi_V c_2 = \phi_S - (\kappa_1 c_2 c_1^{1/2} - \kappa_1/K_0 c_3) \epsilon V \quad [5]$$

The SO<sub>3</sub> mass balance is obtained as: (SO<sub>3</sub> out) = + (SO<sub>3</sub> produced) - (SO<sub>3</sub> consumed by sorbent sulfation reaction), which results in:

$$\phi_V c_3 = (\kappa_1 c_2 c_1^{1/2} - \kappa_1/K_0 c_3) \epsilon V - k_3 S_3 c_3 \quad [6]$$

The gaseous SO<sub>3</sub> is formed by the following equilibrium reaction:



The equilibrium constant K<sub>0</sub> is calculated from the relation of Meyer (1977):

$$\log K_p = (5022/T) - 4.765 \quad \text{where: } K_p = p_{SO_3} / (p_{SO_2} p_{O_2}^{1/2}) \quad (\text{atm}^{-1/2}) \quad [8]$$

### 2.3 Oxygen concentration

The conversion of freshly added coal in the reactor as a function of time is obtained from the coal mass balance as given in Eq.[1]. At steady state operation the oxygen concentration can be assumed to be constant; consequently the fractional reactive external surface area of the coal as a function of time is obtained as:

$$\sigma_1(t) = \exp\left[-\frac{k_1 - c_1}{\zeta_1 q_1} t\right] \quad [9]$$

$\sigma_1(t)$  is defined as  $S_1(t)/S_{1,0}$ , where  $S_{1,0}$  is the initial total available reactive coal surface area which, theoretically, is equal to the average coal surface area in the bed when no reaction takes place.

The average fractional reactive coal surface area in the bed is calculated with the coal residence time distribution function according to:

$$\sigma_{1,avg} = \int_0^{\infty} E_1(t) \sigma_1(t) dt \quad [10]$$

The residence time distribution function of solids in a fluid bed is determined by Yagi and Kunii (1961) to be equal to that of an ideally stirred tank reactor:

$$E_1(t) = [1/\tau_1] \exp[-t/\tau_1] \quad [11]$$

The solids residence time  $\tau_1$  of the coal can be approximated by:

$$\tau_1 = [q_1 S_{10}] / \phi_C \quad [12]$$

Furthermore, the dimensionless stoichiometric parameter  $\nabla$  is introduced, which is a function of the stoichiometric air ratio  $\lambda$  and is given as:

$$\nabla = [1-\lambda] / \lambda \quad [13]$$

In this equation the stoichiometric air ratio  $\lambda$  is defined by:

$$\lambda = [\phi_v c_{in}] / \phi_C \quad [14]$$

Combination of Eqs.[9]..[14] and the  $O_2$  mass balance leads finally to an expression for the steady state oxygen concentration  $c_1$  in the reactor:

$$c_1 = 1/2 \left( \left[ \{c_0 + \nabla c_{in}\}^2 + 4 c_0 c_{in} \right]^{1/2} - (c_0 + \nabla c_{in}) \right) \quad [15]$$

The parameter  $c_0$  in this equation is defined as the 'equivalent oxygen concentration', because  $c_0 = c_1$  when  $c_0 = 0$  at  $\lambda = 1$ , and is obtained from the following expression:

$$c_0 = [\zeta_1 q_1] / [k_1 \tau_1] \quad [16]$$

Theoretically,  $c_0$  provides a measure for the extent of (in)complete coal combustion. For example, incomplete coal combustion due to a high elutriation rate (low  $\tau_1$ ) in combination with a low coal combustion rate (low  $k_1$ ), leads to a high value of  $c_0$ . In appendix 1 equations are given so as to calculate  $c_0$  from coal and fluid bed system properties.

#### 2.4 (Ca/S) ratio

According to a symmetric reasoning as applied in section 2.3 the conversion of freshly added sorbent in the reactor as a function of time is obtained from the sorbent mass balance as provided in Eq.[2]. At steady state operation the gaseous sulfur species concentration is assumed to be constant, consequently the fractional reactive sorbent surface area as a function of time is obtained as:

$$\sigma_3(t) = \exp\left[-\frac{k_3 - C_3}{\zeta_3 q_3} t\right] \quad [17]$$

The average fractional sorbent surface area is subsequently derived from:

$$\sigma_{3,avg} = \int_0^{\tau_0} E_3(t) \sigma_3(t) dt \quad [18]$$

The sorbent residence time distribution equals:

$$E_3(t) = [1/\tau_3] \exp[-t/\tau_3] \quad [19]$$

$$\text{with the residence time being given by: } \tau_3 = [q_3 S_{30}] / [\alpha_{max} \phi_{Ca}] \quad [20]$$

Furthermore,  $\tau_0$  in Eq.[18] is the maximum possible sulfation reaction time, which equals for example the pore plugging time when the sulfation reaction product blocks the pores prior to total conversion of CaO. It should be noticed that no reactive sorbent surface is present at  $t > \tau_0$  and therefore  $\sigma_3(t > \tau_0) = 0$ . The minimum attainable fractional reactive sorbent surface area is subsequently defined by:

$$\sigma_{3,min} = \exp\left[-\frac{k_3 - C_3}{\zeta_3 q_3} \tau_0\right] = 1 - \alpha_{max} \quad [21]$$

The average sorbent conversion in the reactor is then derived from:

$$\begin{aligned} \alpha_{3,avg} &= \int_0^{\tau_0} E_3(t) (1 - \sigma_3(t)) dt + \int_{\tau_0}^{\infty} E_3(t) (1 - \sigma_3(\tau_0)) dt = \\ &= (1 - \sigma_{3,avg}) - (1 - \alpha_{max}) \exp[-\tau_0/\tau_3] \end{aligned} \quad [22]$$

The degree of sulfur retention R in the reactor is defined as:

$$R = 1 - (\phi_V c_2) / \phi_S = 1 - \frac{x_1}{x_2} \frac{c_1}{c_{in}} \frac{c_2}{(1+\nu)} \quad [23]$$

while further the molar (Ca/S) ratio in the reactor feed equals:

$$(Ca/S) = \phi_{Ca} / \phi_S \quad [24]$$

Combination of these equations results finally in the following expression for the (Ca/S) ratio as a function of the level of retention R, the maximum CaO conversion  $\alpha_{max}$  and the dimensionless model parameter  $M_0$ :

$$(Ca/S) = R / \alpha_{avg} \quad \text{with: } \alpha_{avg} = \sigma_{3,avg} M_0 [1-R] \quad [25a]$$

$$\text{and: } \sigma_{3, \text{avg}} = \frac{1 - (1 - \alpha_{\text{max}}) \exp\left[-\frac{\ln(1 - \alpha_{\text{max}})}{M_0 [1-R]}\right]}{1 + M_0 [1-R]} \quad [25b]$$

To derive these equations it has been assumed that:

$$R / (\epsilon V \kappa_1) \ll [1-R] c_1^{1/2} / \phi_V \quad [26]$$

which is a valid assumption at a relatively high rate of  $\text{SO}_3$  formation.

The dimensionless model parameter  $M_0$  in Eqs. [25a] and [25b] is defined by:

$$M_0 = \frac{[1+\nabla]}{2} \left[ \left( \{M_1 + \nabla M_2\}^2 + 4 M_1 M_2 \right)^{1/2} - \{M_1 + \nabla M_2\} \right]^{1/2} \quad [27]$$

This parameter incorporates the effect of the oxygen-stoichiometry with:

- the 'stoichiometric parameter  $\nabla$ ', which was defined as (Eq. [13]):

$$\nabla = (1-\lambda)/\lambda \quad [28]$$

Furthermore,  $M_0$  is a function of fluid bed, coal and sorbent properties, which are included in two dimensionless parameters:

- the 'combustion parameter  $M_1$ ', which is defined as:  $M_1 = \mu_0 c_0$  [29]

$$\text{where } \mu_0 = \left[ \frac{k_3 K_0 \tau_3 x_s c_{in}}{(3200/12) \zeta_3 q_3} \right]^2 \text{ and } c_0 = \left[ \frac{\zeta_1 - \theta_1}{k_1 \tau_1} \right] \quad [30]$$

In appendix 2 equations are given so as to calculate  $\mu_0$  from sorbent and fluid bed system properties.

- the 'retention parameter  $M_2$ ', which is defined as:  $M_2 = \mu_0 c_{in}$  [31]

When the maximum CaO conversion in the sorbent equals 1, then the retention  $R$  can be written explicitly as a function of the (Ca/S)-ratio as:

$$R = 1/2 \left[ \left( \frac{M_0 + 1}{M_0} + (\text{Ca/S}) \right) - \left\{ \left( \frac{M_0 + 1}{M_0} + (\text{Ca/S}) \right)^2 - 4 (\text{Ca/S}) \right\}^{1/2} \right] \quad [32]$$

### 3. COMPARISON WITH EXPERIMENTAL DATA

#### 3.1 Oxygen concentration

In Figure 1 a comparison is given between, at the one side, experimental data on the oxygen concentration  $c_1$ , as reported by different authors and, at the other side, the calculated concentration according to Eq.[15]. It is observed that the data of Zakkay et al. (1985) are described by an equivalent oxygen concentration  $c_0$  of 0 vol.%, which corresponds with complete combustion of all coal in the bed ( $\tau_1 \rightarrow \infty$ ). The other experimental data are in agreement with higher values of  $c_0$  (in general smaller than 1 vol.%), which corresponds with incomplete in-bed coal combustion due to elutriation ( $\tau_1$  is relatively small).

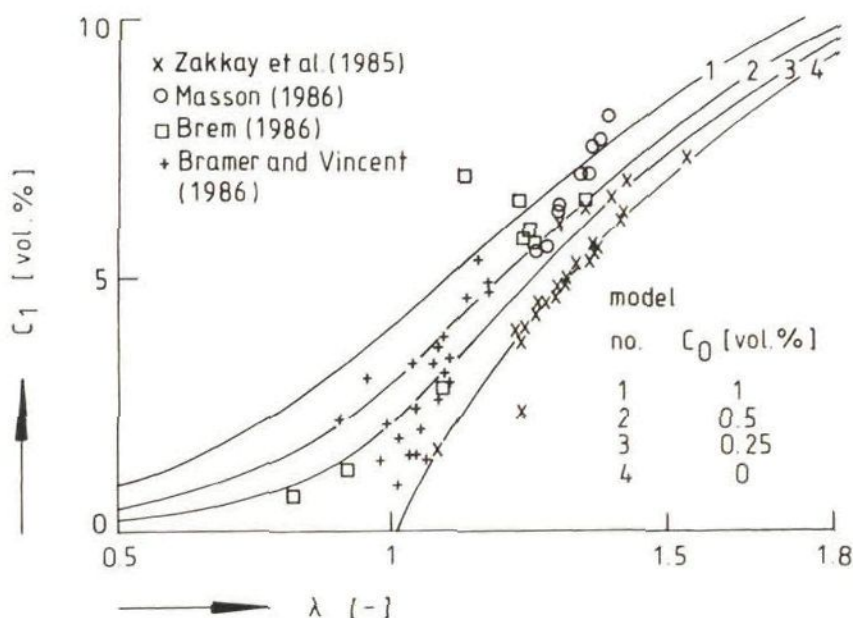


Figure 1: The oxygen concentration  $c_1$  in the reactor outlet as a function of the stoichiometric air ratio  $\lambda$ : a comparison between experimental data and model calculations at different values of the equivalent oxygen concentration  $c_0$ .

#### 3.2 Sensitivity analysis: influence of $\lambda$ on retention

In Figure 2 a plot is given of the level of retention  $R$  as a function of the in-bed air ratio  $\lambda$  at different values of the equivalent oxygen concentration  $c_0$  with common average values for the other main parameters:  $(Ca/S)$

$= 2$ ,  $\alpha_{\max} = 1 [-]$  and  $M_2 = 2.5 [-]$ . From Figure 1 it is concluded that average values of  $c_0$  vary between about 0.1 and 1; this implies that the curves 3 and 4 in Figure 2 give average predictions of the possible effect of oxygen on sulfur retention. In these cases it is observed that the desulfurization efficiency decreases from about 50% at air ratios higher than 1.2 to about 20-35% (or even lower) at air ratios smaller than 0.6. These calculations are qualitatively in good agreement with experimental observations as for example are described in section 1.2.

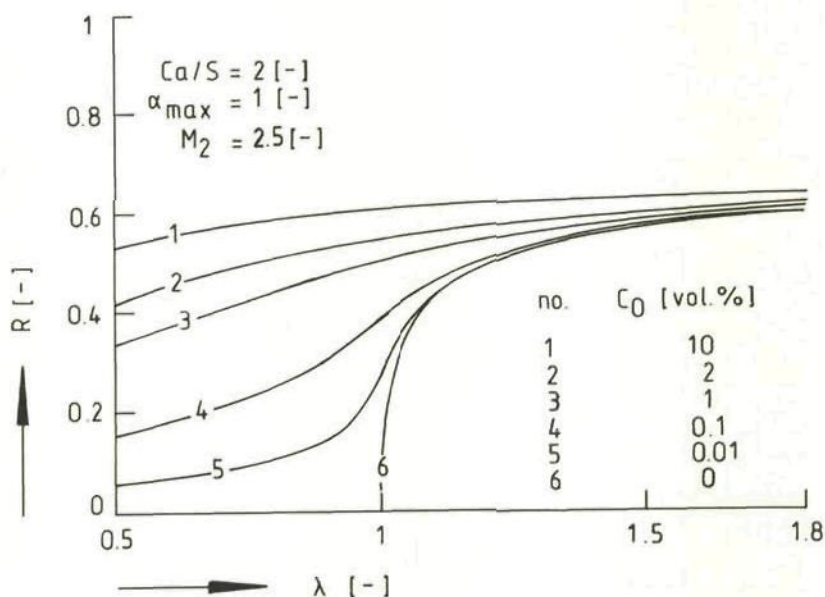


Figure 2: Model sensitivity analysis; the influence of the equivalent oxygen concentration  $c_0$  on the degree of sulfur retention  $R$  as a function of the stoichiometric air ratio  $\lambda$ .

### 3.3 Diagnostic evaluation of model and experiments: the sorbent residence time

In this section the SURE model will be applied as a diagnostic tool for the screening of plant operational data.

An analysis of recent retention data shows that in many cases steady state sulfation data are not reliable, because they were actually obtained at non-steady state conditions due to the fact that during the experimental runs no account was taken of the influence of the sorbent residence time. Due to its rather high value (ranging from about 1 to even over 100 hours (Duqum et al., 1985)) it will take more time than normally expected to reach



a steady state situation after a change in operation conditions. At least 5 times the mean sorbent residence time has to be waited in order to be sure that measurements will not be biased by the history of one (or more) previous experiments. For example, Salib et al. (1987) and Desai et al. (1987) mention maximum experimentation times of, respectively, 14 hours and 17 hours, however, the estimates of the corresponding sorbent residence times are at least, respectively, 50 hours and 10 hours.

This phenomenon will be illustrated in more detail by a comparison of the present SURE model with experimental retention data of Valk et al. (1987) obtained in a 0.6x0.6 m<sup>2</sup> atmospheric facility. An overview of the sorbent and coal properties, the fluid bed properties and the calculated or measured SURE model parameters is given in Table 1.

The equivalent oxygen concentration is taken  $c_o = 0.25 \text{ mol/m}^3$  based on the comparison in Figure 1 of the calculated oxygen concentration  $c_1$  (Eq.[15]) with experimental data of Bramer and Vincent (1986) obtained in the same facility (see also appendix 1).

Table 1: model parameters based on data of Valk et al. (1987).

<u>limestone Carmeuse Engis:</u>		<u>Model parameters:</u>	
$\alpha_{\text{max}}$	= 0.308 [-] (Akse et al., 1983)	$q_3$	= 7 mol/m <sup>2</sup>
$\rho_3$	= 2700 kg/m <sup>3</sup>	$k_{g_3}$	= 0.3 m/s
$d_3$	= 1.62 mm	$k_{s_3}$	= 0.2 m/s
$x_3$	= 0.96 [-]	$K_o$	= 0.154 (m <sup>3</sup> /mol) <sup>1/2</sup>
$\zeta_3$	= 1 [-]		
$k_{s_3}$	= 0.70 m/s (Valkenburg et al., 1987)		
<u>Coal types:</u>	Polish-5:	Br. Marine:	
	$x_s = 0.78 \text{ wt}\%$	$x_s = 0.95 \text{ wt}\%$	
<u>Fluid bed:</u>	H = 1 m	$\phi_v = 0.7 \text{ m}^3/\text{s}$	T = 1123 K
$\epsilon = 0.7$ [-]	F = 0.36 m <sup>2</sup>	$c_{\text{in}} = 2.28 \text{ mol/m}^3$	Sh <sub>3</sub> = 2.5 [-]

No accurate estimate of the sorbent residence time could be made, because no data are available on the volume fraction of sorbent material in the bed. However, the maximum possible sorbent residence time can be readily obtained based on the assumption that all bed material consists of sorbent. This assumption leads to:

$$\tau_3 \leq \frac{\text{total volume of bed material}}{\text{volumetric sorbent feed rate}} = 2000 \left[ \frac{\lambda (1-\epsilon) HF}{(Ca/S) \phi_v c_{in} x_s} \right] \quad [\text{hr}] \quad [33]$$

This equation demonstrates that the sorbent residence time decreases with a decreasing stoichiometric air ratio. Further, using the parameters given in Table 1 (with  $\lambda=1.2$ ), it is easily calculated that in general  $\tau_3 < 140$  hr. This implies that in the realistic case that about half of the bed material consists of sorbent material a relatively high sorbent residence time of about 70 hr will be found (at  $\lambda=1.2$ ).

Subsequently, the sorbent residence time of the experiments of Valk et al. (1987) has been obtained by a fit of the experimental data to the SURE model (Eq.[25]). The results are shown in Table 2.

Table 2: Result of fit of Eq.[25] to experimental data: calculation of  $\tau_3$ .

<u>Coal type: Br. Marine</u>			<u>result of model fit:</u>			
$\lambda$ [-]	R [-]	$\alpha_{\text{avg}} = R/(Ca/S)$	$M_1$ [-]	$M_2$ [-]	$M_0$ [-]	$\tau_3$ [hr]
1.11	0.41	0.273	2.39	21.75	2.40	24.0
1.08	0.39	0.260	1.07	9.77	1.62	16.1
0.93	0.24	0.160	0.034	0.31	0.30	2.9
0.73	0.16	0.107	0.005	0.045	0.15	1.1
0.52	0.16	0.107	0.0063	0.061	0.15	1.3

<u>Coal type: Polish-5</u>			<u>result of model fit:</u>			
$\lambda$ [-]	R [-]	$\alpha_{\text{avg}} = R/(Ca/S)$	$M_1$ [-]	$M_2$ [-]	$M_0$ [-]	$\tau_3$ [hr]
1.2	0.50	0.333	-	-	-	> 140
1.1	0.55	0.367	-	-	-	> 140
1.02	0.45	0.300	-	-	-	> 140
1.01	0.45	0.300	-	-	-	> 140
1.01	0.41	0.273	2.26	20.59	2.40	28.5
0.88	0.36	0.240	0.39	3.57	1.03	11.9
0.83	0.27	0.180	0.055	0.51	0.39	4.5

First, it is observed that the sorbent residence time decreases with a lower air ratio as expected from Eq.[33]. However, the first four experiments of the Polish-5 coal type show experimental average sorbent conversions in the bed ( $= R/(Ca/S)$ ) which are higher or only a little lower than the maximum conversion of 0.308 as measured by Akse et al. (1983) for this specific limestone. Consequently, these data are not reliable; this is also concluded from the fitted values of the sorbent residence time which are higher than the maximum possible residence time according to Eq.[33].

Furthermore, it is observed that the sorbent residence time of the experiments with  $\lambda > 1$  is relatively high: it varies between 16.1 and 28.5 hr. Although these values correspond with realistic volumetric sorbent loadings in the bed (11% to 21% sorbent), it is not expected that a situation of steady state sulfation during the measurements was reached due to the relatively high residence times.

Finally, it is concluded that the experiments with  $\lambda < 1$  show sorbent residence times varying between 1.1 hr (reasonably low!) and 11.9 hr, which corresponds with average sorbent loadings in the bed of less than 11%.

#### 4. CONCLUSION

A simple sulfur retention model is given which describes the influence of oxygen-stoichiometry on the sorbent sulfation reaction during FBC by the relatively fast formation of the intermediate reactant  $SO_3$ .

The oxygen concentration is influenced by one model parameter, the equivalent oxygen concentration, which is a measure of the (in)complete combustion of the coal. The decrease in the sulfur retention at lower stoichiometric air ratios can readily be described by the model equations.

However, a diagnostic evaluation of model and experimental data makes clear that a direct validation or verification of the model predictions is generally prevented due to a neglect of the influence of the sorbent residence time on the steady state character of retention experiments.

#### APPENDIX 1

By definition the molar carbon surface concentration is written as:

$$q_1 = \frac{\text{moles of carbon in a coal particle}}{\text{external surface area of a particle}} = (1000/72) \rho_1 d_1 x_1 \quad [A1.1]$$

The stoichiometric coefficient  $\zeta_1$  varies between 0.5 and 1 (average = 0.85). As an approximation the coal combustion rate constant  $k_1$  can be considered to be equal to the oxygen mass transfer coefficient:

$$k_1 = k_{g_1} = Sh_1 D_1 / d_1 \quad [A1.2]$$

The appropriate Sherwood number  $Sh_1$  can be derived from LaNauze's (1985) equations. Consequently, the equivalent oxygen concentration is written as:

$$c_o = [125/9] \frac{\zeta_1 \rho_1 x_1 d_1^2}{Sh_1 D_1 \tau_1} \quad [A1.3]$$

As example  $c_0$  is approximated from the following general values of the respective parameters in Eq.[A1.3]:

$$\zeta_1 = 0.85 [-]; \rho_1 = 1400 \text{ kg/m}^3; x_1 = 0.8 [-]; d_1 = 2 * 10^{-3} \text{ m}; Sh_1 = 3 [-]; D_1 = 2.2 * 10^{-4} \text{ m}^2/\text{s}; \tau_1 = 5 \text{ min} = 300 \text{ sec.}$$

This leads to  $c_0 = 0.267 \text{ mol/m}^3$ ; this general value of the equivalent oxygen concentration is in good agreement with the data as summarized in Figure 1.

## APPENDIX 2

The molar CaO surface concentration is given as (Schouten and Van den Bleek, 1987):

$$q_3 = (5/3) \rho_3 d_3 x_3 \quad [A2.1]$$

The sulfation rate constant  $k_3$  is calculated from:

$$k_3 = 1 / [1/k_{S_3} + 1/k_{g_3}] \quad [A2.2]$$

$$\text{The mass transfer coefficient is obtained from: } k_{g_3} = Sh_3 D_3 / d_3 \quad [A2.3]$$

The appropriate Sherwood number  $Sh_3$  can be derived from LaNauze's (1985) equations. The sorbent reaction rate constant  $k_{S_3}$  equals 700 mm/s based on  $SO_3$  sulfation data of Valkenburg et al. (1987).

Combination of the equations given above results in the following expression for the parameter  $\mu_0$ , Eq.[30]:

$$\mu_0 = \left( [9/4000] \left[ \frac{K_0 \tau_3 x_s c_{in}}{\rho_3 d_3 x_3 \zeta_3} \right] / [1/k_{S_3} + d_3/(Sh_3 D_3)] \right)^2 \quad [A2.4]$$

## 2.4 Comments

2.4.1 Comment 1: influence of the coal combustion rate on sulfur retention	78
2.4.2 Comment 2: discrepancy between fixed and fluid bed SURE modeling	79
2.4.3 Comment 3: influence of oxygen on unsteady state sorbent sulfation	80
2.4.4 Comment 4: influence of bed temperature on sorbent sulfation rate	82
2.4.5 Comment 5: pore plugging and SURE modeling: a tool for the optimization of sorbent consumption	87
<u>2.4.1 Comment 1: influence of the coal combustion rate on sulfur retention</u>	

Some retention models in literature incorporate an effect of oxygen on sulfur retention by assuming a (linear) relationship between the rate of coal combustion and the rate of sulfur release. However, especially at air ratios higher than 1 to 1.2, it may be assumed that all sulfur which is feeded with the coal is converted into sulfur dioxide. Even at in-bed air ratios lower than 1 (0.6 to 1) this assumption holds when in a steady state situation no sulfur accumulation occurs in the coal ash: then all sulfur feeded will be released either as sulfur dioxide or as reduced sulfur species like  $H_2S$ ,  $COS$  or  $CS_2$ . So it is not necessary to connect the sulfur release rate to the rate of oxygen consumption or coal combustion, which may sometimes even be incorrect (when reduced sulfur species are produced).

For example, Noordergraaf (1985) has discussed in his thesis (Chapters 2 and 11) the effect of the rate of mass transfer on the sulfur retention. He considers the mass transfer of  $SO_2$  as well as of  $O_2$  and concludes that a high coal combustion rate effects the degree of desulfurization. However, in his model (see Chapter 2) the sulfur release rate is directly connected to the coal combustion rate, while furthermore the sulfation rate is taken zero order in oxygen. Consequently, it is more easier to take the sulfur release rate linear dependent on the coal feed rate as is done in the SURE model (papers 2.4, 2.5 and 2.7). Because in the SURE model the retention parameter is linear dependent on the sulfur feed rate, while further the sulfur retention increases with an increasing retention parameter, the SURE model leads to the same conclusion that sulfur retention increases with a higher coal combustion rate.

#### 2.4.2 Comment 2: discrepancy between fixed and fluid bed SURE modeling

All models presented in the present chapter are based on the simple SURE modeling approach which states that the sorbent sulfation rate is first order in the gaseous sulfur component ( $\text{SO}_2$  or  $\text{SO}_3$ ) and first order in the reactive sorbent surface area. However, a main difference is observed between the SURE modeling in the fixed bed and in the fluid bed. In paper 2.6 it is argued that good model fits of the non-steady state fixed bed experimental data (synthetic sorbent material) could only be obtained by assuming in the sorbent two different solid reactive surfaces which have a different reaction rate towards the  $\text{SO}_3$  sulfation reaction. This phenomenon is explained by the possible interaction of  $\text{CaO}$  and  $\text{Al}_2\text{O}_3$ . Both reaction rate constants, which differ an order in magnitude, are based on the total internal reactive sorbent surface area. However, in paper 2.5 it has been shown that the non-steady state sulfation of the same synthetic sorbent material in a fluid bed could easily be described by only one rate constant which is based on the total external sorbent surface area.

A possible explanation for this paradox is that in the fluid bed the sorbent is well mixed, which implies that all sorbent particles have the same overall conversion at each moment at each position in the bed. This overall conversion is the sum of the fractional conversions of the solid reactant at the respective sorbent surface areas, which are the same in all particles. This implies that the overall conversion of the solid reactant can be considered as a 'weighed average', while further the sulfation rate can be considered to be first order in the total sorbent surface area with a rate constant which is also a 'weighed average'. Or in other words: all sorbent particles have the same degree of conversion of  $\text{CaO}$ .

The fixed bed is not well mixed, which results in axial profiles in the fractional conversions of the respective sorbent surface areas. This means that all particles have a different 'weighed conversion', consequently no average surface area and no average rate constant can be used to describe the sulfation as a function of time.

This explanation is strengthened by the calculation of the 'weighed' average rate constant based on the fixed bed measurements, which will now be based on  $\text{SO}_2$  sorption and on the external sorbent surface area so as to compare it with the rate constant  $k_s$  as obtained with the fluid bed experiments (chapter 2.2). With the data of the standard experiment as used in the fixed sorption study (paper 2.6) a rate constant  $k_s$  of 52 mm/s is calculated, which agrees reasonably well with the fluid bed  $k_s$  values (Table 5; page 35) of 38, 51 and 80 mm/s (mean value: 56 mm/s).

Consequently, the main conclusion is that the application of a fixed bed reactor to study the sulfation process may increase the fundamental understanding of the sulfation mechanism: in this case it focusses in on the possible presence of two different reactive sorbent surfaces. This knowledge may further lead to the synthesis of a sorbent material with a much smaller 'slower-reacting' surface area in order to increase the final sulfation rate. However, application of the fixed bed sulfation results to fluid bed circumstances is limited from a modeling point of view: the fluid dynamical behaviour of particles in a fluid bed is very different, which leads in this specific case to the application of a much simpler kinetic term in the sulfur retention model.

#### 2.4.3 Comment 3: influence of oxygen on unsteady state sorbent sulfation

In the first paper (chapter 2.2) an analytical relationship for the dimensionless sulfur breakthrough time is given as a function of the maximum gas exchange ratio  $P_0$  and the maximum CaO conversion  $\alpha_{\max}$ , Eq.[9]. This equation is based on the sorption of  $\text{SO}_2$ . However, when the approach is applied as outlined in papers 2.6 and 2.7 (chapter 2.3), where the sulfation rate is based on  $\text{SO}_3$  sorption (influence of oxygen-stoichiometry!), then a same type of equation for the dimensionless breakthrough time is derived:

$$\theta = t/\tau_{\text{br}} = 1 + (1/P_0) \left( A_0 \ln(P_0) - \frac{(A_0(1-X_2)-1)}{X_2} - A_0 \ln \left[ \frac{(A_0(1-X_2)-1)}{X_2} \right] \right) \quad [3.1]$$

The maximum gas exchange ratio  $P_0$  is here defined as  $(k_3 S_3)_0 / \phi_v$ , while  $X_2$  is the dimensionless  $\text{SO}_2$  outlet concentration. The dimensionless model parameter  $A_0$  is defined as the 'equilibrium parameter' and equals:

$$A_0 = 1 + 1 / [K_0 c_{\text{in}}^{1/2}] \quad (A_0 > 1) \quad [3.2]$$

The derivation of Eq.[3.1] is based on two assumptions:

$$1. \quad c_{\text{in}} \gg (1 + k_3 S_3 / \phi_v) c_3 / 2 \quad [3.3]$$

This first assumption is always valid under practical sulfation conditions, because in these cases it holds that  $c_{\text{in}}$  (21 vol%)  $\gg c_2/2$  (= 0.1 ~ 0.3 vol%), while further always  $c_2 \gg c_3$  and  $k_3 S_3 / \phi_v > 0$ .

$$2. \quad 1/(\kappa_1 \tau_g) \ll c_{\text{in}}^{1/2} \quad (\text{where } \tau_g \text{ is the gas residence time } \epsilon V / \phi_v) \quad [3.4]$$

The validity of this second assumption is basically dependent on the magnitude of  $\kappa_1$ . In paper 2.6 a relatively large forward reaction rate constant  $\kappa_1$  ( $10^4$  [ $1/(\sqrt{\text{kmol}/\text{m}^3})/\text{s}$ ]) has been assumed so as to obtain a high rate of  $\text{SO}_3$  formation. The gas residence time is general in the order of 1 second. So the second assumption is valid under these circumstances, because  $1/(10^4) \ll c_{\text{in}}^{1/2}$  (at 850 °C about 0.05 [ $\sqrt{(\text{kmol}/\text{m}^3)}$ ]).

Further, the initial outlet concentration  $X_{20}$  at  $\theta=0$  is obtained as:

$$X_{20} = (A_0 - 1)/(A_0 + P_0) \quad [3.5]$$

The sulfur dioxide concentration at the end of the breakthrough process (at  $t \rightarrow \infty$ ) is written as:

$$X_2^\infty = 1 - 1/A_0 \quad [3.6]$$

These expressions demonstrate that the influence of the equilibrium formation of  $\text{SO}_3$  on the sorbent sulfation rate is incorporated in the dimensionless model parameter  $A_0$ . The same solution as in case of the  $\text{SO}_2$ -equation as given in paper 2.5 (chapter 2.2) is obtained when  $A_0 \rightarrow \infty$  (which implies that  $K_0 \rightarrow \infty$  and/or  $c_{\text{in}}$  is relatively high).

The dimensionless breakthrough time can also be written as a function of the dimensionless total sulfur ( $\text{SO}_2 + \text{SO}_3$ ) outlet concentration  $X_0$  as:

$$\theta = 1 + (A_0/P_0) \left[ \ln(P_0/A_0) - (1-X_0)/X_0 - \ln[(1-X_0)/X_0] \right] \quad [3.7]$$

In this case the initial outlet concentration at  $t = 0$  is  $A_0/(A_0 + P_0)$ , while of course this concentration at total breakthrough ( $t \rightarrow \infty$ ) equals one. Consequently, the breakthrough of sulfur in a fluid bed during unsteady state operation is now a function of three independent dimensionless parameters: the maximum gas exchange ratio  $P_0$ , the maximum CaO conversion  $\alpha_{\text{max}}$  and the equilibrium parameter  $A_0$ .

The influence of the ratio  $(A_0/P_0)$  on the dimensionless breakthrough time is given in Figure 3.1. It is easily concluded that the shape of the curves is significantly affected by a relatively small change in the ratio  $(A_0/P_0)$ .

Under practical FBC conditions  $A_0$  equals about 4-6 [-] as based on average values of  $K_0$  ( $\approx 0.154$  ( $\sqrt{\text{m}^3/\text{mol}}$ )) and  $c_{\text{in}} = 2.3$  mol/ $\text{m}^3$  (21 vol%; 850 °C). The values of the maximum gas exchange ratio  $P_0$  based on  $\text{SO}_2$  sulfation as given in Tables 3, 4 and 5 in chapter 2.2 are about 13 ( $\approx [93\% \text{SO}_2]/[7\% \text{SO}_3]$ ) times higher when they are based on  $\text{SO}_3$  sulfation; consequently they vary between about 10 [-] and 40 [-] depending on the type



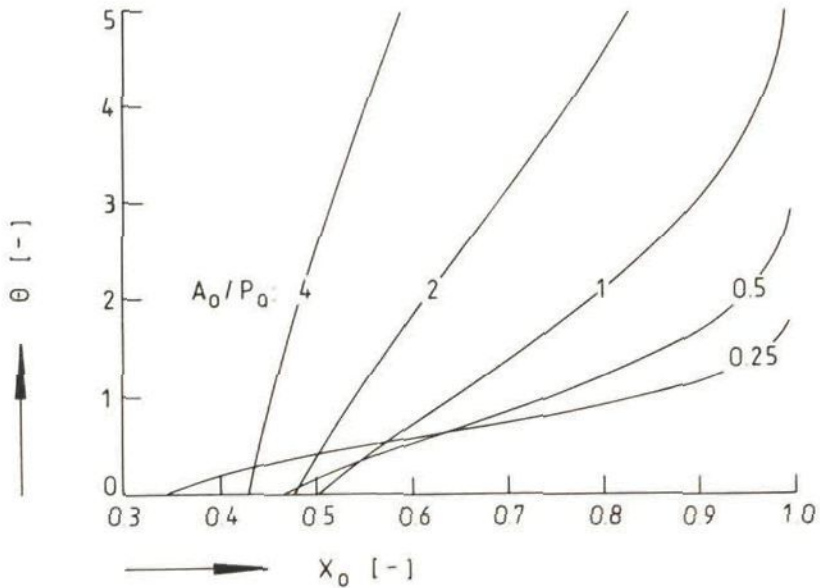


Figure 3.1: The dimensionless breakthrough time  $\Theta$ , Eq.[3.7], as a function of the dimensionless total sulfur ( $\text{SO}_2 + \text{SO}_3$ ) outlet concentration at different values of the ratio between the model parameters  $A_0$  and  $P_0$ .

of sorbent used and depending on the reactor circumstances. This implies that the ratio ( $A_0/P_0$ ) in general will vary between about 0.1 and 0.5 indicating that complete sulfation of the sorbent material will be obtained in about 2 to 4 times the breakthrough time (Figure 3.1).

#### 2.4.4 Comment 4: influence of bed temperature on sorbent sulfation rate

The SURE model as it is presented in the present chapter does not provide directly an explanation for the influence of bed temperature on the rate of sulfation. In general it would predict an increasing sulfation rate at higher temperatures due to an increase of the rate of mass transfer or due to a higher sulfation kinetic rate constant. However, many times an optimum in the sulfation rate (or sulfur retention) as a function of bed temperature is reported in the FBC literature (see literature review: paper 2.1). E.g. Hartman and Coughlin (1976) mention an optimum at 900 °C in case of their limestone sulfation experiments in a differential reactor.

One explanation mentioned in literature is that both sulfation and calcination occur simultaneously, which leads to an optimum temperature resulting from these two opposing tendencies. However, in this comment it will be demonstrated that the occurrence of an optimum can also be

theoretically explained by the rate of  $SO_3$  formation in combination with the  $SO_3$ -sorbent sulfation reaction in the present SURE model. This explanation is illustrated with the experimental conditions provided by Hartman and Coughlin (1976).

First, it is easily seen that the rate of sulfation of the sorbent material (limestone) in the differential reactor, as based on the SURE model assumptions, is given by:

$$\left[ \zeta_3 q_3 \frac{dS_3}{dt} / S_3 \right] = r \text{ [mol } SO_3/m^2/s] = -k_3 c_3 \quad [4.1]$$

Further the  $SO_3$  mass balance over the differential reactor reads ( $SO_3$  reacted with sorbent) = ( $SO_3$  formed by forward reaction) - ( $SO_3$  converted by backward reaction), which results in:

$$k_3 S_3 c_3 = (\kappa_1 c_2 c_1^{1/2} - \kappa_2 c_3) V_{gas} \quad [4.2]$$

where  $V_{gas}$  is the total gas volume in the reactor, which is considered to be equal to the gas which is present between the particles in the reactor.

$$\text{So: } V_{gas} = \epsilon V_{particles} / (1-\epsilon) \quad [4.3]$$

where  $V_{particles}$  is the volume of the limestone particles in the reactor, while  $\epsilon$  is the porosity (in general  $\epsilon=0.4$ ).

Now the initial sulfation rate ( $r(t=0) = r_0$ ) will be considered, which is easily derived with the equations given above to be:

$$r_0 = - \frac{c_2 c_{in}^{1/2}}{\frac{S_{30}}{\kappa_1 V_{gas}} + \frac{1}{K_0 k_3}} \quad [4.4]$$

$S_{30}$  is the external sorbent surface area  $S_3$  at  $t=0$ . When the particles are assumed to be spherical (average diameter  $d_0 = 0.565$  mm) it equals:

$$S_{30} = (6 M_0) / (\rho_0 d_0) \quad [4.5]$$

$$\text{So, it can also be derived that: } S_{30}/V_{gas} = 6 (1-\epsilon) / (\epsilon d_0) \quad [4.6]$$

Furthermore, the reactor inlet concentrations of sulfur dioxide and oxygen in case of the data of Hartman and Coughlin (1976) are respectively  $c_2 = 0.29$  vol% and  $c_{in} = 3.5$  vol% (of course the concentrations given in mol/m<sup>3</sup> are temperature dependent).

The equilibrium constant  $K_0$  is a function of temperature as it is given in chapter 2.3 and paper 2.6.

It is assumed, finally, that the temperature dependency of the rate constants  $\kappa_1$  and  $k_3$  is described according to Arrhenius equations as:

$$\kappa_1 = \kappa_{1,0} \exp[-E_1/R/T] \quad \text{and} \quad k_3 = k_{3,0} \exp[-E_3/R/T] \quad [4.7]$$

The activation energy of  $\text{SO}_3$  formation,  $E_1$ , is strongly dependent on the type of catalysts on which the reaction takes place. E.g. Meyer (1977) reports two very different values: 142.1 kJ/mol in case of a vanadium catalyst, while 41.8 kJ/mol is found with a platinum catalyst. During fluid bed combustion the  $\text{SO}_3$  formation might be catalyzed by e.g. the construction material of the reactor wall or heat exchanger pipes, the coal ash particles as well as by the sorbent material; this will determine to a great extent what the actual value of the activation energy finally will be. In this comment two values are used for the calculation of the temperature dependency: the average of the two values reported and the maximum value, respectively 90 kJ/mol and 140 kJ/mol. In all calculations it is assumed that the rate of  $\text{SO}_3$  formation has a specific value at a bed temperature of 850 °C; this value is varied between  $10^2$  and  $10^5$  (in paper 2.6 the value of  $10^4$  [ $1/\sqrt{(\text{kmol}/\text{m}^3)/\text{s}}$ ] was used to derive the model fits).

The activation energy of the sorbent sulfation reaction,  $E_3$ , is taken as 70 kJ/mol, which is an average value being in agreement with data reported by Marsh and Ulrichson (1985). Here it is also assumed that the rate of sorbent sulfation has a specific value at 850 °C. This value is based on the average  $\text{SO}_2$  kinetic rate constant of 200 mm/s as it is reported in chapter 2.2; this value agrees with a rate constant based on  $\text{SO}_3$  sulfation of about 2.7 m/s.

The result of the calculations is summarized in the Figures 4.1 and 4.2. It is shown in Figure 4.1 that at relative low values of the forward reaction rate parameter  $\kappa_1$  at 850 °C (100 to 5000 [ $1/\sqrt{(\text{kmol}/\text{m}^3)/\text{s}}$ ]) a maximum in the initial reaction rate as a function of temperature is easily obtained: respectively at about 740, 790, 835, 880 and 930 °C. So the maximum of 900 °C reported by Hartman and Coughlin (1976) should correspond with a relatively low value of  $\kappa_1$  between 100 and 500 [ $1/\sqrt{(\text{kmol}/\text{m}^3)/\text{s}}$ ] at 850 °C.

Furthermore it is demonstrated in Figure 4.2 that at higher values of the rate parameter  $\kappa_1$  the maximum disappears and the initial reaction rate decreases gradually with increasing temperature.

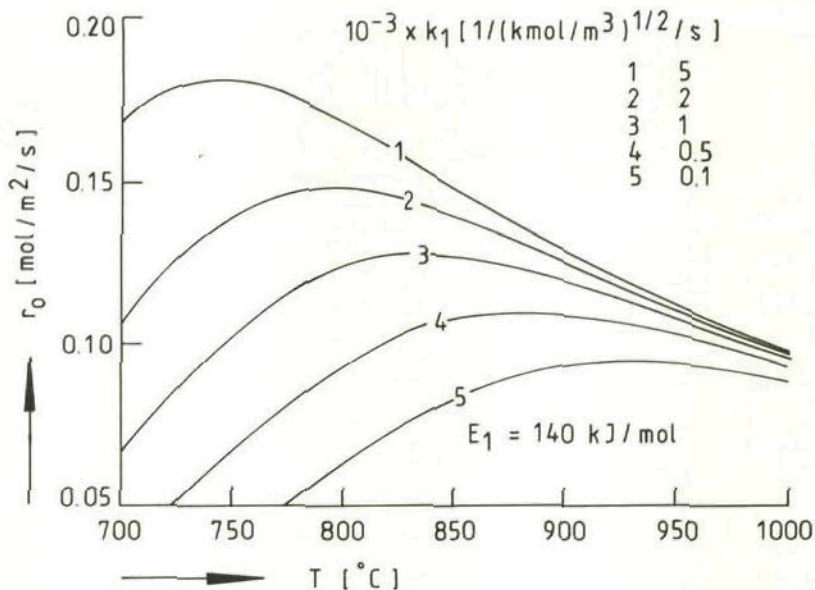


Figure 4.1: The effect of temperature on sorbent sulfation: the initial sorbent sulfation rate  $r_0$  as a function of temperature at different values of the forward  $\text{SO}_3$  formation rate parameter  $\kappa_1$  (values given at 850 °C); the activation energy of  $\text{SO}_3$  formation equals  $E_1 = 140 \text{ kJ/mol}$ .

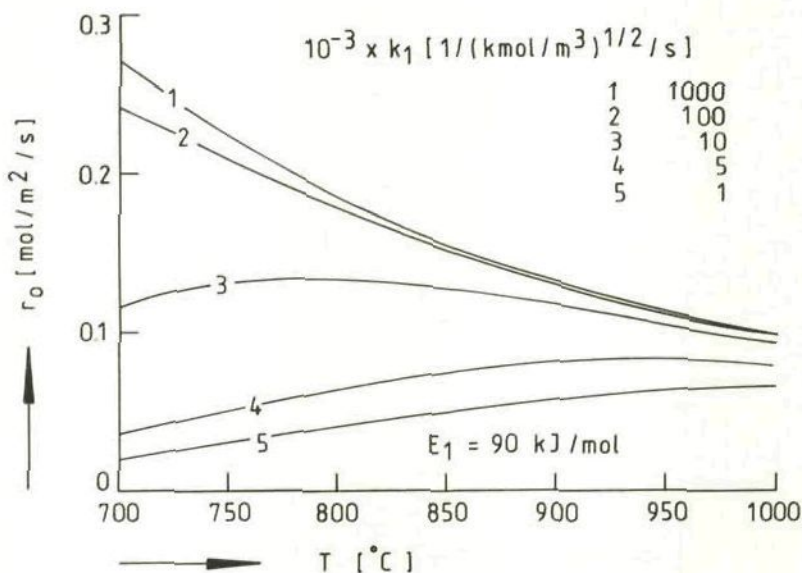


Figure 4.2: The effect of temperature on sorbent sulfation: the initial sorbent sulfation rate  $r_0$  as a function of temperature at different values of the forward  $\text{SO}_3$  formation rate parameter  $\kappa_1$  (values given at 850 °C); the activation energy of  $\text{SO}_3$  formation equals  $E_1 = 90 \text{ kJ/mol}$ .

Consequently, these calculations make clear that the temperature dependency of the rate of sulfation, together with the occurrence of an optimum, can easily be described by the rate of  $\text{SO}_3$  formation in the SURE model. However, it is also observed that hereto a value of the forward reaction rate constant  $\kappa_1$  at 850 °C has to be applied which is significantly lower than the value of  $10^4$  used in paper 2.6.

A same type of approach has been discussed by Burdett (1983). He assumed the pore diffusion and solids diffusion coefficients in an extended pore/grain model as well as the rate of  $\text{SO}_3$  formation to be temperature dependent, which resulted in a maximum sulfation rate between 800 °C and 900 °C. In the calculations an average value of the activation energy of  $\text{SO}_3$  formation of 133 kJ/mol was applied.

In paper 2.6 it has also been reported that the rate of sulfation of the synthetic sorbent material increases continuously when the temperature is increased from 800 to 950 °C. With the expression for  $r_o$  as given above, it is calculated that this increase can only be obtained with values of  $\kappa_1$  at 850 °C lower than 5000. This implies that in these cases  $\kappa_1$  might not always be neglected (which means it might not be assumed to be very high) and should be incorporated in the model equations.

For example, this means that the second assumption as outlined in the previous comment, Eq.[3.4], is not valid anymore. The expression for the dimensionless total sulfur ( $\text{SO}_2 + \text{SO}_3$ ) outlet concentration, Eq.[3.7], becomes under these circumstances:

$$\Theta = B_o (1 - \sigma_3) - (A_o/P_o) \ln[\sigma_3] \quad [4.8]$$

with the dimensionless sorbent surface area  $\sigma_3 = S_3/S_{3o}$  being given as:

$$\sigma_3 = \frac{A_o (1 - X_2)}{P_o [B_o X_o - (B_o - 1)]} \quad [4.9]$$

Here the equilibrium parameter  $A_o$  is defined by:

$$A_o = 1 + 1/[K_o c_{in}^{1/2}] + 1/[\kappa_1 \tau_g c_{in}^{1/2}] \quad [4.10]$$

Furthermore the dimensionless parameter  $B_o$  in this equation [4.9] is defined as the 'formation rate parameter' and is given by:

$$B_o = 1 + 1/[\kappa_1 \tau_g c_{in}^{1/2}] = A_o - 1/[K_o c_{in}^{1/2}] \quad [4.11]$$

$B_o$  approaches 1 at a high rate of  $\text{SO}_3$  formation ( $B_o \rightarrow 1$  at  $\kappa_1 \rightarrow \infty$ ).

#### 2.4.5 Comment 5: pore plugging and SURE modeling: a tool for the optimization of sorbent consumption

The phenomenon of deactivation of a sorbent particle due to pore plugging has been incorporated in the SURE model (see Eq.[15], page 25) by assuming that the sorbent conversion is limited by a maximum possible reaction time  $\tau_0$ . So, for example,  $\tau_0$  may be the pore plugging time at which all the pores in the particle are blocked before total conversion of the sorbent has been reached. The corresponding maximum conversion of the sorbent,  $\alpha_{\max}$ , can be calculated from detailed pore plugging model equations (see for example Eq.[A1.25], page 60).

So, according to this SURE model approach, it is assumed that when  $t \leq \tau_0$  (here  $t$  is the time that the sorbent particle is present in the combustor during steady state operation), still all the unreacted sorbent surface area (i.e.  $\sigma(t)*S_0$ ) 'contributes' to the driving force for the sulfation reaction. So, at  $t = \tau_0$  still a contribution of  $\sigma(t)*S_0 = \sigma_{\min} * S_0 = (1-\alpha_{\max}) * S_0$  to the driving force is present. However, when  $t > \tau_0$  then all the pores are blocked, so no reactive surface is present anymore which implies that  $\sigma(t > \tau_0) = 0$ .

This SURE model approach has as a consequence that, due to its definition, the course of the reactive sorbent surface area ( $\sigma(t)$ ) of one sorbent particle is discontinuous. However, other (more detailed) pore closure models suppose a gradual and continuous change of the reactive surface area as a function of time (see e.g. Simons and Garman (1986)). But it is also obvious that in the actual situation of steady state sulfation of more than one particle in a combustor, the mean conversion (as calculated from the SURE model) as a function of time of a number of particles, which have been feeded one after the other with small time intervals, will demonstrate a more gradual change at  $t = \tau_0$ , than in case of only one single particle. Therefore, the preference has been given to the SURE model approach, because it is also much simpler to apply in overall FBC sulfation models.

Summarizing, it is assumed in the SURE model that in case of the steady state sulfation of a sorbent particle in a combustor it can be written that:

$$t < \tau_0 : \quad \sigma(t) = \exp[-M(1-R)(t/\tau_s)] \quad \text{and} \quad \alpha(t) = 1 - \sigma(t) \quad [5.1a]$$

$$t = \tau_0 : \quad \sigma(t) = \sigma_{\min} = \exp[-M(1-R)(\tau_0/\tau_s)] \quad \text{and} \quad \alpha(t) = \alpha_{\max} \quad [5.1b]$$

$$t > \tau_0 : \quad \sigma(t) = 0 \quad \text{and} \quad \alpha(t) = \alpha_{\max} \quad [5.1c]$$

These equations are demonstrated in Figure 5.1 in case of a practical situation with  $M = 5$  [-],  $R = 0.8$  [-] and  $\tau_s = 10$  hr. It is concluded that the maximum conversion of the particle ( $\alpha_{\max} = 0.42$  [-]) is reached at  $\tau_0 = 5.3$  hr.

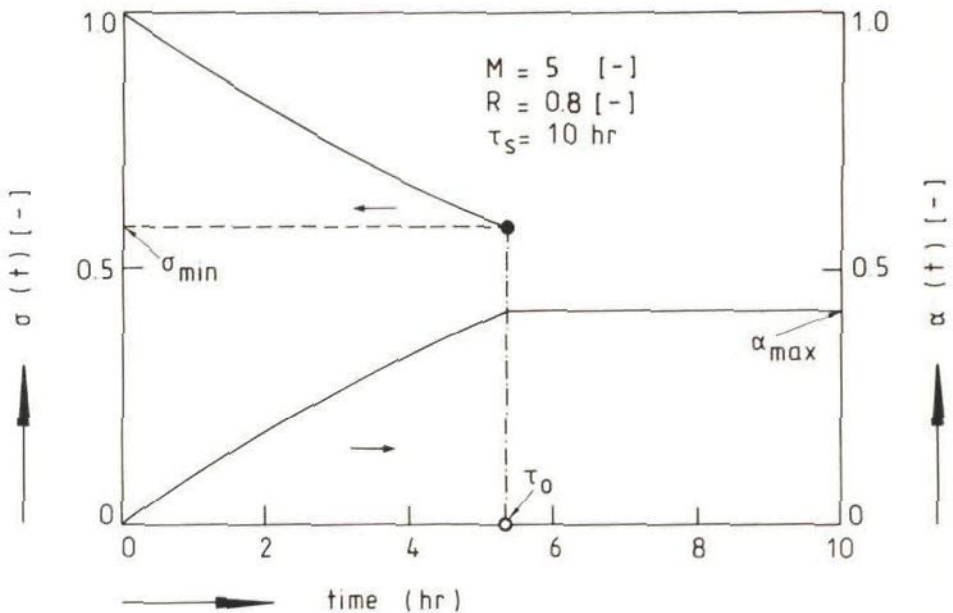


Figure 5.1:  $\sigma(t)$  and  $\alpha(t)$  of one sorbent particle as a function of time.

The ratio between the pore plugging time  $\tau_0$  and the average sorbent residence time  $\tau_s$  is an important system parameter, because it demonstrates whether the sorbent remains too long or too short in the reactor with respect to the time in which it reaches its maximum conversion. For example, the sorbent remains too long in the system when  $\tau_0/\tau_s < 1$ : in this case a part of the sorbent in the reactor is not active anymore because it has already reached its maximum conversion. However, when  $\tau_0/\tau_s > 1$  then sorbent is 'spoiled', because it already leaves the reactor before it has reached its maximum conversion. Consequently, an optimum situation from the point of view of sorbent consumption is obtained at  $\tau_0/\tau_s = 1$ . This ratio can be written according to Eq.[5.1b] as:

$$\tau_0/\tau_s = -\ln(1-\alpha_{\max}) / M / (1-R) \quad [5.2]$$

This relation is plotted in Figures 5.2a and 5.2b for the situation that  $R = 0.8$  [-] at different values of the retention parameter  $M$ . It is concluded from Figure 5.2a that at small values of  $M$  ( $\leq 2$ ) and also at high values of  $\alpha_{\max}$  ( $> 0.8$  [-]), the situation is obtained that  $\tau_0 > \tau_S$ . Furthermore, Figure 5.2b shows that in case of limestone sulfation (with in general  $0.3 < \alpha_{\max} < 0.5$ ), the situation is easily achieved that  $\tau_0 < \tau_S$  when  $M > 2$  [-].

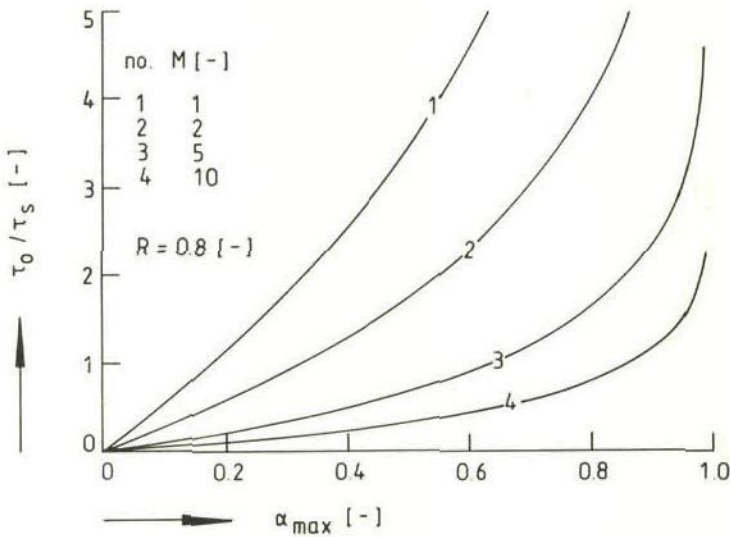


Figure 5.2a: The ratio  $\tau_0/\tau_S$  as a function of the maximum conversion at different values of the retention parameter  $M$  ( $R = 0.8$  [-]).

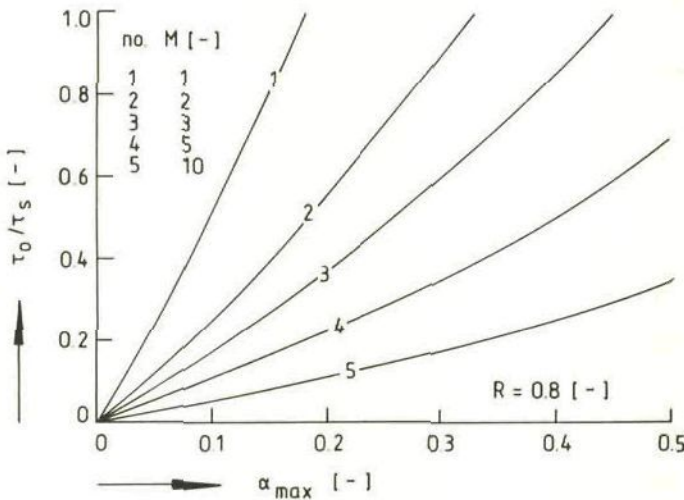


Figure 5.2b: The ratio  $\tau_0/\tau_S$  as a function of the maximum conversion at different values of the retention parameter  $M$  ( $R = 0.8$  [-]).



According to Eq.[5.2] it can be derived at the optimum  $\tau_0 = \tau_s$  that:

$$M = -\ln(1-\alpha_{\max}) / (1-R) \quad [5.3]$$

Substitution of Eq.[5.3] in Eqs.[25]...[27] of chapter 2.2 (page 26) results in an expression for the optimum (Ca/S) ratio at  $\tau_0 = \tau_s$  ( $\alpha_{\max} < 1$  [-]):

$$(Ca/S)_{\text{optimum}} = R \frac{\ln(1-\alpha_{\max}) - 1}{\ln(1-\alpha_{\max})} / [1 - (1-\alpha_{\max}) \exp(-1)] \quad [5.4]$$

This remarkable result illustrates that now the (Ca/S) ratio is not anymore a function of the retention parameter M, because the connection between M and  $\alpha_{\max}$  has been established by Eq.[5.3]. With l'Hôpital's rule it is seen that at  $\alpha_{\max}=1$  the optimum average conversion equals 1 and  $(Ca/S)_{\text{optimum}}=R$ .

Furthermore, from a combination of Eq.[5.3] and the definition of the retention parameter M (Eq.[28] of chapter 2.2 (page 27)), the following expression for the corresponding optimum sorbent residence time  $\tau_s$  can be derived:

$$(\tau_s)_{\text{optimum}} = (\tau_0)_{\text{optimum}} = \frac{-\ln(1-\alpha_{\max})}{(1-R)} \frac{q \phi_v}{k \phi_s} \quad [5.5]$$

These results will now be illustrated with a calculation example. The following average reactor circumstances and sorbent properties are applied:

$$U_0 = 2 \text{ m/s}; \phi_S/F = 0.02 \text{ mol/s/m}^2; d_0 = 1 \text{ mm}; \rho_0 = 2700 \text{ kg/m}^3; x_s = 0.95 [-]; \\ k = 0.1 \text{ m/s}; F = 1 \text{ m}^2; R = 0.8 [-] \text{ and } \alpha_{\max} = 0.40 [-].$$

With these data it is calculated that:

$$(\tau_s)_{\text{optimum}} = 3.03 \text{ [hr]} \text{ and } (Ca/S)_{\text{optimum}} = 3.04 [-].$$

In order to realize this optimum sorbent residence time in the reactor, the appropriate reactor volume has to be designed based on the relationship:  $\tau_s = (\text{volume of sorbent in reactor}) / (\text{volumetric sorbent feed rate})$ . From this equation the required volume of the sorbent in the reactor can be calculated. Subsequently, from this result and with the average bed porosity, the volume of the heat exchanger pipes and the volume of coal and ash in the bed, finally the required total reactor volume can be obtained.

Summarizing, in this comment it has been elucidated how an optimum degree of sorbent consumption can be established: the average residence time of the sorbent in the fluid bed system should equal the time of pore closure, from which the optimum (Ca/S) ratio can be derived.

## CHAPTER 3: PARTICLE MOTION in SLUGGING GAS FLUIDIZED BEDS

### 3.1 Introduction

The fluid dynamical behaviour of bed material used in the fluidized bed combustion of coal is an important phenomenon which greatly influences the mechanism of particle mixing and segregation. In FBC generally large particle systems are applied which give a tendency to the appearance of slugging, especially in smaller diameter systems (as for example are found between the heat exchanger tubes in FBC units).

In the first paper (chapter 3.2) segregation and slugging experiments are presented which have been carried out with a binary large particle system representing the ash-coal/sorbent mixture in a fluid bed combustor. The slugging beds are characterized by dimensionless slug parameters which are obtained from visual bed height measurements. The influence of the superficial gas velocity, the bed diameter and the bed aspect ratio on the extent of segregation is investigated. A simple segregation model is introduced which is based on a mechanism of segregation in slugging gas fluidized beds that is proposed being based on experimental observations.

In the second paper (chapter 3.3) an experimental study is presented with the objective to investigate with a dynamic radioactive tracer technique the movement of sorbent particles in a one- and two-component 10 cm ID fluid bed. Information is obtained on the presence probability of the tracer particle as a function of the bed height, the frequency of passage of the tracer at a given bed level, the probability for a direction change, the magnitude of the up- and downward velocities of the tracer as a function of bed height and on the random diffusion- (or dispersion-) like character of the particles trajectories. This information is sufficient to obtain a useful qualitative description of the mechanism of particle motion in these systems. Furthermore a general model for the motion of particles in slugging fluidized beds is formulated based on this mechanistic description.

accepted for publication in Powder Technology, July 1987

SUMMARY	93
1. INTRODUCTION	93
1.1 Segregation in gas fluidized beds	93
1.2 Segregation of particle systems during FBC	94
1.3 Fluidization behaviour during FBC	95
1.4 Objective of this paper	95
2. EXPERIMENTAL	96
2.1 Slugging and segregation measurements	96
2.2 Extent of segregation	97
3. SLUGGING IN FLUID BEDS	98
3.1 Theoretical	98
3.1.1 Types of slugging	98
3.1.2 Characterization of slugging	98
3.2 Experimental results	99
3.2.1 Minimum fluidization velocity $U_{mf}$	99
3.2.2 Slug parameter a	100
3.2.3 Slug parameter b	101
3.2.4 Observed particle flow	104
4. SEGREGATION IN SLUGGING FLUID BEDS	104
4.1 Theoretical	104
4.1.1 Mechanism of particle flow in slugging fluid beds	104
4.1.2 Modeling of particle flow in slugging fluid beds	106
4.2 Experimental results	109
4.2.1 Effect of $H_{mf}/D$ -ratio	109
4.2.2 Effect of superficial gas velocity	110
4.2.3 Effect of bed diameter	114
4.2.4 Some modeling results	117
5. CONCLUSIONS AND DISCUSSION	119

J.C. Schouten, P.J.M. Valkenburg and C.M. van den Bleek

## SUMMARY

In this paper steady state segregation and slugging experiments are presented which have been carried out with a binary large particle system representing the ash-coal/sorbent mixture in a fluid bed coal combustor. The slugging beds are characterized by dimensionless slug parameters which are obtained from visual bed height measurements. The influence of the superficial gas velocity and the bed diameter on the extent of particle segregation is investigated. It is shown that a critical bed diameter exists beyond which segregation is nil. A simple segregation model is introduced proceeding with a proposed mechanism of segregation in slugging gas fluidized beds, which is based upon the visually observed flow of particles. The segregated particle distribution is characterized by one 'Peclet-like' dimensionless number, which is the ratio between the net particle convective and segregating flows and the dispersive solids flow in the bed.

## 1. INTRODUCTION

## 1.1 Segregation in gas fluidized beds

From a particle point of view a gas fluidized bed is usually assumed to be well mixed. However, segregation may occur when the bed contains more than one type of particles. In that case segregation will take place due to the differences in particle properties, like a. particle density, b. particle size and, c. particle shape. In general segregation is most influenced by density differences.

Furthermore other parameters that determine the extent of particle segregation in a fluid bed system are related to the amount of particles applied. The characteristic parameters in this case are: a. the bed aspect ratio at minimum fluidization (which is related to the total amount of bed material) and b. the weight ratio of the segregating components in the bed.

Finally the extent of segregation is greatly influenced by fluid bed system properties which are independent of the particle mixture applied. Most notably these are: a. fluid bed dimensions, as the (hydraulic) bed diameter and the bed height, and b. bed operating conditions, like the superficial gas velocity.

A comprehensive review on the substantial literature on segregation in gas fluidized beds is provided by Beeckmans et al. (1984). Clearly most of the research on segregation is carried out on the Geldart's A- and B-powders, i.e. the small particle systems. However segregation in large particle B- and D-powder systems has been relatively neglected in literature so far, although these type of systems are more and more common; for example

they are characteristic for the bed material applied during the fluidized bed combustion of coal (FBC).

One main reason for this neglect may be that the mode of fluidization in large particle fluid beds (slugging type of fluidization) differs significantly from that in smaller particle systems (bubbling beds). This causes that the mechanism of segregation, on which generally the mathematical modeling of particle segregation is based, will also strongly differ in both systems which requires another approach in the modeling of segregation in large particle systems.

### 1.2 Segregation of particle systems during FBC

The particles applied in FBC are B- or D-type of powders according to the classification scheme of Geldart (1973) or 'fluid dynamically large' according to Jovanovic and Catipovic (1983). They differ significantly in size and density; coal ash:  $d = 700 \mu\text{m}$ ,  $\rho = 2600 \text{ kg/m}^3$ ; coal:  $d = 1 - 6 \text{ mm}$ ,  $\rho = 800 - 1400 \text{ kg/m}^3$ ; limestone/dolomite:  $d = 300 \mu\text{m} - 5 \text{ mm}$ ,  $\rho = 1200 - 2700 \text{ kg/m}^3$ .

Furthermore the relative amounts of ash, coal and sorbent that are present in the combustor are strongly different; generally the bulk of the bed consists of ash and sorbent, while coal is present in only a small weight percentage.

Consequently, segregation of the bed material during FBC will be enhanced by a. the clear differences in the particle properties as well as by b. the difference in their relative weight ratios.

However, it is clear that a good mixing during FBC has to be accomplished: a. to derive an optimum contact between the gaseous sulfur species released from volatiles and char combustion and the sorbent material in order to obtain an efficient sulfur capture, and b. to avoid defluidization of the particles.

This latter phenomenon is caused by variation of the minimum fluidization velocity along the bed height due to segregation. It occurs especially when the actual superficial gas velocity in the bed becomes smaller than the local minimum fluidization velocity. In general this happens in a region just above the distributor (Chiba and Nienow, 1984; Beekmans, 1984). This phenomenon must be avoided, because: a. it enhances coking, sintering and clinkering of the ash (Cooke et al., 1982), and b. it will decrease the coal combustion efficiency as well as the level of sulfur retention, and c. it can shorten the lifetime of the applied (regenerative) sorbent material.

A complicating factor is further that the rate and extent of sorbent segregation will change as a function of time due to the sulfur-uptake (Valkenburg et al., 1986).

So it is obvious that in FBC the rate and extent of segregation have to be well known in order to select the proper bed dimensions (hydraulic bed diameter) and the correct operating conditions (superficial gas velocity).

### 1.3 Fluidization behaviour during FBC

In general the fluidization behaviour of FBC-large-particle systems is characterized as 'slow bubbling': the bubble rise velocity is smaller than the interstitial velocity; the transition zone between the slow bubble void and the dense phase is not well defined and particles can rain through the voids.

However, the fluidization behaviour in a FBC combustor is also influenced by the closely packed internals as heat exchanger tubes. The space surrounded by the convex side of the tubes may be regarded as a system of small parallel fluidized beds with a hydraulic bed diameter of about 5 to 30 cm. The solids exchange between the parallel sections is low (Chen et al., 1983) and a good vertical mixing takes place with horizontal tubes positioned in line (Raven and Sparham, 1982) or with vertical pipes. The fluidization is mostly of the slugging type and shows remarkable agreement with the mode of fluidization in relatively small diameter fluid beds as is discussed by Noordergraaf et al. (1987).

Consequently, slugging is an important fluid dynamical phenomenon that certainly can influence the extent of segregation of coal and sorbent during fluid bed combustion.

### 1.4 Objective of this paper

Therefore in this paper slugging and segregation experiments in small diameter fluid beds with large particles are presented that are characteristic for FBC-particle-systems.

Further a simple steady segregation model is given which is derived from the mechanism of segregation in slugging beds as it is formulated based upon the observed particle flow.

## 2. EXPERIMENTAL

### 2.1 Slugging and segregation measurements

Bed height and slugging measurements as well as segregation experiments have been carried out at ambient conditions in 3.5 cm, 5 cm, 7.5 cm, 10 cm and 15 cm ID plexiglass fluid beds at superficial gas velocities ranging from the minimum fluidization velocity  $U_{mf} = 0.6$  m/s to 2 m/s. The bed aspect ratio at minimum fluidization ( $H_{mf}/D$ ) is varied between 0.79 and 3.04 in the segregation experiments, while  $H_{mf}/D$  is raised to 14.8 in the bed height measurements in the 10 cm ID bed.

Group D particle systems are used that resemble the composition of an ash-coal/sorbent mixture in a FBC combustor. The ash is represented by sand particles with a mass-averaged diameter of 1 mm (850 - 1200  $\mu$ m). The coal and sorbent are represented by (cylindrical) alumina particles with dimensions (2.9 - 3.7 mm) and densities (1250 - 1285 kg/m<sup>3</sup>) comparable to coal and limestone/dolomite. The material properties are summarized in Table 1. The weight ratio between sand and alumina in the segregation experiments is varied between 2 and 5; an overview is provided in Table 2.

Table 1: Properties of materials.

material	shape	diameter d		length l (mm)	density $\rho$ (kg/m <sup>3</sup> )
		1) (mm)	2)		
sand	spherical	1.0	-	-	2600
$\gamma$ -alumina	cylindrical	3.7	3.1	3.4	1285
calcined $\alpha$ -alumina	cylindrical	2.9	2.5	2.5	1250
iron	spherical	0.45	-	-	7860

- 1) based on spherical shape;  
2) based on cylindrical shape.

In a typical segregation experiment first the minimum and maximum bed heights are measured at the chosen gas velocity by means of visual observation. Further the bed is fluidized for 15 minutes whereupon the gas flow is abruptly stopped. This period of time is sufficient to reach steady segregation conditions; preliminary experiments showed that the steady state situation at a gas velocity of 1 m/s is already obtained after 15 to 20 seconds. Subsequently the bed content is removed in five layers of identical

height by means of a special vacuum equipment. In each layer the particles are separated by sieving after which their amount is determined by weighing. In general the loss of weight in an experiment is less than 2%.

Segregation experiments were also carried out with mixture I (Table 2) in a 10 cm ID fluid bed facility at atmospheric pressure and 850 °C. The superficial gas velocity was varied between  $U_{mf} = 0.38$  m/s and 2 m/s; the  $H_{mf}/D$ -ratio was fixed at 2.1. The same technique of abrupt defluidization and layer by layer analysis was used. The bed height was measured with use of a technique based on heat conduction (Kroon, 1986).

Table 2: Particle mixtures used in segregation experiments.

particle mixture	materials	weight ratio $W_R$
I	sand/calced alumina	3
II	sand/calced alumina	4
III	sand/ $\gamma$ -alumina	2
IV	sand/ $\gamma$ -alumina	4
V	sand/calced alumina	5

To investigate the effect of fluid bed diameter on the extent of segregation also experiments have been carried out at different bed diameters with a strong segregating particle system: a 5:1 weight mixture of iron particles ( $d = 450 \mu\text{m}$ ;  $\rho = 7860 \text{ kg/m}^3$ ) and cylindrical 3.7 mm  $\gamma$ -alumina particles at a  $H_{mf}/D$ -ratio of 2 and an excess gas velocity of 0.30 m/s.

## 2.2 Extent of segregation

The extent of segregation is expressed in a number  $S$  on a scale of 0 to 100 [-], which represents the axial distribution of the segregating (flotsam) alumina particles according to:

$$S = \text{ABS} [(N_{L1} + N_{L2}) - (N_{L4} + N_{L5})] \quad [1]$$

$N_{Li}$  is the percentual weight of the alumina in bed layer  $Li$  ( $i = 1, 2, 4, 5$ ;  $L1$  is the top layer).  $S = 0$  [-] in case of complete mixing, while  $S = 100$  [-] for complete segregation; so the latter situation is obtained when all alumina particles are found in the upper two layers of the bed.



### 3. SLUGGING IN FLUID BEDS

#### 3.1 Theoretical

##### 3.1.1 Types of slugging

In general three major types of slugging can be recognized (Geldart et al., 1978): 1. square-nosed or solids slugging, 2. symmetrical round-nosed slugging (axi-symmetric round-nosed slugging), and 3. asymmetrical round-nosed or wall slugging.

Square-nosed slugs are only encountered for large  $d/D$ -ratios and often involve rough walls. During square-nosed slugging the solids rain through the gas slug from a ceiling above and no clear slug boundary can be observed (Noordergraaf et al., 1987; Thiel and Potter, 1977). Hovmand and Davidson (1971) considered the 'raining slug regime' to be a breakdown of proper fluidization which occurs in beds of a diameter less than 5 cm. However, Thiel and Potter (1977) concluded that coarse particles readily form square-nosed slugs in high aspect ratio beds of a diameter even up to 22 cm.

Symmetrical round-nosed slugs appear in the intermediate region where square-nosed slugs are giving way to the asymmetrical round-nosed (wall) slugs.

##### 3.1.2 Characterization of slugging

The fluidization behaviour of slugging beds is in general completely characterized by three parameters, which are a. the minimum fluidization velocity, and b. two empirical dimensionless slug parameters. These three parameters determine the minimum and maximum expansion of slugging fluidized beds at a given value of the superficial gas velocity.

The minimum ( $H_{\min}/H_{mf}$ ) and maximum ( $H_{\max}/H_{mf}$ ) bed expansion of slugging beds are derived from expressions for the minimum and maximum bed height as given by Kehoe and Davidson (1973) respectively as:

$$E_{\min} = 1 + (1-b) [U_0 - U_{mf}] / U_s^0 \quad \text{and} \quad E_{\max} = 1 + [U_0 - U_{mf}] / U_s^0 \quad [2a]$$

$$\text{or: } (E_{\max} - 1) = (U_0 - U_{mf}) / U_s^0 \quad \text{and} \quad E_{\max} = 1/(1-b) E_{\min} - b/(1-b) \quad [2b]$$

$U_s^0$  is the stable slug velocity which is defined as:

$$U_s^0 = 0.35 [a g D]^{1/2} \quad [3]$$

The empirical slug parameter a is related to the type of slugging and characteristic values have already been obtained in literature. It equals 1 for round-nosed slugs;  $a = 2$  in case of wall slugs, while  $a$  equals 0.26 when it is assumed that the same form of equation can also be applied to square-nosed slugging (Rudolph and Judd, 1986).

Further, the empirical slug parameter b is introduced here: it represents the ratio between the height of a single particle slug ( $T \cdot D$ ) and the bed height at minimum fluidization:  $b = T \cdot D / H_{mf}$ . This parameter provides an indication for the number of particle slugs that is present in the bed: more than two solid slugs will be present when  $b < 0.5$ , while it is likely that generally only one slug is present when  $b \gg 0.5$ .

### 3.2 Experimental results

#### 3.2.1 Minimum fluidization velocity $U_{mf}$

The minimum fluidization velocity is simply obtained from bed height measurements by plotting the minimum and maximum bed height as a function of gas velocity (Noordergraaf, 1985). A typical example is shown in Figure 1 for mixture I in the 5 cm ID bed:  $U_{mf}$  is approximated as 0.59 m/s by linear extrapolation, while the corresponding bed height at minimum fluidization equals 15.2 cm.

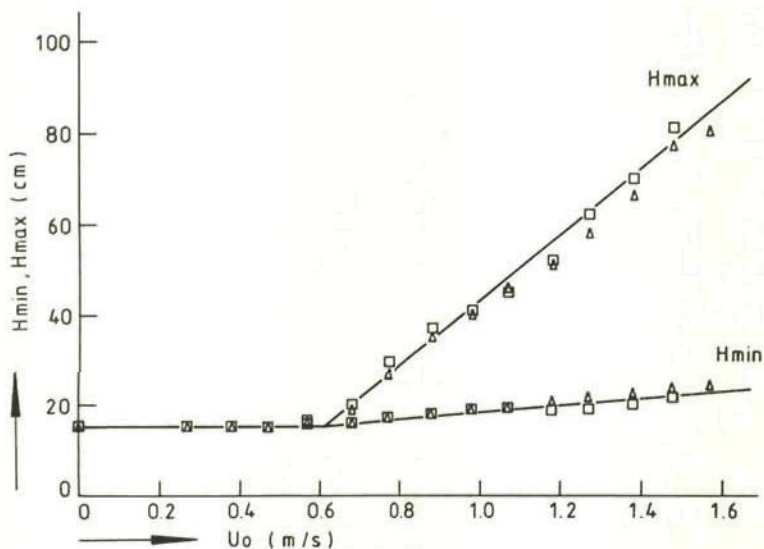


Figure 1: The minimum and maximum bed heights as a function of the superficial gas velocity; duplo experiments have been indicated.  
 (Mixture I;  $D = 5$  cm;  $H_{mf}/D = 3.04$  [-];  $U_{mf} = 0.59$  m/s;  $H_{mf} = 15.2$  cm;  
 $a = 0.89$  [-];  $b = 0.89$  [-];  $m_f = 2.70$  [-]).

It is observed that the minimum bed height is only a few cm's above the bed height at minimum fluidization; the increase with gas velocity is very small. However, the maximum bed expansion is a steep function of the gas velocity, where the difference between  $E_{\max}$  and  $E_{\min}$  reaches a factor of about 4 at 1.6 m/s in case of Figure 1. This implies that generally a slugging bed is characterized by large fluctuations of the bed height, which take place with a high frequency (0.5 to 2 Hz; Noordergraaf et al., 1987).

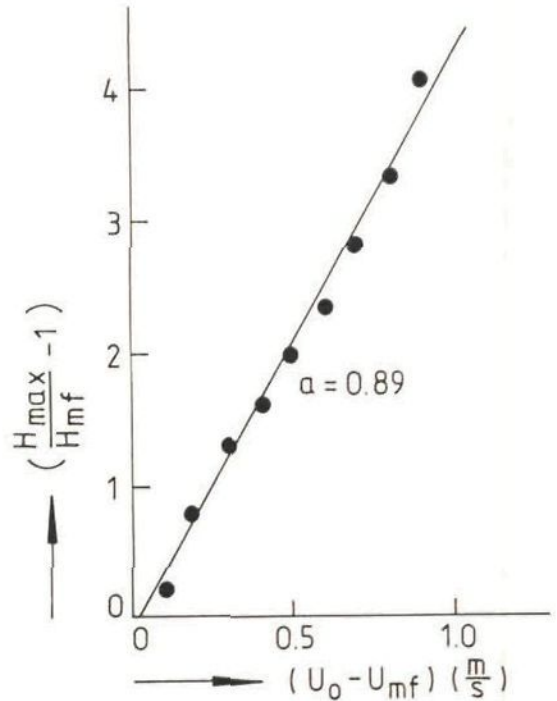
The minimum fluidization velocity of the sand, calcined alumina and  $\gamma$ -alumina are determined in the 10 cm ID bed at ambient conditions respectively as 0.55 m/s, 0.85 m/s and 0.95 m/s.

The minimum fluidization velocities of the sand, calcined alumina and the 1:3 mixture at 850 °C in the 10 cm ID facility are measured to be 0.30 m/s, 0.8 m/s and 0.38 m/s respectively.

### 3.2.2 Slug parameter a

Plotting of  $(E_{\max} - 1)$  against  $(U_0 - U_{mf})$  gives a straight line with slope  $1/U_s^0$  from which the slug parameter  $a$  is calculated, Eq.[2b]. An illustrative example is shown in Figure 2 for mixture I in the 5 cm ID bed at a  $H_{mf}/D$ -ratio of 3.04. The slug parameter  $a$  equals 0.89, which indicates a mode of slugging in between square- and round-nosed slugging.

Figure 2: Determination of the dimensionless slug parameter  $a$  from the slope  $1/U_s^0$  of the straight line which is obtained by plotting  $(E_{\max} - 1)$  as a function of the excess gas velocity  $(U_0 - U_{mf})$ ; conditions: see Figure 1.



In general it is concluded that  $a$  is independent of mixture composition, but strongly dependent on the  $H_{mf}/D$ -ratio as is shown for example in Figure 3 in case of the 10 cm ID bed. This graph demonstrates that  $a < 2$  for  $H_{mf}/D$ -ratios of more than 2. Wall slugging is likely to occur at aspect ratios between 1.5 and 2.5, round-nosed slugging at ratios of 2 to 4, while square-nosed slugging is present at higher  $H_{mf}/D$ -ratios where  $a$  varies between 0.1 and 0.5.

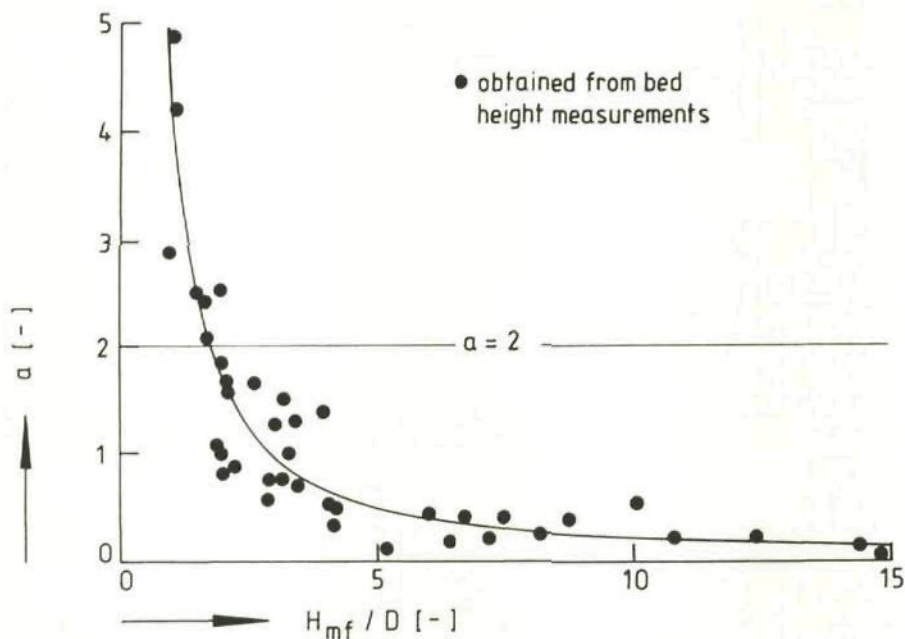


Figure 3: The slug parameter  $a$  as a function of the  $H_{mf}/D$ -ratio in the 10 cm ID bed; bed material is sand and alumina in different weight ratios.

### 3.2.3 Slug parameter $b$

Plotting of  $E_{max}$  against  $E_{min}$  gives a straight line with slope  $1/(1-b)$  and intercept  $-b/(1-b)$  from which the slug parameter  $b$  is obtained, Eq.[2b]. This is illustrated in Figure 4 for mixture I in the 5 cm ID bed at a  $H_{mf}/D$ -ratio of 3.04;  $b$  is calculated from the intercept to be 0.895, while the slope gives a value of 0.893.

$b$  increases clearly with the  $H_{mf}/D$ -ratio as is shown for example in Figure 5 in case of the 10 cm ID bed. At aspect ratios smaller than 2 a steep increase in  $b$  is measured, but this is in the region where no clearly defined type of slugging is present (Figure 3: slug parameter  $a > 2$ ). In the region where  $a < 2$  ( $H_{mf}/D > 2$ ) the slug parameter  $b$  increases very slowly

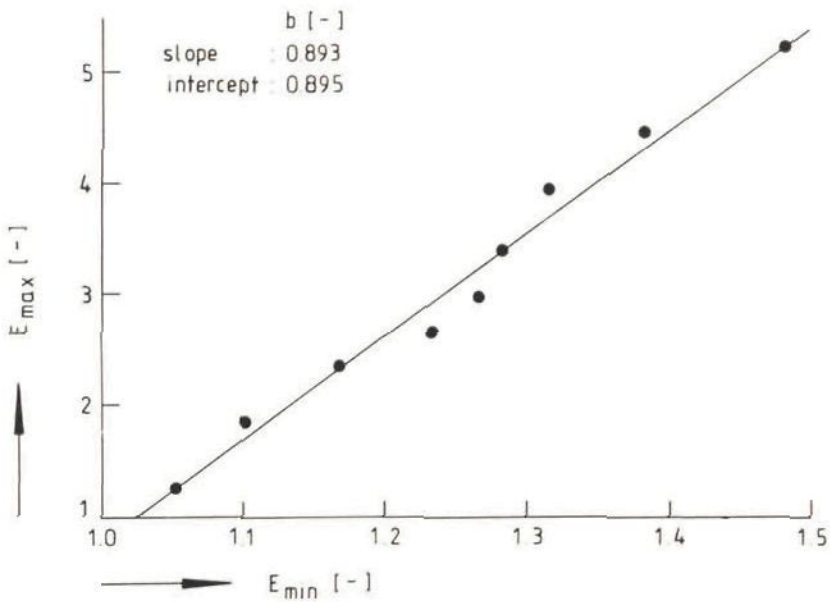


Figure 4: Determination of the dimensionless slug parameter  $b$  from the slope  $1/(1-b)$  or intercept  $b/(1-b)$  of the straight line which is obtained by plotting  $E_{\max}$  as a function of  $E_{\min}$  (conditions: see Figure 1).

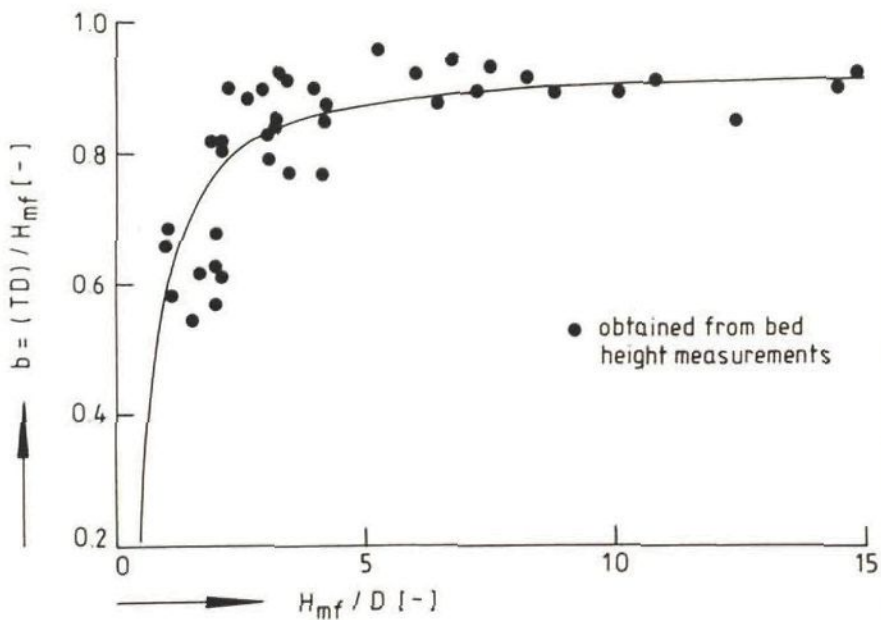
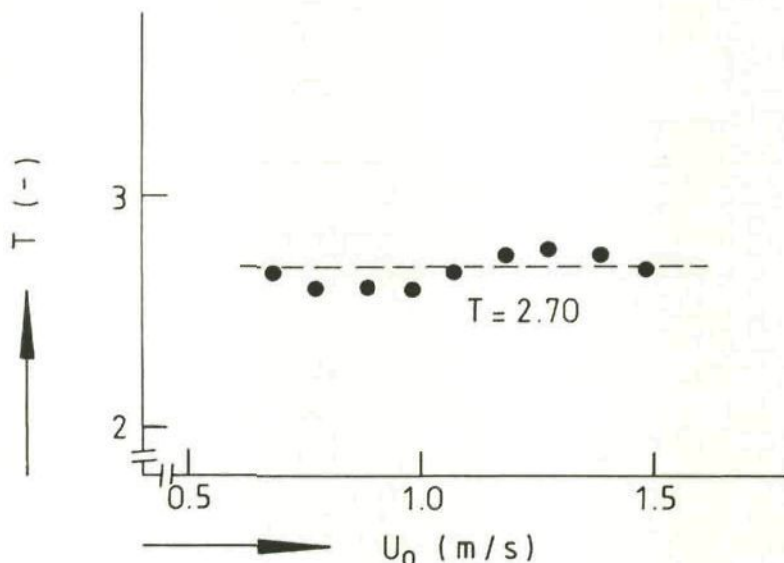


Figure 5: The slug parameter  $b$  as a function of the  $H_{mf}/D$ -ratio (10 cm bed).

from about 0.8 to 0.92 at  $H_{mf}/D = 14.8$ . This means that the average length of a particle slug equals about 80% to even more than 90% of the bed height at minimum fluidization. This implies that in general only one particle slug is present in the bed.

In this section it is implicitly assumed by plotting  $E_{max}$  against  $E_{min}$  that the dimensionless distance  $T$  between two successive gas slugs (expressed in units of bed diameter) is not dependent on the superficial gas velocity. This assumption is confirmed by experiment as is illustrated in case of mixture I in Figure 6.



**Figure 6:** The dimensionless interslug spacing  $T$  as a function of the superficial gas velocity (conditions: see Figure 1).

This result is in agreement with experiments of Hikita et al. (1984); they measured the frequencies of solid plugs ( $d = 2.1$  mm;  $\rho = 2250$  kg/m<sup>3</sup>) to be nearly proportional to the solid flow rate in 5 cm and 15 cm ID pipes. They concluded that the average length of plugs (i.e.  $TD$ ) is almost constant regardless of the solid flow rate and consequently independent of the superficial gas velocity. This latter effect is also reported by Donsi et al. (1984) for the slug flow of glass ballotini (354  $\mu$ m) and silica sand (115  $\mu$ m) in a 20 cm ID bed at ambient conditions.

### 3.2.4 Observed particle flow

Although slug parameters were measured which indicated a mode of slugging in between symmetrical round-nosed and asymmetrical round-nosed slugging at  $H_{mf}/D$ -ratios between about 2 and 4 as discussed in section 3.2.2, we clearly could still visually observe the rise of solids plugs followed by the transition to swarms of particles raining through the next gas slug over the complete cross-sectional bed area. No downwards flow was observed of particles predominantly past the rising gas slug in an annular region on the wall as is frequently reported in literature to be characteristic for round-nosed slugging.

Only in the 15 cm ID bed at low  $H_{mf}/D$ -ratios (smaller than 1) no solids raining is observed anymore. The mode of fluidization seems to be more that as it is attributed to wall slugging: successive dense plugs of solids flow downwards alongside the pipe walls. This implies that the main upwards flow of particles should take place in the center of the bed.

## 4. SEGREGATION IN SLUGGING FLUID BEDS

### 4.1 Theoretical

#### 4.1.1 Mechanism of particle flow in slugging fluid beds

In the same way as is proposed for example by May (1959), Van Deemter (1967) and Gibilaro and Rowe (1974) in case of solids flow in small particle diameter systems, it is assumed here in case of slugging large particle fluid beds that the flow of solids is characterized by four flow mechanisms: convective flow, segregating flow, dispersive flow and/or particle exchange.

The following flow mechanism for segregating particles in round- and square-nosed slugging beds is proposed based upon the measured and observed flow of solids as discussed in section 3.2; a schematical representation is given in Figure 7:

- \* the segregating particles move downwards in the gas slug with a convective velocity ( $v$ ), which is related to the descending velocity of solids in the gas slug due to gravity;
- \* the segregating particles move upwards in the particle slug with a convective velocity ( $k$ ), which contains a **segregating component** that is predominantly caused by an 'Archimedes-like' upwards force due to density differences between the particles (buoyancy);

\* particle exchange takes place at the boundary between the gas and particle slug between the up flowing and down flowing segregating particles and is represented by a transfer coefficient ( $p$ ) expressed in volumes of solids per unit bed volume per unit of time;

\* eventually also a dispersive particle flow may be present; however, in the next section it will be shown that particle exchange and particle dispersion are theoretically interrelated.

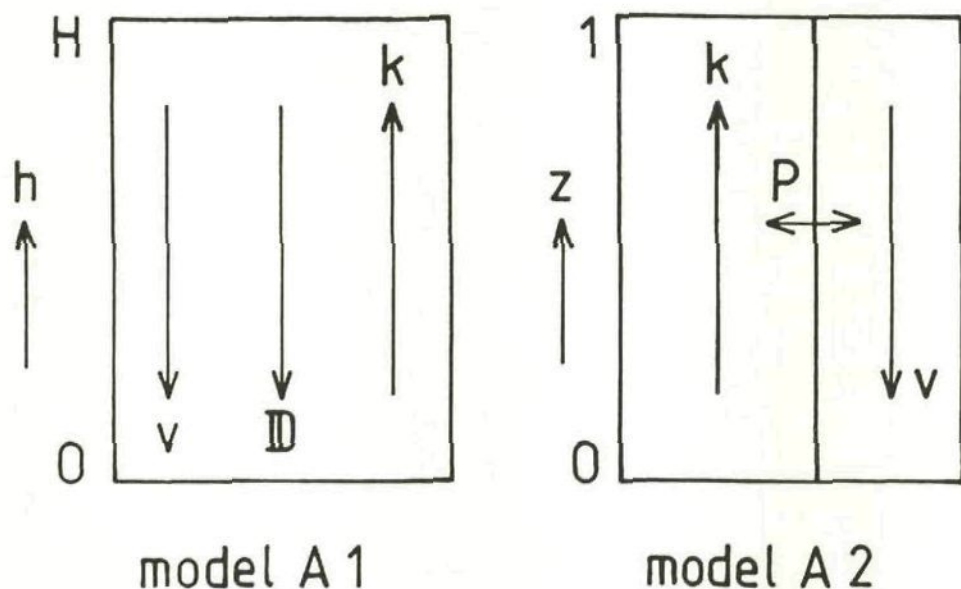


Figure 7: Schematical representation of the particle flows in a slugging fluidized bed.

Model A1: convective particle flows ( $v, k$ ) and particle dispersion ( $D_0$ );  
 Model A2: convective particle flows ( $v, k$ ) and particle exchange ( $p$ ).

$v$  and  $k$  are the average linear velocities of the segregating particles in the respective downwards and upwards solid flows; so  $f_v v$  and  $f_k k$  are the superficial velocities with  $f_v$  and  $f_k$  representing the volume fractions of the solids. It is obvious that  $(f_v + f_k)$  equals  $(1 - f_s - \epsilon)$ , with  $f_s$  is the volume fraction of the non-segregating material and  $\epsilon$  is the bed porosity.

The present authors have already shown that model A1 as indicated in Figure 7 is able to describe the occurrence of a maximum in the non-steady state segregating particle distribution as a function of time due to a pulse-like input of slightly higher density tracer particles in a 10 cm ID bed (Valkenburg et al., 1986).



#### 4.1.2 Modeling of particle flow in slugging fluid beds

Two simple mathematical models are set up based on the flow mechanism as outlined in the previous section and as shown in Figure 7. For both models mathematical equations will be derived, which describe the axial segregating particle distribution.

##### model A1

The following differential equation is derived from a steady state mass balance in case of model A1:

$$D_0 \frac{d^2 c(h)}{dh^2} + (f_v v - f_k k) \frac{dc(h)}{dh} = 0 \quad [4]$$

The two boundary conditions are:

1. no material leaves the bed at the top or at the bottom;

$$\text{at } h=0 \text{ and } h=H: \quad D_0 \frac{dc(h)}{dh} + (f_v v - f_k k) c(h) = 0 \quad [5]$$

2. the total amount of segregating material  $N$  is obtained by integration of  $c(h)$  along the bed height  $h$ :

$$N = \int_0^H c(h) F dh \quad [6]$$

Solution of this set of equations results in an expression for the axial particle concentration:

$$c(z) = c_0 \frac{-\lambda \exp(-\lambda z)}{\exp(-\lambda) - 1} \quad \text{with } c_0 = N/(HF) \text{ and } z = h/H \quad [7]$$

The amount of segregating material  $\Delta n(\Delta z)$  in a bed layer of dimensionless height  $\Delta z = z_2 - z_1$  is subsequently obtained from:

$$\Delta n(\Delta z) = \int_{z_1}^{z_2} c(z) HF dz \quad [8]$$

Combination of Eqs. [7] and [8] leads to:

$$\Delta n(\Delta z) = N \left[ \frac{\exp(-\lambda z_2) - \exp(-\lambda z_1)}{\exp(-\lambda) - 1} \right] \quad [9]$$

This equation shows that the steady state axial segregating particle distribution in case of model A1 is characterized by one dimensionless

'Peclet-like' number  $\lambda$ , which is the ratio between the net particle convective and segregating flows and the particle dispersive flow:

$$\lambda = (f_v v - f_k k) H / D_0 \quad [10]$$

The situation of complete mixing ( $S = 0$  [-]) is obtained when  $\lambda$  equals zero: in that case it can be derived from Eq.[9] that  $\Delta n(\Delta z)/N = \Delta z$ . With the definition of the model parameter  $\lambda$  in Eq.[10] it is directly observed that complete mixing is attained:

- a. at high values of the dispersion coefficient  $D_0$ ,
- b. at low values of the bed height  $H$  (so in shallow beds), and
- c. when the superficial upwards and downwards solids flows, respectively  $(f_v v)$  and  $(f_k k)$ , are equal.

The sign of the model parameter  $\lambda$  depends on the magnitude of the superficial solids flows.  $\lambda$  is positive when  $(f_k k)$  is smaller than  $(f_v v)$ ; in that case a 'jetsam' segregating system is considered. The 'flotsam' systems are related to negative values of  $\lambda$ : the upwards superficial solids flow is larger than the downwards flow ( $f_k k > f_v v$ ).

In Figure 8 the axial 'flotsam' segregating particle concentration  $c(z)$ , Eq.[7], is plotted as a function of the dimensionless bed height  $z$  at different values of the dimensionless model parameter  $\lambda (< 0)$ .

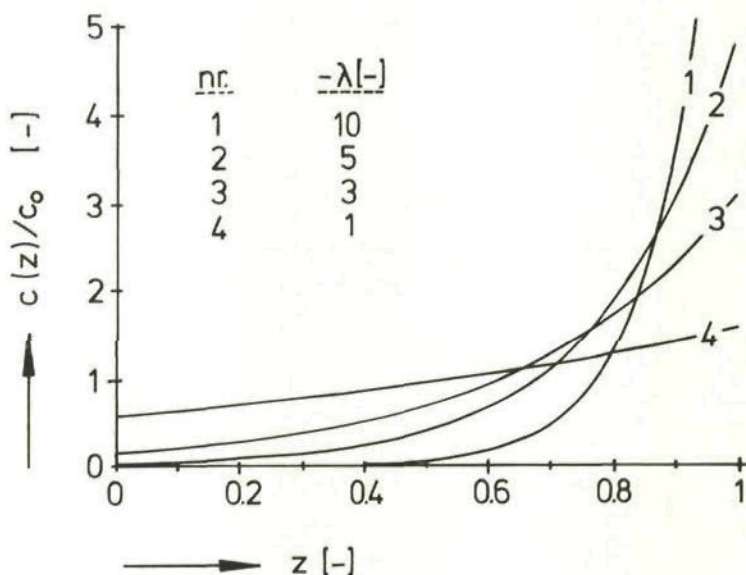


Figure 8: The axial 'flotsam' segregating particle concentration  $c(z)/c_0$ , Eq.[7], as a function of the dimensionless bed height  $z$  at different values of the dimensionless model parameter  $\lambda (< 0)$ .

It is concluded that the local dimensionless concentration  $c(z)/c_0$  equals 1 at an axial position of  $z = 0.53 [-]$  when  $\lambda = -1 [-]$  or  $z = 0.76 [-]$  when  $\lambda = -10 [-]$ . This implies that when  $\lambda < -1 [-]$  the amount of flotsam material in the lower part of the bed ( $z < 0.5 [-]$ ) is always less than in the ideally mixed situation. A steep jetsam segregation profile is found when  $\lambda < -5 [-]$ ; here is in general  $c(z)/c_0 \gg 1$  when  $z > 0.8 [-]$ .

### model A2

Steady state mass balances on phases 'a' and 'b' in model A2 as given in Figure 7 result in the following differential equations:

$$\text{phase 'a': } \frac{d c_a(h)}{d h} = \left( \frac{f_v}{f_k} - \frac{p}{k} \right) [c_a(h) - c_b(h)] \quad [11a]$$

$$\text{phase 'b': } \frac{d c_b(h)}{d h} = \left( \frac{f_v}{f_v} - \frac{p}{v} \right) [c_a(h) - c_b(h)] \quad [11b]$$

The two boundary conditions are:

1. the upwards and downwards flows are equal at each axial position in the steady state situation:

$$f_k k c_a(h) = f_v v c_b(h) \quad \text{for } 0 < h < H \quad [12]$$

2. the second b.c. is the same as for model A1:

$$N = \int_0^H (c_a(h) + c_b(h)) F dh \quad [13]$$

Solution of these equations leads to the following expression for the steady state axial segregating particle distribution in case of model A2:

$$\Delta n(\Delta z) = N \left[ \frac{\exp(-\alpha z_2)}{\exp(-\alpha)} - \frac{\exp(-\alpha z_1)}{1} \right] \quad [14]$$

Consequently the same type of equation is obtained as for model A1, where the dimensionless parameter  $\alpha$  in case of model A2 is given by:

$$\alpha = \frac{p (f_v v - f_k k) H}{f_v v f_k k} \quad [15]$$

This is a remarkable result from a mechanistic point of view, because it suggests that the 'first order' solids exchange between two separate upwards

and downwards particle flows can theoretically be described by a 'second order' dispersive particle flow which is superimposed on the one net convective flow of solids. So the dispersion coefficient  $D_0$  is a function of the solids exchange parameter  $p$ ; this relationship is derived from  $\alpha = \lambda$ , Eqs.[10] and [15], to be:

$$D_0 = f_v v f_k k / p \quad [16]$$

Consequently, a large dispersion coefficient  $D_0$ , which causes a low extent of segregation, corresponds with a small value of the solids exchange coefficient  $p$ . In other words: this implies mechanistically that a high rate of particle exchange between the upwards and downwards solids flows is favorable to segregation. So when particles have a tendency to segregate due to for example significant differences in their densities, this tendency is reduced by a decrease of the 'in-bed freedom of particle movement', which is related to a lower solids exchange between the phases. In practice this may be observed for example with 'finned' heat exchanger tubes which lower the extent of solids movement and therefore decrease the segregation tendency in comparison with smooth exchanger pipes.

#### 4.2 Experimental results

In section 1.1 it has been discussed that segregation is influenced by a. particle properties, b. the amount of particles in the bed, and by c. fluid bed system properties. In this section 4.2 it will be shown how the variables b and c influence the extent of segregation in case of the FBC particle system used. The effect of the amount of particles ( $H_{mf}/D$ -ratio) is demonstrated in section 4.2.1, the influence of the bed system properties as the gas velocity and the bed diameter are discussed respectively in sections 4.2.2 and 4.2.3, while some modeling results are outlined in section 4.2.4.

##### 4.2.1 Effect of $H_{mf}/D$ -ratio

In Figure 9 the extent of segregation is demonstrated as a function of the  $H_{mf}/D$ -ratio for mixture I at a superficial gas velocity of 0.9 m/s. The effect of the amount of solids is very significant:  $S$  increases from about 15 [-] at  $H_{mf}/D = 1$  to about 65 [-] at a ratio of 3. Other experiments show the same effect at a gas velocity of 1.1 m/s: in that case  $S$  increases from 7.5 [-] at  $H_{mf}/D = 1$  to 60 [-] at a ratio of 3. In both cases the absolute difference is about 50 units, which proves the importance of the amount of bed material with respect to segregation.

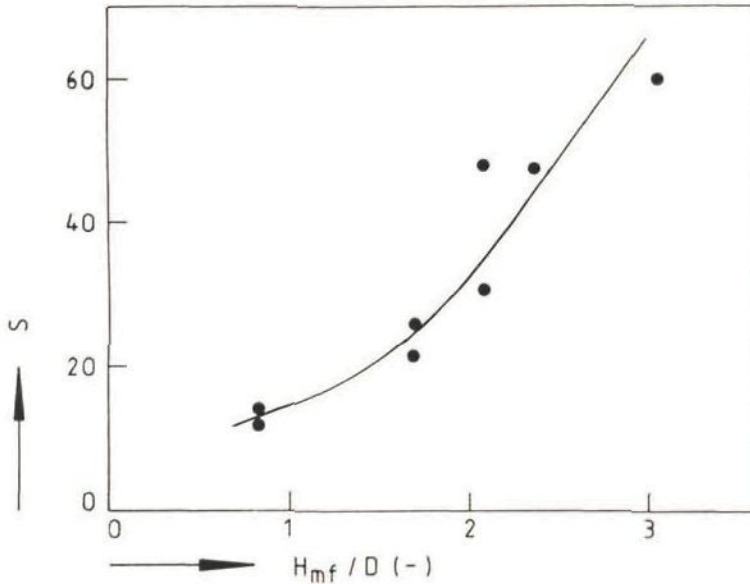


Figure 9: The influence of the bed aspect ratio at minimum fluidization,  $H_{mf}/D$ -ratio, on the extent of segregation (mixture I:  $U_0 = 0.9$  m/s).

#### 4.2.2 Effect of superficial gas velocity

In Figure 10 (see also Table 3) six typical examples of the extent of segregation  $S$  of several bed mixtures have been plotted as a function of the superficial gas velocity at different  $H_{mf}/D$ -ratios in the 5 cm, 7.5 cm, 10 cm and 15 cm ID fluid beds at ambient conditions. It is concluded that the extent of segregation decreases with increasing gas velocity as can be expected.

Table 3: Experimental conditions in Figures 10a to 10f: the influence of the superficial gas velocity on the extent of segregation.

Fig.	Mixture	$D$ [cm]	$H_{mf}/D$ [-]	$U_{mf}$ [m/s]	$a$ [-]	$b$ [-]
10a	I	5	2.08	0.64	2.10	0.84
10b	IV	5	2.08	0.68	2.21	0.91
10c	I	5	3.04	0.59	0.89	0.89
10d	I	7.5	2.36	0.56	2.10	0.78
10e	I	10	1.68	0.54	2.08	0.83
10f	I	15	0.83	0.57	2.88	0.87

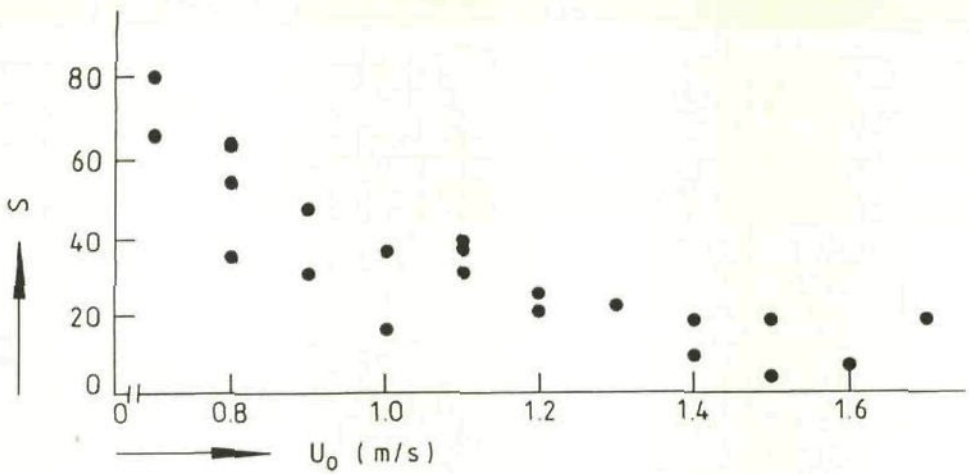


Figure 10a (see Table 3).

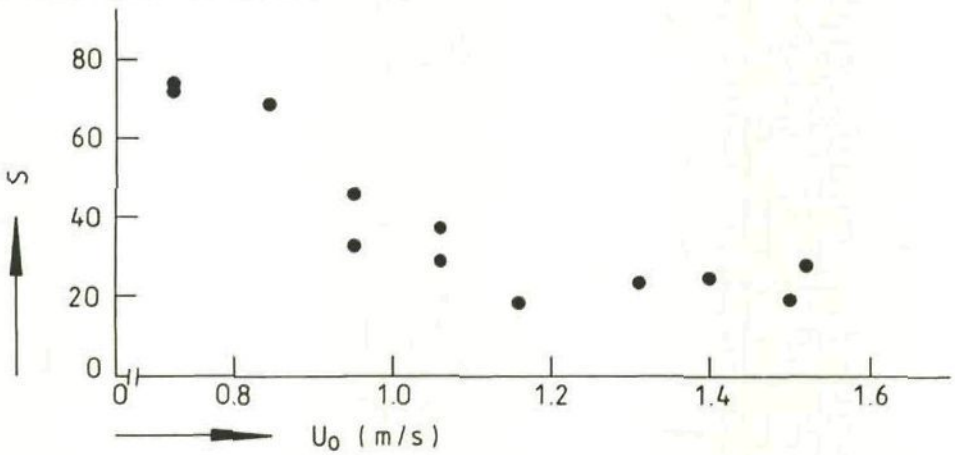


Figure 10b (see Table 3).

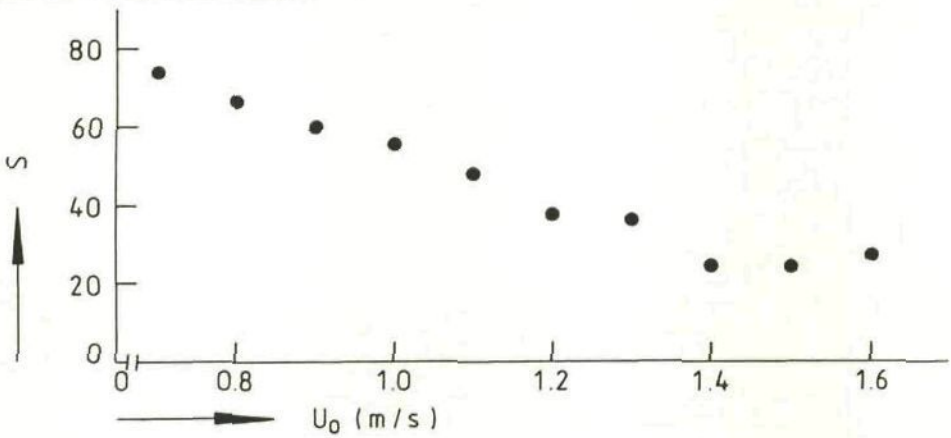


Figure 10c (see Table 3).

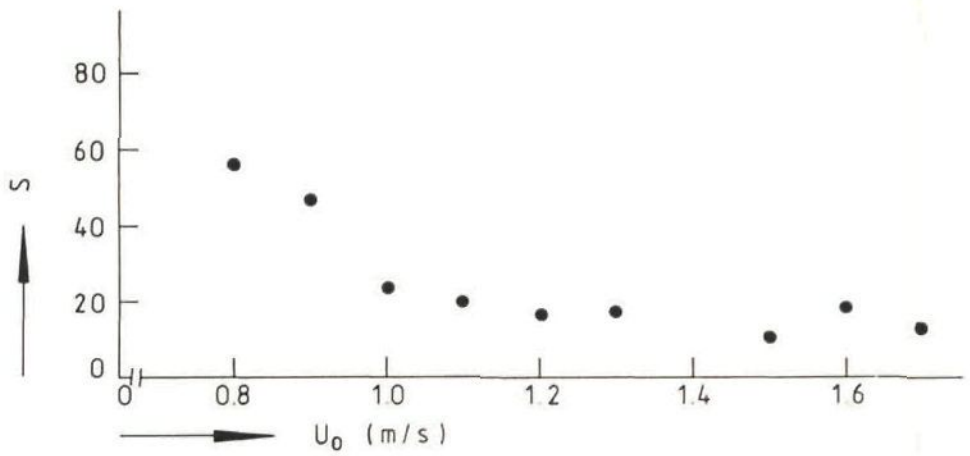


Figure 10d (see Table 3).

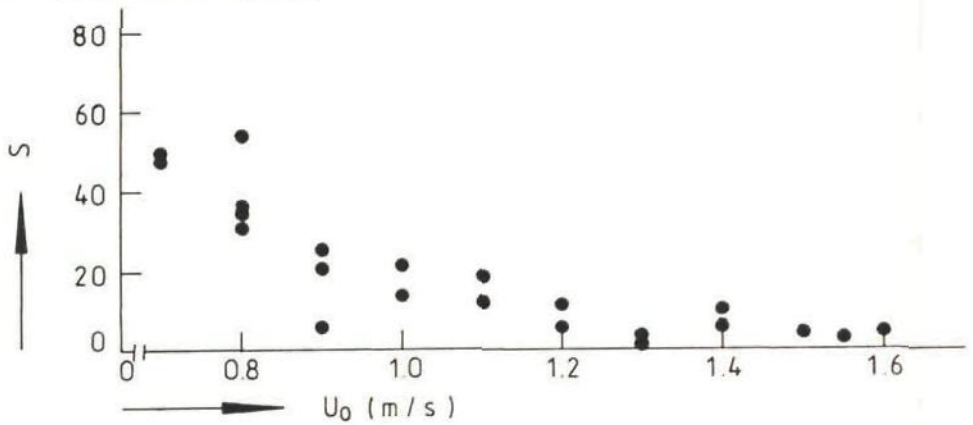


Figure 10e (see Table 3).

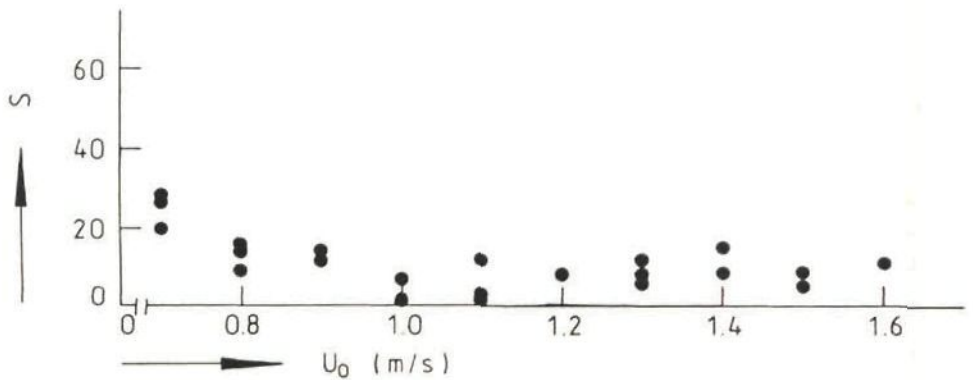


Figure 10f (see Table 3).

Further, it is shown that still a significant degree of segregation is present at superficial gas velocities of about three times the minimum fluidization velocity, resulting in a value of  $S$  of less than 10 [-] in the 10 cm ID bed to more than 20 [-] in the 5 cm ID bed.

It is remarkable that the extent of segregation in the 15 cm ID bed remains constant at an average level of about 10 [-], even at the low  $H_{mf}/D$ -ratio of 0.83 applied and at relative high gas velocities ( $> 1$  m/s).

In Figure 11 the extent of segregation is given as a function of gas velocity at 850 °C in the 10 cm ID bed.  $S$  shows a steep decrease between 0.5 m/s and 1.0 m/s; hereafter  $S$  decreases rather slowly and is still about 10 [-] at a superficial gas velocity of 2.0 m/s, which is even more than 5 times the minimum fluidization velocity.

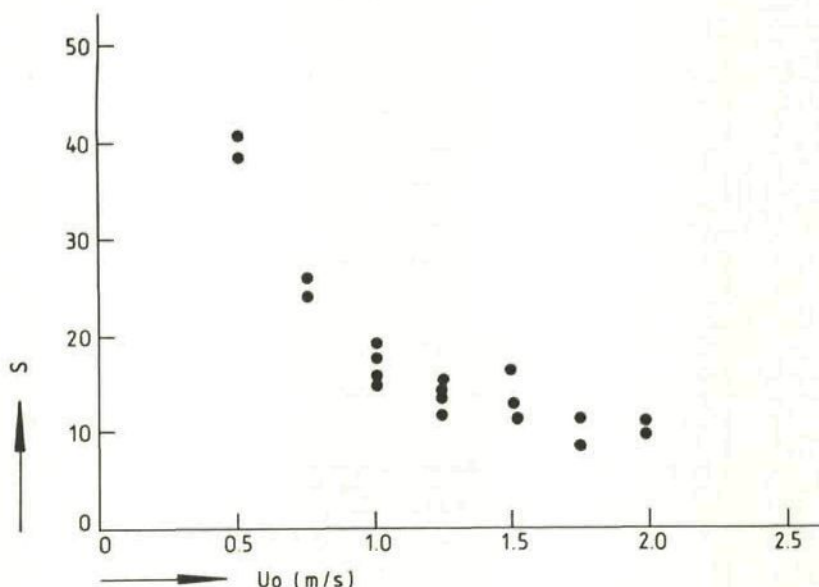


Figure 11: The influence of the superficial gas velocity on the extent of segregation in the 10 cm ID bed at 850 °C; (Mixture I;  $H_{mf}/D = 2.1$  [-];  $U_{mf} = 0.38$  m/s).

Consequently, it is concluded from the above results that always a fixed extent of segregation is present in the order of  $S = 10$  [-] to  $S = 20$  [-] at superficial gas velocities (1 - 2 m/s) and (hydraulic) bed diameters ( $< 15$  cm ID) that are of relevance in fluid bed combustion.

This observation may be explained by the fact that a slugging bed becomes more and more "divided" in two regions at higher gas velocities; the



first region is found between the distributor and the minimum bed height, while the second exists between the minimum and maximum bed heights (see Figure 1). In this second region a high degree of mixing is present due to the large fluctuations in bed height between  $H_{\min}$  and  $H_{\max}$  that are caused by large upwards and downwards movements of the particles (where  $H_{\max}/H_{\min}$  can be even higher than 4; the frequency of fluctuations is also high: 0.5 to 2 Hz according to Noordergraaf et al., 1987). A considerable less degree of mixing exists in the less violent fluidizing first bed region where the slugs are formed. So a state of dynamic equilibrium exists between the two regions, where the slugs that are generated in region 1 will "entrain" particles in region 2, which can be regarded as a large "splash zone".

Further, the 'entrained' flotsam solids are balanced by an opposite flux of particles from region 2 to region 1. However, it is likely that this flux is rather small, because it is visually observed that at the boundary between region 1 and 2 at  $H_{\min}$  mainly solids slugs are moving upwards; while the observed downward movement of particles, caused by 'solids raining' through the successive gas slugs, begins at higher positions in the bed. This implies that the downwards movement of flotsam particles from the upper region 2 to the lower region 1 will be small, especially at higher gas velocities, which causes that always a small degree of segregation will remain.

#### 4.2.3 Effect of bed diameter

The effect of a larger bed diameter on solids circulation has been reported in literature several times. Werther (1973) concluded that the influence of bed diameter is progressively stronger especially at low bed diameters, i.e. smaller than 20 cm; the bed diameter influences the transition to slugging and so the solids circulation pattern. Glicksman and McAndrews (1985) reported a significant effect of bed width on the fluid dynamics of large particle fluidized beds. They also showed that a horizontal tube bank in the bed acts to reduce the effective cross-section of the bed.

In Figure 12 the extent of segregation  $S$  is explicitly plotted as a function of the bed diameter  $D$  at a constant  $H_{mf}/D$ -ratio of 2.0 and at a constant excess gas velocity ( $U_0 - U_{mf}$ ) of 0.30 m/s. It is concluded that segregation decreases linearly with increasing bed diameter:  $S$  decreases from an average value of about 57 [-] in the 3.5 cm ID bed to an average value of about 18 [-] in the 15 cm bed.

This graph clearly suggest that the extent of segregation  $S$  approximates  $S = 0$  [-] at a specific critical value of the bed diameter  $D$ , which equals

23 cm in this particular case as is determined from linear extrapolation. This implies that not only the gas velocity is an important variable with respect to segregation, but also the (hydraulic) bed diameter is very significant.

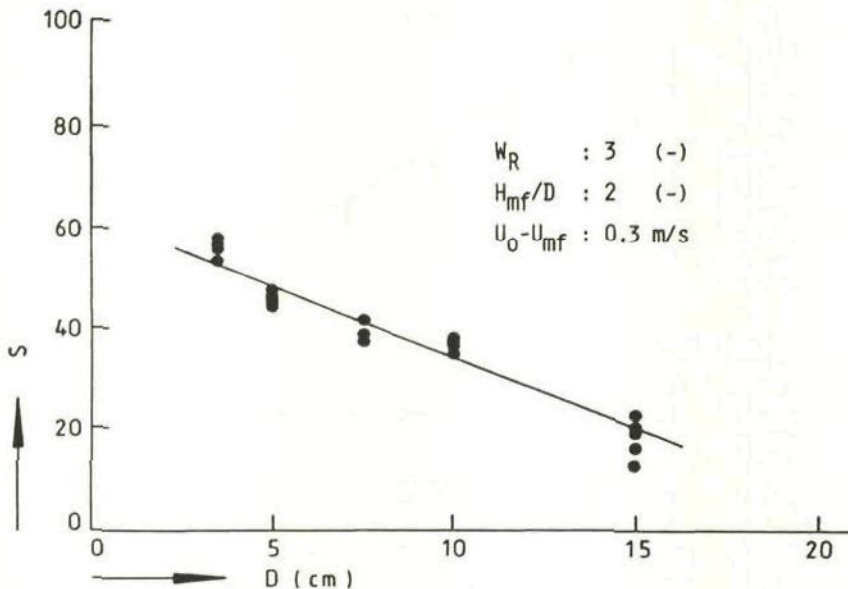


Figure 12: The influence of the bed diameter on the extent of segregation (Mixture I;  $H_{mf}/D = 2.0$  [-];  $U_0 - U_{mf} = 0.30$  m/s).

The effect of bed diameter is also indicated in Figure 13 at a  $H_{mf}/D$ -ratio of 2 and an excess gas velocity of 0.30 m/s for a complete other, stronger segregating, type of particle system: a 5:1 weight mixture of iron and  $\gamma$ -alumina particles, which will be compared with the results of Figure 12. The extent of segregation at the bed diameter of 3.5 cm is in absolute units 18 larger than in case of the sand/alumina-mixture; the average value of  $S$  is about  $S = 75$  [-]. However, the extent of segregation at the bed diameter of 15 cm is significantly decreased and equals about 28 [-], which is in absolute units only 10 higher than in case of the sand/alumina-mixture.

This influence of bed diameter on segregation can be predicted by an evaluation of the proposed segregation model. It has been shown in Eq.[10] that the model parameter  $\lambda$  decreases with an increasing solids dispersion coefficient  $D_0$ , which leads to a decrease in segregation (Eq.[9]). Thiel and Potter (1978) proposed a theoretical relation for the solids dispersion coefficient in slugging beds, which shows that  $D_0$  increases with a larger

bed diameter. This effect has been experimentally confirmed by several authors as is summarized by Avidan and Yerushalmi (1985).

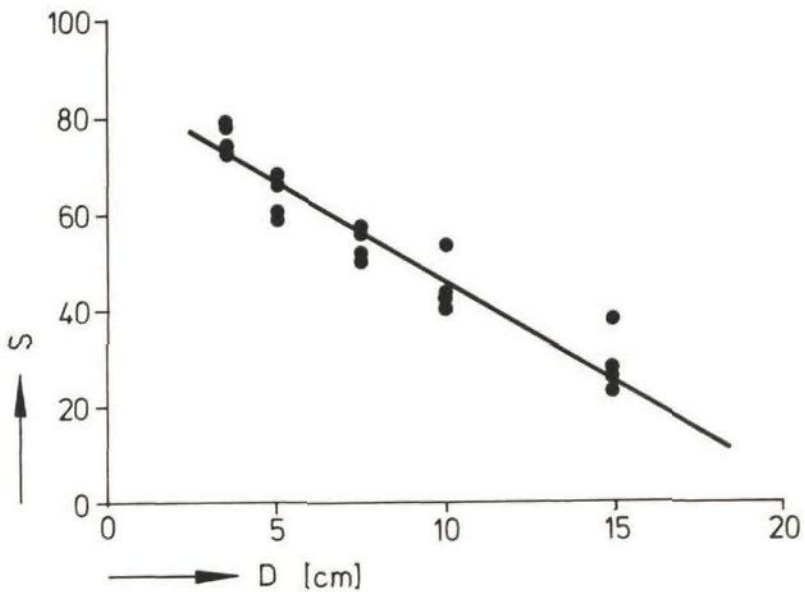


Figure 13: The effect of the bed diameter on the extent of segregation in a 5:1 weight mixture of iron particles and  $\gamma$ -alumina particles; ( $H_{mf}/D = 2.0$  [-];  $U_o - U_{mf} = 0.30$  m/s).

The effect of bed diameter on the extent of mixing and segregation can be generally explained by the fact that the mechanism of solids transport gradually changes. At small bed diameters the downwards and upwards solids movements are predominantly axially positioned at fixed bed regions and take place over the complete cross-sectional area (as during square-nosed slugging). However, the solids movement at higher bed diameters is not anymore only axial fixed, but also the radial position becomes important; particles move upwards along the centerline of the bed, while the downwards movement is located along the pipe walls (as observed with wall slugging in the 15 cm ID bed). Of course this will greatly enhance the degree of overall solids mixing in the bed.

Consequently, in general it can be concluded that a larger bed diameter leads to a considerable decrease in the extent of segregation, which therefore might be a more 'powerful tool' in the reduction of segregation than increasing the superficial gas velocity. However, it should be noticed with regard to fluid bed scale-up considerations that the avoidance of

segregation by applying a larger (hydraulic) bed diameter is clearly a means which has to be dealt with in the design and construction phase of a FBC boiler, while influencing segregation by the superficial gas velocity is obviously a more dynamic operational tool.

#### 4.2.4 Some modeling results

The experimental axial segregating particle distributions are fitted to the model distribution as expressed by Eqs.[9] or [14], by minimalization of the difference between the model and experimental amount of particles in the successive bed layers L1 to L5. Two typical examples are given in Figure 14, which show that the model is able to fit the experimental distributions very well.

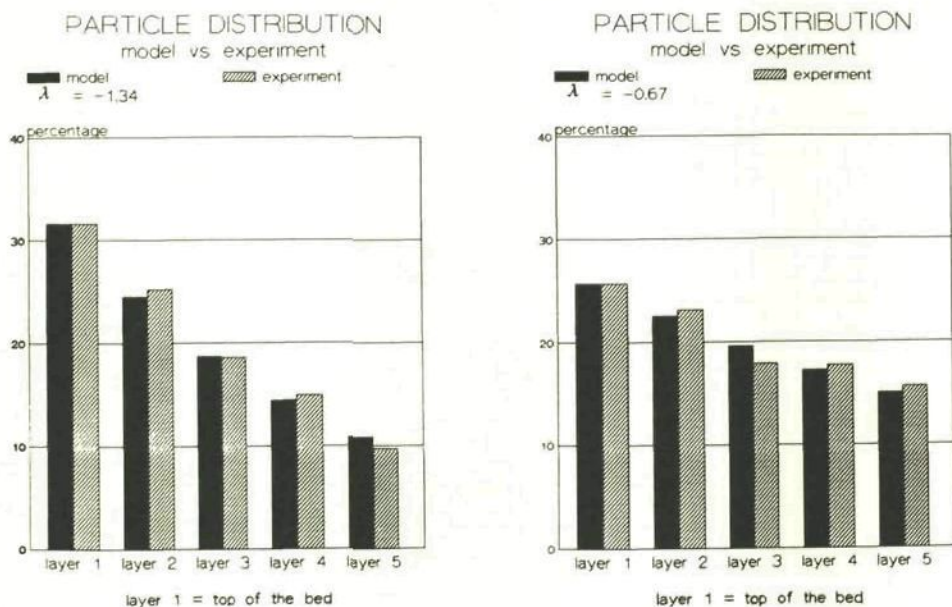


Figure 14a, 14b: Comparison between two experimental segregation particle distributions and the respective model fits:

Fig.	Mixture	D [cm]	$H_{mf}/D$ [-]	$U_{mf}$ [m/s]	$U_o$ [m/s]	a [-]	b [-]
14a	I	5	2.08	0.64	1.10	2.10	0.84
14b	II	10	1.98	0.51	1.00	2.52	0.75

Further it is shown that in the 5 cm ID bed at 1.10 m/s ( $S = 30$  [-]) the top layer 1 of the bed contains about three times as much flotsam alumina particles as the bottom layer 5. In the 10 cm ID bed ( $S = 15$  [-]) this

difference is reduced to about 1.7 times at almost the same experimental conditions. This difference between top and bottom layer is important from a sulfur retention point of view, because it may influence the position choice of the coal feed in relation to the rate of sulfur release during coal devolatilization.

The agreement between model and experiment can also be concluded from Figure 15, which gives the theoretical relationship between the model parameter  $\lambda$ , Eq.[9], and the extent of segregation  $S$ , Eqs.[1] and [10]. It is observed that the relationship between  $\lambda$  and  $S$  is linear. Further in this graph some typical fitted values of  $\lambda$  have been indicated as a function of the experimental extent of segregation of mixture I in the 5 cm, 10 cm and 15 cm ID beds at different gas velocities.

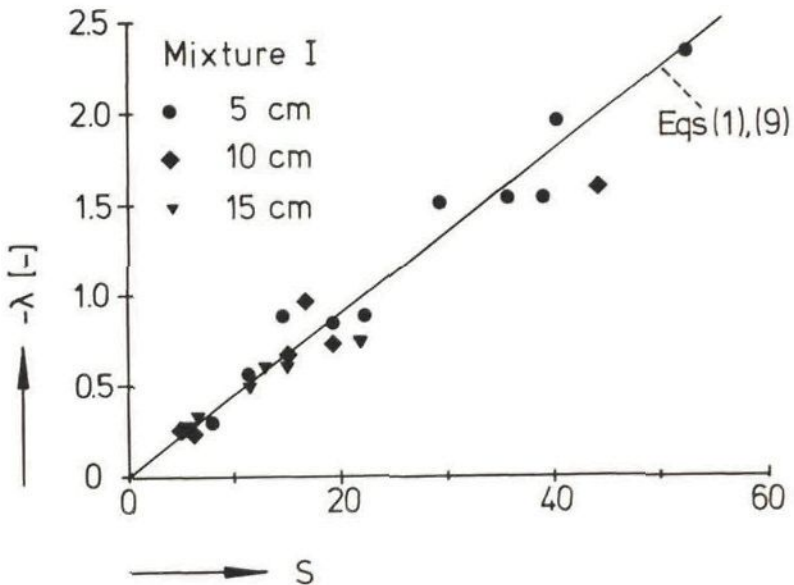


Figure 15: Comparison of the theoretical relationship between the model parameter  $\lambda$ , Eq.[10], and the extent of segregation  $S$ , Eqs.[1] and [9], with values of  $\lambda$  obtained from model fits.

The agreement between the experimental data and the theoretical curve is good, which suggests that the mechanistic and modeling approach to segregation based on convective solids flow and solid dispersion is realistic and applicable in practical situations.

## 5. CONCLUSIONS AND DISCUSSION

Slugging and segregation experiments have been performed with Geldart's D-group solids in small diameter fluid beds ( $\leq 15$  cm ID) that are of relevance in the fluidized bed combustion of coal. The results on slugging in a 10 cm ID bed at ambient conditions showed that:

1. square-nosed slugging is likely to occur at  $H_{mf}/D$ -ratios of more than 4;
2. the distance between two successive gas slugs is independent of the superficial gas velocity;
3. the average length of a solids slug equals about 80% to more than 90% of the bed height at minimum fluidization; this percentage depends on the  $H_{mf}/D$ -ratio. This implies that in general only one particle slug is present in the bed.

The following results have been obtained with respect to segregation:

4. the extent of segregation increases with a larger  $H_{mf}/D$ -ratio, a smaller bed diameter and a decreasing gas velocity. However, at a gas velocity of three times the minimum fluidization velocity still a significant degree of segregation is measured. It is further suggested that segregation becomes nil at a critical value of the (hydraulic) bed diameter.
5. a segregation mechanism in slugging fluidized beds is proposed, which is based on a downwards solids flow in the gas slug, an upwards solids flow in the particle slug and solids dispersion (which can also be described by a solids exchange between upwards and downwards moving solids flows);
6. this mechanism leads to an one-parameter-model, which is in good agreement with experimental axial segregating particle distributions. Furthermore, the decrease of segregation at larger bed diameters is qualitatively explained by the model.

This model can be helpful in the up-scaling of segregation results to FBC pilot plants and industrial facilities, especially when it is possible to derive theoretical expressions for the particle velocities  $v$  and  $k$  and the dispersion coefficient  $D_0$ . For example  $D_0$  can be taken from the expression given by Thiel and Potter (1978), while further the downwards velocity  $v$  can be calculated from the 'free-falling' velocity due to gravity. The upwards velocity  $k$  may contain, among others, a segregation velocity component caused by an 'Archimedes-like' upwards force due to density differences between the segregating particle and the bulk of the bed (buoyancy). Preliminary results of this type of modeling approach to segregation in slugging beds have already been obtained and showed good agreement with experiments (Schouten et al., 1987b).

3.3 The MOTION of PARTICLES in a SLUGGING GAS FLUIDIZED BED  
submitted for publication in Powder Technology, 1987.

SUMMARY	121
1. INTRODUCTION	121
1.1 Particle motion and Fluidized Bed Combustion	121
1.2 Previous work	122
1.3 The objective of this paper	122
2. EXPERIMENTAL METHOD	123
2.1 Particle system	123
2.2 Experimental facility	123
2.3 Overview of experiments	125
3. EXPERIMENTAL RESULTS	126
3.1 Particle velocities	126
3.1.1 Upward particle velocity	126
3.1.2 Downward particle velocity	129
3.1.3 Particle velocity ratio	131
3.1.4 Large amplitude upward and downward velocities	133
3.2 Probability of direction change p	133
3.2.1 ABCD/BC and EFGH/FG	134
3.2.2 AB/A, ABC/AB and ABCD/ABC	135
3.2.3 EF/E, EFG/EF and EFGH/EFG	136
3.2.4 ABGH/A and GHAB/G	137
3.2.5 BG/B and GB/G	139
3.2.6 BGBG/B and CFCF/C	140
3.2.7 Particle cycling times	141
3.2.8 Solids fractions	142
3.3 Particle presence probability pp	143
4. GENERAL MODEL OF PARTICLE MOTION	146
4.1 Model assumptions	147
4.2 Mass balances	148
4.3 Solids concentrations	149
4.4 Modeling results	151
5. CONCLUSIONS	153

J.C. Schouten, H.A. Masson and C.M. van den Bleek

### SUMMARY

In this paper an experimental study is presented on the motion of particles in a slugging 10 cm ID gas fluidized bed at ambient conditions. A particle system is used that resembles the composition of an ash-coal/sorbent mixture in a FBC combustor. A radioactive tracer technique is applied to measure the upward and downward tracer velocities, the probabilities of changes in the direction of the displacement of the tracer as well as the tracer's axial presence probability. The influence of the superficial gas velocity and the ratio between the bed height at minimum fluidization and the bed diameter on the tracer velocities and probabilities is investigated. A general model for the description of solids motion in slugging fluidized beds is introduced; a comparison between the model and experimental results shows good agreement.

### 1. INTRODUCTION

#### 1.1 Particle motion and Fluidized Bed Combustion

Fluidized beds are used for many different chemical engineering applications. One of these is the production of energy from coal in the Fluidized Bed Combustion of coal (FBC); however, this technique is still under development and many problems concerning fluidization aspects and the fundamentals of phenomena like gas transfer, combustion, sulfur retention,  $\text{NO}_x$ -reduction, heat exchange etc. have to be solved yet before FBC 'becomes of age' (Proc. Int. Conf. on FBC, Boston, USA, May 3-7, 1987).

One of these important phenomena is also the 'fluid dynamical behaviour' of the bed material which is applied during the Fluidized Bed Combustion of coal, because it greatly influences the mechanism of particle motion, mixing and segregation.

The importance of the understanding of the mechanism of particle motion and of the mixing and segregation phenomena is clear when we think of e.g. the modeling of different processes in the reactor (like coal devolatilization or sulfur retention) or when we have to deal with design considerations as the choice of the position of the coal feed or sorbent and ash removal.

The rate of particle mixing strongly determines the position of the coal feed; the coal particles devolatilize generally in a period of about 10 to 30 seconds. Subsequently, it is important to know whether the particles remain in the feed zone during this time period or that the mixing is fast resulting in a continuous devolatilization and subsequent even sulfur release throughout the whole bed.



Furthermore, it is of importance to know whether a fluid bed coal combustor can be considered from a particle point of view as an ideally stirred tank reactor as it is in literature generally assumed to be. Or in other words: it has to be determined what the mean time of displacement of the particles will be between the distributor and the maximum bed height in relation to e.g. the coal burnout time or the average sorbent residence time.

Also of relevance is the magnitude of the average presence probability of the particle in the axial direction in the bed. Or in other words: it has to be determined whether the particles segregate and by what bed conditions this segregation is influenced.

### 1.2 Previous work

In previous work the present author(s) have already paid attention to some aspects of these topics. Noordergraaf et al. (1987) have pointed out that in FBC generally large particle systems (B- or D-type of powders) are applied which give a tendency to the appearance of slugging, especially in smaller diameter systems (as for example are met between the heat exchanger tubes in FBC units). They argued that experiments performed in small diameter beds (around 10 cm ID) already provide useful information about the expected behaviour of solids in larger FBC units. Schouten et al. (1987a) presented segregation and slugging experiments in small diameter beds; they showed the influence of the superficial gas velocity, the bed aspect ratio and the bed diameter on the extent of segregation. Based on these experimental observations Schouten et al. (1987b) presented a segregation model which characterizes the segregating particle distribution by one 'Peclet-like' dimensionless number, which is the ratio between the net particle convective and segregating flows and the dispersive solids flow in the bed.

### 1.3 The objective of this paper

The present paper reports about the continuation of our work on these topics of *particle motion in relation to fluid bed combustion of coal*. In this paper an experimental study is presented on the motion of one tracer particle in a one- and two-component slugging gas fluidized bed. In this study a non-disruptive dynamic radioactive tracer technique is applied for the investigation of the axial presence probability of the particle, the probability for a change in the direction of the displacement of the particle, the magnitude of the upward and downward particle velocities and on the random diffusion-like character of the particle's trajectories. This experimental investigation is applied to obtain a qualitative description of

the mechanism of particle motion in these systems. Furthermore a simple general model for the motion of particles in slugging fluidized beds is formulated based on this mechanistic description.

## 2. EXPERIMENTAL METHOD

### 2.1 Particle system

Group D particle systems are used that resemble the composition of an ash-coal/sorbent mixture in a FBC combustor. The ash is represented by sand particles (density  $2600 \text{ kg/m}^3$ ) with a mass-averaged diameter of 1 mm (850 - 1200  $\mu\text{m}$ ). The coal and sorbent are represented by (cylindrical)  $\gamma$ -alumina particles with dimensions ( $l = d = 3 \text{ mm}$ ) and a density ( $829 \text{ kg/m}^3$ ) which are comparable to devolatilized coal and calcined limestone.

### 2.2 Experimental facility

The experiments are carried out in a 10 cm ID plexiglass fluid bed with a length of 1.5 m. A distributor plate with 100 holes of 1 mm ID is used.

A fully automatic analysis method based on the application of a radioactive tracer techniques as described by Masson et al. (1981, 1982), is used for the investigation of the motion of the particles in the bed. Hereto a 200  $\mu\text{m}$   $\text{Co}^{60}$  source ( $\gamma$ -emitter of 300  $\mu\text{Cu}$ ) is glued in a small hole that is bored in one alumina particle (size and weight increase negligible). This particle will further be referred to as the tracer particle.

The radiation is detected by two photomultipliers which are equipped with NaI crystals and connected to rapid rate-meters. Two overlapping measurement windows are defined by lead block collimators. The collimators can be moved vertically along the plexiglass column in a supporting rack with use of a pulley system. In this way different sections of the bed may be exposed to the photomultipliers. Furthermore, an electronic chain is present which mainly consists of two signal make-up devices (amplifier and trigger) that are connected to a transition identifier.

Eight different transitions in the position of the tracer particle are possible of which four upward and four downward transitions. The transitions are labelled from A to H (see Figure 1). A digital code is associated to each transition.

The identification code is generated by combining the state signal of one channel and the signal of a slope detector relative to the other channel. This slope detector is just a differentiator to the corresponding

state signal. The transition code is sent to an on-line computer with monitor display and printing facilities.

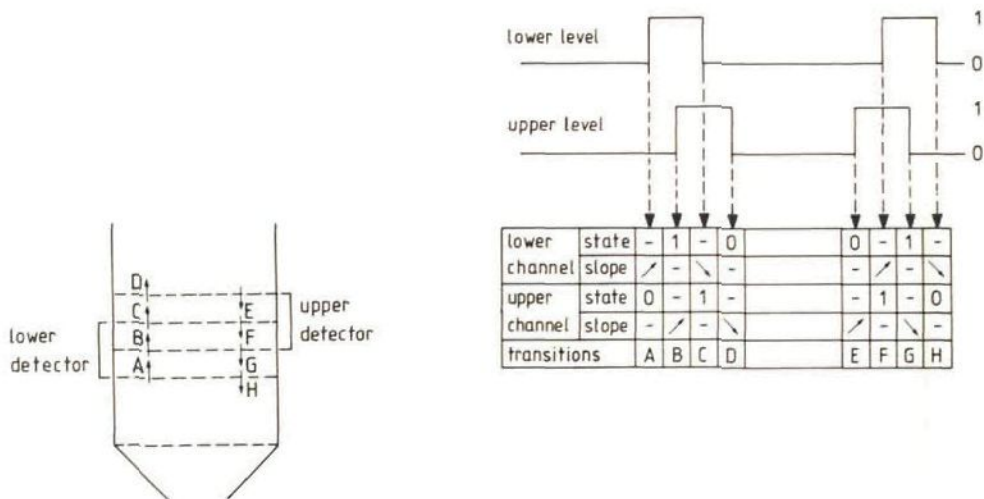


Figure 1: The logic transition identifier (Masson et al., 1981; 1982).

The digital code is recorded in a chronological way and so is also the time interval between two successive transitions. All the transitions separated by more than 100  $\mu$ sec are detected; a typical experiment consists of the recording of 1181 transitions (which takes in general about 10 to 20 minutes). The computer program computes the frequency of the different transitions and of remarkable doublets, triplets or quadruplets of transitions. It provides also a histogram of time intervals between two successive transitions and it computes the corresponding mean value and standard deviation.

Next to the digital code also a five level analogue signal is generated of which the amplitude is proportional to the position of the tracer particle in the bed. The analogue signal measurements are stored in a five class amplitude histogram; the proportion of measurements falling in a given class is proportional to the probability of presence (pp) of the tracer particle in the corresponding window. In the absence of segregation, this presence probability must be equal to the ratio of the volume of the solids in the measurement window and the total volume of the solids in the bed.

### 2.3 Overview of experiments

Three different sets of experiments are performed at ambient conditions. Experiments are carried out with the tracered alumina particle in a bed of:

1. sand particles (experimental set 1);
2.  $\gamma$ -alumina particles (experimental set 2);
3. sand and  $\gamma$ -alumina particles with a fixed ratio of 4 between the height at minimum fluidization of the sand bed and the  $\gamma$ -alumina bed (experimental set 3).

The minimum fluidization velocities (measured in the 10 cm ID bed) of the sand and the  $\gamma$ -alumina are respectively 0.55 m/s and 0.9 m/s.

The aspect ratio at minimum fluidization,  $H_{mf}/D$ , is varied between 2.4 and 5.1, while the superficial gas velocity ranges between 0.8 m/s and 1.8 m/s.

Table 1: overview of experiments.

experimental set 1 (sand bed)			experimental set 2 (alumina bed)			experimental set 3 (sand/alumina bed)		
no.	$H_{mf}/D$ [-]	$U_0$ [m/s]	no.	$H_{mf}/D$ [-]	$U_0$ [m/s]	no.	$H_{mf}/D$ [-]	$U_0$ [m/s]
1.1	2.4	0.8	2.1	2.85	1.2	3.1	2.7	0.8
1.2	2.4	1.0	2.2	2.85	1.4	3.2	2.7	1.0
1.3	2.4	1.25	2.3	2.85	1.6	3.3	2.7	1.2
			2.4	2.85	1.8	3.4	3.0	1.0
			2.5	3.85	1.4	3.5	3.3	0.8
			2.6	4.85	1.2	3.6	3.3	1.0
						3.7	3.3	1.2
						3.8	3.65	0.8
						3.9	3.65	1.0
						3.10	4.0	0.8
						3.11	4.0	1.0
						3.12	4.0	1.2
						3.13	4.5	0.8
						3.14	4.5	1.0
						3.15	4.7	0.8
						3.16	5.1	0.8

At each  $H_{mf}/D$ -ratio and at each superficial gas velocity at least six recordings of the 1181 transitions are established at different axial positions along the column; in this way a total number of 186 recordings has been obtained.

An overview of the experimental sets is given in Table 1. Each experiment in a set is given a specific number (1.1 .. 1.3, 2.1 .. 2.6, 3.1 .. 3.16) as is indicated in Table 1. References are made to these experiment numbers in the captions of relevant figures in this paper.

### 3. EXPERIMENTAL RESULTS

In this section some typical experimental results are demonstrated on the particle velocities and on the probability of direction changes.

#### 3.1 Particle velocities

##### 3.1.1 Upward particle velocity

The upward particle velocity is obtained from:

$$v_{up} = L_{window} / (B.C) \quad [1]$$

where  $L_{window}$  is the width of the middle measurement window (64 mm) and (B.C) represents the mean of the time interval distribution between a B transition followed directly by a C transition.

In Figure 2 a characteristic example is given of the upward velocity of the tracer in a bed of sand particles (experimental set 1). The upward velocity is plotted as a function of the axial position in the bed at different values of the superficial gas velocity. It is clearly observed that  $v_{up}$  strongly increases with an increasing gas velocity, which may be caused by an increased drag force on the particle. Furthermore, a significant influence of the axial position of the particle on its velocity is found.

In Figure 3 a typical example is shown of the influence of the superficial gas velocity on the upward velocity of the tracer particle in a bed of alumina particles (experimental set 2).

First, it is clearly observed that the upward velocity is not constant along the bed height, but it increases until a maximum is reached. The axial position of this maximum is a function of the gas velocity. The occurrence of this maximum is obvious because the upward velocity at  $h=H_{max}$  will be zero.

Furthermore, in this case the upward velocity increases also with an increasing superficial gas velocity; for example, the maximum value increases from about 0.4 m/s to 0.7 m/s when the gas velocity is increased from 1.2 to 1.8 m/s.

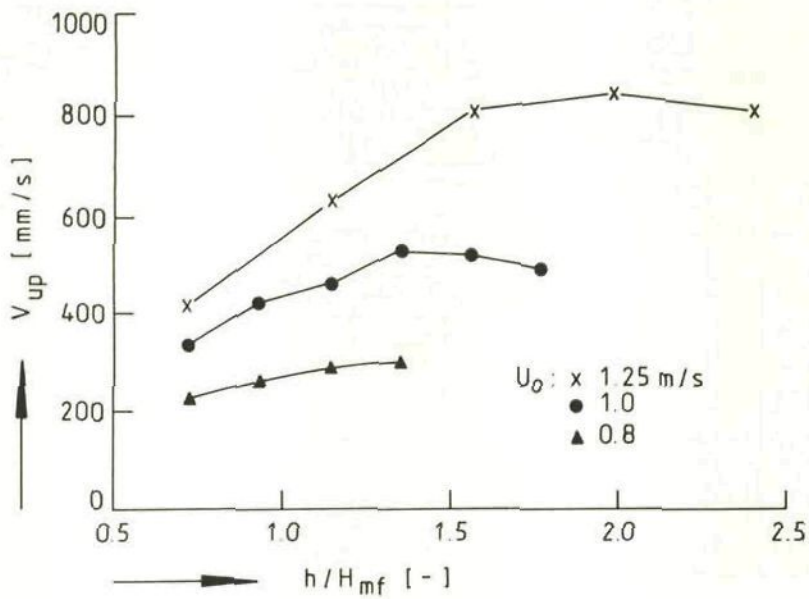


Figure 2: The upward tracer velocity as a function of the axial position in the bed (experimental sets 1.1, 1.2 and 1.3).

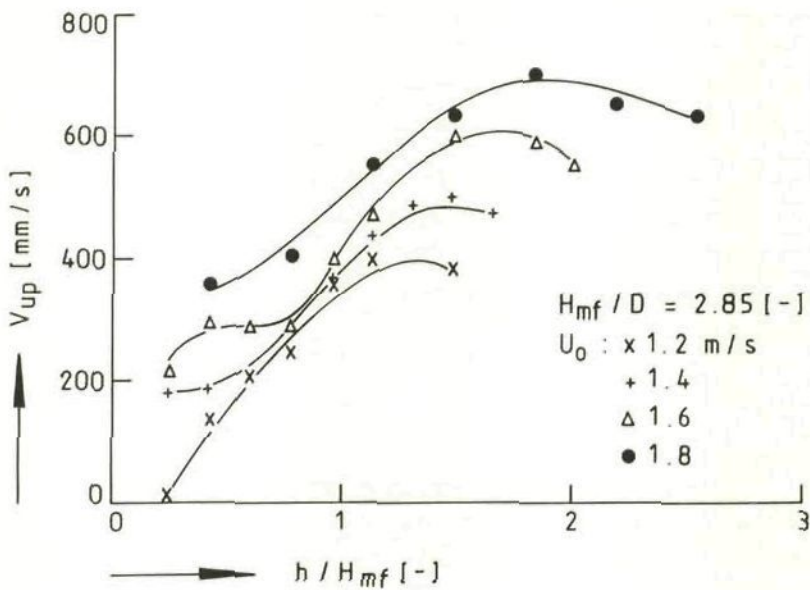


Figure 3: The upward tracer velocity as a function of the axial position in the bed (experimental sets 2.1 .. 2.4).

The effect of the  $H_{mf}/D$ -ratio on the upward velocity at a constant gas velocity is illustrated in Figure 4. This typical example shows the general phenomenon that no influence can be observed at values of the  $H_{mf}/D$ -ratio lower than about 5.

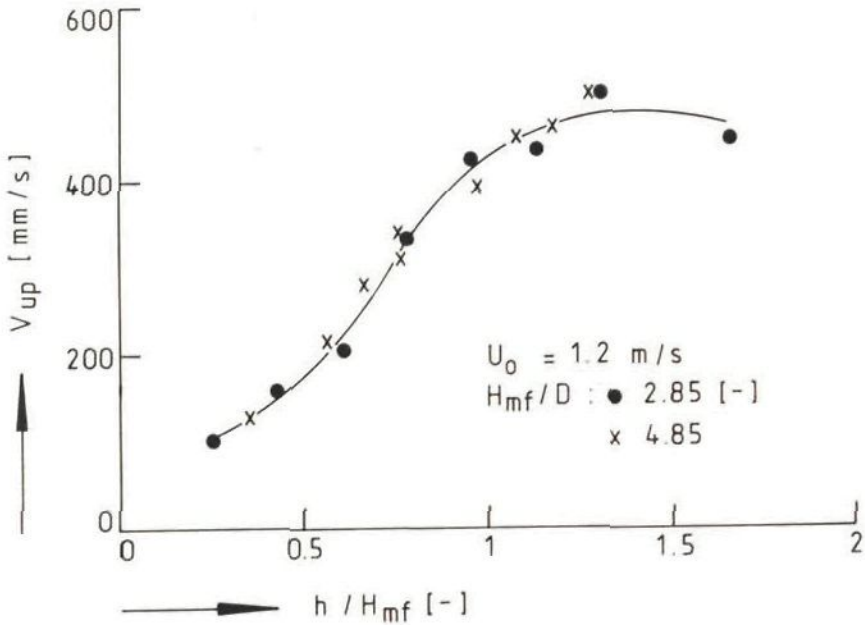


Figure 4: The upward tracer velocity as a function of the axial position in the bed (experimental sets 2.1 and 2.6).

It is realistic to consider that the measured upward particle velocity and the solid slug rise velocity are equal. However, the upward particle velocity and the gas slug rise velocity may differ. The gas slug rise velocity is generally calculated from relations of the following form (Schouten et al., 1987b):

$$U_s = (U_0 - U_{mf}) + 0.35 (a g D)^{1/2} \quad [2]$$

$a$  is a dimensionless slug parameter which characterizes the type of slugging (see Schouten et al., 1987a). When, for example, the data are applied which correspond to the data-sets in Figure 4 ( $U_0 = 1.2$  m/s;  $U_{mf} = 0.8$  m/s;  $a = 1.5 [-]$ ;  $D = 0.10$  m), it is obtained that the average value of  $U_s$  equals about 0.8 m/s.

First, this result clearly indicates that in the present case the gas slug is flowed through with gas, because the superficial gas velocity is

about 1.5 times higher. Furthermore, the corresponding measured upward particle velocity increases from about 0.1 m/s (at  $h/H_{mf} = 0.3$ ) to the maximum of about 0.5 m/s (at  $h/H_{mf} = 1.3$ ), which is clearly smaller than the average gas slug rise velocity.

This means that in this case the average gas slug rise velocity is about 2 to even 8 times higher than the solid slug rise velocity. This implies that the solid slug is also flowed through with gas.

### 3.1.2 Downward particle velocity

The downward particle velocity is obtained from:

$$v_{\text{down}} = L_{\text{window}} / (E.F) \quad [3]$$

where  $L_{\text{window}}$  is the width of the measurement window (64 mm) and (E.F) represents the mean of the time interval distribution between an E transition followed directly by a F transition.

In Figure 5 a typical example is shown of the influence of the superficial gas velocity on the downward velocity of the tracer particle in a bed of alumina particles (experimental set 2).

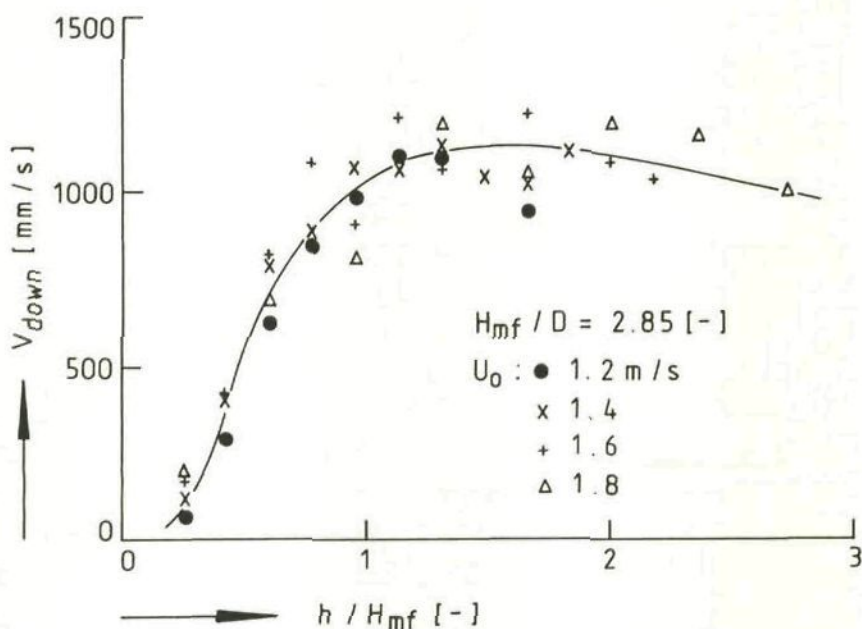


Figure 5: The downward tracer velocity as a function of the axial position in the bed (experimental sets 2.1 .. 2.4).



First, it is observed that the superficial gas velocity has no influence on the downward particle velocity.

Furthermore, the downward velocity is clearly bed height dependent: it increases steeply from about 0.1 m/s at  $h/H_{mf} = 0.3$  to about 1 m/s at  $h/H_{mf} = 1$ ; hereafter it becomes almost constant at about 1.1 m/s until  $h/H_{mf} = 1.5$  whereupon it slightly levels off.

This graph illustrates also that the downward particle velocity is much more effected by the position of the bed height at minimum fluidization ( $h/H_{mf} = 1$ ) than the upward particle velocity. The explanation is that the slugging behaviour of the bed is fully developed above the axial position  $h/H_{mf} = 1$ , while at  $h/H_{mf} < 1$  slugs are being formed. This implies that the average length of a gas slug above  $h/H_{mf} = 1$  will be almost constant, while this length increases from about nil to its final value (at about  $h=H_{mf}$ ) in the bed section below  $h=H_{mf}$ . Visual observation of the bed showed that the downward particle movement takes place in the gas slug, so the length of the gas slug will determine the final value of the downward particle velocity.

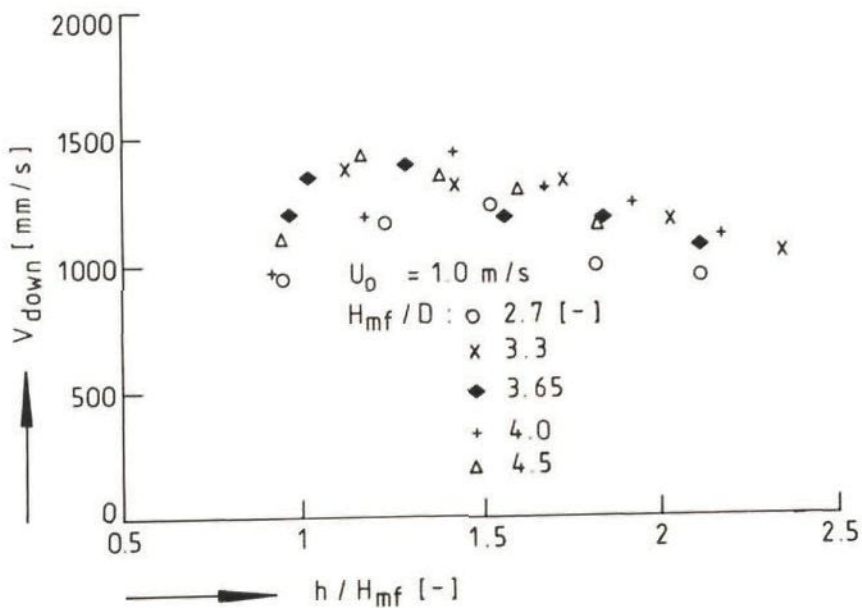


Figure 6: The downward tracer velocity as a function of the axial position in the bed (experimental sets 3.2, 3.6, 3.9, 3.11 and 3.14).

In Figure 6 the effect of the  $H_{mf}/D$ -ratio on the downward particle velocity is illustrated; in this specific case data of experimental set 3 have been applied, however, all other sets show the same effect. It is

observed that the downward particle velocity is not effected by the relative amount of material ( $H_{mf}$ ), however, it is slightly bed height dependent.

Figures 5 and 6 demonstrate that the downward particle velocity shows a clear scatter above a value of  $H_{mf}/D = 1$ : generally the downward velocity varies between about 1 m/s and 1.5 m/s, independent of gas velocity and  $H_{mf}/D$ -ratio. The reason for this scatter may be the fact that in general the axial position of the gas slugs in the bed is more or less fixed; e.g. it has been visually observed that particles which are 'raining through' a gas slug always drop onto the successive solid slug at more or less fixed positions along the bed height. Or put into other words: this implies that the 'axial presence probability' of a gas slug is not independent of the bed height. The velocity of particles that 'fall' through a gas slug increases until the steady state velocity has been reached, consequently, particles that are moving downward through a gas slug will have different velocities at different positions in the gas slug and so at different axial positions along the bed height.

Finally, it is remarked that Figures 5 and 6 indicate that it is useful to distinguish the 'expanded' bed aspect ratio  $H/D$  (influenced by the gas velocity) and the 'static' ratio  $H_{mf}/D$ . Therefore it is suggested to make this distinction also in empirical relationships which predict phenomena closely related to solids movement (like elutriation rates).

### 3.1.3 Particle velocity ratio

In Figure 7 a typical example of the ratio between the downward and upward particle velocity is plotted in case of one tracer particle in a sand bed (experimental set 1). It is observed that this ratio is a clear function of the superficial gas velocity as well as of the axial bed position. At a relatively low gas velocity of 0.8 m/s ( $U_{mf} = 0.6$  m/s) the velocity ratio increases at higher positions in the bed and reaches even a value of 3; however, at superficial gas velocities higher than 1.0 m/s the ratio decreases with increasing bed height and ranges between 2 and 1.

This specific system (experimental set 1) is a segregating system wherein it is observed that the particle presence probability increases along the bed height with a decreasing gas velocity. So the results on the particle velocity ratio as presented in Figure 7 are in agreement with the segregation model of Schouten et al. (1987b) which predicts that the extent of segregation is effected by the velocity ratio of the upward and downward moving particles.

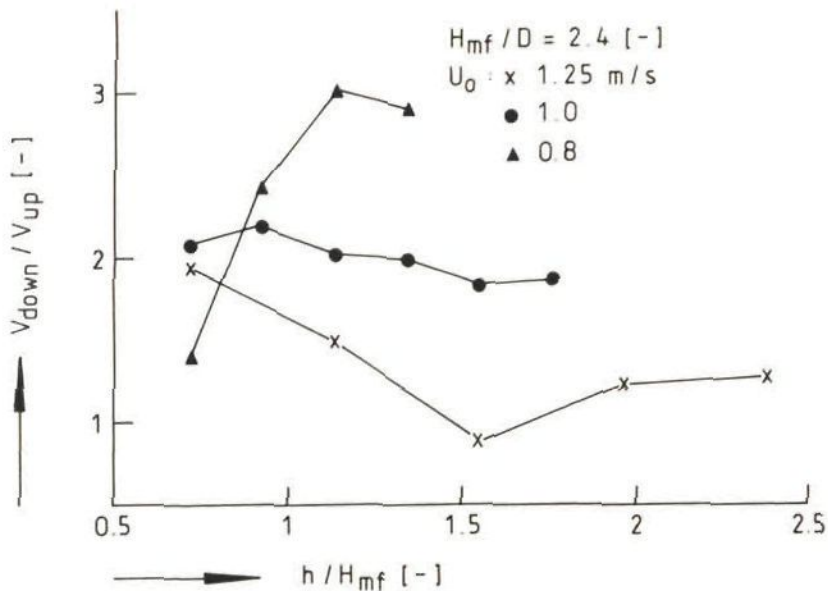


Figure 7: The ratio between the upward and downward tracer velocities as a function of the axial position in the bed (experimental sets 1.1, 1.2 and 1.3).

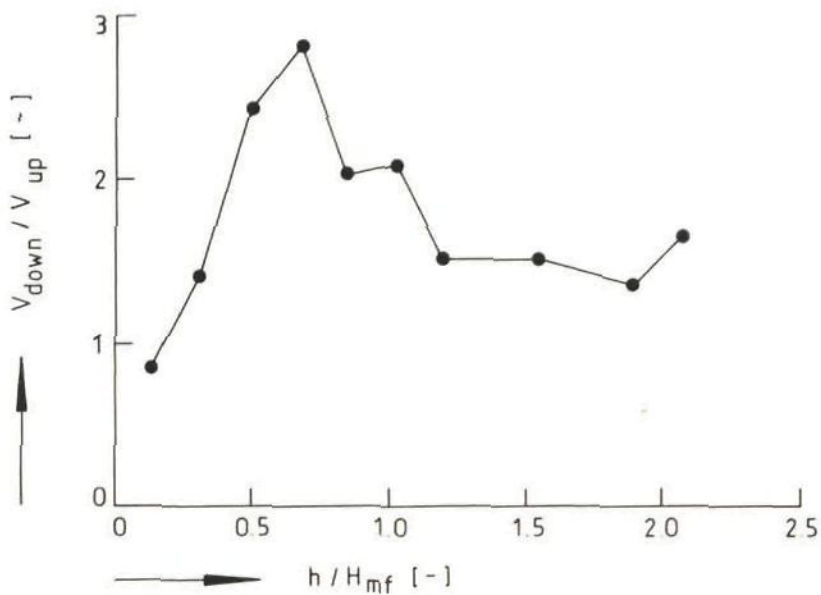


Figure 8: The ratio between the upward and downward tracer velocities as a function of the axial position in the bed (experimental set 2.3).

A typical example of the shape of the velocity ratio in a non-segregating system (experimental set 2) at a relatively high superficial gas velocity (1.6 m/s) is shown in Figure 8. Here a steep increase of the particle velocity ratio until a value of nearly 3 is observed between the distributor and  $h/H_{mf} = 0.5$ , whereupon the ratio decreases and reaches more or less a constant value of about 1.5 at  $h/H_{mf} > 1$ .

Consequently, a clear difference is present between the velocity ratio in a segregating and in a non-segregating system at higher superficial gas velocities: in a non-segregating system a clear maximum in the velocity ratio is found, while further a significant change in its vertical profile is observed above the static bed height ( $h/H_{mf} = 1$ ).

#### 3.1.4 Large amplitude upward and downward velocities

The particle velocities discussed in the previous sections are based on the small amplitude displacement of the particle in the middle measurement window (width 64 mm). However, the particle velocities can also be calculated based on a large amplitude displacement: in this case the time interval between a B and a consecutive C transition is used only if this happens in a AB,CD sequence; in the same way the time interval EF,GH is applied in case of the downward particle movement.

The small and large amplitude displacements can be compared by considering the ratio between the velocities calculated using time intervals B,C, AB,CD and F,G, EF,GH respectively for the upward and downward displacements.

The results of all experimental sets demonstrate that this ratio is not dependent on the superficial gas velocity nor on the axial bed position in the upper part of the bed ( $h/H_{mf} > 1$ ) where its mean value is 1 (variation between about 0.7 and 1.3). The upward velocity ratio is also about 1 in the lower part of the bed ( $h/H_{mf} < 1$ ), while the downward velocity ratio generally shows an increase from 0.5 to 1.

So this means that especially above  $h/H_{mf} = 1$  no distinction can be made between the particle velocities of small and large amplitude displacements. This suggests that the particle already reaches its steady state velocity during its movement in the measurement window or/and that predominantly large amplitude movements take place (see also section 3.2.1).

#### 3.2 Probability of direction change p

Useful information with respect to the mechanism of particle motion can be obtained from an analysis of the probabilities (p) of possible direction changes of the tracer particle. Especially, it is of importance to know

whether the particle possesses a 'memory' with regard to its previous 'history' or that the particle behaviour can be described by its present state and a transition probability associated to this state. When the latter proposition is correct, then the process of particle motion in slugging fluidized beds is a markovian one and can be described by a purely diffusive mechanism.

### 3.2.1 ABCD/BC and EFGH/FG

ABCD/BC and EFGH/FG define the conditional probabilities for respectively an upward and downward displacement of the tracer particle with an amplitude larger than 16 cm once it takes place over 6.4 cm. This phenomenon can be characterized as 'direction keeping'.

A typical example is shown in Figure 9 in case of experimental set 2 (tracer in alumina bed). Both probabilities demonstrate almost the same shape; first, a clear increase is observed until about  $h/H_{mf} = 0.8$ , whereupon a slight decrease is found with a minimum around  $h/H_{mf} = 1.0-1.1$ . Above  $h/H_{mf} = 1.2$  both probabilities vary between 0.75 and 0.5.

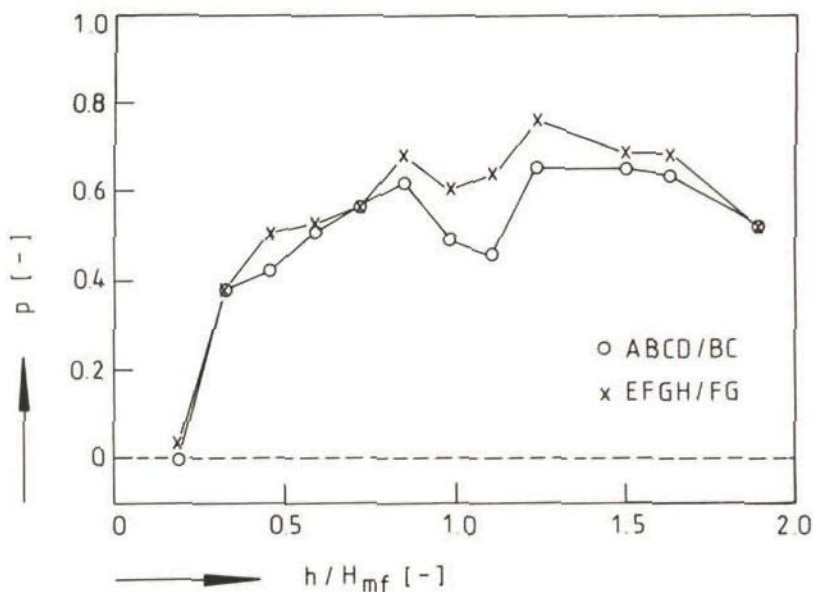


Figure 9: The probabilities ABCD/BC and EFGH/FG as a function of the axial position in the bed (experimental set 2.5).

In general these values indicate that above  $h/H_{mf} = 0.5$  the probability is about 50% or more for the particle in the alumina bed to make a large

amplitude displacement once its motion already takes place over a distance of more than 6 cm.

In a segregating system (experimental set 1: tracer particle in sand bed) a slightly different behaviour is found: this is illustrated in Figure 10. First, the probabilities  $ABCD/BC$  and  $EFGH/FG$  decrease from about 0.3 at  $h/H_{mf} = 0.7$  to 0.15 at about  $h/H_{mf} = 0.95$ . Hereupon both probabilities increase to about 0.5 to 0.6 at  $h/H_{mf} = 1.6$  whereafter they decrease. So in this segregating system the probabilities to make large amplitude displacements are more dependent on the axial bed position and therefore a larger variation above  $h/H_{mf} = 0.8$  (15% to 60%) is found.

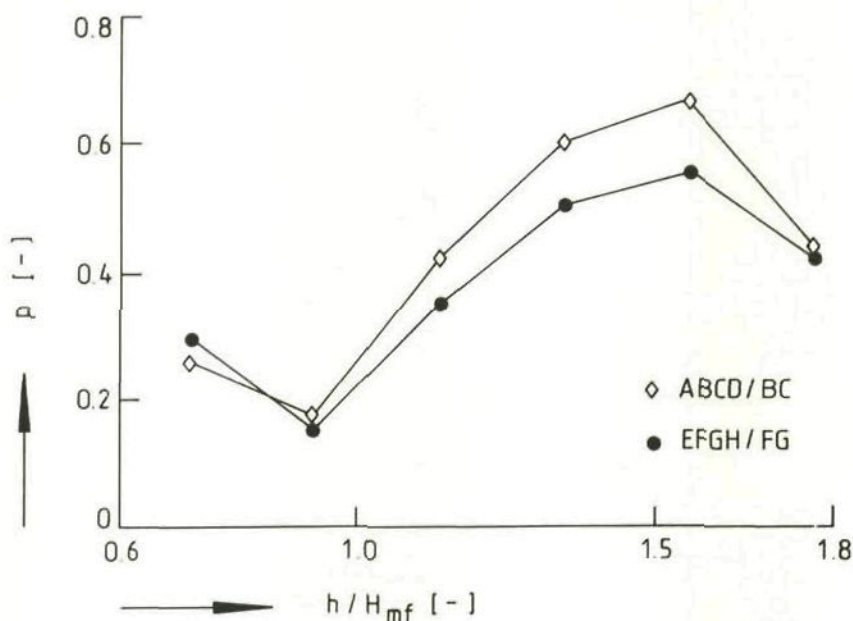


Figure 10: The probabilities  $ABCD/BC$  and  $EFGH/FG$  as a function of the axial position in the bed (experimental set 1.2).

### 3.2.2 $AB/A$ , $ABC/AB$ and $ABCD/ABC$

For a large number of observed transitions  $AB/A$ ,  $ABC/AB$  and  $ABCD/ABC$  are unbiased estimators of the conditional probability to continue upwards once the tracer particle is engaged in an ascending displacement.

When  $AB/A = ABC/AB = ABCD/ABC = 0.5$  the solids movement is characterized by a typical diffusive mechanism: radial and axial displacements have the same probability. However, when  $ABCD/ABC > ABC/AB > AB/A$  then a clear 'memory effect' is present: the particles tend to move upwards once they are present in an upwards movement.

A typical example of experimental set 2 (alumina bed) is given in Figure 11. It is observed that in general  $AB/A$ ,  $ABC/AB$  as well as  $ABCD/ABC$  are much larger than 0.5 and in most cases vary between 0.7 and 0.9 for  $h/H_{mf} < 1$ . A slight dependency on the axial bed position is found: above  $h/H_{mf} = 1$  the respective probabilities decrease a little and now vary between 0.5 and 0.7. These measurements point to an anisotropic behaviour of the particles with respect to the axial dispersion.

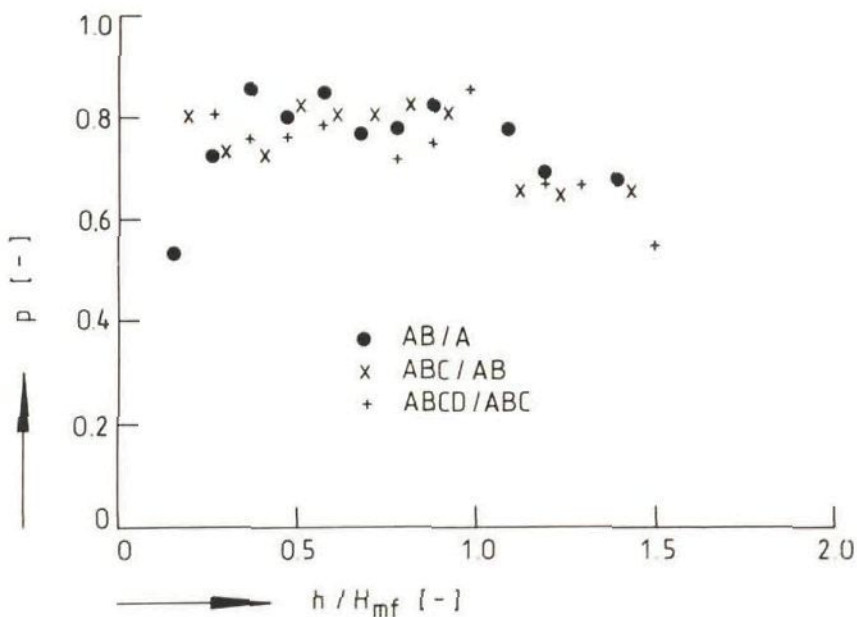


Figure 11: The probabilities  $AB/A$ ,  $ABC/AB$  and  $ABCD/ABC$  as a function of the axial position in the bed (experimental set 2.6).

So the upward motion is clearly not characterized by a purely diffusive mechanism. Furthermore, a clear memory effect as defined above cannot be recognized. However, the relatively large values of the transition probabilities ( $\gg 0.5$ ) indicate that the particle has still an obvious tendency to continue in the same direction once it is engaged in an upwards movement.

### 3.2.3 $EF/E$ , $EFG/EF$ and $EFGH/EFG$

A symmetric reasoning can be applied to the downward displacement of the tracer particle. For example, in Figure 12 the  $EF/E$ ,  $EFG/EF$  and  $EFGH/EFG$  transition probabilities of experimental set 1 (tracer particle in a sand bed) are presented. It is observed that the respective probabilities

increase significantly at higher bed height positions: when  $h/H_{mf} < 1$  then  $p < 0.5$ , while the three probabilities approach  $p=1$  when  $h/H_{mf} > 1.5$ .

However, under strong segregating conditions some averaging of the simplets, doublets and triplets is in fact necessary over the width of the four concerned measurement levels. In the situation of downward displacements the quantities to compare are:

$$\frac{4(EF + FG + GH)}{3(E + F + G + H)} \quad \text{and} \quad \frac{3(EFG + FGH)}{2(EF + FG + GH)}$$

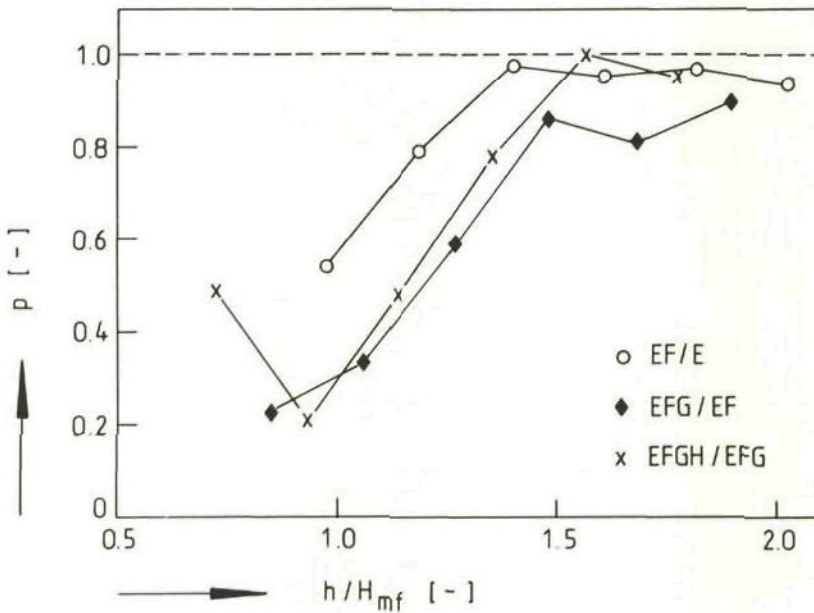


Figure 12: The probabilities  $EF/E$ ,  $EFG/EF$  and  $EFGH/EFG$  as a function of the axial position in the bed (experimental set 1.2).

The results of experimental set 3 (segregating sand/alumina system) demonstrate in general that both quantities vary around 0.5 at  $0.8 < h/H_{mf} \leq 1$ , while they increase upto  $h/H_{mf} = 1.2$  where they reach values higher than 0.85 (varying between 0.85 and 1) which are not dependent on the superficial gas velocity nor on the axial bed position.

These results indicate that the tracer particle preferentially continues its downward displacement in the upper part of the bed (in general  $p \gg 0.5$  at  $h/H_{mf} > 1.2$ ) once it is engaged in it, however, no 'memory effect' is observed. Furthermore, also the downward solids displacement demonstrates an anisotropic behaviour with respect to axial dispersion.



### 3.2.4 ABGH/A and GHAB/G

ABGH/A defines the probability for a 'clean' change of the direction of movement of the particle. A typical result in case of the experimental set 1 is summarized in Figure 13.

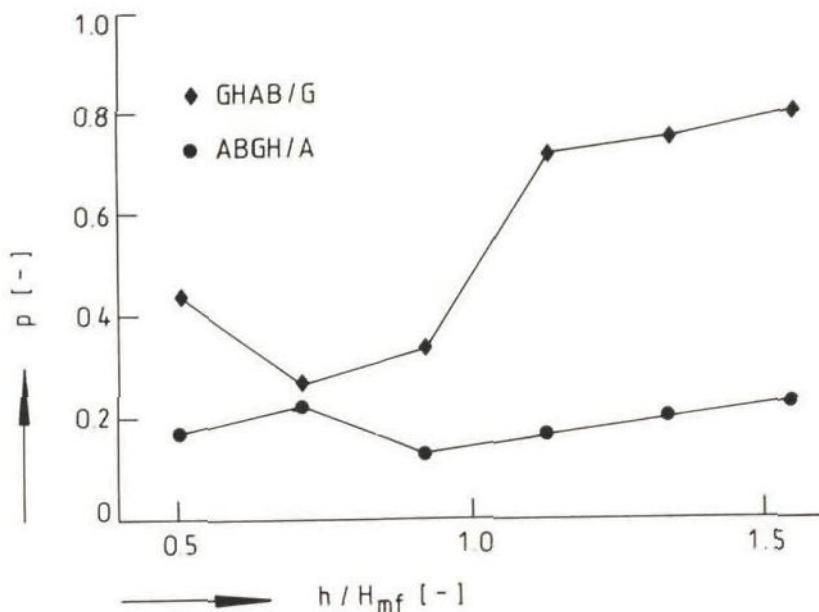


Figure 13: The probabilities ABGH/A and GHAB/G as a function of the axial position in the bed (experimental set 1.2).

It is observed that the probability of the direction change ABGH/A is in general smaller than 20% and is only a slight function of the axial bed position. So, this type of 'clean' direction change is not likely to occur often; or in other words: this result implies that an upward movement will not easily be transferred into a downward movement (probability less than 20%). Of course, when  $h \rightarrow H_{max}$  then ABGH/A will approach 1.

The probability GHAB/G shows another type of behaviour: below  $h/H_{mf} = 0.9$  it varies between about 0.25 and 0.45. This indicates that the probability varies between 55% and 75% that the particle will change its direction into an upward motion in this lower bed section. However, above  $h/H_{mf} = 0.9$  GHAB/G increases steeply and becomes more or less constant at 0.75 at  $h/H_{mf} > 1.1$ .

So in this upper part of the bed the probability is about 25% that the particle will change its direction into an upward motion. This result is obvious because the particle is present in a segregating ('flotsam') system,

where the tendency to segregate will increase at lower bed positions respectively decrease at higher positions.

### 3.2.5 BG/B and GB/G

BG/B and GB/G represent the probability for the tracer particle to change its displacement direction during respectively its upward or downward movement in the measurement window (width 64 mm).

A typical result is given in Figure 14 in case of experimental set 2 (tracer in alumina bed). BG/B and GB/G demonstrate the same pattern until about  $h/H_{mf} = 1.2$ . The probability decreases strongly between  $h/H_{mf} = 0$  and 0.2 in case of BG/B and between  $h/H_{mf} = 0$  and 0.5 in case of GB/G. Further until  $h/H_{mf} = 1.2$ , BG/B and GB/G remain constant at about respectively 0.18 and 0.28. Subsequently, GB/G decreases steeply and becomes 0 at  $h/H_{mf} > 1.4$ , while BG/B decreases strongly and remains constant at 0.35 beyond  $h/H_{mf} = 1.4$ .

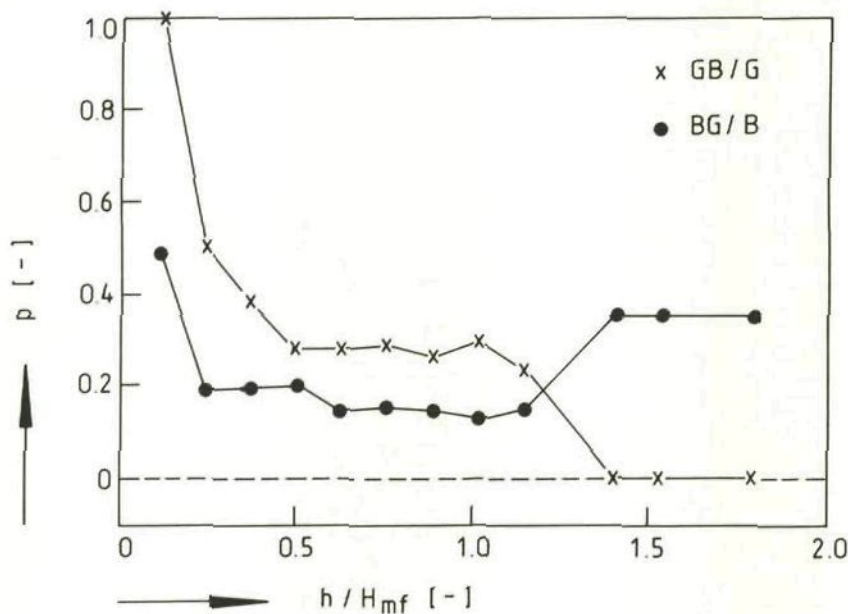


Figure 14: The probabilities BG/B and GB/G as a function of the axial position in the bed (experimental set 2.5).

These results indicate that beyond  $h/H_{mf} = 1.4$  it is very unlikely that a downwards movement is changed into an upward movement during the motion in one window. Furthermore, between  $h/H_{mf} = 0.2$  and  $h/H_{mf} = 1.4$  the probability for such a direction change in one window is also not high: in general smaller than 30%. This implies that direction changes of the particle

predominantly take place over longer distances than the width of the measurement window (64 mm).

In a segregating system the probability GB/G shows a different type of behaviour: see Figure 15 (experimental set 1: tracer particle in sand bed).

The probability BG/B demonstrates the same general shape as in Figure 14: between  $h/H_{mf} = 0.6$  and 1 it decreases a little from 0.22 to 0.12, whereafter it increases gradually to a constant value of about 0.28 at  $h/H_{mf} > 1.4$ . However GB/G first increases from about 0.4 at  $h/H_{mf} = 0.6$  to 0.68 at  $h/H_{mf} = 0.8$ , whereupon it decreases gradually to about 0 beyond  $h/H_{mf} = 1.4$ .

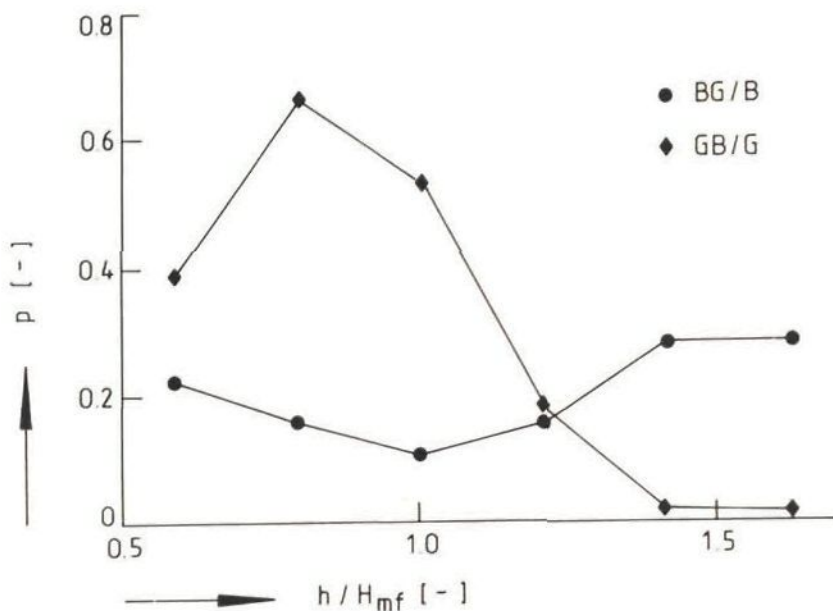


Figure 15: The probabilities BG/B and GB/G as a function of the axial position in the bed (experimental set 1.2).

This implies that in a segregating system at lower bed positions ( $h/H_{mf} < 1.2$ ) an obvious much larger tendency than in a non-segregating system exists for the particle to change a downward movement into an upward displacement over the width of the measurement window, which is in agreement with the last remark in the previous section 3.2.4.

### 3.2.6 BGBG/B and CFCF/C

BGBG/B and CFCF/C give the probabilities for oscillating displacements with an amplitude smaller than the width of the measurement window (64 mm).

For all experimental sets it is observed that these probabilities are very small (in general much smaller than 5%) and no dependency on the superficial gas velocity nor on the axial bed position is observed.

These results confirm that the particle has a strong tendency to continue its movement in a specific direction in the measurement window once it is engaged in it (see also section 3.2.5) and consequently oscillating displacements are very unlikely.

### 3.2.7 Particle cycling times

The particle cycling times above or under a given plane are given respectively by the time intervals D.E and H.A.

As example in Figure 16 a plot is given of the cycling time D.E in case of experimental set 2 as a function of the axial bed position.

It is observed that above the plane at  $h/H_{mf} = 0.5$  the particle will spend about 1.5 to not more than 3 seconds in the upper part of the bed before reemerging. However, above the plane at  $h/H_{mf} = 0.7$  the cycling time does not change much and decreases slowly from about 0.8 sec to about 0.25 sec at  $h/H_{mf} = 1.7$ .

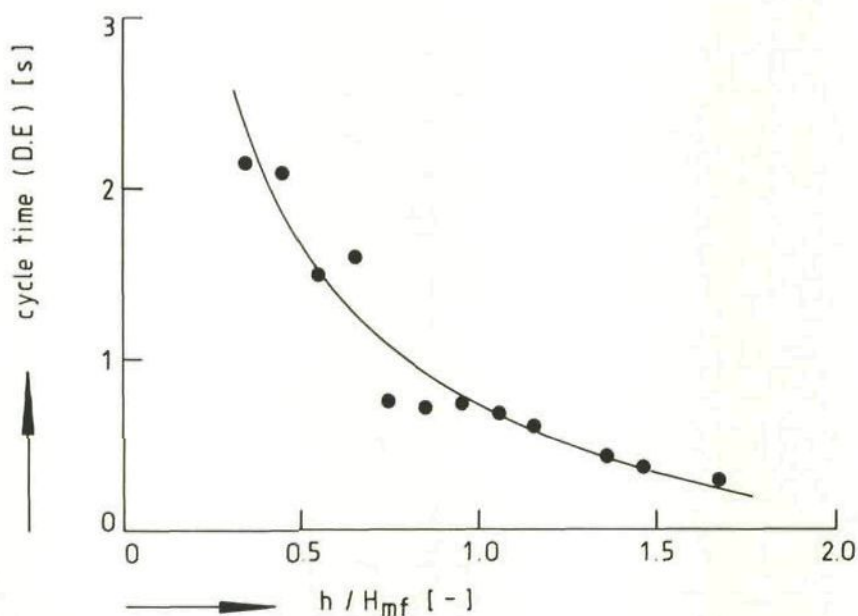


Figure 16: The tracer cycling time D.E as a function of the axial position in the bed (experimental set 2.6).

In general the cycling time H.A. shows a similar type of behaviour.

It is observed that for all experimental sets the mean values of D.E and H.A. do not exceed a period of 5 seconds along the total bed height (varying between 40 and 120 cm). However, it should be remarked that the actual cycling times sometimes vary between less than 0.1 second to even more than 1 minute, where the latter time is obtained in segregating systems with the measurement plane located at low bed positions. The mean values, however, indicate that a slugging fluid bed may be considered from a particle point of view as a perfectly mixed system when a comparison is made between the particle cycling times for axial displacements in the bed (less than 5 sec.) and e.g. the average coal burnout time (about 50 to 500 sec.) or the sorbent sulfation time (in general  $\gg$  2000 sec.) in a fluidized bed combustor.

### 3.2.8 Solids fractions

All results so far clearly point out that in a slugging gas fluidized bed particles move upward and downward. The upward movement of the particles is directly related to the ascending displacement of the solid slugs, while the downward movement of the particles takes place in the gas slugs ('raining through'). Consequently, a relevant parameter is the distribution of the solids over respectively the solid and the gas slugs. For example, it has already been demonstrated (Schouten et al., 1987b) that this distribution can be an important parameter in a segregation model.

The magnitude of this parameter can be approximated by the ratio of the time the tracer particle is engaged in an upward motion (time of transitions A.B, B.C and C.D) and the total time of upward and downward displacements (time of transitions A.B, B.C, C.D, E.F, F.G and G.H). In this way the fraction of solids ( $f$ ) which are present in the solid slugs is obtained; further  $(1-f)$  represents the fraction of solids which are raining through the gas slugs.

Two typical examples are demonstrated in Figure 17. In the segregating system (experimental set 3)  $f$  is only slightly dependent on the axial bed position: between  $h/H_{mf} = 0.5$  and 2,  $f$  varies between about 0.7 and 0.8. However, in the non-segregating system (experimental set 2) the axial influence on  $f$  is more pronounced: first  $f$  increases strongly to more than 0.8 at  $h/H_{mf} = 0.8$ , whereupon it decreases slightly and varies between about 0.65 and 0.7 for  $1 < h/H_{mf} < 2$ .

Furthermore, in general the experiments show that  $f$  is clearly dependent on the  $H_{mf}/D$ -ratio, while only a slight dependency on the superficial gas velocity is observed (see Schouten et al., 1987b). In general  $f$  increases

with a larger  $H_{mf}/D$ -ratio, indicating that relatively more solids are engaged in an upward displacement when the amount of solids in the bed is enlarged. This suggests that the extent of segregation will increase with a larger  $H_{mf}/D$ -ratio; this qualitative result is in agreement with segregation measurements (Schouten et al., 1987a).

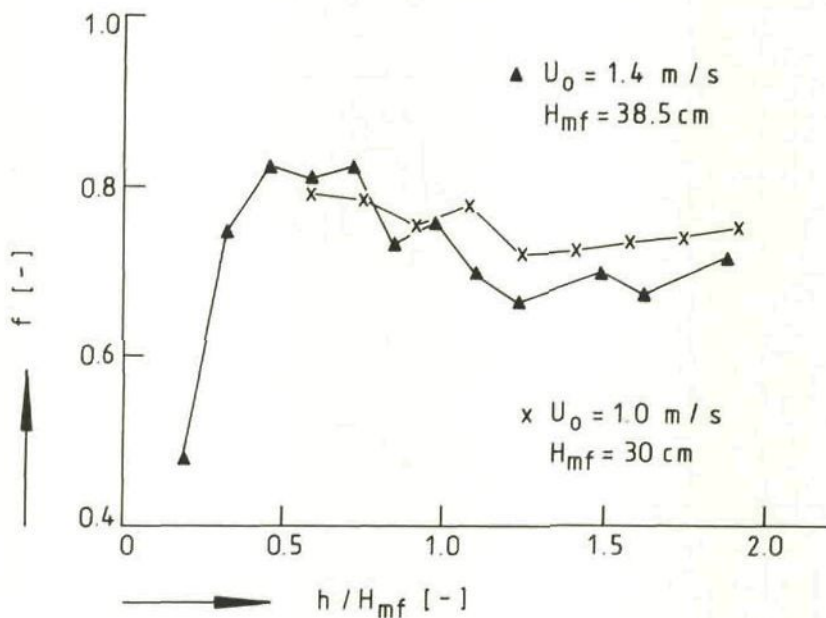


Figure 17: The solids fraction  $f$  as a function of the axial position in the bed (experimental sets 2.5 and 3.4).

### 3.3 Particle presence probability pp

The preceding sections tended to give insight about the way a particle moves in a slugging gas fluidized bed. The main conclusion so far may be that the particle shows a clear and strong tendency to continue its movement in one direction once it is engaged in it; furthermore the particle motion is clearly influenced by its position in the bed. It seems obvious that this will effect the presence probability of the particle along the bed height; in this section it is tried to bring an answer to this suggestion.

The particle's presence probability (pp) in the measurement window can be obtained by counting the cumulative presence time of the tracer in the window and divide this presence time by the total time of the experiment. In absence of any kind of segregation, this presence probability equals the ratio of the solids volume in the measurement window and the total volume of

the solids in the bed. In a segregating system this probability will change along the bed height.

A typical example is given in Figure 18 in case of a segregating alumina/sand mixture (experimental set 3) at a relatively low superficial gas velocity (0.8 m/s). It is observed that the particle presence probability clearly changes along the bed height: first it increases from about 0.055 at  $h/H_{mf} = 0.9$  to about 0.11 at  $h/H_{mf} = 1.5$ , whereupon it decreases to a value of about 0.07 at  $h/H_{mf} = 1.8$ . Consequently, it may be concluded that the concentration of the (segregating) solids increases along the bed height, however, just until a maximum is reached which indicates that in the upper part of the bed de-segregating forces are active which lead to a significant decrease of the solids concentration.

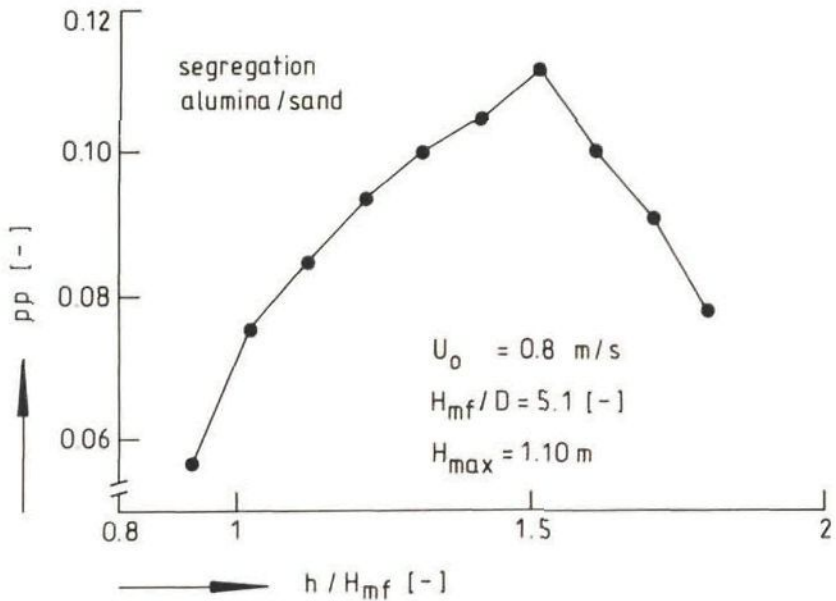


Figure 18: The tracer's presence probability  $pp$  as a function of the axial position in the bed (experimental set 3.16).

An evaluation of the tracer presence probability in a non-segregating system provides an explanation for this phenomenon as will be discussed now.

The presence probability of the tracer divided by the volume fraction occupied by the measurement window may be used as a measure for the local extent of mixing (or segregation): this measure is defined as the normalized presence probability,  $pp_{norm}$ :

$$pp_{\text{norm}} = \frac{\text{cumulative presence time in measurement window}}{\text{total time of experiment}} * \frac{\text{total bed volume}}{\text{window volume}}$$

It must be remarked that this is only true when the average porosity of the bed in the measurement window is equal to the average porosity of the whole bed.

In Figure 19 an example is given of the  $pp_{\text{norm}}$  of the tracer in case of a non-segregating system (experimental set 2: tracer in alumina bed). In this type of system of course no segregation is expected, however, it is clearly observed that the normalized presence probability is not equal to 1 but it decreases along the bed height. Near the distributor  $pp_{\text{norm}}$  is rather high ( $> 1.5$ ), while it is smaller than 1 in the lower part of the bed (at  $h/H_{\text{mf}} > 1.2$ ). Also the effect of the superficial gas velocity on the axial presence probability can be observed: in the lower part of the bed ( $h/H_{\text{mf}} < 0.7$ ) it is found that  $pp_{\text{norm}}$  is higher for the lower gas velocity, while in the rest of the bed  $pp_{\text{norm}}$  is significantly smaller in case of the lower gas velocity.

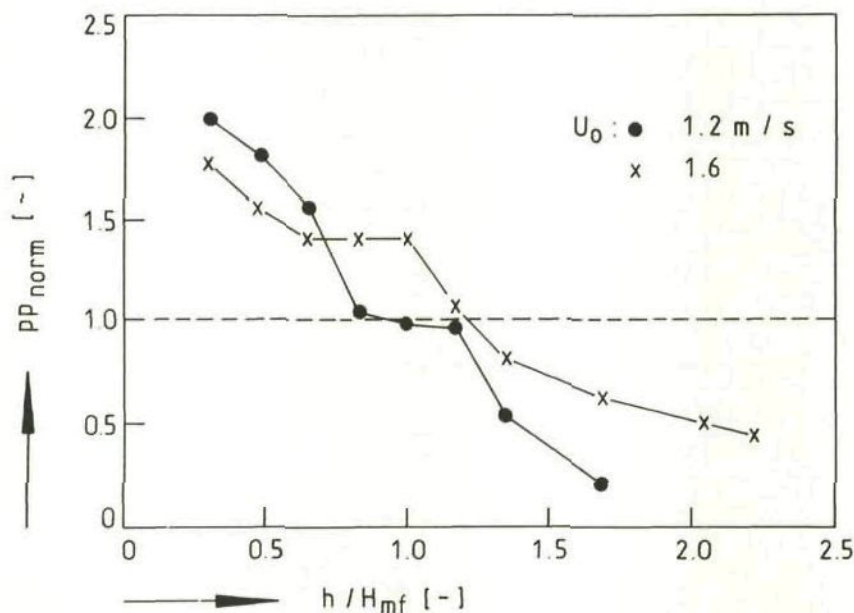


Figure 19: The tracer's normalized presence probability as a function of the axial position in the bed (experimental sets 2.1 and 2.3).

This remarkable phenomenon of a  $pp_{\text{norm}} \neq 1$  in a non-segregating system is defined here as 'solids dilution': the solids concentration decreases



along the bed height which is obviously not caused by segregating forces (due to e.g. density or diameter differences between the solids in the bed) because all particles are equal, but it may be attributed to an axially decreasing upward (convective) flow of particles due to an increasing difference between the downward directed gravity force on the solids and the upward directed drag force caused by the gas flow (which is a function of the superficial gas velocity). This explanation is in agreement with the observed influence of the gas velocity (see Figure 19): a lower gas velocity will lead to a smaller drag force on the solids which causes a relatively larger effect of the gravity force and therefore a larger downward solids flow and consequently a steeper decrease of the solids concentration along the bed height.

This effect of solids dilution provides also an explanation for the observed decrease of the presence probability in the segregating system of Figure 18. In this case one extra upward force acts on the (flotsam) particles: a segregation force due to buoyancy. However, when as caused by this segregation phenomenon the (flotsam) particle concentration increases along the bed height, then at the same time the local net segregation force will decrease due to the decreasing difference between the flotsam particle density and the local bulk density of the bed. At some point (there where the maximum in the presence probability is observed) the sum of the drag force and the buoyancy (segregation force) will become smaller than the gravity force which will subsequently lead to a larger convective downward solids flow and consequently to a decreasing (flotsam) particle concentration.

In the next section some more experimental results will be shown on the particle presence probability in a non-segregating system (experimental set 2) in relation to a general model for particle motion in slugging gas fluidized beds.

#### 4. GENERAL MODEL OF PARTICLE MOTION

In previous work a segregation model has been presented, which is based upon a flow mechanism of segregating particles in round- and square-nosed slugging fluidized beds (Schouten et al. 1987a; 1987b). This mechanism states that the segregating particles move downwards in the gas slug with a convective velocity  $v$  which is related to the descending velocity of solids in the gas slug due to gravity. The segregating particles move upwards in the particle slug with a convective velocity  $k$ , which includes a segregating

component that is predominantly caused by an 'Archimedes-like' upwards force due to density differences between the solids (buoyancy). Furthermore, it is also assumed that a dispersive flow of particles is present which is directed downwards.

#### 4.1 Model assumptions

This modeling approach will be extended based upon the experimental observations in the present work (section 3), so as to derive a general model for the description of particle motion in slugging fluidized bed. Hereto the following three assumptions are introduced:

\* first, it is assumed that a slugging bed consists of two layers. Based on the experimental observations it is assumed that the boundary between these two layers is situated at  $h/H_{mf} = 1$ . In each layer solids move upwards and downwards caused by convective, dispersive and possible segregative solids flows. These solids flows are caused by different forces on the solids, which are predominantly the drag force, the gravity force and buoyancy.

\* secondly, it is assumed that in each layer the upward and downward solids velocities as well as the axial solids dispersion coefficient are constant and do not change as a function of the bed height. The only change is observed at the boundary between the two layers in the bed.

Clearly this assumption does not agree with for example the results on the downward and upward particle velocities, which are bed height dependent. However, it is supposed that the division of the bed in two parts is a more important phenomenon which will effect the particle distribution more significantly than other axial influences. Therefore it is supposed that it will be sufficient to take for example average particle velocities in both bed sections.

\* finally, the assumption is introduced that the distribution of the solids over the particle and the gas slug is no function of the bed height. This implies that the volume fractions of solids in respectively the particle slug and the gas slug are the same in both bed layers.

A schematical representation of the model is given in Figure 20.

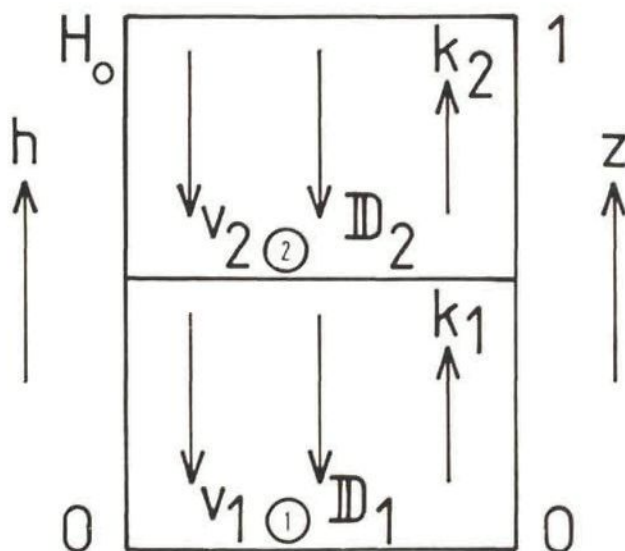


Figure 20: A schematical representation of the general model for particle motion in a slugging gas fluidized bed.

#### 4.2 Mass balances

The following mass balances are formulated as based upon the assumptions given. First, in the lower part of the bed it can be derived that:

$$D_1 \frac{d^2 c_1(h)}{d h^2} + (f_v v_1 - f_k k_1) \frac{d c_1(h)}{d h} = 0 \quad (0 \leq h \leq H) \quad [4]$$

Further, in the upper part it is obtained that:

$$D_2 \frac{d^2 c_2(h)}{d h^2} + (f_v v_2 - f_k k_2) \frac{d c_2(h)}{d h} = 0 \quad (H \leq h \leq H_0) \quad [5]$$

$f_v$  and  $f_k$  are respectively the solids volume fractions in the downward and upward moving solids flows.  $v_1, v_2$  and  $k_1, k_2$  represent the downward and upward velocities of the particles in the lower and upper part of the bed; these velocities can also include a segregating component.  $D_1$  and  $D_2$  are the axial solids dispersion coefficients in respectively the lower and upper bed part.

The boundary conditions of the differential Eqs.[4],[5] are formulated as:

- 1) no material leaves the bed at the top or at the bottom;

$$\text{at } h=0: \quad D_1 \frac{d c_1(h)}{d h} F + (f_v v_1 - f_k k_1) c_1(h) F = 0 \quad [6]$$

$$\text{at } h=H_0: \quad D_2 \frac{d c_2(h)}{d h} F + (f_v v_2 - f_k k_2) c_2(h) F = 0 \quad [7]$$

2) the solids concentrations in the lower and upper part of the bed are the same at the boundary between these two bed layers:

$$\text{at } h=H: \quad c_1(h) = c_2(h) \quad [8]$$

3) the total amount of segregating solids  $N$  is obtained by integration of the solids concentration along the bed height according to:

$$N = \int_0^{H_0} c(h) F dh = \int_0^H c_1(h) F dh + \int_H^{H_0} c_2(h) F dh \quad [9]$$

#### 4.3 Solids concentrations

Solution of these equations results in two expressions for the dimensionless axial solids concentrations  $X_1(z)$  and  $X_2(z)$  in respectively the lower and upper part of the bed:

$$z \leq z_H: \quad X_1(z) = c_1(z)/c_0 = \exp[-\lambda_1 z] \exp[\lambda_1 z_H] / \Omega \quad [10]$$

$$z \geq z_H: \quad X_2(z) = c_2(z)/c_0 = \exp[-\lambda_2 z] \exp[\lambda_2 z_H] / \Omega \quad [11]$$

In these expressions is  $c_0$  the overall solids concentration which equals  $N/(H_0 F)$ ; the dimensionless bed heights are defined as  $z = h/H_0$  and  $z_H = H/H_0$ , while the dimensionless parameter  $\Omega$  is written as:

$$\Omega = [1/\lambda_1] [\exp(\lambda_1 z_H) - 1] + [1/\lambda_2] [1 - \exp(\lambda_2 z_H) \exp(-\lambda_2)] \quad [12]$$

It should be noticed that  $X_1(z)$  and  $X_2(z)$  are local concentrations which can be larger than 1; furthermore, they equal by definition the normalized particle presence probability  $pp_{\text{norm}}$ .

The dimensionless boundary  $z_H$  is located at the bed height at minimum fluidization, while the expanded bed height  $H_0$  is equal to the maximum bed height of a slugging bed  $H_{\text{max}}$  (see Schouten et al., 1987). Therefore, by definition it can be written that  $z_H = H_{\text{mf}}/H_{\text{max}}$ .

$\lambda_1$  and  $\lambda_2$  are dimensionless model parameters which will be defined as distribution coefficients. They represent the ratio between the net particle convective and possible segregative flows and the particle dispersive flow:

$$\lambda_1 = (f_v v_1 - f_k k_1) H_0 / D_1 \quad \text{and} \quad \lambda_2 = (f_v v_2 - f_k k_2) H_0 / D_2 \quad [13]$$

It is easily observed that the second boundary condition leads to a simple expression for the solids concentration at  $z = z_H$ , which is given as:

$$X_1(z=z_H) = X_2(z=z_H) = 1 / \Omega \quad [14]$$

The absolute amount of solids  $\Delta n(\Delta z)$  in a bed layer of dimensionless height  $\Delta z = z_2 - z_1$  is subsequently obtained from:

$$\Delta n_1(\Delta z) = \int_{z_1}^{z_2} c_1(z) F dz \quad \text{where } z_1, z_2 \leq z_H \quad \text{and} \quad [15]$$

$$\Delta n_2(\Delta z) = \int_{z_1}^{z_2} c_2(z) F dz \quad \text{where } z_1, z_2 \geq z_H \quad [16]$$

With these expressions it is easily derived that:

$$\Delta n_1(\Delta z) = [\exp(-\lambda_1 z_1) - \exp(\lambda_1 z_2)] \exp(\lambda_1 z_H) / [\lambda_1 \Omega] \quad [17]$$

$$\Delta n_2(\Delta z) = [\exp(-\lambda_2 z_1) - \exp(\lambda_2 z_2)] \exp(\lambda_2 z_H) / [\lambda_2 \Omega] \quad [18]$$

Consequently, these expressions demonstrate that the axial solids distribution is a function of three dimensionless model parameters: the dimensionless bed height  $z_H$  and the distribution coefficients  $\lambda_1$  and  $\lambda_2$ .

The situation of complete mixing of the solids, with  $c_1(z) = c_2(z) = c_0$ , is obtained when  $\lambda_1 = \lambda_2 = 0$ . The distribution coefficients become zero when the convective and/or segregative upward and downward flows are equal, possibly in combination with a large axial solids dispersion coefficient.

Furthermore, the situation can be distinguished wherein only one part of the bed is completely mixed, while in the other part an axial solids distribution is present. This case is described by two possible combinations of the distribution coefficients:

1. the lower part of the bed is completely mixed:  $\lambda_1 = 0$  and  $\lambda_2 = 0$ .

In this case the solids concentration in the lower bed part is constant and no function of the bed height. It is remarkable that the magnitude of this concentration is completely determined by the magnitude of the distribution coefficient in the upper bed part:

$$z \leq z_H: X_1(z) = \lambda_2 / [1 - \exp(\lambda_2 z_H) \exp(-\lambda_2 z)] \quad [19]$$

The concentration in the upper bed part as a function of bed height is:

$$z \geq z_H: X_2(z) = \lambda_2 \exp[\lambda_2 (z_H - z)] / [1 - \exp(\lambda_2 z_H) \exp(-\lambda_2 z)] \quad [20]$$

2. the upper part of the bed is completely mixed:  $\lambda_1 \neq 0$  and  $\lambda_2 = 0$ .

In this case the solids concentration in the lower bed part is dependent on the bed height, while the concentration in the upper bed layer is constant. In this situation it is derived that:

$$z \leq z_H: X_1(z) = \lambda_1 \exp[\lambda_1 (z_H - z)] / [\exp(\lambda_1 z_H) - 1] \quad [21]$$

$$z \geq z_H: X_2(z) = \lambda_1 / [\exp(\lambda_1 z_H) - 1] \quad [22]$$

#### 4.4 Modeling results

In the Figures 21 and 22 a comparison is given between model fits of Eqs.[10],[11] and the experimentally obtained normalized particle presence probabilities  $pp_{norm}$  of the tracer in a bed of alumina respectively of experimental set 2.3 ( $U_0 = 1.6$  m/s;  $H_{mf}/D = 2.85$  [-];  $z_H = 0.32$  [-]) and experimental set 2.5 ( $U_0 = 1.4$  m/s;  $H_{mf}/D = 3.85$  [-];  $z_H = 0.37$  [-]).

It is concluded that the model describes the data very well with respectively the following values of the fitted distribution coefficients  $\lambda_1 = 1.3$  [-] and  $\lambda_2 = 2.8$  [-] in case of set 2.3 and  $\lambda_1 = 0.5$  [-] and  $\lambda_2 = 4.0$  [-] in case of set 2.5.

First, it is observed that in both cases the distribution coefficients are positive, which indicates that in the lower as well as in the upper bed part the downward convective solids flows are larger than the upward flows:  $f_v v_1 > f_k k_1$  and  $f_v v_2 > f_k k_2$ . This is, of course, in agreement with the phenomenon of solids dilution as mentioned in section 3.3.

Furthermore, it is found that the ratio  $\psi$  between  $\lambda_2$  and  $\lambda_1$  is very different:  $\psi = 2.15$  [-] for experimental set 2.3, while it equals 8.0 [-] for experimental set 2.5. A large value of  $\psi$  indicates in general a considerable difference between the magnitude of the respective particle flows in the upper and lower bed part:  $(f_v v_1 - f_k k_1) \ll (f_v v_2 - f_k k_2)$  and  $D_1 \gg D_2$ . This causes that a much more significant transition in the solids concentration will be found at the position of the boundary  $z = z_H$  between both bed parts in case of a larger value of the ratio  $\psi$ . This is in good agreement with the experimentally achieved transitions of  $pp_{norm}$  at  $z = z_H$  in Figures 21 and 22.

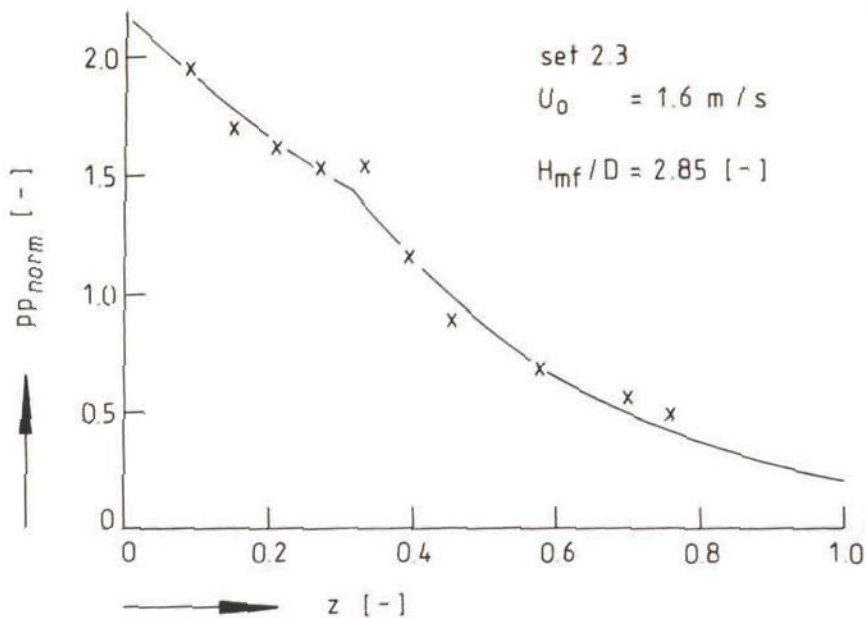


Figure 21: Model fit of the normalized presence probability in case of experimental set 2.3:  $U_0 = 1.6 \text{ m/s}$ ;  $H_{mf}/D = 2.85 [-]$ ;  $z_{mf} = 0.32 [-]$ . Model parameters:  $\lambda_1 = +1.3 [-]$ ;  $\lambda_2 = +2.8 [H]$ .

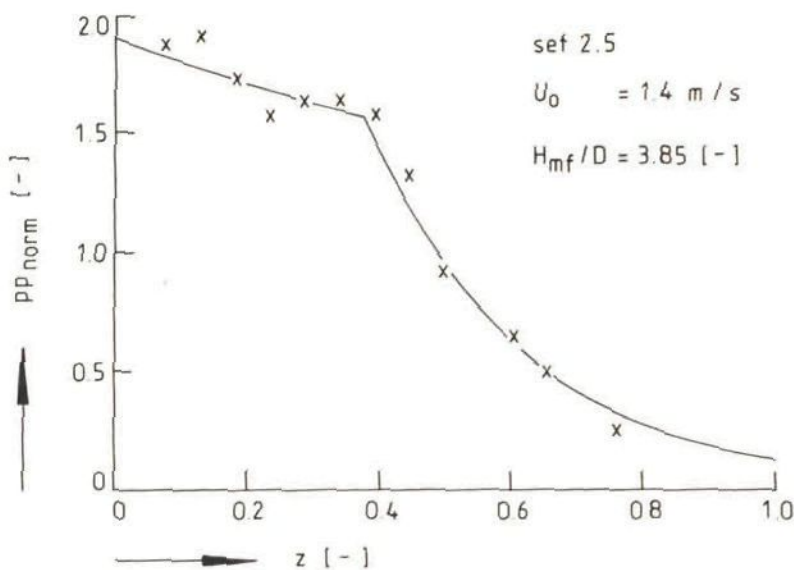


Figure 22: Model fit of the normalized presence probability in case of experimental set 2.5:  $U_0 = 1.4 \text{ m/s}$ ;  $H_{mf}/D = 3.85 [-]$ ;  $z_{mf} = 0.37 [-]$ . Model parameters:  $\lambda_1 = +0.5 [-]$ ;  $\lambda_2 = +4.0 [H]$ .

Finally, it is observed that the transition becomes less clear at a higher gas velocity and a lower  $H_{mf}/D$ -ratio (compare experimental set 2.3 and 2.5). Consequently, at these conditions the ratio  $\psi$  decreases which might partly be due to an increased upwards solids flow as a result of a larger drag force.

## 5. CONCLUSIONS

The main conclusions as obtained in this paper can be summarized as follows:

1. The upward particle velocity is a function of the axial position in the bed and increases with increasing superficial gas velocity, while it is not dependent on the  $H_{mf}/D$ -ratio ( $< 5$ ).
2. From calculations it is concluded that the average gas slug rise velocity is higher than the solid slug rise velocity, which indicates that the solid slug is flowed through with gas.
3. The downward particle velocity increases along the bed height; further no influence of the  $H_{mf}/D$ -ratio nor of the superficial gas velocity is observed. It is concluded that the position of the bed height at minimum fluidization  $H_{mf}$  effects the magnitude of the upward velocity, which is explained by the development of the slugs below  $h=H_{mf}$ .
4. A clear difference is present between the upward and downward velocity ratio as a function of the bed height in a segregating and in a non-segregating system at higher superficial gas velocities: in a non-segregating system a clear maximum is found, while further a significant change in its shape is observed at  $h=H_{mf}$ .
5. Above  $h=H_{mf}$  no distinction can be made between the particle velocities of small and large amplitude displacements. This suggest that the particle already reaches its steady state velocity during its movement in one single measurement window or/and that predominantly large amplitude movements take place.
6. A particle in a slugging gas fluidized bed shows a very strong tendency to continue its movement in an upward or downward direction once it is engaged in it. No strict diffusive mechanism is found, while also no memory effect is present. The solids displacement is considered to be anisotropic with respect to axial disperison.
7. It is observed that direction changes of the particle predominantly take place over longer distances than the width of the middle measurement window (64 mm). Oscillating displacements are very unlikely.



8. In general the mean particle cycling times are smaller than 5 seconds, however in a segregating system variations between 0.1 sec and more than 1 minute are observed dependent on the axial position in the bed.
9. The phenomenon of 'solids dilution' influences the axial presence probability of the particle which decreases along the bed height. The effect of solids dilution and segregation can be explained by a balance of forces acting on a particle (drag force, buoyancy and gravity).
10. A general model for particle motion in a slugging gas fluidized bed is formulated based on convective, dispersive and segregative solids flows which are different in the upper and lower part of the bed; the boundary is situated at the bed height at minimum fluidization ( $H_{mf}$ ). A comparison between experimental results and model calculations leads to useful results which can be applied for a diagnostic evaluation of the motion of solids in the upper and lower part of the bed.

### 3.4 Comments

- 3.4.1 Comment 1: critical gas velocity  $U_c$  and bed aspect ratio  $(H_{mf}/D)_c$  155
- 3.4.2 Comment 2: the axial solids dispersion coefficient in slugging beds 157
- 3.4.3 Comment 3: experimental evaluation of the general 'two-layer' model 161
- 3.4.1 Comment 1: critical gas velocity  $U_c$  and bed aspect ratio  $(H_{mf}/D)_c$

It has been concluded in the first paper in this chapter (chapter 3.2) and in paper 3.2 that segregation is influenced by the superficial gas velocity, the bed aspect ratio at minimum fluidization  $(H_{mf}/D)$  as well as by the bed diameter. Consequently, these factors have to be taken into account during the design phase of a fluid bed boiler so as to obtain the required level of segregation during the operation of the combustor. However, in general the (hydraulic) bed diameter can only be varied between narrow boundaries that are determined predominantly by the heat transfer requirements. Therefore, in a practical situation, only the gas velocity and the  $H_{mf}/D$ -ratio can be varied during operation in order to influence the extent of segregation.

The segregation model as discussed in chapter 3.2 and paper 3.2 provides the possibility to calculate the required magnitude of the values of the gas velocity and the  $H_{mf}/D$ -ratio at which a specific degree of segregation is present in the bed.

This specific level of segregation is defined as the critical level of segregation  $S_0$  which corresponds to a critical value of the model parameter  $\lambda$  being defined as  $\lambda_0$ . It has been shown in paper 3.2 that  $\lambda$  is a function of the ratio between the upward and downward particle velocities  $(k/v)$  as well as of the ratio between the solids volume fractions in respectively the particle and gas slug  $(m)$ . In the same way it will be defined here that:

$$\lambda_0 = 2 - (mk/v)_0 - (v/mk)_0 \quad [1.1]$$

Consequently, the critical level of segregation  $S_0$  is reached at a corresponding critical value of the ratio  $x_0 = (mk/v)_0$ . It can easily be

seen that always  $x_0 > 0$ , so subsequently the following explicit expression between  $x_0$  and  $\lambda_0$  is derived from Eq.[1.1]:

$$x_0 = [1 - \lambda_0/2] + [(\lambda_0/2)^2 - \lambda_0]^{1/2} \quad [1.2]$$

The procedure for the derivation of  $x_0$  is now in principle very simple. First, the required critical extent of segregation  $S_0$  is chosen; further, the corresponding value of  $\lambda_0$  is calculated, whereafter  $x_0$  is calculated with the equation given above. For example, when only a small extent of segregation is desired, e.g.  $S_0 = 5$  [-], then  $\lambda_0 = -0.20$  [-] and  $x_0 = 1.56$  [-].

In paper 3.2 relationships have been summarized which describe the upward and downward velocities, respectively  $k$  and  $v$ , as a function of fluid bed conditions ( $D$ ,  $H_{mf}$ ,  $U_0$ ,  $a$ ,  $b$  and  $m$ ) and particle system properties (expressed by the parameter  $R$ ). When these relationships are substituted in the expression  $x_0 = (mk/v)_0$ , finally, equations can be derived for the critical gas velocity ( $U_c$ ) as well as for the critical bed aspect ratio at minimum fluidization ( $(H_{mf}/D)_c$ ) at which the segregation level  $S_0$  will be reached. In this way the critical gas velocity is subsequently obtained as:

$$U_c = U_{mf} + \frac{[m^2 g R b H_{mf} / 2]^{1/2} + [x_0 0.35(agD)]^{1/2}}{x_0^2 [b H_{mf} / \{(0.35 m)^2 2 a D R\}]^{1/2} - x_0} \quad [1.3]$$

And the critical bed aspect ratio is further derived as:

$$(H_{mf}/D)_c = \left[ \frac{x_0 [(U_0 - U_{mf}) + 0.35(agD)]^{1/2}}{x_0^2 (U_0 - U_{mf}) [b / \{(0.35 m)^2 2 a R\}]^{1/2} - [g R b D / 2]^{1/2}} \right]^2 \quad [1.4]$$

As example the critical velocity is calculated in case of mixture I (see chapter 3.2) in the 5 cm ID bed at  $S_0 = 10$  [-]; a value of  $U_c = 1.74$  m/s is achieved which agrees well with the experimental value of  $U_c = 1.6$  to 1.7 m/s as it can be derived from Figure 10a in chapter 3.2.

In Figure 1.1 the calculated values of  $(U_c - U_{mf})$  have been plotted as a function of the bed aspect ratio  $H_{mf}/D$  (in case of the 5 cm ID bed; conditions of mixture I). It is clear that  $U_c$  increases with increasing  $H_{mf}/D$ -ratio as it was expected. Further, it is shown that  $U_c$  at  $S_0 = 5$  [-] is much larger than  $U_c$  at  $S_0 = 10$  [-] when  $H_{mf}/D > 1.5$ : at  $H_{mf}/D = 1$  the difference is about 0.1 m/s, but at  $H_{mf}/D = 2$  and 3 the difference is

already respectively 0.7 m/s and 3.6 m/s. So, these calculations indicate that rather large values of the gas velocity are needed to obtain a critical extent of segregation  $S_0 < 5$  [-] at practical levels of the  $H_{mf}/D$ -ratio; for example at  $H_{mf}/D = 3$  a value of  $U_c > 7$  m/s for mixture I in the 5 cm bed is necessary for  $S_0 < 5$  [-]; in case of  $S_0 = 10$  [-] a value of  $U_c = 2.9$  m/s is sufficient).

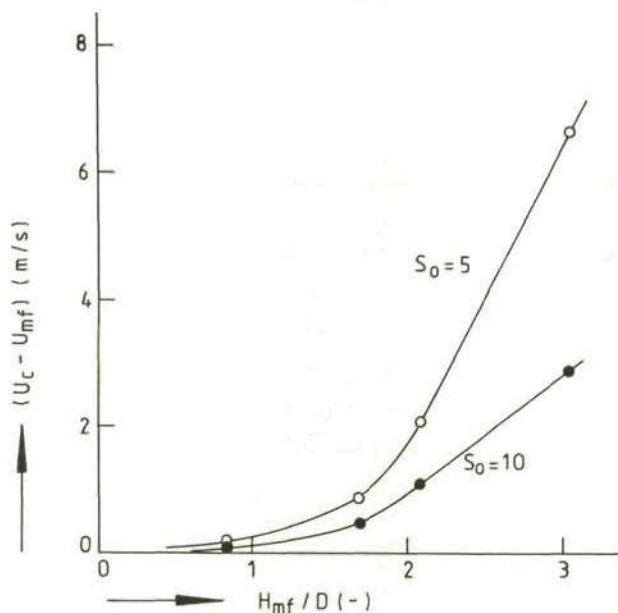


Figure 1.1: Model calculation of the critical gas velocity  $U_c$ , Eq.[1.3], as a function of the bed aspect ratio at minimum fluidization  $H_{mf}/D$  (Mixture I;  $D = 5$  cm; see chapter 3.2)

Consequently, it is obvious that always segregation of bed material has to be expected at superficial gas velocities in the range of 1 to 3 m/s as applied during fluidized bed combustion. A possible mechanistic explanation for this phenomenon has been given in the first paper (chapter 3.2).

### 3.4.2 Comment 2: the axial solids dispersion coefficient in slugging beds

In paper 3.2 it has been demonstrated that the segregation model enables the calculation of the axial particle dispersion coefficient. In this comment some more model results will be shown, which are further compared with data given in literature.

Some typical examples of the particle dispersion coefficient, as obtained from the segregation model, as a function of the superficial gas

velocity are given in the Figures 2.1 and 2.2. It is demonstrated that these calculations agree rather well with the dispersion coefficient given by Thiel and Potter (1978). These authors have developed a model to predict the axial solids mixing in a slugging fluidized bed containing round-nosed slugs. Their model supposes that each gas slug is followed by a well-mixed and a piston flow region. The model gives a prediction of the axial solids dispersion coefficient as:

$$D_o = (f^2/2) (1-\epsilon_{mf}) TD [U_o - U_{mf} + 0.35(gD)^{1/2}] \quad [2.1]$$

$f$  is the fraction of the interslug volume which is perfectly mixed. Its value, as required by Thiel and Potter (1978) to fit their experimental results, varies between 0.5 and 0.85. Their model gives a reasonable prediction of the data with  $f = 0.5$  in a 5.1 cm ID bed,  $f = 0.75$  in a 10.2 cm ID bed and  $f = 0.85$  in a 21.8 cm ID bed. They proposed for  $f$  the average value of  $f = 0.7$ , which they also used for comparison of their model with literature data. The results predicted by their equation of  $D_o$  are shown to be in good agreement with the values reported by other authors. E.g., their model predicts the scale effect of bed diameter, as first reported by May (1959) with a fair degree of accuracy. The dispersion coefficient as given in Figures 2.1 and 2.2 in case of mixture I in the 5 cm ID and the 7.5 cm ID bed are calculated with values for  $f$  obtained from interpolation, these are respectively  $f = 0.5$  and  $f = 0.67$ .

The relationship of Thiel and Potter (1978) is based on the length of the gas slug as is given by Eq.[13] in paper 3.2. However, their equation does not contain the influence of the type of slugging which is expressed by the dimensionless slug parameter  $a$ . This influence is probably incorporated in the value of the fraction  $f$  which they obtained by fitting the equation to experimental data.

Viswanathan and Subba Rao (1984) show that the axial solids dispersion coefficient is predicted by their solids circulation model to be proportional to  $(U_o - U_{mf})$  to the power 0.2. This result showed to be at least in qualitative agreement with the data summarized by Van Deemter (1980).

Further, Avidan and Yerushalmi (1985) presented literature data and own measurements which show the axial dispersion coefficient to be linear dependent on the gas velocity. The calculations based on the segregation model as shown in Figures 2.1 and 2.2 indicate that in these cases the dispersion coefficient of segregating particles is predicted to be proportional to  $(U_o - U_{mf})$  to the power 0.64 and 0.75 respectively.

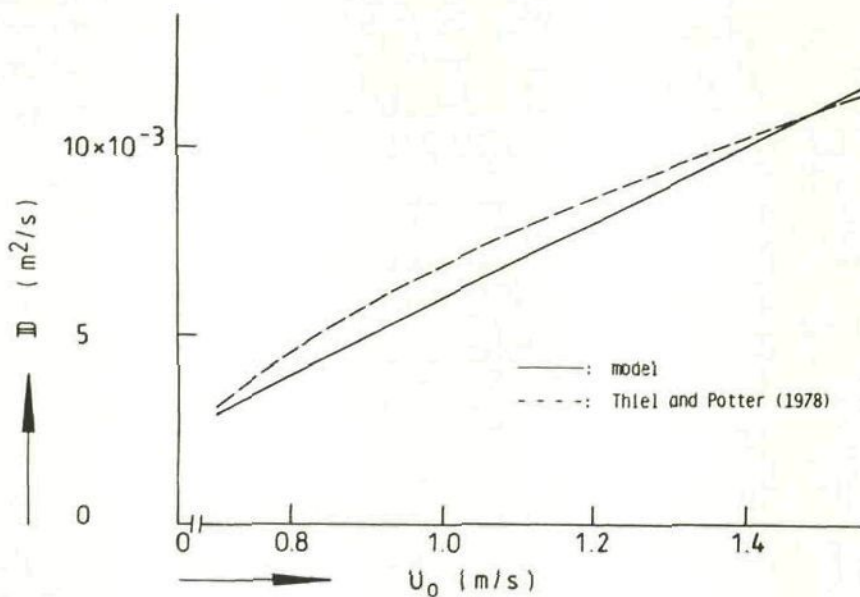


Figure 2.1: Comparison between the particle dispersion coefficient calculated with the segregation model and the equation of Thiel and Potter (1978) (Mixture I;  $H_{mf}/D = 3.04$  [-];  $U_{mf} = 0.58$  m/s;  $D = 5$  cm).

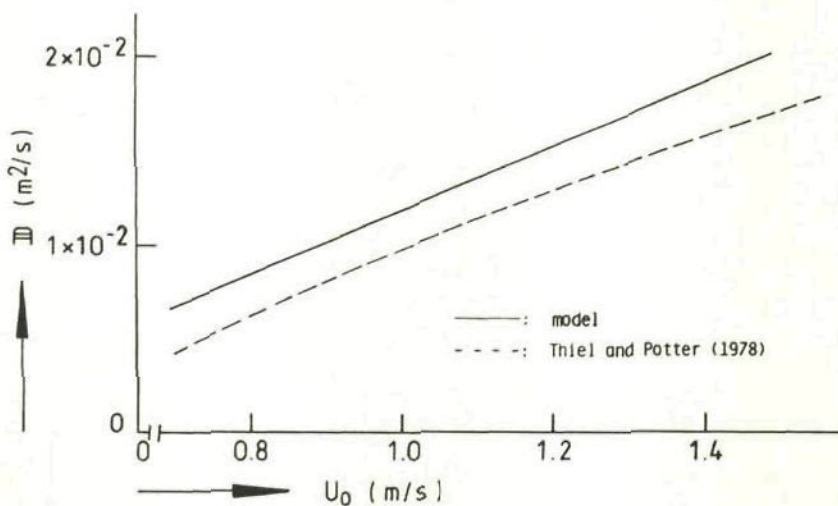


Figure 2.2: Comparison between the particle dispersion coefficient calculated with the segregation model and the equation of Thiel and Potter (1978) (Mixture I;  $H_{mf}/D = 2.36$  [-];  $U_{mf} = 0.56$  m/s;  $D = 7.5$  cm).

In Figure 9 in paper 3.2 it has been shown that also a good agreement is found between the experimentally obtained dispersion coefficient as a function of the bed diameter and the equation of Thiel and Potter (1978).

Viswanathan and Subba Rao (1984) reported that the axial solids dispersion coefficient is predicted by their model to be proportional to the fluid bed diameter raised to the power 1.4 (for beds with  $H/D > 0.625$ ), which is in excellent agreement with the data summarized by Van Deemter (1980).

In general, the results of the segregation model demonstrate that  $D_0$  is proportional to the bed diameter raised to the power 1.25, which is in good qualitative agreement with the value of 1.4.

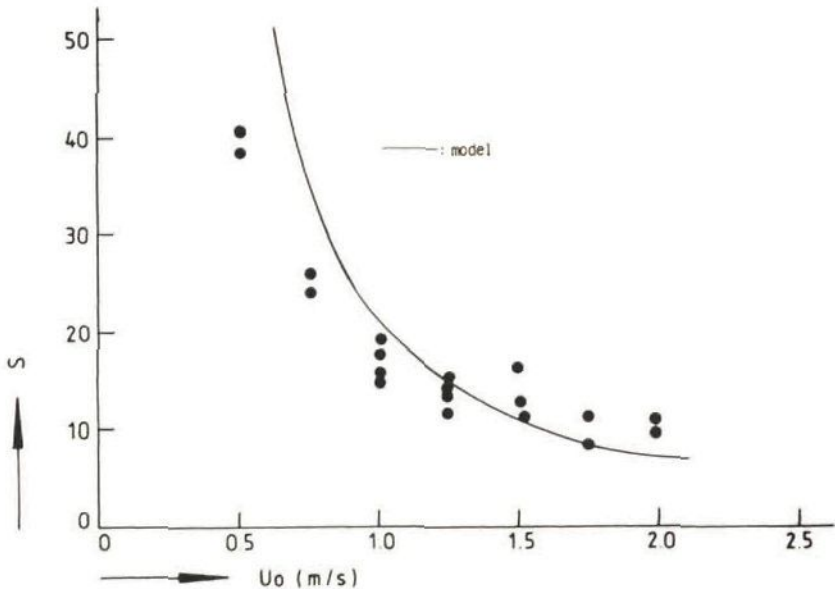


Figure 2.3: The extent of segregation  $S$  as a function of the superficial gas velocity at  $850^\circ\text{C}$ : a comparison between model and experiment (Mixture I;  $H_{mf}/D = 2.1$  [-];  $U_{mf} = 0.38$  m/s;  $D = 10$  cm; fitted value of  $f_m = 0.68$  [-]).

In Figure 2.3 the agreement between the segregation model and the experimental results of the extent of segregation is shown as a function of the superficial gas velocity in the 10 cm ID bed at  $850^\circ\text{C}$ . It is observed that the model predicts a value of the extent of segregation which is more than 30% higher than the experimental value at gas velocities smaller than 0.7 m/s. Especially at  $U_o = 0.5$  m/s the difference between model and experiment is considerable. The best fit between model and experiment is obtained with a value of the fraction of particles in the particle slug,  $f_m$ ,

of 0.68 [-]. This value implies that 32% of the segregating particles is 'raining through' the gas slugs. Under ambient conditions (20 °C) a value of  $f_m = 0.61$  [-] is obtained, which differs not much from the value at high temperature. In Figure 2.4 it is demonstrated that the segregation model predicts at 850 °C a solids dispersion coefficient which is qualitatively in agreement with the equation of Thiel and Potter (1978), however, the model value is in general about 70 mm<sup>2</sup>/s smaller.

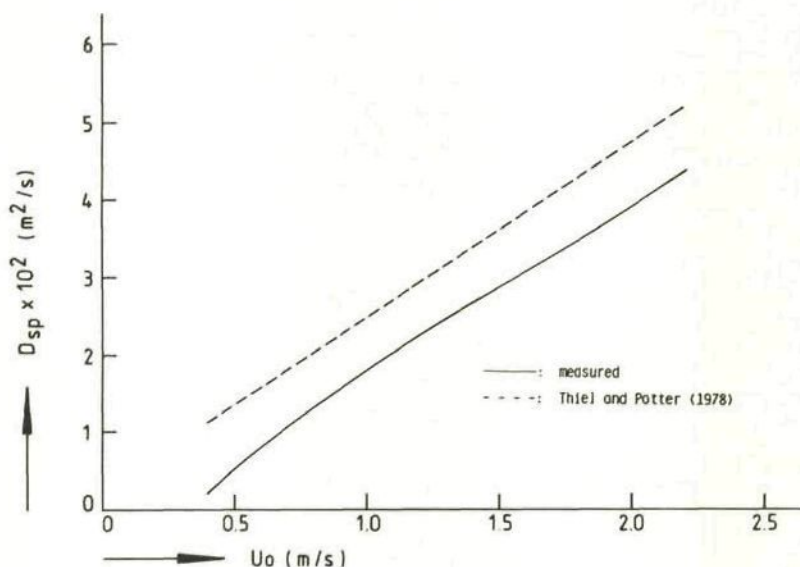


Figure 2.4: Comparison of the calculated particle dispersion coefficient and the equation of Thiel and Potter (1978) as a function of the superficial gas velocity at 850 °C (conditions: see Figure 2.3).

### 3.4.3 Comment 3: experimental evaluation of the general 'two-layer' model

In the second paper (chapter 3.3) in this chapter a general model has been introduced for the description of particle motion in slugging gas fluidized beds. A key element of the model is that it assumes that a slugging bed consists of two layers with different magnitudes of the upward and downward solids flows. The axial solids distribution is obtained as a function of the axial position of the boundary between the two layers as well as of two distribution coefficients which describe the ratio between the net convective/segregative flows and the dispersive flow in the respective bed layers. This model has been applied to explain the experimentally obtained solids presence probability during the radioactive tracer measurements.



In this third comment it will be demonstrated that this model is also able to describe particle distributions due to segregation. Hereto the static segregation experimental results will be applied which have been described in the first paper (chapter 3.2).

In general a significant maximum in the axial distribution of 'flotsam' particles is observed at low superficial gas velocities ( $U_0 - U_{mf} < 0.3$  m/s), while nearly no particles are present in the two bottom layers of the bed (L4 and L5); a typical example is shown in Figure 3.1 ( $U_0 = U_{mf}$ ). This same phenomenon has also been reported in chapter 3.3 where a maximum in the presence probability of the 'flotsam' tracer particle is found. This maximum occurs in the upper section of the bed (at  $z = 0.8$  [-]) and is explained by the opposite action of segregation forces and the occurrence of 'solids dilution' above the bed height at minimum fluidization.

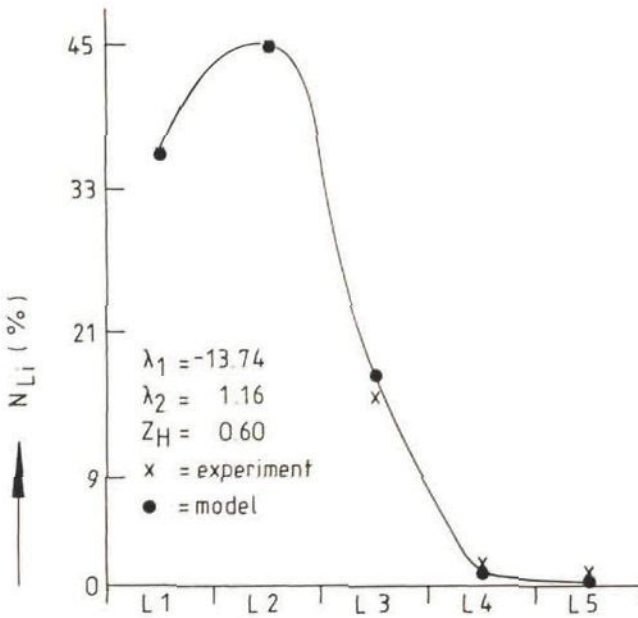


Figure 3.1: Comparison between the experimental and the model particle distributions (Mixture I;  $D = 5$  cm;  $H_{mf}/D = 2.08$  [-];  $U_0 = 0.65$  m/s).

Figure 3.1 points out that a good fit between model and experiment is obtained at  $z_H = 0.60$  [-],  $\lambda_1 = -13.74$  [-] and  $\lambda_2 = +1.16$  [-]. The negative value of the distribution coefficient  $\lambda_1$  in the lower bed section ( $z < z_H$ ) implies that  $f_k k_1 > f_v v_1$ , which indicates that the upward convective/segregative flow of the 'flotsam' alumina in this section of the bed is larger than the downward flow. This causes the particles to segregate,

however, the distribution coefficient  $\lambda_2$  in the upper section is positive which means that here the net convective/segregative flow is directed downwards ( $f_k k_2 < f_v v_2$ ), which clearly explains the occurrence of the 'solids dilution' in this upper part of the bed.

The maximum disappears at higher gas velocities where probably the influence of 'solids dilution' becomes small in comparison with the convective/segregative flow. In Figure 3.2 it is illustrated that the model fits the data well in such a case with values of the distribution coefficients which are both negative. Furthermore the dimensionless boundary position  $z_H$  has been shifted to  $z_H = 0.20$  [-]. However, it should be noticed that at a higher gas velocity the average bed height  $H_0$  has increased, which will decrease the ratio  $H/H_0$  when  $H$  remains constant.

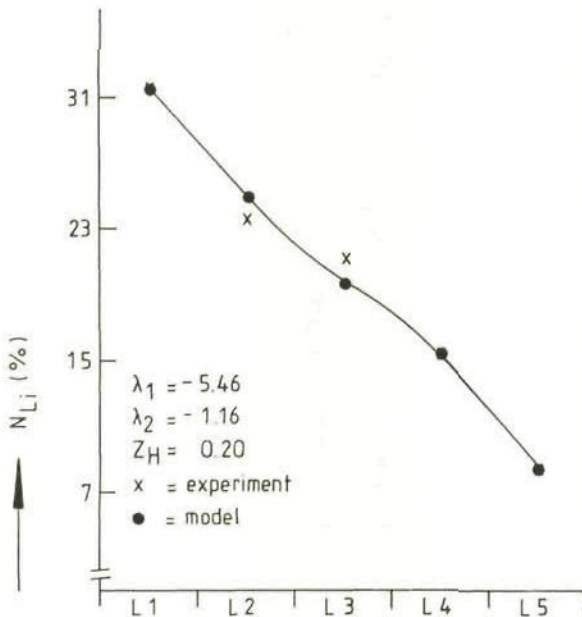


Figure 3.2: Comparison between the experimental and the model particle distributions (Mixture I;  $D = 5$  cm;  $H_{mf}/D = 2.08$  [-];  $U_0 = 0.90$  m/s).

The influence of the superficial gas velocity on the model parameters is clearly demonstrated in the Figures 3.3 ( $z_H$ ), 3.4 ( $\lambda_1$ ) and 3.5 ( $\lambda_2$ ) for mixture I. Figure 3.3 shows that in general three regions can be distinguished with respect to  $z_H$ :  $z_H$  is almost constant at a value of 0.6 between the minimum fluidization velocity ( $U_{mf} = 0.64$  m/s) and  $U_0 = 0.9$  m/s;  $z_H$  decreases from 0.6 to 0.2 between 0.9 m/s and 1.4 m/s, whereafter it remains at 0.2 at gas velocities higher than 1.4 m/s.

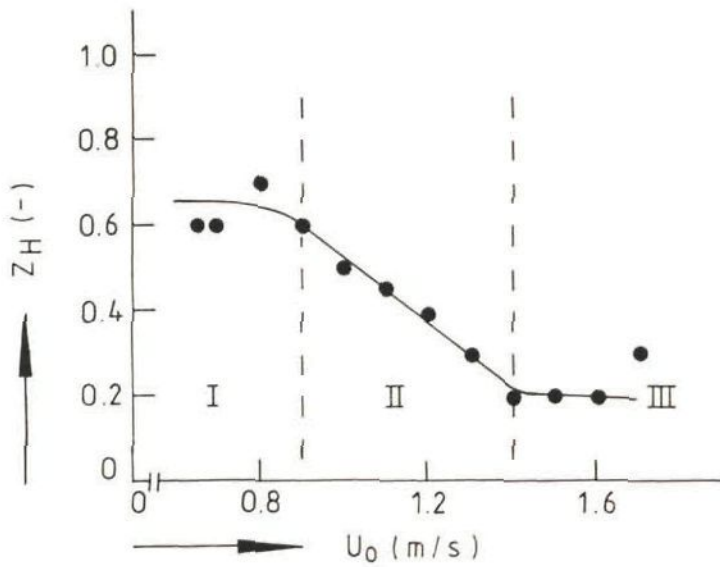


Figure 3.3: The dimensionless position of the boundary  $z_H$ , as a function of the superficial gas velocity (Mixture I;  $D = 5$  cm;  $H_{mf}^H/D = 2.08 [-]$ ).

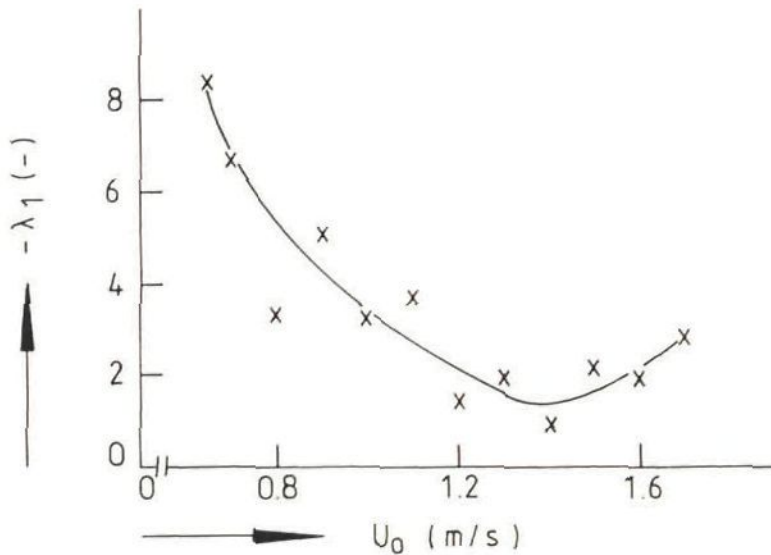


Figure 3.4: The distribution coefficient  $\lambda_1$ , as a function of the superficial gas velocity (Mixture I;  $D = 5$  cm;  $H_{mf}^H/D = 2.08 [-]$ ).

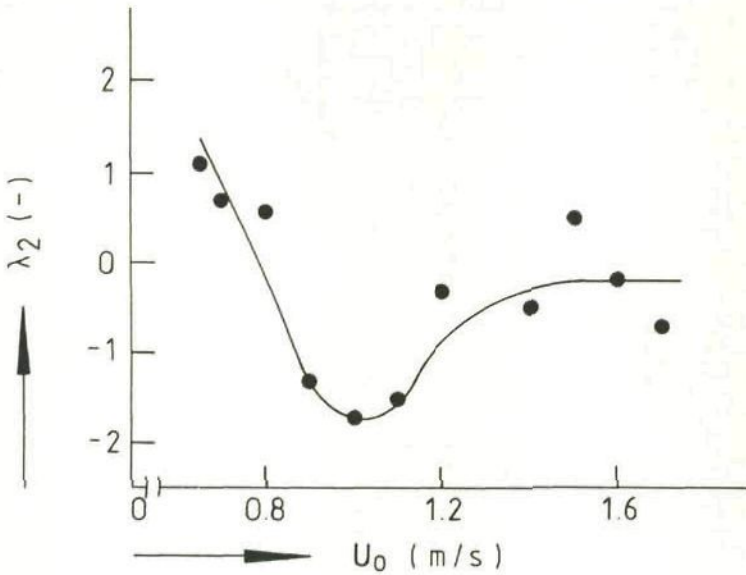


Figure 3.5: The distribution coefficient  $\lambda_2$  as a function of the superficial gas velocity (Mixture I;  $D = 5$  cm;  $H_{mf}/D = 2.08$  [-]).

$\lambda_1$  decreases with increasing gas velocities and shows a minimum at about  $U_0 = 1.4$  m/s which corresponds with the gas velocity where  $z_H$  remains constant at 0.2. So  $\lambda_1$  does not become zero, but even increases a little at higher gas velocities, indicating that the net upward solids flow increases. The reason for this phenomenon is not clear.

The distribution coefficient  $\lambda_2$  shows also a minimum, but this is in all cases present at a gas velocity of about 1 m/s. Further in general  $\lambda_2$  becomes about zero at higher velocities ( $U_0 > 1.6$  m/s), which indicates that the upper section of the bed is completely mixed (the axial particle concentration is constant). However, still some segregation is present,  $c_2(z) > c_0$ , due to the fact that  $\lambda_1 < 0$ .

In Figures 3.6 and 3.7 two typical examples are plotted of the distribution coefficient  $\lambda_2$  as a function of the extent of segregation  $S$ . It is observed that  $\lambda_2 > 0$  when  $S > 60$  [-] and  $S > 30$  [-] in respectively the 5 cm ID ( $H_{mf}/D = 2.08$  [-]) and the 15 cm ID bed ( $H_{mf}/D = 0.79$  [-]). Consequently, the net effect of 'solids dilution' and segregation in the 15 cm bed is much larger; obviously this will predominantly be the result of the much smaller segregative flow in the 15 cm bed caused by the larger bed diameter and the smaller  $H_{mf}/D$ -ratio, because both effects decrease the extent of segregation significantly (see chapter 3.2).

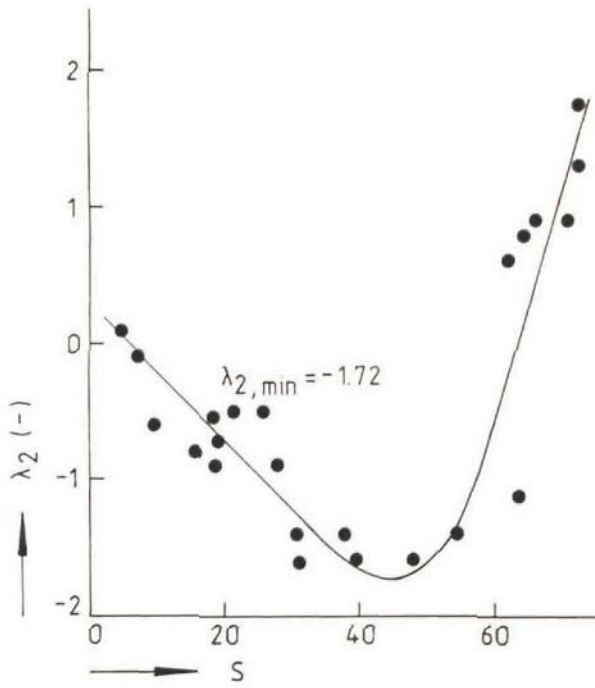


Figure 3.6: The distribution coefficient  $\lambda_2$  as a function of the extent of segregation  $S$  (Mixture I;  $D = 5$  cm;  $H_{mf}/D = 2.08$  [-]).

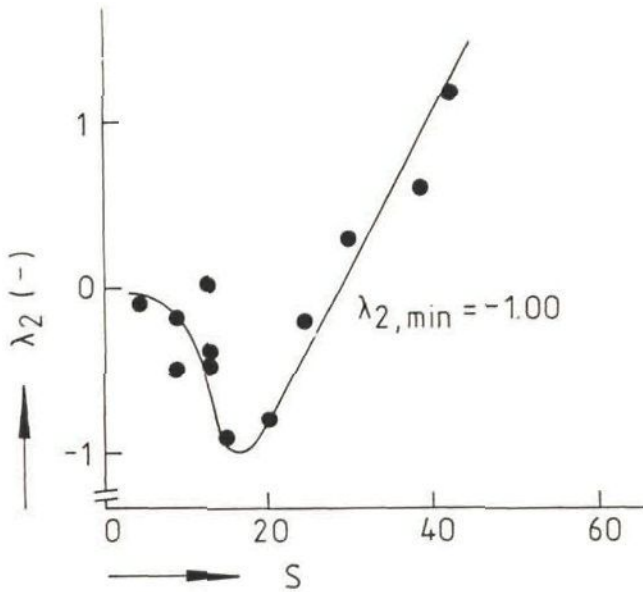


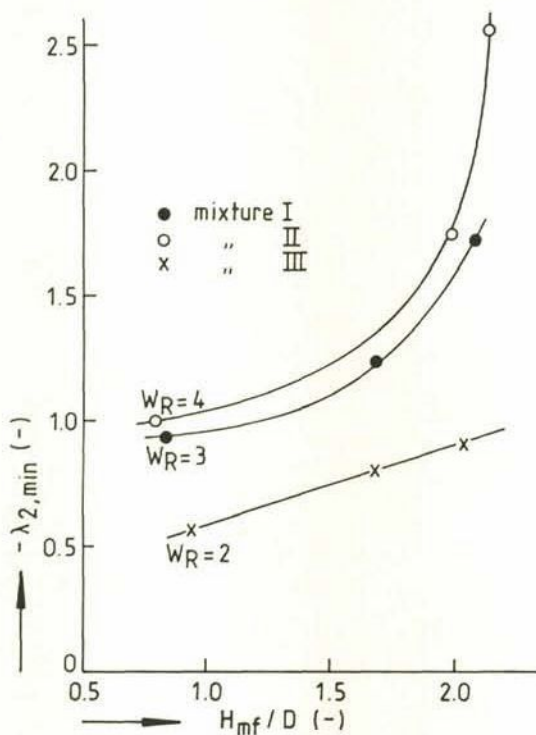
Figure 3.7: The distribution coefficient  $\lambda_2$  as a function of the extent of segregation  $S$  (Mixture II;  $D = 15$  cm;  $H_{mf}/D = 0.79$  [-]).

The magnitude of the minimum value of the distribution coefficient  $\lambda_2$ ,  $\lambda_{2,\min}$ , is a measure of the extent of segregation  $S$  at a superficial gas velocity of about 1 m/s. For example,  $S \approx 45$  [-] at  $\lambda_{2,\min} = -1.72$  [-] in the 5 cm ID bed in Figure 3.6, while  $S \approx 18$  [-] at  $\lambda_{2,\min} = -1.00$  [-] in the 15 cm ID bed in Figure 3.7.

In Figure 3.8 the effect of the  $H_{mf}/D$ -ratio on  $\lambda_{2,\min}$  in the 5 cm ID bed is demonstrated for three different mixtures corresponding with different weight ratios  $W_R$  between sand and alumina of respectively 2 (mixture III), 3 (mixture I) and 4 (mixture II). In all cases it is observed that  $\lambda_{2,\min}$  becomes more negative with increasing  $H_{mf}/D$ -ratio, which implies an increase of segregation. This effect of the bed aspect ratio has already been shown and discussed in chapter 3.2.

**Figure 3.8:** The minimum distribution coefficient  $\lambda_{2,\min}$  as a function of the  $H_{mf}/D$ -ratio ( $D = 5$  cm;  $U_0 = 1$  m/s).

Furthermore, Figure 3.8 clearly illustrates the general effect of the relative amount of the segregative material on the extent of segregation (see chapter 3.2):  $\lambda_{2,\min}$  decreases with increasing  $W_R$ , so the extent of segregation decreases with a higher relative amount of alumina present in the bed (consequently, no segregation is present when  $W_R \rightarrow 0$ , in this case all bed material is alumina).



This effect of the weight ratio on the extent of segregation might also be predicted from the segregation model equations given in paper 3.2 (Eqs. [7], [8] and [10]). When  $W_R \rightarrow 0$  it is obvious that  $\rho_{\text{bulk}} \rightarrow \rho_{\text{alum}}$  and consequently  $R \rightarrow 0$ , so no segregation will occur. Furthermore, when  $W_R \rightarrow \infty$  it is clear that  $\rho_{\text{bulk}} \rightarrow \rho_{\text{sand}}$  and so in this case  $R \rightarrow (\rho_{\text{sand}}/\rho_{\text{alum}} - 1)$ , which is theoretically the highest value of  $R$ , indicating that in this situation the extent of segregation will be maximum.

## NOTATION

a	= dimensionless slug parameter	[-]
$a_0$	= initial sorbent interfacial area	$[m^2/m^3]$
$a_A$	= total initial sorbent interfacial area	$[m^2/m^3]$
$A_0$	= equilibrium parameter	[-]
Ar	= Archimedes number	[-]
b	= dimensionless slug parameter	[-]
$B_0$	= formation rate parameter	[-]
c	= chapter 2: gaseous sulfur concentration chapter 3: solids concentration	$[mol/m^3]$ $[\#/m^3]$
$c_{in}$	= oxygen reactor inlet concentration	$[mol/m^3]$
$c_{uit}$	= oxygen reactor outlet concentration	$[mol/m^3]$
$c_0$	= chapter 2: initial gaseous sulfur concentration equivalent oxygen concentration	$[mol/m^3]$ $[mol/m^3]$
	= chapter 3: overall solids concentration	$[\#/m^3]$
$c_1$	= oxygen concentration	$[mol/m^3]$
$c_2$	= sulfur dioxide concentration	$[mol/m^3]$
$c_2(z)$	= axial solids concentration in upper bed section	$[\#/m^3]$
$c_3$	= sulfur trioxide concentration	$[mol/m^3]$
Ca/S	= molar calcium to sulfur ratio in the reactor feed	[-]
d	= particle diameter	[m]
$d_0, d_3$	= initial average sorbent particle diameter	[m]
$d_1$	= average coal particle diameter	[m]
$d_b$	= average bubble diameter	[m]
$d_{max}$	= maximum bubble diameter	[m]
$d_p$	= average bed particle diameter	[m]
D	= chapter 2: sulfur dioxide diffusion coefficient chapter 3: bed diameter	$[m^2/s]$ [m]
$D_0$	= axial solids dispersion coefficient	$[m^2/s]$
$D_1$	= oxygen diffusion coefficient	$[m^2/s]$
$D_3$	= sulfur trioxide diffusion coefficient	$[m^2/s]$
$E_1(t)$	= coal residence time distribution function	[1/s]
$E(t), E_3(t)$	= sorbent residence time distribution function	[1/s]
$E_{max}$	= maximum bed expansion	[-]
$E_{min}$	= minimum bed expansion	[-]
$E_1$	= activation energy of $SO_3$ formation	[kJ/mol]
$E_3$	= activation energy of sorbent sulfation reaction	[kJ/mol]
f	= fraction of the interslug volume which is perfectly mixed	[-]
$f_k$	= volume fraction of solids in upward moving particle flow	[-]
$f_m$	= volume fraction of solids in particle slug	[-]
$f_v$	= volume fraction of solids in downward moving particle flow	[-]
$f_s$	= volume fraction of non-segregating solids in the bed	[-]
F	= bed cross-sectional area	$[m^2]$
g	= acceleration due to gravity = $9.814 m/s^2$	
h	= bed height	[m]
H	= average expanded bed height	[m]
$H_{max}$	= maximum bed height	[m]
$H_{mf}$	= bed height at minimum fluidization	[m]
$H_{mf}/D$	= bed aspect ratio at minimum fluidization	[-]
$(H_{mf}/D)_c$	= critical value of $H_{mf}/D$	[-]
$H_{min}$	= minimum bed height	[m]

K	= bubble-emulsion phase mass transfer coefficient (based on total reactor volume)	[1/s]
$K_{be}$	= idem (based on total bubble volume)	[1/s]
$K_p$	= equilibrium constant	[atm <sup>-1/2</sup> ]
$K_o$	= equilibrium constant	[1/√(mol/m <sup>3</sup> )]
k	= chapter 2: overall sulfation rate constant based on SO <sub>2</sub> sulfation	[m/s]
	= chapter 3: upward (segregation) particle velocity	[m/s]
$k_1$	= chapter 2: overall coal combustion reaction rate parameter	[m/s]
	= chapter 3: upward particle velocity in the lower bed section	[m/s]
$k_2$	= upward particle velocity in the upper bed section	[m/s]
$k_3$	= overall sulfation rate constant (based on SO <sub>3</sub> sulfation)	[m/s]
$k_{30}$	= pre-exponential factor of sorbent sulfation rate constant	[m/s]
$k_g$	= mass transfer coefficient	[m/s]
$k_{g1}$	= oxygen mass transfer coefficient	[m/s]
$k_{g3}$	= sulfur trioxide mass transfer coefficient	[m/s]
$k_s$	= sulfation rate constant (based on SO <sub>2</sub> sulfation)	[m/s]
$k_{s3}$	= sulfation rate constant (based on SO <sub>3</sub> sulfation)	[m/s]
l	= height of cylindrical alumina particle	[mm]
m	= chapter 2: two-phase gas flow parameter	[-]
	= chapter 3: ratio between volume fraction of particles in the particle and the gas slug	[-]
$M, M_2$	= retention parameter	[-]
$M_o$	= initial sorbent weight (before calcination)	[kg]
	= dimensionless model parameter	[-]
$M_1$	= combustion parameter	[-]
$M_{CaCO_3}$	= molar mass of CaCO <sub>3</sub>	[g/mol]
$\Delta n$	= amount of segregating particles in a bed layer of height $\Delta z$	[#]
N	= total amount of segregating particles in the bed	[#]
$N_o$	= number of transfer units	[-]
$N_{CaO,o}$	= initial amount of CaO in the bed	[mol]
$N_{Li}$	= percentual amount of segregating particles in bed layer Li	[%]
p	= solids exchange coefficient	[m <sup>3</sup> solids/m <sup>3</sup> bed/s]
	= probability of direction change	[-]
pp	= presence probability of tracer particle	[-]
$P_o$	= maximum gas exchange ratio	[-]
P	= average gas exchange ratio	[-]
$q, q_3$	= CaO molar surface concentration	[mol/m <sup>2</sup> ]
$q_1$	= carbon molar surface concentration	[mol/m <sup>2</sup> ]
r	= sulfation rate	[mol SO <sub>3</sub> /m <sup>2</sup> /s]
$r_o$	= initial sulfation rate (r at t=0)	[mol SO <sub>3</sub> /m <sup>2</sup> /s]
R	= chapter 2: level of sulfur retention	[-]
	= chapter 3: dimensionless parameter which is a function of solids weight ratio and densities	[-]
RI	= retention index	[-]
S	= chapter 2: average reactive sorbent surface area	[m <sup>2</sup> ]
	= chapter 3: extent of segregation	[-]
$S_A$	= initial total available reactive sorbent surface area	[m <sup>2</sup> ]
$Sh_1, Sh, Sh_3$	= Sherwood number (resp. O <sub>2</sub> , SO <sub>2</sub> and SO <sub>3</sub> gas transfer)	[-]
$S_o$	= chapter 2: initial reactive sorbent surface area	[m <sup>2</sup> ]
	= chapter 3: critical value of extent of segregation	[-]
$S_1(t)$	= surface area of freshly added coal as a function of time	[m <sup>2</sup> ]



$S_{10}$	= initial total available reactive coal surface	[m <sup>2</sup> ]
$S_3$	= surface area of freshly added sorbent	[m <sup>2</sup> ]
$S_{3,0}$	= initial total available reactive sorbent surface area	[m <sup>2</sup> ]
$t$	= time	[s]
$t_0$	= time constant	[s]
$T$	= Chapter 2: absolute temperature	[K]
	= Chapter 3: length of particle slug in units of bed diameter	[-]
$u$	= dimensionless excess gas velocity in the bubble phase	[-]
$u_b$	= bubble rise velocity	[m/s]
$U_0$	= superficial gas velocity	[m/s]
$U_C$	= critical value of superficial gas velocity	[m/s]
$U_e$	= superficial gas velocity in the emulsion phase	[m/s]
$U_{mf}$	= minimum fluidization velocity	[m/s]
$U_S^0$	= stable slug velocity	[m/s]
$v$	= downward particle velocity	[m/s]
$v_1$	= downward particle velocity in the lower bed section	[m/s]
$v_2$	= downward particle velocity in the upper bed section	[m/s]
$V$	= reactor volume	[m <sup>3</sup> ]
$V_{gas}$	= total gas volume in the reactor	[m <sup>3</sup> ]
$V_{particles}$	= volume of (sorbent) particles in the reactor	[m <sup>3</sup> ]
$W_{bed}$	= total mass of bed material	[kg]
$W_{CaCO_3}$	= mass of CaCO <sub>3</sub> in a sorbent particle	[kg]
$W_R$	= weight ratio of sand (or iron) and alumina	[-]
$W_0$	= initial reactive mass of sorbent in the bed	[kg]
$W_A$	= total initial reactive mass of sorbent in the bed	[kg]
$x_{CaCO_3}$	= weight fraction of CaCO <sub>3</sub> in a sorbent particle	[-]
$x_S$	= weight percentage of sulfur in coal feed	[%]
$x_0$	= dimensionless parameter equal to $(mk/v)$ at $S=S_0$	[-]
$x_1$	= molar fraction of carbon in coal	[-]
$x_2$	= molar fraction of sulfur in coal	[-]
$x_3$	= weight fraction of calcium in sorbent	[-]
$X$	= dimensionless SO <sub>2</sub> outlet concentration	[-]
$X_0$	= dimensionless sulfur (SO <sub>2</sub> + SO <sub>3</sub> ) outlet concentration	[-]
$X_2$	= dimensionless SO <sub>2</sub> outlet concentration	[-]
$X_{2,0}$	= initial dimensionless SO <sub>2</sub> outlet concentration	[-]
$X_{2^\infty}$	= SO <sub>2</sub> dimensionless outlet concentration at $t \rightarrow \infty$	[-]
$z$	= chapter 2: ratio between molar volumes of sulfation reaction product and reactant	[-]
	= chapter 3: dimensionless bed height	[-]
$z_H$	= axial position of boundary between bed layers	[-]

#### Greek letters

$\alpha_{avg}$	$\alpha_{2,avg}$ = average CaO sorbent conversion	[-]
$\alpha_{max}$	= maximum CaO sorbent conversion	[-]
$\bar{V}$	= stoichiometric parameter	[-]
$\epsilon$	= bed porosity	[-]
$\epsilon_b$	= bubble fraction	[-]
$\epsilon_p^0$	= initial porosity of CaO in calcined sorbent	[-]
$\epsilon_{mf}$	= bed porosity at minimum fluidization	[-]
$\Phi_C$	= molar carbon feed rate (based on C in coal)	[mol/s]
$\Phi_{Ca}$	= molar calcium feed rate (based on Ca in sorbent)	[mol/s]

$\phi_{\text{coal}}$	= coal feed rate	[kg/s]
$\phi_{\text{H}}$	= molar hydrogen feed rate (based on H in coal)	[mol/s]
$\phi_{\text{N}}$	= molar nitrogen feed rate (based on N in coal)	[mol/s]
$\phi_{\text{O}}$	= molar oxygen feed rate (based on O in coal)	[mol/s]
$\phi_{\text{S}}$	= molar sulfur feed rate (based on S in coal)	[mol/s]
$\phi_{\text{solids}}$	= solids feed rate	[kg/s]
$\phi_{\text{v}}$	= gas flow rate	[m <sup>3</sup> /s]
$\kappa_1$	= forward SO <sub>3</sub> reaction rate constant	[1/√(mol/m <sup>3</sup> )/s]
$\kappa_{10}$	= pre-exponential factor of forward SO <sub>3</sub> reaction rate constant	[1/√(mol/m <sup>3</sup> )/s]
$\kappa_2$	= backward SO <sub>3</sub> reaction rate constant	[1/s]
$\lambda$	= chapter 2: stoichiometric air ratio	[mol O <sub>2</sub> /mol C]
	chapter 3: dimensionless parameter in segregation model	[-]
$\lambda_0$	= critical value of $\lambda$ (chapter 3)	[-]
$\lambda_1$	= distribution coefficient in lower bed section	[-]
$\lambda_2$	= distribution coefficient in upper bed section	[-]
$\lambda_{2,\text{min}}$	= minimum distribution coefficient in upper bed section	[-]
$\mu$	= gas viscosity	[Pa.s]
$\eta$	= oxygen conversion	[-]
$\Omega$	= dimensionless parameter	[-]
$\Lambda$	= dimensionless parameter $\alpha/\alpha_{\text{max}}$	[-]
$\Pi$	= dimensionless parameter $t/t_0$	[-]
$\rho$	= solids density	[kg/m <sup>3</sup> ]
$\rho_0, \rho_3$	= initial sorbent density (before calcination)	[kg/m <sup>3</sup> ]
$\rho_1$	= coal density	[kg/m <sup>3</sup> ]
$\rho_{\text{alum}}$	= density of alumina particle	[kg/m <sup>3</sup> ]
$\rho_{\text{bulk}}$	= density of bulk material in the solids slug	[kg/m <sup>3</sup> ]
$\rho_{\text{g}}$	= gas density	[kg/m <sup>3</sup> ]
$\rho_{\text{p}}$	= average density of bed material	[kg/m <sup>3</sup> ]
$\rho_{\text{sand}}$	= density of sand particle	[kg/m <sup>3</sup> ]
$\sigma$	= fractional reactive sorbent surface area	[-]
$\sigma_{1,\text{avg}}$	= average fractional coal surface area	[-]
$\sigma_{\text{avg}}, \sigma_{3,\text{avg}}$	= average fractional reactive sorbent surface area	[-]
$\sigma_{\text{min}}$	= minimum fractional reactive sorbent surface area	[-]
$\sigma_1$	= fractional coal surface area	[m <sup>2</sup> ]
$\sigma_3$	= fractional sorbent surface area	[-]
$\tau, \tau_0$	= maximum reaction time (e.g. pore plugging time)	[s]
$\tau_1$	= average coal residence time	[s]
$\tau_{\text{br}}$	= sulfur breakthrough time	[s]
$\tau_{\text{g}}$	= gas residence time	[s]
$\tau_3, \tau_{\text{S}}$	= average sorbent residence time	[s]
$\theta$	= dimensionless sulfur breakthrough time	[-]
$\psi$	= ratio between distribution coefficients $\lambda_2$ and $\lambda_1$	[-]
$\zeta, \zeta_1, \zeta_3$	= stoichiometric coefficients	[-]

## REFERENCES

- Almstedt, A.-E., *Chem. Eng. Sci.*, 42 (3), 581-590, 1987.
- Almstedt, A.-E. and Ljunstrom, E.B., Proc. 9th Int. Conf. on FBC, volume 1, 575-585, Boston, USA, May 3-7, 1987.
- Akse, H.A., Vincent, Ch.J. and Spitsbergen, U., *VDI-Berichte*, 498, 107, 1983.
- Anthony, E.J., Becker, H.A., Code, R.K., Liang, D.T. and Stephenson, J.R., Proc. 8th Int. Conf. on FBC, Houston, USA, 1985.
- Avidan, A. and Yerushalmi, J., *AIChE J.*, 31 (5), 835, 1985.
- Babu, S.P., Shah, B. and Talwalkar, A., *AIChE Symp. Ser.*, 74, No. 176, 1978.
- Bass III, J.W. and High, M.D., Proc. 3rd Int. Fluid. Conf., KN/1B/2-1, The Institute of Energy, London, 1984.
- Beeckmans, J.M., Bergstrom, L. and Large, J.F., *Chem. Eng. J.*, 28, 1, 1984.
- Beeckmans, J.M., in: Fluidization, D. Kunii and R. Toei (Eds.), Engineering Foundation, New York, 177, 1984.
- Bethell, F.V., Gill, D.W. and Morgan, B.B., *Fuel*, 52, 121, 1973.
- Bhatia, S.K. and Perlmutter, D.D., *AIChE Journal*, 27, 226, 1981.
- Bhatia, S.K., *AIChE Journal*, 31, 642, 1985.
- Borgwardt, R.H., *Environ. Sci. Technol.*, 4, 59, 1970.
- Borgwardt, R.H. and Harvey, R.D., *Environ. Sci. Technol.*, 6 (4), 350, 1972.
- Borgwardt, R.H., Roache, N.F. and Bruce, K.R., *Environ. Prog.*, 3, 129, 1984.
- Bramer, E.A. and Vincent, Ch., Internal report, Department of Thermal Power Engineering, Twente University of Technology, Enschede, The Netherlands, September 1986.
- Brem, G., TNO report, no. 8726-16334, The Netherlands, August 1986.
- Burdett, N.A., Proc. Int. Conf. Inst. Energy, V-3-1, London, 1980.
- Burdett, N.A., *J. Inst. Energ.*, 198-208, 1983.
- Burdett, N.A., Hotchkiss, R.C. and Squires, R.T., Proc. Int. Conf. on Coal Science, 610, Pittsburgh, USA, 1983.
- Chen, T.P. and Saxena, S.C., *Fuel*, 56, 401, 1977.
- Chen, M.M., Chao, B.T. and Liljegen, J., Proc. 4th Int. Conf. on Fluid., Japan, 1983.
- Chiba, T. and Nienow, A.W., in: Fluidization, D. Kunii and R. Toei (Eds.), Engineering Foundation, New York, 195, 1984.
- Christman, P.G. and Edgar, T.F., *AIChE Journal*, 29, 388, 1983.
- Chrostowski, J.W. and Georgakis, C., Proc. Int. Symp. on Chemical Reaction Engg., 225, Houston, 1978.
- Clift, R., Ghadiri, M., Monteiro, J.L., Tan, B.K.C. and Thambimuther, K.V., Proc. 4th Eng. Found. Conf. on Fluid., 1.11.1-1.11.8, Japan, 1983.
- Cooke, M.J., Napier, B.A., Parkinson, M.J. and Rogers, E.A., Proc. 7th Int. Conf. on FBC, volume II, 792, Philadelphia, USA, 1982.
- De Kok, J.J., Stark, N.L. and Van Swaaij, W.P.M., Proc. 5th Eng. Found. Conf. on Fluid., in: Fluidization, K. Østergaard and A. Sørensen (Eds.), Engineering Foundation, New York, 433, 1986.
- Dennis, J.S. and Fieldes, R.B., *Chem. Eng. Res. Des.*, 64, 279, 1986.
- Desai, D.L., Engstrom, F., Alderton, W.B., Vayda, S.H., Wood, C.E. and Friedrich, F.D., Proc. 9th Int. Conf. on FBC, volume 1, 312-321, Boston, USA, May 3-7, 1987.
- Dogu, T., *Chem. Eng. J.*, 21, 213, 1981.

- Donsi, G., Lancia, M., Massimilla, L. and Volpicelli, G., in: Fluidization, D. Kunii and R. Toei (Eds.), Engineering Foundation, New York, 347, 1984.
- Duqum, J.N., Tang, J.T., Morris, T.A., Esakov, J.L. and Howe, W.C., Proc. 8th Int. Conf. on FBC, Houston, USA, 1985.
- Ekinci, E., Turkay, S. and Fells, I., Proc. 7th Int. Conf. on FBC, volume 2, 875, Philadelphia, USA, 1982.
- Fan, L.-S., Miyanami, K. and Fan, L.T., Chem. Eng. J., 13, 13, 1977.
- Fan, L.-S., Fan, L.T., Tojo, K. and Walawender, W.P., Can. J. Chem. Eng., 56, 603, 1978.
- Fan, L.-S., Satija, S., Wilson, W.I., Fee, D.C., Myles, K.M. and Johnson, I., Chem. Eng. J., 28, 151, 1984.
- Fee, D.C., Wilson, W.I., Myles, K.M., Johnson, I. and Fan, L.-S., Chem. Eng. Sci., 38 (11), 1917, 1983.
- Fee, D.C., Myles, K.M., Marroquin, G. and Fan, L.-S., Chem. Eng. Sci., 39 (4), 731, 1984.
- Fieldes, R.B., PhD Dissertation, University of Cambridge, United Kingdom, 1979.
- Fieldes, R.B., Burdett, N.A. and Davidson, J.F., Trans. Instn. Chem. Engrs., 57, 276, 1979.
- Geldart, D., Powder Technol., 7, 285, 1973.
- Geldart, D., Hurt, J.M. and Wadia, P.H., AIChE Symp. Ser., 74, No. 176, 60, 1978.
- Georgakis, C., Szekely, J., Chang, C.W., Chrostowski, J.W. and Trinh, T., Proc. 5th Int. Conf. on FBC, volume II, 787, 1977.
- Georgakis, C., Chang, C.W. and Szekely, J., Chem. Eng. Sci., 34, 1072, 1979.
- Gibilaro, L.G. and Rowe, P.N., Chem. Eng. Sci., 29, 103, 1974.
- Glicksman, L., Lord, W., Valenzuela, J., Bar-Cohen, A. and Hughes, R., AIChE Symp. Ser., 205, 77, 139, 1981.
- Glicksman, L.R. and McAndrews, G., Powder Technol., 42, 159, 1985.
- Hartman, M. and Coughlin, R.W., AIChE Journal, 22, 490, 1976.
- Hatfield, J.D., Dim, Y.K., Mullins, R.C. and McClellan, G.H., NTIS Publication, No. PB 202 407, 1970.
- Hikita, T., Ikeda, M. and Asano, H., in: Fluidization, D. Kunii and R. Toei (Eds.), Engineering Foundation, New York, 169, 1984.
- Hirama, T., Takeuchi, H. and Horio, M., Proc. 9th Int. Conf. on FBC, volume 1, 898-905, Boston, USA, May 3-7, 1987.
- Ho, Tho-Ching, Lee, Hom-Ti and Hopper, J.R., AIChE Journal, 32 (10), 1754, 1986.
- Hovmand, S. and Davidson, J.F., in: Fluidization, J.F. Davidson and D. Harrison (Eds.), Chapter 5, Academic Press, New York, 1971.
- Inoue, T., Tamanuki, S., Shimizu, T., Kawada, S. and Takada, T., Proc. 7th Int. Conf. on FBC, volume 2, 915-928, Philadelphia, USA, October 25-27, 1982.
- Ishida, M. and Wen, C.Y., Chem. Eng. Sci., 26, 1031, 1971.
- Jonke, A.A., Vogel, G.J., Carls, E.L., Ramaswami, D., Anastasia, L., Jarry, R. and Haas, M., AIChE Symp. Ser., No. 126, 68, 241, 1972.
- Jovanovic, G.N. and Catipovic, N.M., Proc. 4th Int. Conf. on Fluid., Japan, 1983.
- Kamphuis, B., Potma, A.W. and Van Werven, C., Paper presented at the 3rd discussion meeting of the Netherlands WUB-workgroup "Fluidized Combustion", Liège, Belgium, February 6, 1987.
- Kehoe, P.W.K. and Davidson, J.F., AIChE Symp. Ser., 69 (128), 41, 1973.

- Kroon, J.A., MSc Thesis, Department of Chemical Engineering and Chemistry, Delft University of Technology, Delft, The Netherlands, 1986.
- Kool, R.J.M., PhD Thesis, Laboratory of Thermal Power Engineering, Delft University of Technology, The Netherlands, 1985.
- LaNauze, R.D. and Jung, K., Proc. 7th Int. Conf. on FBC, volume II, 1040, Philadelphia, USA, October 25-27, 1982.
- LaNauze, R.D., Chem. Eng. Res. Des., 63, 3, 1985.
- Lee, D.C., Hodges, J.L. and Georgakis, C., Chem. Eng. Sci., 35, 302, 1980.
- Lee, D.C. and Georgakis, C., AIChE Journal, 27, 472, 1981.
- May, W.G., Chem. Eng. Progress, 55 (12), 49, 1959.
- Marsh, D.W. and Ulrichson, D.L., Chem. Eng. Sci., 40 (3), 423, 1985.
- Masson, H.A., Dang Trang, K. and Rios, G., Proc. Fluid. Comb. Conf., Energy Research Institute, University of Cape Town, South Africa, January 28 - 30, 1981.
- Masson, H.A., Dang Trang, K. and Rios, G., AIChE Symp. Ser., No. 65, 1982.
- Masson, H.A., Report INIEX, Liege, Belgium, July 1986.
- Meyer, B., Sulfur, Energy and Environment, Elsevier, Amsterdam, 1977.
- Molayem, B., Bardakci, T., Hall, A.W. and Hewitt, D.R., Proc. 7th Int. Conf. on FBC, volume I, 239, Philadelphia, USA, October 25-27, 1982.
- Mori, S. and Wen, C.Y., AIChE Journal, 21, 109, 1975.
- Noordergraaf, I.W., PhD Thesis, Delft University of Technology, The Netherlands, Delft University Press, 1985.
- Noordergraaf, I.W., Van den Bleek, C.M. and Van den Berg, P.J., Proc. 8th Int. Conf. on FBC, Houston, USA, 1985.
- Noordergraaf, I.W., Van Deemter, J.J., Van den Bleek, C.M. and Van den Berg, P.J., Proc. 5th Eng. Found. Conf. on Fluid., in: Fluidization, K. Østergaard and A. Sørensen (Eds.), Engineering Foundation, New York, 579, 1986.
- Noordergraaf, I.W., Van Dijk, A. and Van den Bleek, C.M., Powder Technol., 52, 59, 1987.
- Olofsson, J., Mathematical Modelling of Fluidised Bed Combustors, Report number ICTIS/TR14, IEA Coal Research, London, November 1980.
- Park, D., Levenspiel, O. and Fitzgerald, T.J., Proc. 6th Int. Conf. on FBC, 791, 1980.
- Preto, F., Report of CANMET to the IEA, Canada Centre for Mineral and Energy Technology, 1985.
- Rajan, R.R., Krishnan, R. and Wen, C.Y., AIChE Symp. Ser., No. 176, 74, 112, 1978.
- Rajan, R.R. and Wen, C.Y., AIChE Journal, 26, 642, 1980.
- Ramachandran, P.A. and Doraiswamy, L.K., AIChE Journal, 28, 881, 1982.
- Ramachandran, P.A. and Smith, J.M., AIChE Journal, 23, 353, 1977.
- Ranade, P.V. and Harrison, D.P., Chem. Eng. Sci., 34, 427, 1979.
- Raven, P. and Sparham, G.A., Proc. 7th Int. Conf. on FBC, volume I, 275, Philadelphia, USA, 1982.
- Rudolph, V. and Judd, M.R., in: Circulating Fluidized Bed Technology, P. Basu (Ed.), Pergamon Press, Toronto, 437, 1986.
- Salib, P.F., Barua, S.K., Robson, K.B. and Kissell, R.K., Proc. 9th Int. Conf. on FBC, volume 1, 340-344, Boston, USA, May 3-7, 1987.
- Schouten, J.C. and Van den Bleek, C.M., submitted for publication in Chem. Eng. Sci., 1986.
- Schouten, J.C. and Van den Bleek, C.M., submitted for publication in Chem. Eng. Sci., 1987a.

- Schouten, J.C. and Van den Bleek, C.M., Proc. 9th Int. Conf. on FBC, volume 1, 749-761, Boston, USA, May 3-7, 1987b.
- Schouten, J.C., Singh, P.C., Valkenburg, P.J.M. and Van den Bleek, C.M., submitted for publication in Chem. Eng. Res. Des., 1986.
- Schouten, J.C., Valkenburg, P.J.M. and Van den Bleek, C.M., accepted for publication in Powder Technol., 1987a.
- Schouten, J.C., Masson, H.A. and Van den Bleek, C.M., Proc. Int. Symp. on Multiphase Flows, ISMF 1987, volume 1, 237-243, Zhejiang University, Hangzhou, People's Republic of China, August 3-5, 1987b.
- Schouten, J.C., Hakvoort, G., Valkenburg, P.J.M. and Van den Bleek, C.M., Thermochimica Acta, 114, 171-178, 1987c.
- Spitsbergen, U., de Groot, H.J., Schouten, J.C. and Akse, H.A., Proc. 7th Int. Conf. on FBC, volume II, 1087, Philadelphia, USA, October 25-27, 1982.
- Simons, G.A. and Garman, A.R., AICHE Journal, 32 (9), 1491, 1986.
- Simons, G.A. and Rawlins, W.T., Ind. Eng. Chem. Process Des. Dev., 19, 565, 1980.
- Sit, S.P. and Grace, J.R., Chem. Eng. Sci., 36, 327, 1981.
- Tang, J.T., Duqum, J.N., Modrak, T.M. and Aulisio, C.J., Proc. 7th Int. Conf. on FBC, volume I, 373, Philadelphia, USA, October 25-27, 1982.
- Terada, H., Takagi, M., Shimizu, T., Tamanuki, S. and Tatebayashi, J., Proc. 7th Int. Conf. on FBC, volume 2, 876-885, Philadelphia, USA, October 25-27, 1982.
- Thiel, W.J. and Potter, O.E., Ind. Eng. Chem. Fundam., 16 (2), 242, 1977.
- Thiel, W.J. and Potter, O.E., AICHE J., 24 (4), 561, 1978.
- Valk, M., Bramer E.A. and Toissant, H.H.J., Proc. 9th Int. Conf. on FBC, volume 2, 784-792, Boston, USA, May 3-7, 1987.
- Valkenburg, P.J.M., Schouten, J.C. and Van den Bleek, C.M., Proc. 5th Eng. Found. Conf. on Fluid., in: Fluidization, K. Østergaard and A. Sørensen (Eds.), Engineering Foundation, New York, 193, 1986.
- Valkenburg, P.J.M., Singh, P.C., Schouten, J.C. and Van den Bleek, C.M., Proc. 9th Int. Congress of Chem. Eng., Chem. Equipm. Des. and Autom., CHISA 1987, Prague, Czechoslovakia, August 30 - September 4, 1987.
- Van Deemter, J.J., Proc. Int. Symp. on Fluid., (Ed. A.A.H. Drinkenburg), Netherlands University Press, Amsterdam, 334, 1967.
- Van Deemter, J.J., in: Fluidization, J.R. Grace and J.M. Matsen (Eds.), Plenum Press, New York, 75, 1980.
- Van den Bleek, C.M. and Schouten, J.C., Written comment on Proc. 9th Int. Conf. on FBC (Boston, USA, May 3-7, 1987), to be published by the Amer. Soc. Mech. Eng. (ASME); Delft University of Technology, June 3rd, 1987.
- Viswanathan, K. and Subba Rao, D., in: Fluidization, D. Kunii and R. Toei (Eds.), Engineering Foundation, New York, 291, 1984.
- Weimer, A.W. and Clough, D.E., AICHE Journal, 29, 411, 1983.
- Wells, J.W., Krishnan, R.P. and Byrd, J.R., Proc. 7th Int. Conf. on FBC, volume I, 284, Philadelphia, USA, October 25-27, 1982.
- Wen, C.Y. and Ishida, M., Environ. Sci. Technol., 7, 703, 1973.
- Wen, C.Y. and Yu, Y.H., AICHE Journal, 12, 610, 1966.
- Werther, J., AICHE Symp. Ser., 141 (70), 53 (1973).
- Yacono, C. and Angelino, H., Proc. 2nd Eng. Found. Conf. on Fluid., 25, Cambridge, United Kingdom, 1978.
- Yagi, S. and Kunii, D., Chem. Eng. Sci., 16, 364, 1961.

- Yates, J.G., Fundamentals of Fluidized-Bed Chemical Processes, Butterworths Monographs in Chemistry, Butterworths, London, 1983.
- Zakkay, V. and co-workers, Report of Contract no. DE-AS21-80MC 14322 (U.S. D.O.E., Morgantown (WV)), New York University, Department of Applied Science, New York (N.Y.), USA, August 1985 (245 pages).
- Zheng, J., Yates, J.G. and Rowe, P.N., Chem. Eng. Sci., 37 (2), 167, 1982.

CURRICULUM VITAE van JAAP SCHOUTEN

Geboren 29 juni 1959 te Apeldoorn.

- 1971-1977: Voorbereidend Wetenschappelijk Onderwijs (VWO) aan het Myrthus College te Apeldoorn;  
16 juni 1977: diploma Atheneum B.
- 1977-1981: Baccalaureaat technische wetenschappen aan de Afdeling der Chemische Technologie van de Technische Hogeschool Twente te Enschede;  
16 september 1981: diploma Baccalaureus technische wetenschappen (Btw).
- 1981-1983: Vrije Studierichting Chemische Technologie aan de Afdeling der Chemische Technologie van de Technische Hogeschool Twente te Enschede; afstudeeropdracht verricht bij prof. dr. P.J. Gellings (Anorganische Chemie en Materiaalkunde);  
14 september 1983: ingenieursdiploma (met lof).
- 1984-1987: Wetenschappelijk assistent in dienst van de Stichting voor de Technische Wetenschappen (STW). Werkzaam onder leiding van prof. drs. P.J. van den Berg bij het Laboratorium voor Chemische Technologie van de Faculteit der Scheikundige Technologie en der Materiaalkunde aan de Technische Universiteit Delft.  
De onderzoeksresultaten verkregen tijdens deze periode zijn deels vastgelegd in dit proefschrift.
- Vanaf 1 januari 1988 werkzaam bij de sectie 'Washing Processes and Machines' van het Unilever Research Laboratorium te Vlaardingen.